Investigating the role of a *FAM111B* mutation in Hereditary Fibrosing Poikiloderma (POIKTMP) using Induced Pluripotent Stem Cell (iPSC) model

by

Dimakatso B. Gumede

Submitted for the degree of
Doctor of Philosophy

Department of Medicine
UNIVERSITY OF CAPE TOWN

Supervisors

Prof. Susan H. Kidson, Dr. Robea Ballo, Prof. Bongani M. Mayosi

2019

This PhD-project was financially supported by:
National Research Foundation (NRF)
Postgraduate funding Office, University of Cape town
Department of Medicine, University of Cape Town

Plagiarism Declaration

"This thesis/dissertation has been submitted to the Turnitin module (or equivalent similarity and originality checking software) and I confirm that my supervisor has seen my report and any concerns revealed by such have been resolved with my supervisor."

Name: Dimakatso Bertha Gumede

Student number: GMDDIM001

Signature: Signed by candidate

Date:16/10/2019

Abstract

Hereditary fibrosing poikiloderma is an autosomal dominant disorder that is characterised by mottled pigmentation and telangiectasia, accompanied by tendon contractures, myopathy and pulmonary fibrosis (POIKTMP). Mutations in POIKTMP cases have been shown to harbour the *Family with sequence similarity 111B* (*FAM111B*) gene. However, its function is unknown. The aim of this study was to investigate the causative role of the *FAM111B* mutation (c.1861T>G) in the multi-systemic fibrosis affecting the South African kindred with POIKTMP.

Dermal fibroblasts from two affected siblings and a familial control were reprogrammed into induced pluripotent stem cells (iPSCs) via the Sendai virus vector (SeVdp) packaged with pluripotency transgenes (*OCT4; SOX2; KLF4; C-MYC*). The derived iPSCs successfully showed a) endogenous expression of pluripotency markers (OCT4; NANOG; TRA-1-60), b) *in vitro* differentiation into the three germ layers (endoderm; mesoderm; ectoderm) and c) normal karyotyping. Next, the iPSCs from two patients, a Familial control and a Non-familial control were differentiated into mesenchymal stem/stromal cells (iPSC-MSCs) as a cell model in this study. Characterisation of derived iPSC-MSCs indicated positive expression of MSC markers (CD73; CD90; α-SMA). Differentiation of iPSC-MSCs demonstrated adequate osteogenicity but limited adipogenicity. Patient-derived iPSC-MSCs were thereafter analysed by qPCR and collagen staining to determine whether the *FAM111B* mutation alters endogenous expression of pro-fibrotic markers as well as collagen synthesis in patient cells compared to controls. Messenger RNA expression of pro-fibrotic markers (COL1A1; COL3A1; α-SMA) was similar between patient and control iPSC-MSCs. Collagen staining and quantification also showed no statistical differences between patient and control cells. These results suggest that FAM111B does not directly alter the expression of these pro-fibrotic genes in this *in vitro* model system.

Growth curves were then carried out to investigate if the *FAM111B* mutation modulates cell proliferation and it was found that patient cells proliferated at a higher rate compared to controls. To explore the mechanisms underlying the rate change, analyses of FAM111B expression during cell cycle progressions were conducted. Extensive optimization experiments using the double thymidine block approach were necessary to establish the appropriate synchronization protocol, keeping in mind the extended doubling time of iPSC-MSCs. The results revealed that FAM111B mRNA expression was temporally regulated, with a peak at the S-phase and low at the G2/M phase. While there were no pattern differences between patient and control cells, FAM111B mRNA expression was significantly higher in the patient cells compared to controls at the G1- and S-phase. These results suggest that the mutation in FAM111B might affect the stability or perdurance of the mRNA. Unfortunately, analysis of the FAM111B protein data was inconclusive. Problems related to synchronization of the cells and the specificity of the antibody would have to be rectified in order to follow this further.

The overall findings in this *in vitro* study reveal that the *FAM111B* mutation does not alter expression of pro-fibrotic markers but does affect the cell proliferation rate of patient cells compared to controls. Future work will focus on further optimisation of iPSC-MSCs synchronisation to determine correlation of FAM111B mRNA and protein expression during cell cycle progression in the patient cells. Furthermore, 3D *in vitro* cellular models that recapitulate some parts of the POIKTMP phenotype will need to be created. Future work will also explore the gain-of-function hypothesis to further understand the role of FAM111B in fibrosis and cancer phenotype in POIKTMP.

Dedication

For Professor Bongani Mayosi

Acknowledgments

I would firstly like to thank God for granting me the strength and perseverance to complete this PhD journey.

A very special thanks to my supervisors for going above and beyond academic support during the course of my study: the late Prof. Bongani Mayosi, without whom this project would not have been possible; Prof. Susan Kidson for welcoming me into her lab, for supervising, mentoring and spending many hours teaching me the art of scientific writing. Thanks for making learning an exciting and fulfilling experience; Dr. Robea Ballo for patiently teaching me all the laboratory techniques and spending many hours training me in the arduous and highly specialised process of reprogramming fibroblasts.

Thanks to Dr Janine Scholefield (CSIR, Pretoria) for taking me under her wing these last few months and assisting so readily in the completion of this thesis.

Thanks to the members of the "FAM111B" group at the University of Cape Town: Dr Gasnat Shaboodien (Hatter Institute for Cardiovascular Research, UCT), Prof. Ed Sturrock (Dept. of biochemistry, UCT) Dr Afolake Arowolo (Dept. of Dermatology, UCT), Prof. Dirk Lang (Dept. of Human Biology, UCT), Dr Christopher Maske (QLAB Inc.), Ms Komala Pillay (Dept. of pathology, UCT) and Prof. Nonhlanhla Khumalo (Dept. of Dermatology, UCT).

My years spent in the Prof Kidson lab (aka UCT Stem Cell Initiative) was especially enjoyable because of good relationships with my peers. Special thanks to Thulisa Mkathazo, Dennis Lin, Dr Alice Brown, Ms Sylvia Kamanzi-Wa and Austin Malise for their peer support, great laughs and help in times of need. Thank you to Prof. Elizabeth van der Merwe and Ms Viantha Naidoo for their advice, especially with regards to immunocytochemistry.

The cell cycle experiments conducted in this project were challenging and I would like to thank Prof. Sharon Prince for taking time out of her busy schedule to provide invaluable advice for these experiments.

Thank you also to the Prince lab and the Cell Biology support staff (Dept. of Human Biology, UCT) for their assistance during the course of my study.

Thank you to Dr Gasnat Shaboodien, the Mayosi cardio-genetics group and the Hatter Institute for Cardiovascular Research in Africa for the training and support at the start of my PhD.

Special thanks to my friends in Johannesburg, Durban and Cape Town for their prayers and words of encouragement through this journey.

Last, but not least, I would like to thank my family for their prayers, support and patience as I embarked on this PhD journey. A special thank you to my cousin Sifiso More for assisting with the table of contents and hyperlinks for this thesis.

Table of Contents

List of Figures

Tables

1. µl	micro-litres
2. µM	micro-molar
3. 2D	Two-dimension
4. 3D	three-dimension
5. AEC	Alveolar epithelial cells
6. ALP	Alkaline phosphatase
7. ARS	Alizarin red stain
8. ATP13A2	Probable cation-transporting ATPase 13A2
9. AURKA	Aurora kinase A
10. bFGF	basic fibroblast growth factor
11. C/EBPα	CCAAT/enhancer binding protein α
12. CANP	Cancer-associated nuclear protein
13. CCL	Chemokine (C-C motif) ligand
14. CD	Cluster of differentiation
15. CDK	Cyclin-dependent kinase
16. cDNA	complementary DNA
17. ChIP	Chromatin immunoprecipitation
18. COL	Collagen
19. COL1A1	Collagen type 1α1
20. COL3A1	Collagen type 3α1
21. CTGF	Connective tissue growth factor
22. DMEM	Dulbecco's modified eagle's medium
23. DNA	Deoxyribonucleic acid
24. EB	Embryoid body
25. ECM	Extracellular matrix
26. EDTA	Ethylenediaminetetraacetic acid
27. EMT	Epithelial-mesenchymal transition
28. ESC	Embryonic stem cells
29. FABP-4	Fatty-acid binding protein-4
30. FAM	Family with sequence similarity
31. FBS	Foetal bovine serum
32. FOXA2	Forkhead box protein A2
33. HDF	Human dermal fibroblasts
34. hESC	Human embryonic stem cell
35. ICC	Immunocytochemistry
36. IFN-γ	interferon-gamma
37. IL	interleukin
38. iMEFs	inactivated mouse embryonic fibroblasts
39. IPF	Idiopathic pulmonary fibrosis
40. iPSC	Induced pluripotent stem cells
41. iPSC-MSCs	iPSC-derived mesenchymal stem cells
42. KLF	Kruppel-like factor
43. KO SR	Knockout serum replacement
44. MAPK	mitogen-activated protein kinase
45. MCM	MEF-conditioned medium

46. MEF	Mouse embryonic fibroblasts
47. MET	Mesenchymal-epithelial transition
48. miRNA	Micro-RNA
49. MMP	Matrix metalloproteinases
50. MSC	Mesenchymal stem cells
51. NEAA	Non-essential amino acids
52. ng	nanograms
53. NHLS	National Health Laboratory Service
54. OCT	Octomer
55. ORO	Oil red O
56. P/S	Penicillin-streptomycin
57. PBS-T	Phosphate-buffered saline-Tween-20
58. PCNA	Proliferating cell nuclear antigen
59. PCNA	Proliferating cell nuclear antigen
60. PCR	Polymerase chain reaction
61. PDGF	Platelet-derived growth factor
62. POIKTMP	Poikiloderma with tendon contractures, myopathy and pulmonary fibrosis
63. PPARγ	Peroxisome proliferator-activated receptor γ
64. PSR	Picrosirius Red
65. PTEN	Phosphatase and tensin homolog
66. qPCR	Quantitative real-time PCR
67. RIPA	Radioimmunoprecipitation assay
68. RNA	Ribonucleic acid
69. ROCK inhibitor	Rho-associated protein kinase inhibitor
70. RT	Room Temperature
71. RTS	Rothmund-Thomson syndrome
72. RUNX2	Runt-related transcription factor 2
73. SCNT	Somatic cell nuclear transfer
74. SDS-PAGE	Sodium-dodecyl-sulphate polyacrylamide gel electrophoresis
75. SeV	Sendai virus
76. SeVdp	Defective and persistent Sendai virus vector
77. siRNA	Small interfering RNA
78. SOX2	SRY (sex determining region Y)-box 2
79. SV40 LT	Simian virus Large T antigen
80. TBS-T	Tris-buffered saline-Tween-20
81. TGFR	TGF receptor
82. TGF-β	Transforming growth factor-beta
83. TIMP	Tissue inhibitors of metalloproteinases
84. TNF	Tumour necrosis factor
85. V	Volts
86. Xist	X-inactive specific transcript
87. α-SMA	Alpha smooth muscle actin

Chapter 1

Literature review

1.1 Introduction

Hereditary fibrosing poikiloderma with tendon contractures, myopathy and pulmonary fibrosis (POIKTMP[MIM#615704) is a rare autosomal dominant genetic disorder. First described in a South African family of Dutch descent in 2006, there have been 13 independent families and 9 sporadic cases of this genetic disorder reported to date (Chasseuil et al., 2019). The key features being i) poikiloderma which presents in early childhood and is associated with telangiectasia, hypohidrosis and mottled pigmentation, particularly in sun-exposed areas; ii) muscle contractures of the triceps surae leading to Achilles tendon contractures, iii) myopathy with fatty infiltration. and iv) progressive pulmonary fibrosis (Mercier et al., 2015; Mercier et al., 2013; Zhang et al., 2019). It also associated with exocrine pancreatic insufficiency as well as pancreatic cancer (Chasseuil et al., 2019; Goussot et al., 2017; Takeichi et al., 2016). The causative gene has been identified, but the link between the mutation and the phenotype has not been elucidated. Therefore, to help understand and appreciate the complexity of this condition as it involves dermal sclerosis, myopathy and pulmonary impairment, this chapter will address on a broader context the phenotype of this condition, focusing on the pathogenesis of fibrosis, which is the cause of death in the affected persons. This chapter will also address the aims and objectives of this study which will be discussed in detail in the subsequent chapters.

1.2 Hereditary Poikiloderma Syndromes

Poikiloderma is a dermatological condition that presents with epidermal atrophy, alopecia, telangiectasia and mottled pigmentation (Larizza et al., 2010; Nofal & Salah, 2013). Hereditary poikiloderma is associated with syndromes such as the Rothmund-Thomson (RTS), Kindler, Werner, Weary and Bloom's syndromes, which are rare autosomal recessive disorders (Ellis et al., 1995; Larizza et al., 2010; Lindor et al., 2000; Willis & Lindahl, 1987). There have been 300 cases reported for RTS in 2010, and less than 100 cases have been

reported for the Kindler syndrome (Fischer et al., 2005; Larizza et al., 2010). From 1916 to 2002, 1300 cases have been reported for the Werner syndrome (Sert et al., 2009). Bloom's syndrome was reported to have 1:50 000 prevalence persons due to its founder effect, with 1% of it occurring in the European Ashkenazi Jews (Liu & West, 2008).

These syndromes present with poikiloderma and overlap in their clinical features. For example, the Rothmund-Thomson syndrome (RTS), Werner syndrome and Bloom's syndrome indicate adult progeria, chromosomal instability and predisposition to cancer malignancies (Lindor et al., 2000). The Kindler syndrome and Weary syndrome also demonstrate similarities, particularly in progressive poikiloderma with blisters and acral keratosis (Fig. 1.1). However, there are also clear differences in these syndromes, for instance, RTS, Bloom's syndrome and Kindler syndrome present in early childhood while the Werner syndrome presents later in life (see Table 1.1) (Larizza et al., 2010; Lindor et al., 2000). Due to the overlapping clinical features in some of these syndromes there are no set guidelines to properly classify poikiloderma cases. Reliable diagnoses have therefore been performed based on genetic and cytogenetic differences (Lindor et al., 2000). For example, Bloom's syndrome which presents with mutations in the *RECQ2* gene has a high rate of chromatid gaps and breaks that cause genome instability with increased risk of carcinogenesis (Ellis et al., 1995). The RTS presents with mutations in the *RECQ4* gene and commonly presents with cataract and cases of osteosarcoma (Larizza et al., 2010).

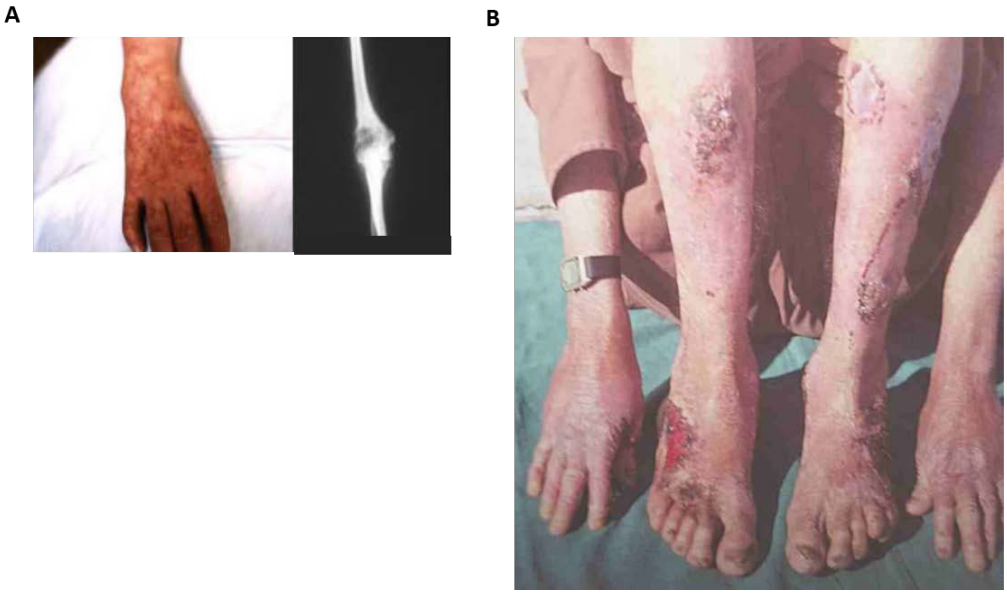

Figure 1.1: Clinical presentations of Rothmund-Thomson and Kindler syndromes.
(A) Poikiloderma and bone defects (X-ray) in patients with RTS. **(B)** Kindler syndrome is shown by the crusted lesions of acral bullae (Larizza et al., 2010; Macris et al., 2006)

The genes associated with some of these syndromes are well characterised. Most seem to be caused by autosomal recessive mutations in the *RECQ* genes which encode DNA helicase enzymes. The human *RECQ* genes are homologous to the *recq* gene found in *E. coli*, and the protein has ATPase-dependent helicase activity which functions in unwinding of the DNA complementary strand during replication (Ellis et al., 1995; Liu & West, 2008). The RECQ proteins are also involved in DNA repair as well as maintenance of genome stability, and mutations in these genes produce a truncated protein resulting in loss-of-function and genome instability (Bahr et al., 1998; Kitano et al., 2010). Mutations in the *RECQ2* gene cause chromosomal breakage and increased sister chromatid interchange in somatic cells resulting in genome instability and predisposition to cancer (Bahr et al., 1998). Similarly, mutations in *RECQ3* cause genome instability resulting in malignancy, particularly osteosarcoma (Larizza et al., 2010; Macris et al., 2006). Mutations in a different gene, *KIND1*, are responsible for the Kindler syndrome (Lindor et al., 2000). The *KIND1* gene encodes the Kindlin-1 protein which is involved in the attachment of the actin cytoskeleton to the extracellular matrix at the focal adhesion sites, and is expressed in epithelial cells such as keratinocytes (Jobard et al., 2003; Ussar et al., 2008). Mouse models have shown that loss of function in the Kindlin-1 protein leads to skin atrophy which is typical of poikiloderma but also causes decreased proliferation of keratinocytes and detachment of intestinal epithelia (Ussar et al., 2008).

Table 1.1: Differential Diagnosis of Hereditary poikiloderma syndromes

Number	Syndrome	Inheritance	Gene	Poikiloderma Features	Additional Features
1	Bloom	AR	*RECQ2*	Present (when exposed to sunlight) with telangiectasia	Excessive sister chromatid exchange (chromosome instability), increased risk of cancer (myelodysplasia, leukaemia) and minor immune deficiency
2	Werner	AR	*RECQ3*	Limited to neck & upper chest. Onset within 1st year of life	Poor dentition, Enteropathy

3	Rothmund-Thomson Syndrome	AR	*RECQ4*	Present (when exposed to sunlight)	Cataract, Dwarfism, Hypogonadism, Bone abnormalities
4	Kindler	AR	*KIND1*	Widespread, Involves Sun exposed & Non- sun exposed body areas.	Defective gene mapped to chromosome 20p12.3. Stenosis of Oesophagus Webbing of digits, Dental Abnormalities Anhidrosis
5	Weary/Hereditary sclerosing poikiloderma	AD		Accentuated in flexors with sclerotic bands	Poor dentition, Calcinosis cutis
6	POIKTMP	AD	*FAM111B*	Widespread with telangiectasia, hypohidrosis, alopecia	Tendon contractures, myopathy with fatty infiltration and pulmonary fibrosis

Table modified from Mahajan et al. (2005) (AD = Autosomal; Dominant, AR =Autosomal Recessive)

1.3 Hereditary Fibrosing Poikiloderma (POIKTMP)

Due to its overlapping features of poikiloderma, alopecia, hypohidrosis and sclerosis, hereditary fibrosing poikiloderma (POIKTMP) was first thought to form part of the Rothmund-Thomson syndrome or the Weary/Werner syndrome (Khumalo et al., 2006; Mercier et al., 2013). Additional clinical features observed in the South African family (Fig. 1.2) which include myopathy and pulmonary fibrosis thus suggested POIKTMP to be a new form of hereditary poikiloderma (Khumalo et al., 2006). There have since been thirteen families and nine sporadic POIKTMP cases reported (Kazlouskaya et al., 2018). Genetic screening by Whole exome-sequencing (WES) showed that none of the *RECQ* and *KIND1* genes were involved (Mercier et al., 2013). Mutations were identified in the *Family with sequence similarity 111, member B* (*FAM111B*) gene which encodes a trypsin-like cysteine/serine peptidase (Goussot et al., 2017; Kazlouskaya et al., 2018; Mercier et al., 2013; Seo et al., 2016; Takeichi et al., 2016).

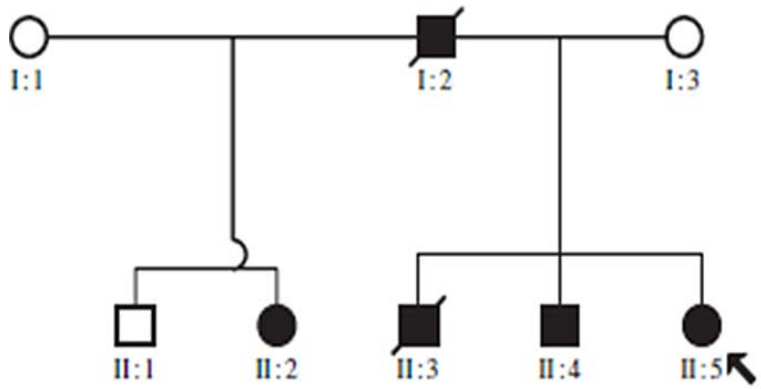

Figure 1.2: Pedigree of the South African kindred with POIKTMP. The affected individuals are represented by solid square (male) or circle (female). The index case (proband) is indicated by an arrow (Khumalo et al., 2006)

1.3.1 Clinical presentation of POIKTMP

This condition in the South African family spans two generations, the second-generation female, who is the proband presented with poikiloderma, alopecia of the scalp and eyebrows, tendon contractures and sclerosis of the digits (Khumalo et al., 2006). The family history indicated that the proband's father, who is deceased presented with similar clinical features and died from interstitial pulmonary fibrosis. An autopsy report of the older brother who also died from interstitial pulmonary fibrosis indicated that he developed poikiloderma, skeletal muscle abnormalities with fatty infiltration and tendon contractures. The surviving brother of the proband is also affected and is reported to experience pulmonary restriction with high chance of requiring lung transplantation (*pers comm, data not shown*).

More POIKTMP cases of similar phenotype as the South African kindred have been reported by Mercier et al. (2015; 2013). The affected individuals reported Mercier et al. (2013) are of Moroccan, Egyptian, Algerian and of Italian descent, and present with tendon contractures, myopathy, and pulmonary fibrosis (Fig. 1.3). Some patients showed evidence of growth retardation and anhidrosis which causes heat intolerance. Magnetic resonance imaging (MRI) results further indicated that myopathy is caused by fragmentation of the skeletal muscle fascicles and increased fatty infiltration (Fig. 1.3D). Skin histology of the affected person also indicated formation of elastin globes on the papillary dermis due to elastin degeneration (Fig. 1.3C). In their follow-up case report, Mercier et al. (2015) reported

six additional cases of individuals with POIKTMP, with additional phenotype such as pancreatic insufficiency and minor liver impairment. The most recent POIKTMP case report is of a French family, of whom the proband was a 64-year old male (father) presenting with classic poikiloderma, including mottled pigmentation, telangiectasia, marked hypohidrosis due to heat intolerance and tendon contractures. The proband did not present with pulmonary fibrosis but with pancreatic cancer (Goussot et al., 2017). The proband was reported to have none of the risk factors (obesity, smoking and type 2 diabetes) associated with pancreatic cancer. The children of the proband, a son and daughter are affected and have been shown to carry the mutation indicating autosomal dominance. They also presented in early childhood with the same clinical features as their father, except for pancreatic cancer. This is the only case to report pancreatic cancer as another feature of POIKTMP. It is unclear at this stage whether this is related to POIKTMP. This potential link will be expanded in detail in latter chapters, especially because there have been other papers where a link between fibrosis and cancer have been posited (Vancheri et al., 2010). The overall analysis of these case reports demonstrates that though the onset of POIKTMP is in early childhood, the clinical features of this condition vary from patient to patient, with some showing varied muscle atrophy ranging from diffuse to severe and pulmonary restrictive patterns beginning in childhood and interstitial pulmonary fibrosis or pancreatic cancer occurring in older individuals. (Goussot et al., 2017; Mercier et al., 2015; Mercier et al., 2013; Takeichi et al., 2016).

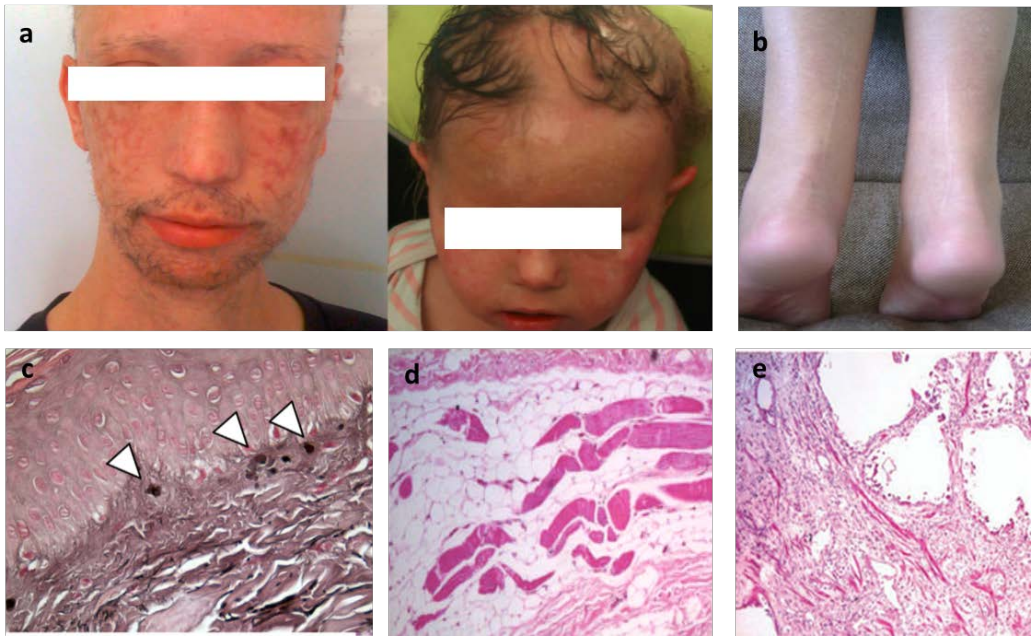

Figure 1.3: Clinical presentation of POIKTMP. The images show poikiloderma with telangiectasia **(A)** surgical scars of lengthened Achilles tendon **(B)**, elastin globules in the skin **(C)** myopathy with fatty infiltration **(D)** and pulmonary fibrosis (Khumalo, 2006; Mercier et al. 2013).

1.3.2 Genetic and molecular basis of POIKTMP

To date, only three familial cases of autosomal dominant inheritance and ten *de novo* cases have been reported globally (Goussot et al., 2017; Khumalo et al., 2006; Mercier et al., 2015; Mercier et al., 2013; Seo et al., 2016; Takeichi et al., 2016). An autosomal dominant mutation was detected in the South African kindred [c.1861T>G (p.Tyr621Asp)] with the classic POIKTMP phenotype (Mercier et al., 2013). Another family with an autosomal dominant mutation [c.1261_1263del (p.Lys421del)] in the *FAM111B* gene was reported to further show POIKTMP phenotype with pancreatic exocrine dysfunction (Seo et al., 2016). In a new case report from Goussot et al. (2017) of autosomal dominant *FAM111B* mutation [c.1884T > A (p.Ser628Arg)] indicated an additional feature of pancreatic cancer. The *de novo* cases reported indicated the same mutations in unrelated individuals (see Table 1.2). The most common de novo mutations are **c.1883G > A (p.Ser628Asn)**, **c.1879A > G (p.Arg627Gly)** and **c.1289A > C (p.Gln430Pro)** (Mercier et al., 2015; Takeichi et al., 2016). All mutations were absent in all public genetic variant databases such as 1000 Genomes Project, Exome Variant Server and (dbSNP142 (http://www.ncbi.nlm.nih.gov/snp/) (Mercier et al., 2015; Seo et al., 2016). Bioinformatic tools (SIFT and PolyPhen) predicted all mutations to be deleterious as they affect amino acids that are conserved across mammalian species (Mercier et al., 2015; Mercier et al., 2013; Seo et al., 2016).

Table 1.2: *FAM111B* mutations in POIKTMP

Case No.	Origin	Inheritance	Mutation	Literature
1	South Africa	AD	c.1861T > G (p.Tyr621Asp)	Mercier et al. (2013; 2015)
2	France	De novo	c.1874C > A (p.Thr625Asn)	
3	Algeria	*De novo* (with paternal inheritance)	c.1879A > G (p.Arg627Gly)	
4	France	De novo	c.1879A > G (p.Arg627Gly)	
5	Italy	De novo	c.1879A > G (p.Arg627Gly)	
6	France/Morocco	N/A	c.1883G > A (p.Ser628Asn)	
7	France	De novo	c.1883G > A (p.Ser628Asn)	
8	Ireland	De novo	c.1883G > A (p.Ser628Asn)	
9	Dominican Republic	De novo	c.1883G > A (p.Ser628Asn)	
10	France	N/A	c.1289A > C (p.Gln430Pro)	
11	United States of America	AD	c.1261_1263del (p.Lys421del)	Seo et al. (2016)
12	Kuwait	De novo	c.1289A > C (p.Gln430Pro)	Takeichi et al. (2016)
13	France	AD	c.1884T > A (p.Ser628Arg)	Goussot et al. (2017)

AD = Autosomal Dominant; AR =Autosomal Recessive

Although the *FAM111B* gene encodes a protein with a trypsin-like cysteine/serine catalytic domain, its function is currently unknown (Mercier et al., 2013). The *FAM111* genes (*FAM111A* and *FAM111B*) are located on the long arm (q) of chromosome 11, position q12.1. The *FAM111A* gene, which is a paralogue of *FAM111B* encodes a protein with 611 amino acid and is located 16 Kb from *FAM111B* (Fig. 1.4) [provided by RefSeq, Apr 2014]. The *FAM111B* gene spans 3.48 Kb of genomic DNA and consists of 4 exons. It undergoes alternative mRNA splicing which gives rise to three transcript variants (http://ncbi.org). Transcript variant 1 (NM_198947.3) encodes the longer isoform with 734 amino acids. Transcript variants 2 (NM_001142703.1) and 3 (NM_001142704.1) both encode the same isoform of 704 amino acids that lacks an exon containing the translational start codon as well as a 5' UTR (transcript variant 3). Both transcript variant 2 and 3 also have a shorter N-terminus compared to variant 1.

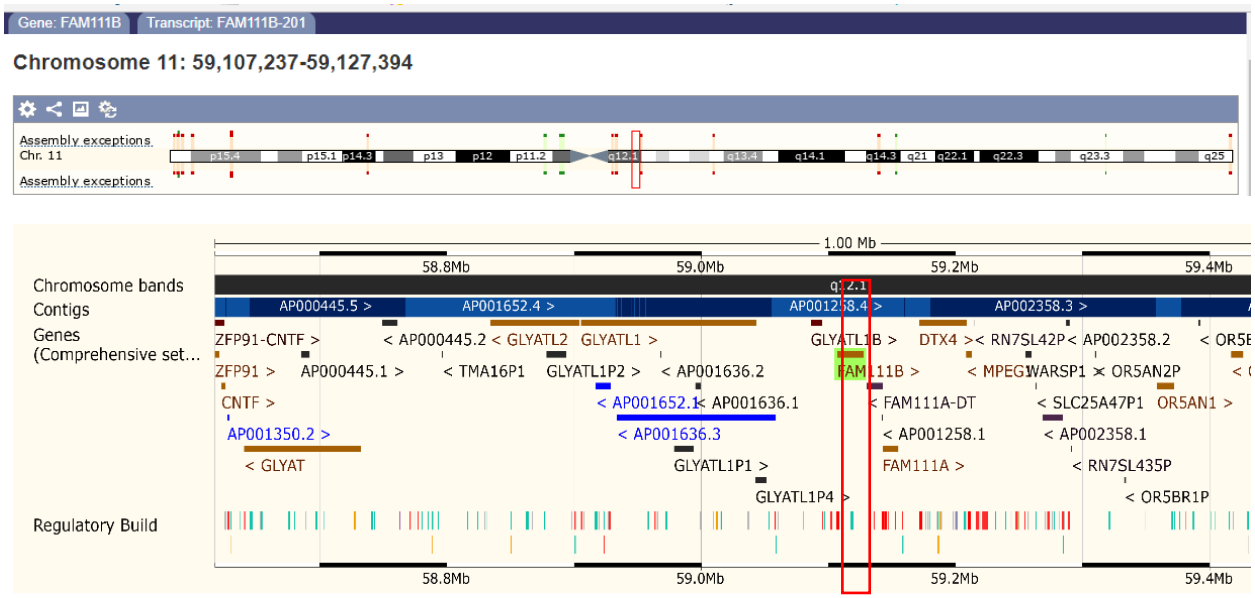

Figure 1.4: Chromosomal localisation of FAM111 genes. FAM111 (*FAM111A* and *FAM111B*) genes are located on the long arm (q) of chromosome 11, position q12.1. ENSEMBL genome browser (ensembl.org/index.html).

The reported *FAM111B* mutations are shown to be localised in the loop region of the catalytic domain (Goussot et al., 2017; Mercier et al., 2015; Mercier et al., 2013), except for the mutation identified in one of the French and a Kuwait patient, which is located on codon 430 (c.1289A>C) (p. Gln430Pro) upstream of the loop domain (Fig. 1.5). The mutations located in codon 621, 627 and 628 are reported to be associated with early onset POIKTMP (Goussot et al., 2017; Mercier et al., 2015; Mercier et al., 2013; Takeichi et al., 2016). However, there are also varying poikiloderma features in individuals carrying mutations in codons 621, 627 and 628. For example, some patients with c.1879A > G (p.Arg627Gly) presented with sclerosis of the digits while others with the same mutation did not (Mercier et al., 2015). A mutation in codon 628 [c.1883G > A (p.Ser628Asn)] indicated pancreatic impairment (Mercier et al., 2013) and the other [c.1884T > A (p.Ser628Arg)] was associated with pancreatic cancer (Goussot et al., 2017). Additionally, it appears that the mutations located in codons 621, 627 and 628 are associated with respiratory abnormalities (Mercier et al., 2015), except for the case reported by Goussot et al. (2017), which did not present with respiratory abnormalities, but rather with pancreatic cancer. The *FAM111B* mutation c.1289A > C (p.Gln430Pro) was reported to present with a mild form of POIKTMP as one of the cases

did not present with tendon contractures and myopathy (Takeichi et al., 2016). However, pulmonary impairment was detected in an adult (40 years old), while a 14-year old girl with the same mutation did not present with pulmonary impairment, thus suggesting that pulmonary abnormalities present at adulthood (Mercier et al., 2015; Takeichi et al., 2016). Another case of a family with an insertion/deletion (INDEL) mutation c.1261_1263del (p.Lys421del), which is located upstream of the loop region presented with pulmonary abnormalities and pancreatic exocrine dysfunction affecting persons of different age groups (Seo et al., 2016). These *FAM111B* mutations appear to cause varying severity of the disease irrespective of the location of the mutations. The genetic and molecular variation between the reported cases therefore highlight the need to understand the function of FAM111B and molecular pathogenesis of these mutations in POIKTMP.

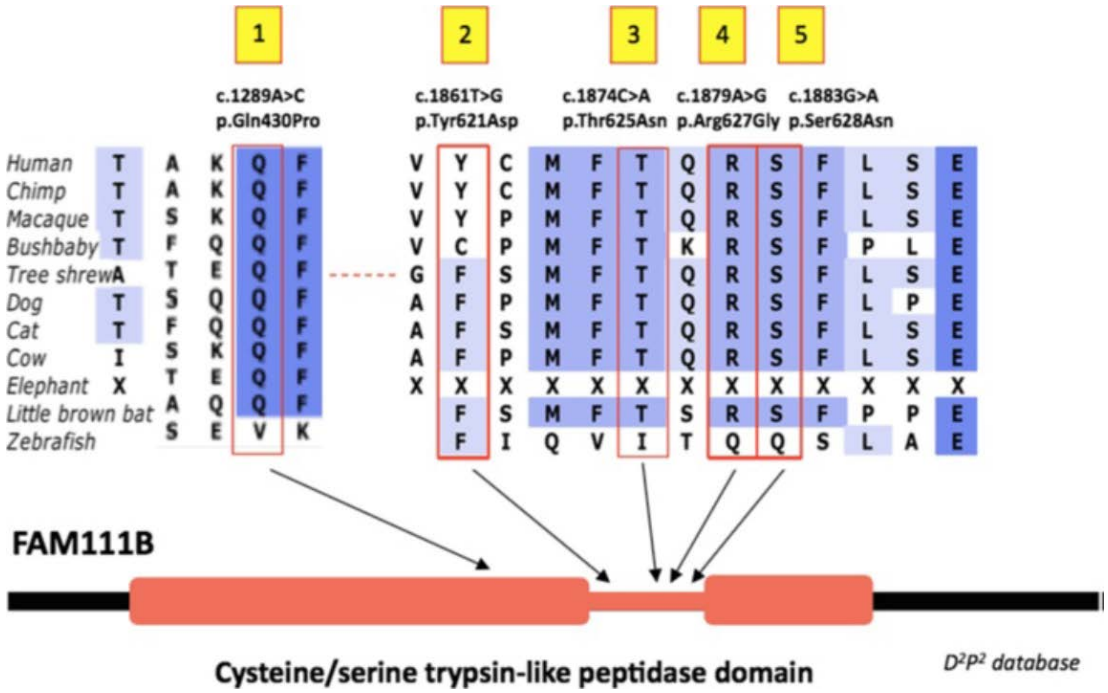

Figure 1.5: FAM111B mutations associated with POIKTMP. The diagram obtained from the database of disordered protein prediction (D^2P^2) shows amino acids changes (POIKTMP) that are conserved across primates. It also shows that mutations c.1861T > G (p.Tyr621Asp); c.1874C > A (p.Thr625Asn), c.1879A > G (p.Arg627Gly) and c.1883G > A (p.Ser628Asn) as well as c.1884T > A (p.Ser628Arg) are located in the loop region of the catalytic domain. The c.1289A > C (p.Gln430Pro) mutation is located upstream of the loop region within the catalytic domain (Mercier et al., 2015).

1.4 Functions of FAM1111A and FAM111B proteins

The microarray database (www.uniprot.org) reports FAM111A and FAM111B to be ubiquitously expressed, with FAM111B showing the highest expression in the kidneys, skeletal muscle and the skin (Mercier et al., 2013). Both proteins have trypsin-like catalytic activity and both seem to play a part in cell cycle regulation, but the link between trypsin-like domain and cell cycle regulation is unknown. The STRING network database reports FAM111B to have strong interactions with the ATP13A2 and SET proteins (http://string-db.org/cgi/network). The ATP13A2 protein, which belongs to the ATPase family is reported to be involved in regulating the transport of membrane cations as well as maintaining neuronal integrity (Ramonet et al., 2012). The SET protein is reported to link the transcription complex with chromatin during cellular replication (Fan et al., 2002). This suggests that it might play a role in the cell cycle.

Cell division is essential for embryonic development and cellular function required for events such as exercise, immune activation, wound healing and tissue repair, to mention a few. Cell cycle entry is tightly regulated by the checkpoints and key regulatory proteins which form the dimerization partner, retinoblastoma-like p130 and p107, E2F and MuvB (DREAM) complex. The DREAM complex is known to mediate repression of most of the cell cycle genes at the quiescent (G0) phase. Phosphorylation of RB-like p130 protein leads to its dissociation from E2F (E2F4 and E2F5) repressors and activation of other E2F transcription factors such E2F1 and E2F2, which promote cell cycle progression from G0 to G1/S (Sadasivam & DeCaprio, 2013); other proteins of the DREAM complex such as MuvB bind to the BMYB protein to promote expression of genes required in the G2/M phase (Fischer & Müller, 2017; Sadasivam & DeCaprio, 2013). The first phase in cell division is DNA synthesis, commonly known as the S-phase. This phase is preceded by gap-1 (G1)/restriction point, which involves the “sensing” of metabolic, stress and environmental cues that determine whether the cell undergoes division, differentiation or death (Massague, 2004). The cell cycle checkpoints are regulated by cyclin proteins and cyclin-dependent kinases (CDKs), which mediate cell cycle progression and division. The G1 phase is mediated by phosphorylation of cyclin D and cyclin E by CDK4/6 and CDK2, respectively. When cyclin D complexes with CDK4 or CDK6 it hypo-phosphorylates the retinoblastoma protein (pRB)- a tumour suppressor and potent inhibitor of G1→S transition (Bertoli et al., 2013). Hypo-phosphorylation of pRB by cyclin D-CDK4/6 complex keeps it bound to the

E2F transcription factor and prevents cell cycle progression into the S-phase. The complexing of cyclin E-CDK2 required for S-phase progression is inhibited by the CDK inhibitor (CDKI) protein p27. However, with the increase of cyclin D levels, CDK2 dissociates from p27 and binds to cyclin E, leading to hyperphosphorylation of pRB and liberation of E2F to initiate the transcription of genes required for S-phase progression (Foster et al., 2010; Massague, 2004). Mutations in the *Rb* gene have been shown in cells to escape the G1 checkpoint, which increases the risk of oncogenesis (Foster et al., 2010). Once the cell passes the G1 restriction point it commits to progress into the S-phase for DNA replication. Upon completion of chromosome replication, the cell enters the G2 phase which ensures that no replication errors are duplicated (Barnum & O'Connell, 2014). This is regulated by the p53 protein which induces cell cycle arrest and apoptosis should replication errors be detected and not corrected. Transition of the cell from G2 to M (mitosis) phase is mediated by the cyclin B-CDK1 complex (Kastan & Bartek, 2004). Cellular stress at the G2 phase, leads to inhibition of cyclin B-CDK1 interaction via p21, or inhibition of CDC25C phosphatase which also prevents CDK1 activation (Foster et al., 2010; Kastan & Bartek, 2004). At the Mitotic (M) phase the cell nucleus membrane is lost (prophase), followed by the centriole positioning forming the mitotic spindle required for chromosome metaphase plate. This step is followed by the separation of the sister chromatids to the opposite spindle poles of the cell (anaphase). Upon separation of the sister chromatids, the nucleoli and nuclear envelopes form around the daughter chromosomes followed by cytokinesis which divides the cell into two daughter cells.

There are various ways that a protein could affect the cell cycle. There is an interesting link between FAM111A and the ability of a cell to protect itself against adenovirus infection in mammalian cells by inducing host cell restriction (Fine et al., 2012). Host cell restriction is a process whereby a specific protein prevents virus binding and entry in a cell (and thereby the disruption of cell cycle machinery). Adenovirus infection requires the Simian Virus 40 (SV40) large T antigen (LT) for replication and cell transformation. The study by Fine et al. (2012) indicated that the C-terminus of the SV40 LT physically binds to FAM111A for cell cycle entry and replication in the host cell. Using human osteosarcoma epithelial cells (U-2 OS), this study further showed that the SV40 virus hijacks the restriction property of FAM111A and uses it for viral replication. Importantly, they demonstrated that only FAM111A and not FAM111B interacts with the C-terminus of the SV40 LT antigen.

Another study by Alabert et al. (2014), which aimed to understand chromatin dynamics and to identify uncharacterised DNA replication factors established that FAM111A contains a proliferating cell nuclear antigen (PCNA) interaction motif (PIP box) to which it uses to physically bind to PCNA at the early S-phase of the cell cycle. The PCNA is known an homotrimeric DNA sliding clamp protein, which encircles double-stranded DNA during replication (Dieckman et al., 2012; Moldovan et al., 2007). It also recruits and regulates other proteins such as DNA polymerase δ required for replication of the lagging strand during DNA synthesis (Moldovan et al., 2007). Its expression levels have been shown to be cell cycle dependent, peaking at the G1/S phase and low at the G0 and G2/M phase (Moldovan et al., 2007). Proteins that contain PIP motif are reported to enhance the binding affinity of PCNA to the DNA strand (Choe & Moldovan, 2017). The binding of FAM111A to the PCNA PIP box therefore suggests its involvement during DNA replication. Alabert et al. (2014) further showed that knockdown of FAM111A by siRNA delays S-phase entry in mammalian cells and inhibits cell proliferation. Furthermore, this study indicated that FAM111A localises with PCNA and that its knockdown delays progression of the cell from the G1/S to G2/M phase, thus delaying cellular replication.

Interestingly, a recent study showed that FAM111B is also involved in the cell cycle (Aviner et al., 2015). Using an integrative multi-omic study approach, Aviner et al. (2015) revealed that the FAM111B expression pattern increases at the mRNA level during the G1 phase, with protein accumulation at the S-phase in synchronised HeLa cells. This expression pattern is reported to follow similar expression to PCNA and MCM2. This link to the cell cycle will be expanded in detail in chapter 4, this leads next to the pivotal question of the relationship between cell cycle and fibrosis. In order to understand this, a detailed appreciation of fibrosis is needed.

1.5 Aetiology and pathogenesis of fibrosis

Fibrosis is the overproduction, deposition and accumulation of collagen and other extracellular matrix (ECM) proteins caused by chronic injury and aberrant tissue repair (Krieg et al., 2007; Wynn & Ramalingam, 2012). Most organ failures result from excessive scarring (fibrosis) of the tissue parenchyma which leads to cellular dysfunction and eventually death. Fibrosis is responsible for 45% of deaths in the developed world (Usunier et

al., 2014). The commonly investigated fibrotic diseases are systemic sclerosis (SSc), hepatic fibrosis, interstitial renal failure and idiopathic pulmonary fibrosis (Ley & Collard, 2013; Rockey et al., 2015). Systemic sclerosis/scleroderma (SSc) is an autoimmune disease characterised by abnormal connective tissue, autoantibody production and fibrosis of the skin and other tissues (Maurer & Distler, 2011). The cause of death in SSc patients is commonly SSc-related pulmonary fibrosis and myocardial disease (Barnes & Mayes, 2012). Idiopathic pulmonary fibrosis (IPF) is a progressive form of interstitial pneumonia with severe prognosis and poor survival rate of 3-5 years from the time of diagnosis (Caminati et al., 2015). The pathogenesis is poorly understood but is associated with genetic and environmental risk factors (Denham & Hauer-Jensen, 2002; Wynn, 2011). Since fibrosis is an irreversible disorder, current treatments aim to prevent disease progression and prolong survival (Bonella et al., 2015).

The patients with POIKTMP develop systemic fibrosis primarily in the skin, lungs and display fibrosis-associated myopathy (Goussot et al., 2017; Khumalo et al., 2006; Mercier et al., 2015; Mercier et al., 2013; Takeichi et al., 2016). While it was initially thought that the skin fibrosis in POIKTMP patients was similar to that of SSc patients, the dermal features were however distinct as the dermis of POIKTMP patients show elastic globes caused by elastin degeneration, as well as sclerosis of the digits. The SSc patients do not show elastin degeneration but present with thickening of the hypodermis and anti-mononuclear antibodies, features that are absent in POIKTMP patients (Khumalo et al., 2006; Shi-Wen et al., 1997). This section will therefore focus on collagen synthesis and regulation in skin, muscle and lungs to understand wound healing and onset of fibrosis in these tissues that are affected in POIKTMP patients.

1.5.1 The role of the ECM in wound healing

The connective tissue which is composed of the extracellular matrix and fibroblasts, provides the microenvironment with structural support and cellular network responsible for cell adhesion (Parker et al., 2014). During inflammation the activated inflammatory cells (e.g. eosinophils, basophils, mast cells & macrophages) are recruited to the site of injury to prevent infection. The release of cytokines, chemokines and growth factors from inflammatory cells stimulates activity effector cells, which include resident fibroblasts, pericytes, fibrocytes and

mesenchymal cells. The effector cells are known to be key players in scar formation as well as fibrosis. Following the inflammatory phase, resident fibroblasts proliferate and secrete matrix metalloproteinases (MMPs) for resorption of the old ECM and deposition of new collagen and ECM (see review by (Diegelmann & Evans, 2004)).

A key feature of wound healing and tissue remodelling is the activation of quiescent fibroblasts which are trans-differentiated into contractile myofibroblasts that express high levels of alpha-smooth muscle actin (α-SMA), type I and III collagen as well as other ECM proteins such as fibronectin, elastin and integrins (Barrientos et al., 2008). Normal wound healing is therefore tightly regulated by homeostasis of collagen deposition and degradation (summary in Fig. 1.6).

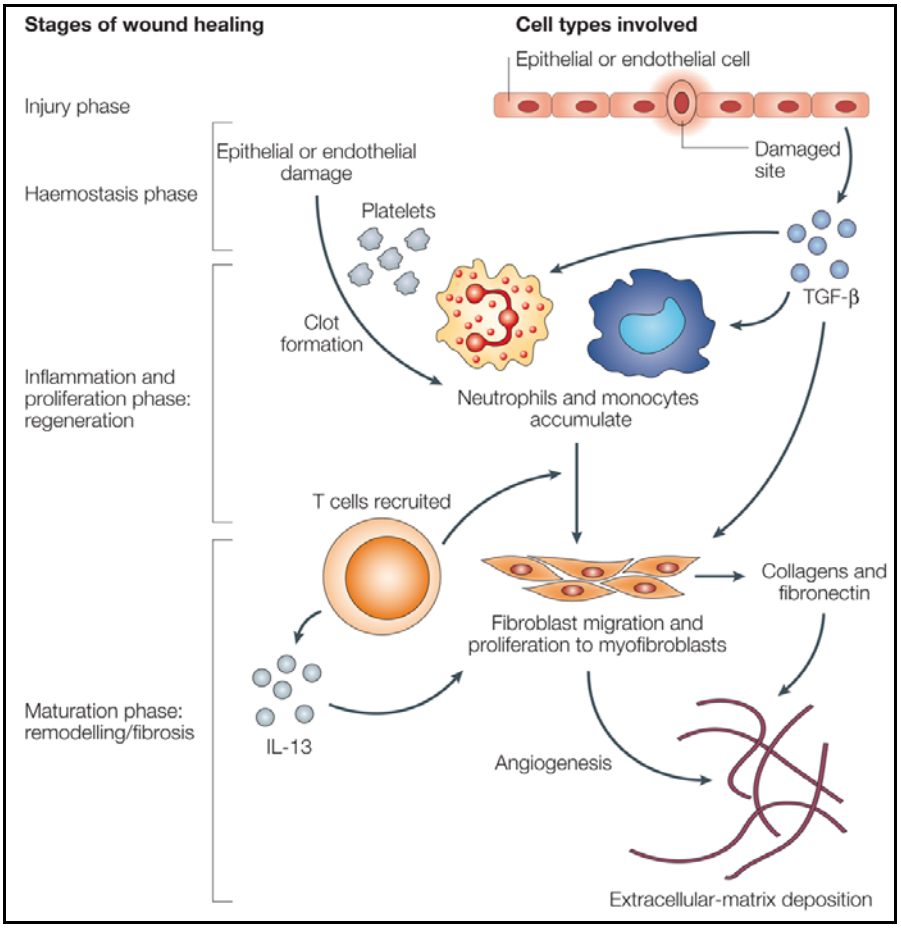

Figure 1.6: Normal wound healing. During injury the damaged cells release chemokines and cytokines which activate and recruit platelets and other inflammatory cells to site of injury (haemostasis phase). The recruited inflammatory cells (inflammatory phase) also release cytokines (e.g. TGF-β and IL-13) which in turn activate fibroblasts to proliferate and differentiate into myofibroblasts for production of collagen, ECM and MMPs for tissue repair/remodelling (maturation/remodelling phase). Dysregulation of tissue remodelling leads to fibrosis (image illustrated by (Wynn, 2004).

1.5.2 Collagen synthesis and turnover

Changes in the homeostasis of ECM production, particularly during wound healing leads to fibrosis, resulting in overproduction and accumulation of type I and III collagen. Therefore, understanding the molecular mechanism of collagen synthesis and regulation provides insight into the pathology and approaches that can be used for treatment.

Collagen constitutes over 30% of the body's total protein and is essential in human physiology as it is involved in structural integrity of tissues (Hulmes, 2002; Minor, 1980). The collagen molecule is a triple-helix with a Gly-X-Y motif, where the X is mostly proline and Y is often hydroxyproline (Jinnin, 2010; Viguet-Carrin et al., 2006). The transcribed collagen mRNA (procollagen) interacts with ribosomes to form procollagen polypeptide chains which are imported into the lumen of the rough endoplasmic reticulum for translation and post-translational modification initiated by the hydroxylation of proline and lysine residues by prolyly-3-hydroxylase, prolyly-4-hydroxylase and lysyl hydroxylase respectively (Trackman, 2005). Hydroxylation of proline and lysine residues initiates the cross-linking and stable conformation of procollagen chains into triple helices which cannot be hydroxylated once formed. Procollagen chains are then chaperoned to the Golgi apparatus by the heat shock protein 47 (HSP47) for packaging of procollagen into secretory vesicles and exported to the extracellular space for further modification (Sluijter et al., 2004; Trackman, 2005). In the extracellular space the non-helical pro-peptides are cleaved at the N- and C-termini by procollagen proteinases. Cleavage of the N- and C-termini leads to the soluble collagen becoming insoluble to form collagen fibrils. The final step is the crosslinking of the collagen fibrils through a catalytic reaction by the lysyl oxidase (LOX) enzyme (Trackman, 2005; Viguet-Carrin et al., 2006) (See Fig. 1.7).

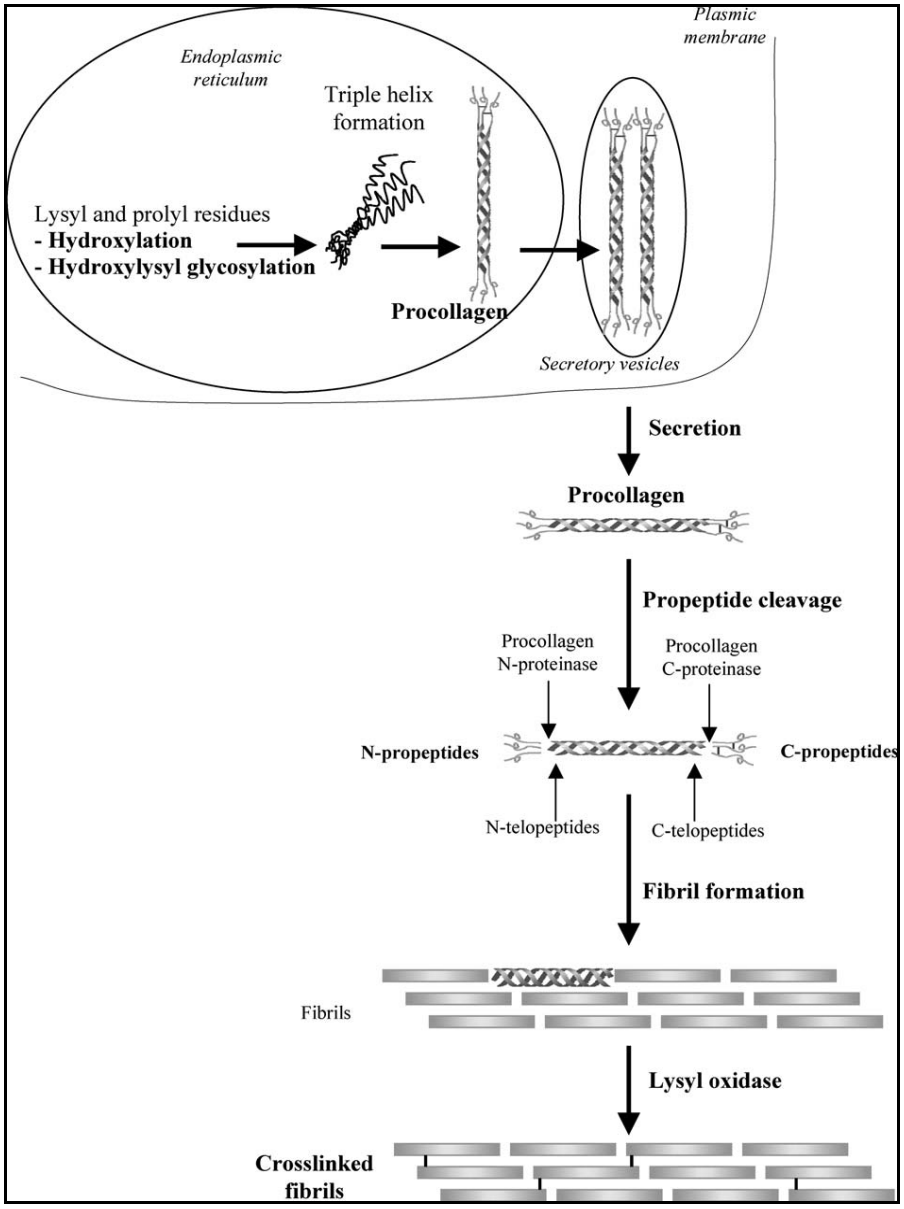

Figure 1.7: Collagen synthesis. A shematic diagram showing the steps and enzymes involved in collagen synthesis. Illustration by (Viguet-Carrin et al., 2006).

Collagen turnover in the ECM is regulated by matrix metalloproteinase proteins (MMPs) that have a catalytic domain with zinc binding motif that binds to three histidines for collagen degradation, and a C-terminus that has the hemopexin domain required for cleavage of helical interstitial collagens (Marion & Mao, 2006; Nagase & Woessner, 1999). The MMPs are classified into collagenases (MMP-1, -8 and -13) which breakdown collagen type I, II, and III; gelatinase (MMP-2 and -9) and membrane-type MMP (MMP 14-16), to mention a few. The secretion of MMP collagenase by fibroblasts results in their binding to collagen to

unwind the collagen triple helix, and the single collagen strands are further degraded by gelatinase (MMP-2 & MMP-9) as well as serine proteinases such as cathepsin K (Lauer-Fields et al., 2009; Laurent, 1987; McKleroy et al., 2013; Nagase & Woessner, 1999). The MMP activity is regulated by tissue inhibitors of metalloproteinases (TIMPs), which are known to be involved in development and tissue remodelling as well as preventing tumour cell invasion (Nagase & Woessner, 1999). There are four known TIMP isoforms (TIMP 1-4) whose N- and C-termini contain cysteine residues that form disulphide bonds for interaction with the hemopexin domain of MMPs required for downregulating MMP activity (Arpino et al., 2015; Baker et al., 2002).

1.5.3 Activation of fibroblasts and transcriptional regulation of collagen synthesis

Chemokines, growth factors and cytokines such as interferon-gamma (IFN-γ), interleukin-6 (IL-6), platelet-derived growth factor (PDGF), connective tissue growth factor (CTGF) and transforming growth factors (TGFs) are known to mediate activation and regulation of collagen synthesis (Krieg et al., 2007; Narayanan et al., 1989). The TGF-β cytokine is a master regulator of this process (Gelse et al., 2003). It is primarily secreted by fibroblasts and macrophages during this process (Desmouliere et al., 1993; Leask & Abraham, 2004). There are three known protein isoforms of TGF-β, namely TGF-β1, TGF-β2 and TGF-β3. The TGF-β1 isoform has a higher binding affinity to their receptors (TGF-βRI and TGF-βRII), and is the major isoform regulating collagen synthesis (Biernacka et al., 2011; Cheifetz et al., 1990). It is synthesised and secreted into the ECM in its inactive form (latent precursor TGF-β). Protease-dependent activation is required Through protease-dependent conformational modification of LAP, the LAP-bound TGF-β is released into its active form. Phosphorylation of TGFβRI receptor activates phosphorylation of SMAD (R-SMAD2 and R-SMAD3) proteins. Upon phosphorylation the R-SMAD2 or R-SMAD3 form a hetero-trimer complex with SMAD4 which translocate to the nucleus to initiate transcription of target genes such as type I, III and V collagen, α-SMA and other ECM genes (Diegelmann & Evans, 2004; Hall et al., 2003). In addition, the TGF-β pathway is regulated by activation of SMAD7 which inhibits the formation of SMAD2/3-SMAD4 complex thereby downregulating expression of collagen and other ECM proteins under normal conditions (Nagase & Woessner, 1999).

1.5.4 Abnormal wound healing and fibrosis

Chronic inflammation and aberrant tissue repair/remodelling are the common causes for the imbalance between synthesis and degradation of collagen and other ECM components, which alters the architecture of the stroma resulting in compromised function of the affected tissues (Wynn, 2007). Chronic inflammation is due to a persistent immune response which maintains the activation of inflammatory cells such as neutrophils, mononuclear cells and macrophages, which secrete cytokines and growth factors such as TGF-β that stimulate the trans-differentiation of resident fibroblasts into myofibroblasts as well as expression of pro-fibrotic genes (Borthwick et al., 2013; Wynn, 2008). The secretion of cytokines such as interleukin-4 (IL-4) and IL-13 have been shown to also play key roles in fibrosis (Borthwick et al., 2013). Interestingly, both IL-4 and IL-13 have been reported to have similar functionality and share common receptors for activation and differentiation of stromal fibroblasts and circulating fibrocytes into myofibroblasts (Coward et al., 2010; Desmouliere et al., 1993; Wynn, 2008).

Macrophages have further been shown to be extensively involved in fibrogenesis due to their plasticity (Laskin et al., 2011). The plasticity produces two subpopulations that have been shown to be active during wound healing; the classic M1 subpopulation is activated by proinflammatory cytokines such as tumour necrosis factor-α (TNF-α) and IFN-γ which induce an immune response during wound healing. The alternative M2 subpopulation acts to downregulate inflammation, thus inducing tissue repair and remodelling by releasing anti-inflammatory cytokines such as IL-4, IL-10 and IL-13 as well as activating TGF-β expression (Laskin et al., 2011; Novak & Koh, 2013). Moreover, studies have reported M2 to interact with mesenchymal stem/stromal cells for immune modulation, myofibroblast formation and recruitment of pericytes during tissue repair. However, it has been suggested that in aberrant tissue repair the MSC-macrophage interaction may lead to fibrosis and maintain the hyperactivity of M2 macrophages which contributes to the fibrotic state in affected tissues (Chung & Son, 2014).

The activation of resident fibroblasts and circulating fibrocytes by growth factors such as TGF-β and CTGF not only leads to their trans-differentiation but also induces increased proliferation of these effector cells (Yang et al., 2015). It been indicated that in conditions such as IPF that IPF-derived fibroblasts increase their proliferation by overriding the negative

feedback that is mediated by the phosphatase and tensin homolog (PTEN)-a tumour suppressor protein that is involved in cell cycle regulation (Xia et al., 2008). Increased proliferation of fibroblasts and other effector cells during fibrosis is also reported to be caused by modulation of the TGF-β as well as the Wnt/β-catenin signalling pathways which will be discussed in section 1.5.6 below. Furthermore, proliferation of these cells during fibrosis has been shown to be due to altered cell cycle progression. For instance, aberrant induction of integrin proteins activates signalling of Rho kinase pathways which increases expression of cell cycle genes such as cyclin D1 (Moreno-Layseca & Streuli, 2014; Watts et al., 2006). Due to its importance in fibrosis and in POIKTMP, cell proliferation will be discussed extensively in chapter 4.

1.5.5 Origin of myofibroblasts involved in wound healing and fibrosis

Resident fibroblasts in the injured tissue are the primary source of myofibroblast cells as shown in a study by(Gabbiani et al., 1972) using male wistar rats to study the ultrastructure of fibroblasts during wound healing. The key feature of myofibroblasts is their high expression of α-SMA which provides myofibroblasts their contractile property during tissue repair (Darby et al., 1990; Masur et al., 1996). They also produce high levels of type I and III collagen and other ECM proteins for wound repair (Ansorge et al., 2017; Hinz, 2007). Treatment of corneal or dermal fibroblasts with TGF-β *in vitro* showed formation of myofibroblasts as they were larger than fibroblasts, have a well-developed rough endoplasmic reticulum and can revert into fibroblasts upon cell-to-cell contact (Masur et al., 1996). In normal wound healing, quiescent fibroblasts are activated for differentiation into myofibroblasts by TGF-β, CTGF and other cytokines; and upon scar formation they are removed either by reverting into fibroblasts or phagocytosed by macrophages. However, in chronic inflammation or chronic injury fibroblasts continuously maintain their myofibroblast state thus resulting in increased collagen and ECM production which causes fibrosis (Desmouliere et al., 1993).

It has been shown that myofibroblasts can also be derived from other cell sources of mesenchymal origin (Wynn, 2008). These include perivascular mesenchymal cells and fibrocytes from the bone marrow which serve as myofibroblast progenitors, and have also been suggested to contribute to liver cirrhosis in post-hepatic transplants due to excessive

scar formation (Forbes et al., 2004; Gabbiani, 2003). In other tissues such as the liver, it has been reported that activation of hepatic stellate cells by TGF-β1 and other cytokines also leads to their differentiation into myofibroblasts, which further contributes to liver fibrosis in aberrant tissue repair (Berardis et al., 2015). In skeletal muscle, mesenchymal progenitor cells known as fibro/adipogenic progenitors localised in the intermuscular region and express PDGF receptor-α (PDGFRα), have been shown to contribute to muscle fibrosis by differentiating into fibrofatty tissue (Uezumi et al., 2014; Uezumi et al., 2011). Interstitial cells in the lung septa have also been reported to differentiate into myofibroblasts during lung injury and can persist in chronic inflammation (Desmouliere et al., 1993).

Other sources of myofibroblasts have been suggested to be derived from resident endothelial and epithelial cells that undergo a reversible process known as endothelial-to-mesenchymal transition (EndMT) and/or epithelial-to-mesenchymal transition (EMT) respectively (Fig. 1.8) (Kalluri & Neilson, 2003; Willis et al., 2006; Zeisberg et al., 2007). Zeisberg et al. (2007) for example, showed that endothelial cells stimulated by TGF-β undergo EndMT during cardiac fibrosis for production of the ECM and collagen. Chronic injury in the lungs has also been shown to induce metaplasia of type II alveolar epithelial cells (AECs) into myofibroblasts, thus activating the EMT process in a TGF-β-dependent manner (Coward et al., 2010). The EMT has also been reported in kidney injury, where tubular epithelial cells differentiate into α-MSA-positive myofibroblast-like cells during tissue repair (Berardis et al., 2015; Strutz & Zeisberg, 2006). The differentiation of these cells into myofibroblasts also contributes to fibrosis in chronic wound healing in different tissues. Therefore, targeting of these cells to prevent myofibroblast formation could delay or prevent fibrosis progression.

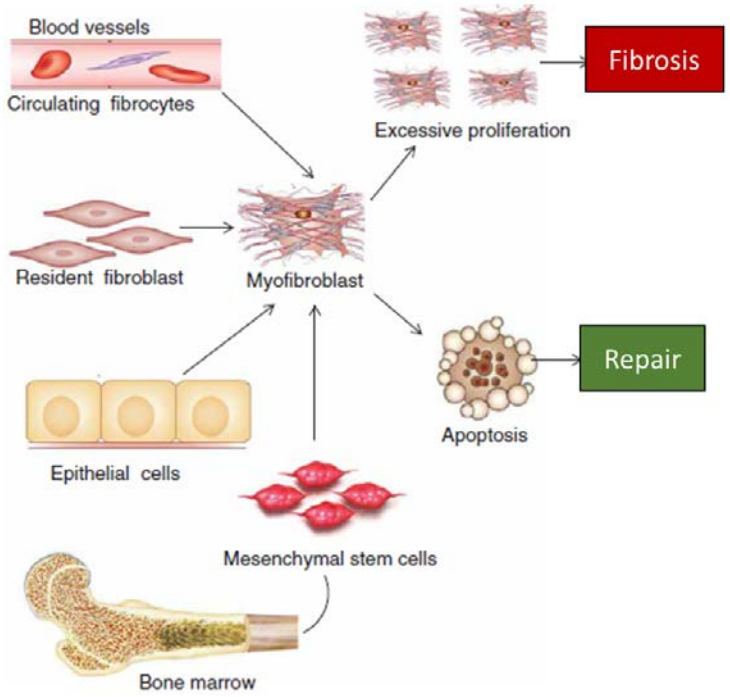

Figure 1.8: Origin of myofibroblasts. Besides resident fibroblasts that form myofibroblasts, circulating fibrocytes and bone marrow-derived mesenchymal stem cells are also recruited and activated, commonly by TGF-β, to form myofibroblasts. Epithelial cells undergo EMT process to form myofibroblasts during wound healing. After normal wound healing the myofibroblasts either revert to their original cell type or undergo apoptosis or phagocytosis. In abnormal wound healing however, there is excessive proliferation of myofibroblasts which increase ECM and collagen production leading to fibrosis. Diagram modified from (Chakraborty et al., 2014).

1.5.6 Molecular pathways involved in fibrosis

The common pathway in fibrogenesis in many affected tissues occurs via the canonical TGF-β1 pathway as TGF-β is a potent profibrotic factor (Pohlers et al., 2009; Rockey et al., 2015; Wynn & Ramalingam, 2012). The constitutive secretion of TGF-β1 by fibroblasts and macrophages in chronic injury activates the SMAD2/3 and SMAD4 complex, which translocate to the nucleus to induce expression of collagen type I, type III and other ECM components (Borthwick et al., 2013; Pohlers et al., 2009). In systemic sclerosis (SSc), collagen I (COL1A1; COL1A2) levels have been shown to be elevated in dermal fibroblasts of SSc patients following analysis of collagen mRNA and quantification of soluble collagen protein (LeRoy, 1974; Shi-Wen et al., 1997). In lung fibrosis, activation of TGF-β1 is shown to promote apoptosis of epithelial cells as well as EMT resulting in the formation of myofibroblasts (Borthwick et al., 2013; Guarino et al., 2009; Iwano et al., 2002). In aberrant

skeletal muscle repair, TGF-β1 inhibits proliferation and differentiation of myoblasts and satellite cells into myotubes by altering the expression of myogenic proteins such as desmin, MyoD and myogenin. Instead, it promotes their differentiation into myofibroblasts (Garg et al., 2015; Li et al., 2004; Mann et al., 2011). Other cytokines such as CTGF and PDGF have also been shown to act in concert with TGF-β1, further augmenting its activity (Leask & Abraham, 2004).

Signalling pathways that act in a TGF-β-dependent and independent manner have also been reported to play a role in fibrogenesis. Additional pathways involved in fibrogenesis are the Wnt/β-catenin and Hedgehog pathways (Rosenbloom et al., 2013). Both pathways have been shown to be activated in lung, kidney, skin and muscle fibrosis (Akhmetshina et al., 2012; Clevers & Nusse, 2012; Ding et al., 2012; Nusse, 2005; Stewart et al., 2003). Both Wnt/β-catenin and Hedgehog pathways are well characterised in embryonic development as they play a role in cell proliferation, body axis formation, stem cell maintenance and cell-fate determination (Cerdan & Bhatia, 2010; Ding et al., 2012; Ribes & Briscoe, 2009; van Amerongen & Nusse, 2009). The canonical Wnt/β-catenin pathway is activated by the binding of the Wnt ligands to the Frizzled transmembrane receptor and low-density lipoprotein receptor-related protein 5/6 (LRP5/6) complex, which activates the complexing of Disheveled (Dvl), Axin-2 and Adenomatosis Polyposis Coli (APC) proteins. This complex leads to the dephosphorylation and accumulation of β-catenin in the cytoplasm and eventual translocation into the nucleus where it binds to the T-cell factor/lymphoid enhancer-factor (TCF/LEF) for transcriptional activation of target genes (van Amerongen & Nusse, 2009). Inhibition of the Wnt/β-catenin pathway is mediated by binding of the Dickkopf-1 (Dkk-1) ligand on the LRP5/6 receptor which stimulates the formation of Dvl, axin, APC and glycogen synthase kinase-3β (GSK-3β) complex. This complex phosphorylates β-catenin thus leading to its degradation via ubiquitination (Nusse, 2005; van Amerongen & Nusse, 2009). The involvement of the Wnt/β-catenin signalling in fibrosis has been primarily shown by the accumulation of β-catenin in the nucleus (Akhmetshina et al., 2012; Carthy et al., 2011; Chilosi et al., 2003). In human or animal studies where fibroblast cells were treated with Wnt-1, Wnt-3a or Wnt-10b there was an observed elevation of pro-fibrotic proteins such as type I collagen, α-SMA and MMP-7 (Carthy et al., 2011; Chilosi et al., 2003; Lam & Gottardi, 2011a). It was also reported that Wnt/β-catenin signalling induces the EMT process for myofibroblasts formation further inducing fibrosis (Gonzalez & Medici, 2014).

Furthermore, it was shown that aberrant Wnt/β-catenin signalling results in 60-80% downregulation of Dkk-1 in fibrotic diseases such as SSc, lung and liver fibrosis (Akhmetshina et al., 2012). Moreover, there is lack of Dkk-1 compensation by other Dkk proteins such as Dkk-2, which was observed in mice treated with a neutralising antibody against Dkk-1 (Akhmetshina et al., 2012). Furthermore, Akhmetshina et al. (2012) showed that TGF-β activates Wnt/β-catenin signalling via the p38 pathway by decreasing the expression of Dkk-1 in cultured human fibroblasts. Other studies have also shown that Wnt/β-catenin signalling can be activated via the canonical TGF-β pathway through phosphorylation of SMAD2/3 (Carthy et al., 2011; Lam & Gottardi, 2011b). These studies therefore suggest that the Wnt/β-catenin signalling can be activated in a TGF-β-dependent and independent manner, thereby contributing to fibrosis progression.

Though Sonic Hedgehog (SHH) signalling is active during embryonic development, it is reported to be deactivated in healthy adults, but is activated during wound healing and tissue repair, as well as in fibrosis (Ding et al., 2012; Jia et al., 2017). The canonical SHH pathway involves binding of the SHH ligand to the Patched-1 (Ptch-1) transmembrane receptor which induces the de-repression of the Smoothened (Smo) protein that when repressed is localised in intracellular endosomes. The de-repressed Smo protein activates the Gli-1 transcription factor which translocates to the nucleus for expression of its target genes. It was shown that SHH secretion in kidney fibrosis is very high thus resulting in increased α-SMA, type I collagen and high induction of EMT in tubular epithelial cells, while in a knockout model reverses the fibrotic phenotype (Ding et al., 2012).

1.6 Disease models for fibrosis

1.6.1 In vivo fibrosis models

In vitro and *in vivo* models have been developed to study the complexity of fibrosis and the pathways involved therein. Various animal models have been developed to identify specific mediators and molecular pathways that drive fibrogenesis. The various mouse models that have been developed for studying skin fibrosis include bleomycin-induced fibrosis, the tight-skin (*Tsk* mutant), Graft-vs-Host Disease (GvHD) and the TGFβRI/II (Cre-Lox) mouse model (Aso et al., 1976; Denton et al., 2007; Do & Eming, 2016; Green et al.,

1976; Ruzek et al., 2004; Smith & Chan, 2010; Yamamoto et al., 1999). Bleomycin, an anti-cancer reagent was previously used to block the progression of cancerous cells to the G2 phase of the cell cycle by causing DNA double strand breaks. The side effects of the treatment however, included scleroderma accompanied by lung fibrosis in humans (Aso et al., 1999). Bleomycin treatment in mouse skin induces scleroderma at the treated site when injected subcutaneously daily for four weeks, and causes an inflammatory response by infiltration of mononuclear cells in skin lesions as well as thickening of the dermis (Yamamoto et al., 1999). Furthermore, it was shown to cause fibroblast trans-differentiation into myofibroblasts leading to increased collagen synthesis and production of anti-mononuclear antibodies, which mimicked the scleroderma phenotype observed in humans. This model has been shown to be effective at identifying the pro-fibrotic mediators which can be targets for anti-fibrotic drug treatment. However, the challenge of this model is that the skin lesions and thickened dermis are localised at the injected site while the clinical features observed in SSc patients are diffused (Do & Eming, 2016). Also, the scleroderma phenotype in mouse models is strain-dependent, with the C57/BL6 strain being susceptible to bleomycin treatment and the BALB/C strain being resistant (Moore et al., 2013; Beyer et al., 2010; Harrison & Lazo, 1988). The BALB/C strain is indicated to be resistant to bleomycin injection due to the suppressor T-cells it produces in the spleen that prevent a fibrotic response (Schrier & Phan, 1984).

The *Tsk*-1 (mutant) model, first discovered in the Jackson laboratory, is a mouse carrying a spontaneous autosomal dominant mutation in the *Fibrillin* gene (Green et al., 1976). The *Tsk-1* mice develop tight-skin two weeks postnatal, and present with hyperplasia of the loose connective tissue, bone and cartilage, which are some of the features observed in skin fibrosis. Moreover, the *Tsk-1* mouse fibroblasts produce high levels of type I and III collagen (Beyer et al., 2010). It was also reported that other growth factors such as CTGF and Wnt3a levels are increased in this model (Green et al., 1976). However, the limitation of the *Tsk-1* model is that it does not induce an inflammatory response, which is one of the primary features of scleroderma (Green et al., 1976).

The *Tsk-2* (mutant) model was observed in the offspring of the 101/H mouse strain treated with the mutagenic ethylnitrosourea (ENU), which caused an autosomal dominant mutation in the alpha-1 propeptide chain of type III collagen (Beyer et al., 2010; Christner et al., 1995; Denton et al., 2007). In contrast to the *Tsk-1* model, the *Tsk-2* mice produce anti-

mononuclear antibodies and display inflammatory cell infiltration in the affected tissue, which is lacking in the *Tsk-1* model. However, the *Tsk-2* model is less well characterised than the *Tsk-1* model. Furthermore, both mouse models display thickening of the hypodermis but incompletely recapitulate the phenotype observed in SSc humans (Baxter et al., 2005; Beyer et al., 2010).

Although the pathogenesis of pulmonary fibrosis is poorly understood, the animal model that is widely used and well established for this disease is the bleomycin model (Aso et al., 1976). It is not known how bleomycin specifically induces lung fibrosis, but its systemic administration in mice causes destruction of the pulmonary vascular endothelium and alveolar epithelial cells by breaking down the basement membrane. This therefore leads to an inflammatory response, proliferation and differentiation of resident epithelial and fibroblast cells (Moore et al., 2013; Coward et al., 2010). Due to the hyperplasia of alveolar epithelial cells (AECs) and metaplasia of the squamous cell, the integrity of the basement membrane remains disrupted further increasing the infiltration of myofibroblasts and collagen deposition in the stroma. Bleomycin has therefore been used to study the pro-fibrotic pathways and cell-to-cell interaction for drug targets (Moore et al., 2013).

1.6.2 In vitro fibrosis models

In vitro fibrosis models that are well established are those where fibroblasts are constitutively treated with TGF-β or CTGF to mimic their trans-differentiation into myofibroblasts and overproduction of collagen as well as other ECM proteins (Desmouliere et al., 1993). Some *in vitro* SSc studies have shown that fibroblasts obtained from SSc patients maintain their myofibroblast phenotype and express high levels of type I collagen without TGF-β induction (LeRoy, 1974). Two-dimensional (2D) co-culture systems have also been used to determine the effect of cell signalling and cell-to-cell interaction during fibrosis. For example, Holt et al. (2010) performed a fibroblast-macrophage co-culture to determine the effect of cell signalling via the paracrine (non-contact) effect using macrophage- or fibroblast-conditioned medium and by juxtacrine (co-culture) mechanism. They observed that fibroblasts cultured in macrophage-conditioned medium increased the production of pro-inflammatory cytokines such as IL-6, while macrophages maintained in fibroblast-conditioned medium produced reduced levels of pro-inflammatory cytokines. This

study therefore indicated the role of paracrine and juxtracrine mechanisms that influence changes in cellular activity and response during the inflammatory and remodelling phases of wound healing. While *in vitro* monocellular or co-culture systems have yielded invaluable knowledge in understanding some the mechanisms involved in fibrosis, their limitation involves the inability to create a cell culture model where most, if not all the cell types involved in fibrosis are included. This is also due to the complexity of mimicking the *in vivo* microenvironment *in vitro*. For example, macrophages have been shown to undergo alternative activation to secrete anti-inflammatory cytokines such as IL-10 and TGF-β, induced by autocrine effect and/or by secretion of IL-4 or IL-6 by epithelial or endothelial cells (Ayaub et al., 2017; Laskin et al., 2011). Alternatively-activated macrophages (M2) together with endo/epithelial cells further induce fibroblast proliferation and trans-differentiation into myofibroblasts, which further drives overproduction of collagen and other ECM proteins that are involved in fibrosis. Also, it is difficult to determine the positive or negative feedback signals of such systems in 2D *in vitro* cell culture. Furthermore, exogenously activated cells can induce an attenuated response *in vitro*, which does not adequately mimic the effects observed *in vivo* (Holt et al., 2010). Furthermore, fibrosis is a progressive condition and its effects manifest over a long period, therefore, to circumvent some of these limitations better *in vitro* models need to be further developed.

Three-dimensional (3D) culture systems have since been established and demonstrate great promise in mimicking the *in vivo* fibrosis milieu. The 3D culture system uses collagen gels or hydrogels to construct matrix scaffolds which can be used to study cell migration, invasion, remodelling and cell-to-cell interaction as well as signalling (Smithmyer et al., 2014; van Spreeuwel et al., 2017). Furthermore, the 3D matrix composition can be adjusted to mimic the matrix stiffness observed in fibrosis, thus making it possible to study changes in cellular response in such conditions. For instance, hydrogels have been used to mimic the ECM and induce a fibrotic state in cardiac fibrosis studies where the stiffness of the matrix determined differentiation of fibroblasts into myofibroblasts, thus mimicking key fibrotic processes that occur *in vivo* (Smithmyer et al., 2014; Zhao et al., 2014). 3D culture systems hold great promise in further understanding the involvement of specific cell types in fibrosis as well as using them as screening potentials for anti-fibrotic drugs. Moreover, with increasing application of pluripotent or multipotent stem cells, there is a greater avenue for developing better *in vitro* disease models.

1.7 Using stem cells for disease-modelling

Stem cells have been used for decades to study and understand animal and human development as well as genetic disorders. They have also been used where animal models failed to recapitulate the phenotypes observed in specific human diseases (Avior et al., 2016). Stem cells have been advantageously used *in vitro* because of their capacity to self-renew and differentiate into different cell lineages (Lewandowski et al., 2017). Totipotent stem cells have an infinite spectrum of differentiation and can form both the embryo and placenta. Pluripotent stem cells have the capacity to self-renew and differentiate into the three embryonic germ layers. Multipotent stem cells have a limited capacity to self-renew and differentiate into other cell lineages (Lewandowski et al., 2017). Stem cells can be derived from adult tissues such as the bone marrow, blood, skin, muscle and liver (Boisset & Robin, 2012). Adult stem cells, which are primarily active during wound healing and tissue remodelling are multipotent and therefore have a limited capacity to self-renew and differentiate into various cell lineages (Blanpain et al., 2004; Seaberg & van der Kooy, 2003). They are most commonly found in a specific microenvironment or niche as stem cell precursors; for example, satellite cells found in skeletal muscle are localised in the sublaminar regions, stellate cells are localised between hepatic lobules, and haematopoietic stem cells are found in the bone marrow (Blanpain et al., 2004; Lewandowski et al., 2017). Due to their limited number and capacity to self-renew, especially *in vitro*, it is challenging to use adult stem cells for therapeutic applications (Blanpain et al., 2004; Potten & Loeffler, 1990).

Pluripotent stem cells are therefore an excellent source to study embryonic development, various diseases as well as the development of regenerative medicine due to their limitless self-renewal as well as the potential to differentiate into the three germ layers (Lewandowski et al., 2017; Thomson et al., 1998; Xu et al., 2015). Embryonic stem cells (ESCs) which were first derived by Thomson et al. (1998) from the inner cell mass of a 5-day old blastocyst fertilised *in vitro* are pluripotent cells and have been used to further study embryonic development, human diseases as well as the development of potential cell therapies and drug discovery (Avior et al., 2016; Merkle & Eggan, 2013; Stadtfeld & Hochedlinger, 2010). Embryonic stem cells have also been derived by the somatic cell nuclear transfer (SCNT) method, where a somatic cell nucleus is transferred into an enucleated oocyte (Gurdon, 1962; Wilmut et al., 1997) to create ESC-like cells by the

electrical impulses and extraction and culture of the inner cell mass (Wilmut et al., 1997). This method has been successful in animal models but not in human cells due to challenges such as abnormal gene expression, incomplete reprogramming and dysregulation of epigenetics during "reprogramming" (Lewandowski et al., 2017; Stadtfeld & Hochedlinger, 2010; Tachibana et al., 2013; Wakayama & Yanagimachi, 1999). Other challenges in using ESCs or SCNT-derived ESCs include lack of cell therapy development due to immunogenic response. Furthermore, SCNT-derived ESCs are less viable in culture and only contain two types of DNA, the mitochondrial DNA from the egg donor and separate DNA from the somatic nuclear donor (Lewandowski et al., 2017). Moreover, there are ethical concerns with the use of ESCs or SCNT-derived ESCs. Embryonic stem cells are derived from spare embryos fertilised through IVF and/or aborted foetuses. The ethical debate thus includes the argument that the inner cell mass used to derive ESCs is obtained from a viable embryo and that once extracted it is a non-viable embryo (de Wert & Mummery, 2003). The SCNT-derived ESCs are derived from donated oocytes which has been met with social resistance as well as unclear boundaries on reproduction and cell therapy (Lewandowski et al., 2017).

The derivation of induced pluripotent stem cells (iPSCs) from animal and human somatic cells such as dermal fibroblasts, a technique pioneered by Yamanaka and colleagues (Takahashi, 2007; Takahashi & Yamanaka, 2006) has overcome mainly the ethical challenges of using pluripotent stem cells for drug discovery, regenerative medicine and potential cell therapies (de Wert & Mummery, 2003; Stadtfeld & Hochedlinger, 2010). This technology further advanced development of patient-specific pluripotent stem cells to study rare diseases as well as creating cell-based disease models that be studied in vitro. Moreover, this technology has made possible the elimination of immunogenic responses for future cell transplantations in patient-specific treatments.

1.7.1 iPSC-derived disease models

Due to the limitation of animal models to faithfully recapitulate the phenotype of many human disease conditions, establishing a culture system using human cells to mimic the microenvironment and cellular interactions will advance future work of drug screening and clinical trials (Guo et al., 2013). However, the use of primary somatic cells limits long-term *in vitro* experiments required for disease modelling as primary cells have limited proliferation

capacity (Trounson & DeWitt, 2016). Therefore, using iPSCs firstly, eliminates this limitation by providing an endless source of cells, which further reduces the need for tissue biopsies that are obtained by a painful and invasive procedure. Secondly, iPSCs can be differentiated into the different lineages, thus providing the ability to create improved disease models *in vitro*. And thirdly, iPSCs provide the means of personalised medicine and future autologous cell therapies. Recent studies have demonstrated that iPSCs can be differentiated into neuronal progenitors, cardiomyocytes and pancreatic islet-like cells (Arber et al., 2015; Kunisada et al., 2012; Oh et al., 2012). Recent studies have demonstrated that using iPSCs to model diseases such as Parkinson's disease, Alzheimer's and Huntington's diseases (HD) has opened avenues to understanding the molecular events involved in the onset of these diseases (Arber et al., 2015; Hossini et al., 2015; Ryan et al., 2013; Yang et al., 2016; Zhang et al., 2016). For example, the iPSCs derived from a patient with Parkinson's disease caused by an autosomal dominant mutation in the *LRRK2* gene were differentiated into dopaminergic precursors and demonstrated that the mutation leads to increased oxidative stress causing degeneration of dopaminergic neurons (Nguyen et al., 2011). Furthermore, iPSCs can be used to study cardiomyopathies such as arrhythmogenic right ventricular cardiomyopathy (ARVC) and long-QT syndrome (Kim et al., 2013; Ma et al., 2013; Miller et al., 2013; Moretti et al., 2013). A study by Kim et al. (2013) for example, showed that iPSCs derived from fibroblasts of patients affected with ARVC caused mutations in the *PKP-2* gene can be differentiated into cardiomyocytes. They further showed that the iPSC-derived cardiomyocytes can recapitulate the disease phenotype by inducing dysregulated lipogenesis and abnormal PKP-2 translocation into the nucleus.

1.7.2 Using iPSC-derived models to study fibrosis

Studies have shown that iPSC can be differentiated into different cell types to perform *in vitro* studies. There are emerging studies that have explored modelling of renal, cardiac and skin fibrosis using iPSC models. For instance, a study by Itoh et al. (2013) successfully differentiated iPSCs into keratinocytes and fibroblasts, which produce COL7A1 to study recessive dystrophic epidermolysis bullosa (RDEB), a genetic disorder caused by mutations in the *COL7A1* gene which encodes a protein that anchors the fibrils on the basement membrane zone. This study further created a 3D culture model by layering iPSC-derived

keratinocytes onto iPSC-derived fibroblasts polymerised in collagen type1 matrix to mimic the skin layer. The 3D model by Itoh et al. (2013) thereby indicates the potential of iPSCs to create models that can be used and improved to model skin fibrosis. Furthermore, patient-specific iPSCs can be used in rare genetic disorders such as POIKTMP to determine some of the molecular changes that may contribute to the phenotype observed in affected individuals. Another study showed that iPSC-derived alveolar epithelial cells (type II), which are activated to form myofibroblasts during pulmonary fibrosis can be used for future therapeutic interventions such as cell replacement therapy to treat cystic fibrosis as well as pulmonary fibrosis (Ghaedi et al., 2013; Snoeck, 2015).

In addition, the recent emergence of iPSC-derived organoids has made it possible to study organ development as well as disease pathologies. For example, (Przepiorski et al., 2018) generated kidney organoids which developed tubular epithelia after 14 days in culture and revealed that at 26 days of culture the kidney organoids showed increased ECM production and high levels of α-SMA which are features of fibrosis. Another recent study created cardiac spheroids using iPSC-derived cardiomyocytes, fibroblasts and endothelial cells in order to study the physiology and microenvironment of these cells in cardiac tissue (Polonchuk et al., 2017).

The present study focuses on the development of an *in vitro* system to investigate the link between mutations in the *FAM111B* gene and the fibrotic phenotype seen in POIKTMP patients. In particular, the rationale in this study is that in order to investigate the cells that might be playing a role in fibrosis, one needs large numbers of such cells, an ability to drive them along a particular line of differentiation, and in so doing, investigate basic cellular processes by comparing normal cells versus patient-derived cells.

1.8 Aims and Objectives

1.8.1 Aim

To evaluate the role of FAM111B in multi-systemic fibrosis, we asked whether the creation of iPSCs might enable us to model some components of the phenotype, and in doing so, contribute to the understanding of the causes of hereditary fibrosing poikiloderma.

1.8.2 Objectives

The overall objectives of this study are to:

i. derive patient-specific iPSCs containing the *FAM111B* mutation (c.1861T>G) (p. Tyr621Asp).
ii. differentiate the iPSCs into mesenchymal stem/stromal cells to investigate if the pro-fibrotic markers are elevated in patients compared to controls.
iii. determine if FAM111B expression is altered in patient cells compared to controls
iv. determine if cell proliferation and the cell cycle are dysregulated in some way in patient-derived cells compared to controls.

Chapter 2

Derivation and characterisation of patient-specific induced pluripotent stem cells (iPSCs)

2.1 Introduction

It has been a decade since the pioneering of induced pluripotent stem cells by the Yamanaka group. Yamanaka and colleagues (Takahashi, 2007; Takahashi & Yamanaka, 2006) observed that a combination of *OCT3/4*, *SOX2*, *KLF-4* and *C-MYC* (*OSKM*) transcription factors from a panel of 24 candidate genes activated the reprogramming of mouse and human fibroblasts into iPSCs with ESC-like phenotype. Of the four transcription factors selected for reprogramming, octomer-binding protein 3/4 (OCT 3/4) was previously shown to be the master regulator of pluripotency, self-renewal and regulates other key pluripotency-associated genes such as *NANOG* in embryonic stem cells (ESCs) (Loh et al., 2006; Mitsui et al., 2003; Saxe et al., 2009; Takahashi & Yamanaka, 2006). Similarly, the SOX2 transcription factor is also reported to regulate the expression of other pluripotency-associated genes (Okumura-Nakanishi et al., 2005; Schmidt & Plath, 2012). Furthermore, both OCT 3/4 and SOX 2 also act as autoregulators of their respective genes by a positive feedback loop (Schmidt & Plath, 2012). The Kruppel-like factor 4 (KLF-4), also a transcription factor, was first demonstrated to actively bind to *nanog* in mouse ESCs to maintain pluripotency and self-renewal as well as preventing ESC differentiation (Chan et al., 2009; Zhang et al., 2010). The *C-MYC* oncogene is known to promote cell proliferation and survival. Furthermore, it has been reported that *C-MYC* promotes opening of chromatin into an active state during cell reprogramming (Nie et al., 2012; Rahl et al., 2010; Schmidt & Plath, 2012). However, the use of factors such as *C-MYC*, which is a well-known oncogene poses a challenge in that its proliferative property can also induce oncogenesis, thus limiting the future potential of iPSCs (Nie et al., 2012; Takahashi & Yamanaka, 2006). To circumvent this limitation, other studies have since shown that substitution of factors such as *C-MYC* and *KLF-4* with *NANOG*, *LIN28* and oestrogen-related receptor-β (ESRRβ) can induce stem cell reprogramming (Feng et al., 2009; Yu, 2007). Furthermore, studies have demonstrated that other MYC proteins such as L-MYC and N-MYC can perform similar function as C-MYC, with L-MYC indicating minimal oncogenic activity (Nakagawa et al., 2008). *C-MYC* has also

been suggested to be responsible for induction of partially reprogrammed cells which do not fully express endogenous stem cell genes due to its high activity during the early stages of reprogramming (Wernig et al., 2008). Therefore, its substitution reduces the yield of partially reprogrammed cells thus increasing reprogramming efficiency. Reprogramming enhancers such as Gli-like transcription factor (GliS1) have also been suggested as effective substitutes of *C-MYC* for increasing reprogramming efficiency and reducing partial reprogramming (Ebrahimi, 2015; Schmidt & Plath, 2012; Seki & Fukuda, 2015). Like MYC, other KLF proteins such as KLF-2 and KLF-5 can be used to substitute KLF-4 as they have also been shown to activate expression and activity of *NANOG* (Zhang et al., 2010).

It has become evident in recent years that there is an order to the reprogramming process (Polo et al., 2012). A few models were hypothesised to explain the reprogramming process; the first model was thought to be the "Elite" model which suggested that some of the somatic cells that undergo complete reprogramming are stem cell progenitors which can be more readily reprogrammed into iPSCs compared to terminally differentiated somatic cells (Smith et al., 2016). This theory, however, was disproved when terminally differentiated T and B lymphocytes were successfully reprogrammed into iPSCs, thus indicating that any cell type can be reprogrammed into iPSCs (Hanna et al., 2008; Stadtfeld et al., 2008; Takahashi & Yamanaka, 2016). The second hypothesised model was the "Deterministic" model in which it was hypothesised that every cell that is exposed to the overexpression of ectopic pluripotency transcription factors will be reprogrammed in a fixed and synchronised manner. However, due to the findings of partial reprogramming this hypothesis was modified to describe a "Stochastic" model, which states that all somatic cells have the potential to become iPSCs at different time points of reprogramming (Polo et al., 2012; Yamanaka, 2009). The stochastic model further proposes that cell reprogramming is a two-stage process which begins with cell proliferation followed by gene activation due to the epigenetics events that occur during reprogramming (Polo et al., 2012; Zunder et al., 2015). The cellular changes that have been shown to occur during the proliferative stage of reprogramming include mesenchymal-to-epithelial cell (MET) transition that is characterised by expression of E-cadherin which is an epithelial marker, and by the metabolic switch from the oxidative to the glycolytic pathway. The late phase is the epigenetic modification phase which is characterised by demethylation of stem cell genes (Kim et al., 2014; Maherali et al., 2007; Pasque et al., 2014; Polo et al., 2012).

Epigenetic modifications are reported to be the driving force to cellular and molecular changes that somatic cells undergo in the stochastic model (Yamanaka, 2009; Zhang et al., 2012). Cell reprogramming from mature lineage-specific somatic cells to pluripotent cells requires chromatin conformation from heterochromatin to euchromatin for the ectopic reprogramming factors to access DNA regions that have been inactivated. Conformation of chromatin from heterochromatin to euchromatin requires the acetylation and/or methylation of histones at specific sites (Gładych et al., 2015; Maherali et al., 2007). Acetylation of histones occurs when acetyl groups are bound to the lysine groups at the N-terminus of histone tails, a process facilitated by histone acetyltransferases (HATs), resulting in a negative histone charge that leads to conformational changes and active chromatin (Gładych et al., 2015; Handy et al., 2011; Srinageshwar et al., 2016). Histone methylation at specific sites has also been shown to change the chromatin state to euchromatin. The commonly reported methylated sites in a heterochromatin state are H3K4me3 and H3K27me3, but the ectopic expression of *OSKM* factors initiates trimethylation of lysine 9 and 36 in histone H3 (H3K9me3 and H3K36me3) regions leading to gene activation (Buganim et al., 2013; Srinageshwar et al., 2016). Overexpression of ectopic OCT3/4 and SOX2 during reprogramming appears to similarly induce DNA demethylation at *OCT3/4* and *NANOG* promoter regions. Kruppel-like factor-4 (*KLF4*) and *C-MYC* have also been shown to induce histone acetylation and methylation for accessibility of the *OCT3/4* and *NANOG* promoter regions (Evans et al., 2007; Lunyak & Rosenfeld, 2008). The early phase of reprogramming which is characterised by the MET transformation occurs following binding of ectopic factors to the promoter regions of their target pluripotency genes, followed by the late phase where the expression of endogenous stem cell genes leads to the complete reprogramming of cells that pass the partially reprogrammed state (Buganim et al., 2012).

Another key epigenetic modification which is observed in reprogrammed female somatic cells is the reactivation of inactive X-chromosome (Xi) (Kim et al., 2015). As mammalian females have two X chromosomes, their somatic cells undergo random inactivation of the second X-chromosome for dosage compensation, which maintains normal genomic copy number between male and female cells (Barakat et al., 2015; Ercan, 2015). This process is regulated by the expression of a long non-coding RNA known as x-inactive specific transcript (*Xist*) for heterochromatin formation (Cantone et al., 2016; Kim et al., 2015; Panning et al., 1997). The *Xist* RNA transcript induces silencing of the second X-

chromosome by creating a nuclear compartment that is devoid of RNA polymerase II, which leads to the recruitment of the Polycomb Recessive Complex 2 (PRC2) that induces the trimethylation of lysine 27 on histone H3 (H3K27me3) as well as 5-methyl-cytosine incorporation on the *Xi* gene for stable silencing (Cantone et al., 2016). During somatic cell reprogramming however, the Xi chromosome is reactivated by downregulation of *Xist* RNA as well as the removal of heterochromatin marks by downregulation of PRC2 (H3K27me3 and DNA methylation) (Pasque et al., 2014). This process has been shown to occur at the late phase of reprogramming where *Xist* RNA is downregulated by the activation of its anti-sense strand which encodes *Tsix* RNA on the Xi domain. Furthermore, X-chromosome reactivation (XCR) occurs post-endogenous expression of *OCT4*, which has been shown to actively bind onto *Tsix* RNA (Donohoe et al., 2009; Maherali et al., 2007; Pasque et al., 2014). Interestingly, XCR has revealed more insight into the epigenetic modifications that occur during reprogramming and made possible detailed tracking of reprogramming stages thus expanding the understanding of cell reprograming (Pasque et al., 2014).

2.1.1. Gene-delivery system for reprogramming

The transduction of fibroblasts into iPSCs was first performed with the use of integrating retroviral plasmids (Nishimura et al., 2011; Takahashi & Yamanaka, 2006; Takahashi & Yamanaka, 2016) due to their high infection efficiency. Since the first demonstration that iPSC generation was possible, subsequent work in this field focused on improving the reprogramming method for clinical application. One of the primary issues with the original iPSC reprogramming method was the use of retroviral vectors, which are genome-integrating vectors and randomly integrate into the host genome (Han & Yoon, 2011). Therefore, the use of retroviral vectors for derivation of human iPSCs for translational purposes posed a risk of retroviral integration into the host genome, which may cause insertional mutagenesis that can lead to tumorigenicity (Higuchi et al., 2014; Kagawa et al., 2009). Scientific advances have since been applied to circumvent this challenge and generate human iPSCs using non-integrating vectors. One of the early strategies applied was replacing retroviral vectors with lentivirus vectors as they do not integrate near the host genome transcription sites (Han & Yoon, 2011; Wu et al., 2003). Lentivirus vectors were replaced by adenoviruses which do not integrate into the host cell genome. However, transient

transfections with the adenovirus greatly reduces reprogramming efficiency (Yu et al., 2011). Other non-integrating vectors such as cosmids, Sendai virus, RNA molecules, transposons, small and large protein molecules as well as episomal vectors have been investigated and showed promise compared to previous systems (Chou et al., 2011; Fusaki et al., 2009b; Malik & Rao, 2013; Stadtfeld & Hochedlinger, 2010). The use of RNA molecules and other molecules such as episomes, are promising non-integrating viral approaches for delivery of pluripotency transgenes. For example, Yu et al. (2011) demonstrated that cells can be reprogrammed with episomal vectors that do not require transgene packaging or repeated transfections and are easily silenced due to their low copy number once transfected into somatic cells. However, they demonstrated that episomal vectors yielded very low reprogramming efficiency, and reprogramming enhancers were required to increase efficiency. Similarly, cosmid plasmids and synthetic modified mRNA molecules demonstrated low reprogramming efficiency and required repeated cycles of infection (Higuchi et al., 2014). While these methods show promise in developing clinical-grade iPSCs, more improvements are required to ensure efficient gene packaging, stable transfection with reduced cellular stress as well as improved reprogramming efficiency. Some studies have suggested that the use micro-RNA 302 (miRNA-302), which endogenously increases OCT4 expression by targeting its inhibitors such as the Nuclear receptor subfamily 2, group F, member two (NR2F2) in ESC and iPSCs, can enhance reprogramming efficiency when used in combination with these non-integrating vectors (Hu et al., 2013). Valproic acid has also been identified to be one of the reprogramming enhancers which can increase reprogramming efficiency. It is a histone deacetylase (HDAC) inhibitor commonly used to treat epilepsy, bipolar mania and migraine prophylaxis which has been shown to promote global increase of H3K9 acetylation in ESCs (Hezroni et al., 2011). Furthermore, it has been shown to prevent senescence and promote cell proliferation of reprogrammed cells (Chen et al., 2016; Huangfu et al., 2008). The p53 tumour suppressor protein or its suppression pathway has also been reported to improve reprogramming efficiency (Menendez et al., 2010). Studies have indicated that ectopic expression of *C-MYC* and *KLF-4* activates p53 due to high expression of the CDK inhibitor p21 which halts cell cycle progression (Kawamura et al., 2009; Li et al., 2013). Therefore, knockdown of p53 increases induction of iPSCs, however, knockdown of p53 causes genomic instability therefore, other studies have suggested that targeting the p53-upregulated mediator of apoptosis (PUMA) protein which is

part of the p53 suppressor pathway can improve iPSC reprogramming without inducing genomic instability (Li et al., 2013).

To date the most promising vector which is used by most researchers in iPSC-based and drug discovery studies is the Sendai virus (Beers et al., 2015; Fusaki et al., 2009b). The Sendai virus (SeV) belongs to the *Paramyxoviridae* family of viruses and is non-pathogenic to humans (Nishimura et al., 2011). It is a negative-strand RNA virus that replicates in the cytoplasm and does not integrate with the host genome (Li et al., 2000; MacArthur et al., 2012; Nishimura et al., 2011). Nishimura et al. (2017) demonstrated that stable transfection for reprogramming can be generated with the Sendai virus, moreover, they also demonstrated that the coding region of the SeV Cl. 151 strain can be replaced with all four pluripotency transgenes (*Oct4; Sox2; Klf4; c-myc*) and the viral persistence can be eliminated with siRNA. Furthermore, Nakanishi & Otsu (Nakanishi & Otsu, 2012) demonstrated that the replication-defective and persistent Sendai virus (SeVdp) can be silenced by using siRNA and endogenous miRNA (mir-302a) that is expressed by human and mouse ESCs and established iPSCs (Nishimura et al., 2017; Nishimura et al., 2011). Nishimura et al. (2011) demonstrated that the L gene effectively silenced the SeVdp vector after treatment with small interfering mRNA (siRNA). The mechanism by which it is silenced, briefly, is by targeting RNA-dependent RNA polymerase L subunit which contains miRNA-302a sequence at the 3' UTR (Nishimura et al., 2017).The mir-302a target sequences were added to the non-coding region of the L gene to silence the SeVdp vector when pluripotent stem cells have been established (Nakanishi & Otsu, 2012). The expression of mir-302a occurs once the iPSCs have been fully established, therefore, removal of SeVdp genome can be analysed between 10-19 passages in newly derived iPSCs (Miller et al., 2013; Nishimura et al., 2017). Therefore, the SeVdp is an ideal vector for iPSC reprogramming to advance iPSC research studies for future clinical applications.

2.1.2. Feeder and feeder-free culture of iPSCs

Embryonic stem cells (ESCs) and iPSCs have been demonstrated to maintain pluripotency and self-renewal when cultured on inactivated mouse embryonic fibroblasts and human foreskin fibroblasts (Pekkanen-Mattila et al., 2012; Richards et al., 2002; Takahashi & Yamanaka, 2006; Thomson et al., 1998). Mouse and human Feeder cells are known secrete

high levels of activin-A and basic fibroblast growth factor respectively (bFGF) (Warren et al., 2012). Mouse embryonic fibroblasts (MEFs) are most commonly used for culture and maintenance of iPSC pluripotency as they are more accessible compared to human cells. However, the disadvantage of using MEFs is xeno-contamination with animal genome and exogenous antigens which can contaminate human iPSCs thus limiting their future clinical use (Chou et al., 2011; MacArthur et al., 2012). Human feeder cells such as foreskin fibroblasts and epithelial cells have recently been used to replace MEFs, but the contamination of differentiated cells on pluripotent stem cells further indicate a barrier for obtaining clinical-grade iPSCs (Pekkanen-Mattila et al., 2012). Therefore, several studies have tested and shown that human somatic cells can be reprogrammed under feeder-free conditions using extracellular matrix substrates such as collagen type I, gelatin, fibronectin and vitronectin (Yamasaki et al., 2014). Mouse ESCs were shown to grow efficiently on gelatin and collagen matrices. Furthermore, human ESCs and iPSCs were demonstrated to maintain their pluripotency on matrix substrates such as fibronectin and vitronectin (Yamasaki et al., 2014). Feeder-free reprogramming was shown to further require specific matrix substrates and growth factors. For example, a study by Yamasaki et al. (2014) demonstrated that iPSCs can be derived and maintained in an undifferentiated state on fibronectin-coated dishes using serum-free hESC medium that is supplemented with TGF-β1. However, they indicated that TGF-β1 induces pluripotency in the early stages of reprogramming and inhibits the emergence of iPSCs colonies when maintained in the late stages of reprogramming.

Since the breakthrough of iPSC technology, studies have focused on circumventing challenges that hinder the production of clinical grade iPSCs for regenerative medicine and cell therapy. Recent advances in producing clinical-grade iPSCs include the use of non-integrating vectors such as the Sendai virus and episomal vectors for delivery of reprogramming factors (Wang et al., 2015). There is also use of the two-factor system (OCT4 and SOX2) and enhancers to eliminate the use of oncogenes such as *C-MYC* and *KLF-4* to improve reprogramming efficiency (Baghbaderani et al., 2015; Wang et al., 2015). Other studies have also indicated the development of xeno-free reagents to avoid contamination of reprogrammed cells (Wang et al., 2015). However, more approaches are required for robust induction of clinical-grade iPSCs which can also be used to develop *in vitro* disease models for translational studies.

2.1.3 Using induced pluripotent stem cells to study FAM111B in vitro

The dawn of iPSC technology has broadened the scope of studying genetic and sporadic diseases beyond the use of animal models, which often do not faithfully recapitulate the disease phenotype. Diseases mechanisms can be studied and further understood by modelling them *in vitro* using iPSCs (Grskovic et al., 2011). Furthermore, their pluripotent state makes them an ideal cell type to use for studying disease conditions that affect more than one organ in the body as they can be differentiated into different cell lineages *in vitro* (Takahashi, 2007).

Since hereditary fibrosing poikiloderma is a rare autosomal dominant genetic disorder with no animal model available to study the function of FAM111B and disease phenotype *in vivo*, the chosen approach for elucidating the role of *FAM111B* mutation in this study was the use of iPSCs to model the disease phenotype. This chapter will focus on the derivation and characterisation of control and patient-specific iPSCs. I will also discuss the challenges experienced during the generation and characterisation of iPSCs. The next chapter will focus on the differentiation of the patient-specific iPSCs into the affected cell lines in this condition.

2.2 Materials & methods

2.2.1 Ethics Approval

Ethics approval for the study was granted by the University of Cape Town (UCT) Faculty of Health Sciences Human Research Ethics Committee (REC Ref. 492/2007) and was renewed in accordance with REC rules. Informed consents were obtained from the South African Kindred, two affected siblings (brother and sister) and their unaffected mother as shown by the pedigree in Figure 2.1 (Khumalo et al., 2006) to obtain skin biopsies for extraction of dermal fibroblasts.

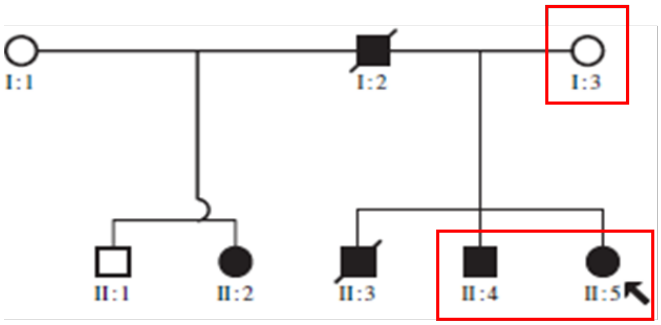

Figure 2.1: Pedigree of South African kindred. The boxed figures indicate individuals from whom informed consents were obtained for this study. The proband is indicated by the arrow.

2.2.2 Cell culture

Skin biopsies were collected from the two affected South African siblings carrying the *FAM111B* gene mutation (c. 1861 T>G) and from their unaffected mother, who was the familial control for this study. Fibroblasts were previously isolated from the dermal explants according to the protocol described by Normand & Karasek (1995). Fibroblasts for the non-familial control were kindly donated by Dr. Robea Ballo (Department of Human Biology, University of Cape town). The dermal fibroblasts were expanded in Dulbecco's Modified Eagle's medium (DMEM (Sigma-Aldrich, St Louis, MO); 10% (v/v) supplemented with heat-inactivated foetal bovine serum (FBS) (Biochrom, Merck-Millipore, Germany) and penicillin (100 U/ml) & streptomycin (100 µg/ml) antibiotic (hereafter 1% Pen-strep) (Sigma-Aldrich, St Louis, MO). The cells were placed in a 37 °C incubator at 5% carbon

dioxide (CO_2) during culture. The cells were maintained in growth medium which was changed every 2-3 days until the cells reached 95% confluence. Mouse embryonic fibroblasts (MEFs) purchased from ATCC (Virginia, USA) were mitotically-inactivated by treatment with Mitomycin-c at passage 6. Following inactivation, the iMEFs were cultured in DMEM supplemented with 10% FBS, 1% (v/v) Pen-strep and 0.05 mM β-mercaptoethanol and used as feeder cells for reprogramming of dermal fibroblasts into iPSCs. Induced pluripotent stem cells (iPSCs) were derived and maintained in human stem cell (hESC) medium that is composed of knockout DMEM (KO-DMEM) supplemented with 20% (v/v) Knockout Serum Replacement (KO-SR), 1% (v/v) non-essential amino acids (NEAA), 1% (v/v) GlutaMax solution, 10 ng/ml basic Fibroblast Growth Factor (bFGF) (Miltenyi Biotec) and 0.05 mM β-mercaptoethanol (all hESC components were purchased from Life Technologies).

2.2.3 Reprogramming of dermal fibroblasts

2.2.3.1 Infection of dermal fibroblasts with SeVdp

Control and patient dermal fibroblasts (P6) were seeded 2 x 10^5 cells per well in a 6-well culture plate overnight in DMEM medium supplemented with 10% (v/v) FBS. The replication-defective and persistent Sendai virus (SeVdp) vector, which simultaneously delivers the four pluripotency factors (*OCT4*; *SOX2*; *KLF4*; *C-MYC*) for reprogramming was kindly provided by Nakanishi (Research Centre for Stem Cell Engineering, National Institute of Advanced Industrial Science and Technology, Tokyo, Japan). When the cells reached 80-90% confluence they were infected with the SeVdp vector at a MOI of 3, per the protocol previously described by Fusaki et al. (2009a) and Nishimura et al. (2011). Briefly, the infected cells were incubated at room temperature for 2 hours (h) before incubating overnight in a 37° C & 5% CO_2 incubator. On the same day, 0.3 x 10^6 iMEFs were seeded onto gelatine-coated wells (35-mm) of a 6-well plate and incubated in 37 °C with 5% CO_2 overnight and thereafter rinsed with twice with 1X phosphate buffered saline (PBS) and maintained in hESC medium. Following overnight incubation, the infected dermal fibroblasts were rinsed twice with 1x PBS and incubated for five minutes with 0.25% trypsin/EDTA at 37° C. The trypsin/EDTA was deactivated by adding growth medium and the cells were centrifuged for five minutes at 450 x g at room temperature. Following centrifugation, the supernatant was removed, and the cell pellet resuspended in 1 ml of growth medium and

counted. The SeVdp-infected dermal fibroblasts were seeded at 1 x 10^4 and 2 x 10^4 cells/ml densities onto the previously prepared ATCC iMEFs and maintained in hESC medium. The hESC medium was changed every 2nd day until the iMEFs were nine days old. After nine days, the SeVdp-infected dermal fibroblasts were maintained in iMEF-conditioned conditioned medium (MCM) till iPSC colonies appeared on the iMEF feeder layer. The MCM was prepared by culturing 4 x 10^6 iMEF cells in a T75 cell-culture flask, maintaining them in hESC medium without bFGF and collecting the medium daily till the iMEFs were nine days old. The MCM was filter-sterilised and supplemented with 10 ng/ml bFGF before adding to the cells undergoing iPSC reprogramming. Figure 2.2 shows the reprogramming timeline used in this study.

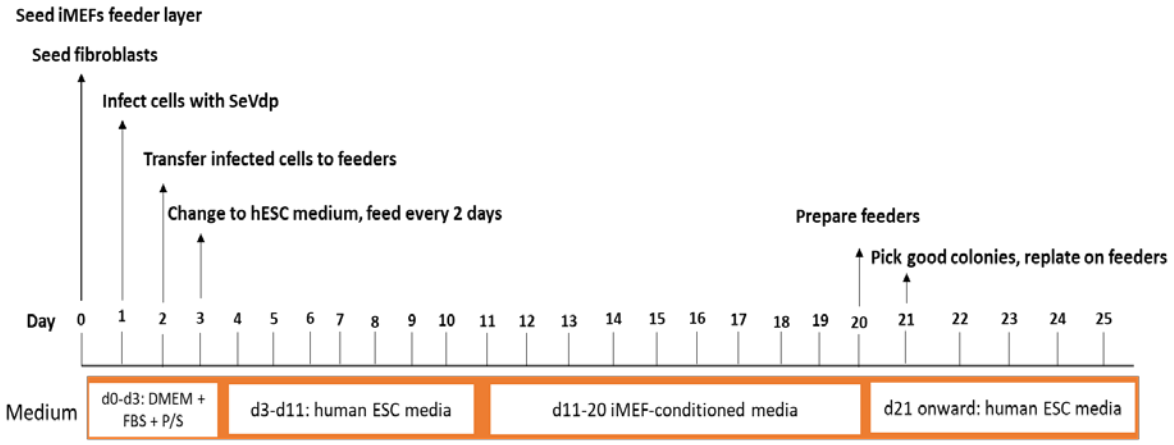

Figure 2.2: iPSC Reprogramming timeline. Mitomycin-inactivated MEFs (iMEFs) were cultured on the same day as patient and control fibroblasts (d0). Fibroblasts were infected with SeVdp vector on day 1 and transferred onto iMEF feeder layer after 24 hours. Between d0 and d3 cells were maintained in DMEM supplement with 10% FBS and 1% Pen-strep. On d2 infected fibroblasts were transferred onto the iMEF feeder layer and maintained in hESC media from d3-d11 for iPSC reprogramming. Reprogrammed cells were thereafter maintained on iMEF-conditioned medium until iPSC clones were picked for expansion.

2.2.3.2 picking and expansion of reprogrammed iPSC clones

After 4-5 weeks, the reprogrammed cells that successfully formed embryonic stem cell-like colonies (see results) were isolated and cultured onto different wells of a 6-well plate that contained with fresh iMEF feeder cells and expanded for characterisation. Each colony that was picked and transferred into a separate well is referred to as a clone. A minimum of

five clones per cell line were picked and expanded or frozen in liquid nitrogen for later use. For expansion, the newly derived iPSCs were cultured on iMEF feeder cells and maintained in hESC medium, with a daily 50% medium change till the cells were ready for manual passaging. The iPSC colonies were passaged every 4-6 days by manual passaging using a sterile 29-gauge syringe needle. The iPSC colonies were dissected to 8-12 patches that were then transferred onto a 35-mm well of a 6-well plate that contained newly seeded iMEFs and maintained in hESC medium until the next passage.

2.2.3.3 Feeder-free iPSC culture

The iPSCs were cultured using a feeder-free method to remove contamination of iMEFs prior to characterisation and further analysis. Briefly, 35 mm or 6-well culture plates were coated with Geltrex (Life Technologies), a basement membrane matrix by incubation at 37° C for 1 h and a further hour at room temperature before use. The iPSC colonies on iMEF feeder cells were aspirated of hESC medium, washed once with 1x PBS and enzymatically passaged with 0.5 mM EDTA (Life Technologies) in 1x PBS by incubation at 37° C for five minutes. Thereafter, the EDTA solution was gently removed using a pipette. The iPSCs were transferred onto a Geltrex-coated 35 mm dish or well that contained feeder-free culture medium prepared in DMEM/F12 supplemented with StemPro hESC supplement, 8 ng/mL bFGF, 25% bovine serum albumin (BSA) and 0.1 mM β-mercapto-ethanol (all feeder-free components were purchased from Life Technologies). The iPSCs were EDTA-passaged every 3-4 days and split in a 1:3 ratio until next passage. To prevent dissociation-induced apoptosis, which occurs when ESCs or iPSC colonies are dissociated into single cells (Watanabe et al., 2007), 10 µM of Rho-associated protein kinase (ROCK) inhibitor (Y-27632) (Sigma-Aldrich, St Louis, MO) was added to the culture dish and incubated overnight at 37° C and 5% CO_2. Feeder-free medium was changed daily, and the cells were passaged every 3-4 days. Furthermore, the iPSCs were maintained in feeder-free culture for 3-10 passages for gene expression assays and further analysis.

2.2.4 Characterisation of derived iPSCs

Two iPSCs clones per cell line from the two patients and one familial control were characterised for pluripotency by firstly determining the expression of stem cell genes (i.e. *OCT4; NANOG, SOX2; KLF4*); secondly, for the potential to differentiate into the three germ layers (endoderm; mesoderm; ectoderm) by *in vitro* differentiation; and thirdly, for normal karyotyping following reprogramming. The iPSCs were characterised between passages eight and 12 (after SeVdp vector was silenced) by quantitative polymerase chain reaction (qPCR) and immunocytochemistry (ICC). The silenced SeVdp in the reprogrammed iPSCs was validated qPCR. A population control iPSC line (Non-familial control), which was used as a positive control for the newly derived iPSCs was previously characterised in our lab by Dr. Robea Ballo.

2.2.4.1 Expression of pluripotency markers in derived iPSCs

2.2.4.1.1 RNA extraction and cDNA synthesis

To determine the pluripotency of derived iPSCs by qPCR the cells were cultured under feeder-free conditions as previously described and lysed for RNA extraction by adding 1 ml Tripure Isolation Reagent (Roche) per 60 mm dish. Total RNA isolation was extracted using the High Pure RNA Isolation Kit (Roche) per the manufacturer's instructions. Briefly, 0.2 ml of 100% chloroform was added to every 1 ml of the cell lysates, vigorously mixed by inverting for 15 seconds (s) and incubated at room temperature for 15 minutes. The lysates were thereafter centrifuged at 4° C and 12 000 x *g* for 15 minutes. After centrifugation, the aqueous phase which contained RNA was transferred into new microfuge tube and equal volume of 70% ethanol was added to aqueous phase and mixed 10 times by pipetting up and down. The aqueous mixture was then transferred into a High Pure filter tube and 2 ml collection tube and thereafter centrifuged at 10 000 rpm for one minute. The flow-through was discarded and each sample was treated with 100 µl of DNase I for removal of genomic DNA contamination and incubated at room temperature for 15 minutes. Following DNase I treatment, the samples were washed by adding 500 µl of Wash Buffer I and centrifuged at 10 000 rpm for one minutes. The flow-through was discarded and the samples were washed again with 200 µl of Wash Buffer I and centrifuged as before. Following washes with Buffer

I the samples were washed by adding 500 µl of Wash Buffer II and centrifuged at 10 000 rpm for one minute. The flow-through was discarded and washed again with 200 µl of Wash Buffer II and thereafter centrifuged at 13 000 rpm for two minutes. The flow-through was discarded and the samples were opened and incubated at room temperature for five minutes to allow evaporation of ethanol from the wash buffers. After five minutes incubation, 30-50 µl of the Elution buffer were added to each sample and total RNA was measured using a nanodrop spectrophotometer (ND-1000, Thermo Fisher). RNA purity was measured at A260/A280 ratio. To determine RNA integrity one µg RNA was run on a non-denaturing 1% agarose gel containing ethidium bromide and electrophoresed at 100 volts (V) for 45 minutes. The gel was viewed under UV light for detection of 28S and 18S ribosomal RNA bands.

For cDNA synthesis, 0.5-1 µg RNA from each sample was reverse transcribed by addition of Oligo (dT) primers and running the reaction in the PCR machine at 42° C for five minutes, followed by adding the cDNA mastermix (1 mM dNTPs; 2.5 mM $MgCl_2$; 1X RT Buffer; 1 U/µl RNase inhibitor; 20 U M-MLV Reverse Transcriptase) [all reagents purchased from Promega except for dNTPs (Bioline)].

2.2.4.1.2 Quantitative real-time PCR (qPCR)

The quantitative PCR (qPCR) mastermix constituted of 200 ng of cDNA, 0.2 µM of forward and reverse primers, 1X (5 µl) SYBR Green I Mastermix (Life Technologies) and water to the final volume of 10 µl per sample. The qPCR reaction was performed using the StepOne Plus machine (Applied Biosystems, Life Technologies) at 95° C denaturation for 15 s, the annealing and extension steps were at 60° C for one minute respectively for 40 cycles. The results were analysed by relative quantitation using the delta delta (ΔΔ) Ct method, where samples were first normalised to β-glucuronidase (GUSβ) and/or β-actin housekeeping genes. Fold change ($2^{-\Delta\Delta Ct}$) was analysed by determining differences between the normalised target sample and normalised calibrator (control sample). Human dermal fibroblasts (HDFs) were used as negative controls for the expression of pluripotency markers.

Table 2.1: Primer sequences for stem cell genes

Gene	Primer sequence	NM Sequence	Size (bp)
hOCT3/- F	5'-GAC AGG GGG AGG GGA GGA GCT AGG-3'	NM_001285987.1	144
hOCT3/4-R	5'-CTT CCC TCC AAC CAG TTG CCC CAA AC-3'		
hNanog-F	5'-CAG CCC CGA TTC TTC CAC CAG TCC C-3'	XM_011520852.1	391
hNanog-R	5'-CGG AAG ATT CCC AGT CGG GTT CAC C-3'		
hSox2-F	5'-GGG AAA TGG GAG GGG TGC AAA AGA GG-3'	NM_003106.3	151
hSox2-R	5'-TTG CGT GAG TGT GGA TGG GAT TGG TG-3'		
hKLF4-F	5'-ACG ATC GTG GCC CCG GAA AAG GAC C-3'	NM_001314052.1	397
hKLF4-R	5'-TGA TTG TAG TGC TTT CTG GCT GGG CTC C-3'		
hMYC-F	5'-GCG TCC TGG GAA GGG AGA TCC GGA GC-3'	NM_002467.4	328
hMYC-R	5'-TTG AGG GGC ATC GTC GCG GGA GGC TG-3'		

2.2.4.1.3 Detection of pluripotency markers by immunocytochemistry (ICC)

For detection of pluripotency markers by immunofluorescence, the reprogrammed iPSC lines were manually passaged onto 0.15 x 10^6 iMEFs plated onto gelatine-coated coverslips per well in a 12-well culture plate. The iPSCs were cultured for two days in hESC medium and analysed for the presence of OCT4, NANOG and/or TRA-1-60. Briefly, the hESC medium was removed and the cells were gently washed three times for three minutes per wash with 1x PBS. Following the PBS washes, the cells were fixed with 4% (wt/vol) paraformaldehyde for 15 minutes at room temperature. After fixing, the cells were permeabilized in ice-cold methanol and incubated at -20° C for five minutes for permeabilization of the nuclear membrane. For detection of surface markers such as TRA-1-60, the permeabilization step was omitted. After permeabilization, the cells were rinsed 3 x 5 minutes with 1X PBS, followed by incubation with the blocking solution (5% FBS; 0. 01% Triton X-100) in 1X PBS for 1 h at room temperature. Following the blocking step, the cells were incubated overnight at 4° C with either OCT3/4 anti-rabbit (1:200), NANOG (1:200) (both OCT3/4 and NANOG were purchased from Abcam, UK) or TRA-1-60 (1:200) (cat #MAB4360A4; Millipore, Germany) antibodies. The cells used as controls were incubated in blocking solution only. Following overnight primary antibody incubation, the cells were rinsed 3 x 5 minutes with 1X PBS. Cells labelled with OCT 3/4 and NANOG were incubated

with donkey anti-rabbit Cy3-fluor secondary antibody (1:1000) for 2 h at room temperature in the dark. No secondary antibody was added to cells labelled with TRA-1-60 as the primary antibody is conjugated to the ALEXA-Fluor 488 tag. The ICC control cells were either incubated with donkey anti-rabbit Cy3-Fluor (Invitrogen, Thermo Fisher) or Alexa-Fluor 488 (Invitrogen, Thermo Fisher) at 1:500 dilution to correct for background fluorescence. After the 2 h incubation with the secondary antibodies, the cells were washed 3 x 5 minutes with 1X PBS. The cells were incubated with Hoechst 33342 (1 µg/ml) for 15 minutes in the dark at room temperature for nuclear staining. The cells were thereafter washed 2 x 5 minutes with 1X PBS and the coverslips were mounted onto slides using mounting fluid (Mowiol) and were stored overnight at 4° C in the dark for the mounting fluid to dry prior to viewing. Images were acquired using a Zeiss Axiovert 200M fluorescence microscope with Axiocam HR charge-coupled device camera and Axiovision 4.7 software.

Table 2.2: Primary and secondary antibodies for pluripotency markers

Antibody	Host species	Antibody dilution	Secondary Ab	Localisation
OCT 3/4	Rabbit pAb	1:200	Cy3-Fluor (Donkey anti-rabbit) (1:1000)	Nuclear
NANOG	Rabbit pAb	1:200	Cy3-Fluor (Donkey anti-rabbit) (1:1000)	Nuclear
TRA-1-60	Mouse pAb	1:200	Alexa-Fluor 488 conjugate	Cell surface

2.2.4.2 In vitro differentiation of iPSCs into the three germ layers

For mesoderm differentiation, the EBs were maintained in EB medium supplemented with 0.5 mM ascorbic acid (Sigma-Aldrich, St Louis, MO) for 3 days. Thereafter, the EBs were transferred onto gelatine-coated coverslips in a 12-well plate and maintained in EB medium supplemented with 0.5 mM ascorbic acid for 15-20 days, with medium change every 2-3 days till immunofluorescence analysis. For ectoderm differentiation, the EBs were maintained in 50% neural basal and 50% DMEM/F12 medium supplemented with 1%

GlutaMax, 1% Pen-strep as well as 0.5% (v/v) N2 and 1% (v/v) B27 supplements (Life Technologies) for 3 days. The EBs were thereafter transferred on a monolayer of PA6 feeder cells cultured on gelatine-coated coverslips previously maintained in MEM-alpha medium supplemented with 10% FBS, 1% GlutaMax and 1% Pen-strep until addition of EBs to the monolayer. Once transferred, the EBs were maintained in ectoderm medium for 14-16 days. Fresh medium added every 2-3 days till immunofluorescence analysis.

Analysis of *in vitro* differentiation was performed as described in section 2.2.4.1.3. For detection of the endoderm cells were incubated with FOXA2 (1:1000), for the mesoderm they were incubated with alpha-smooth muscle actin (α-SMA) (1:100) and for ectoderm detection the cells were incubated with β-III tubulin (1:300) antibody (all primary antibodies were purchased from Abcam). The secondary antibodies used for fluorescence staining are shown in Table 2.3.

Table 2.3: Primary and secondary antibodies for germ layer markers

Antibody	Host species	Dilution	Secondary Ab	Germ layer
Alpha SMA	Mouse mAb	1:100	Alexa Fluor-488 (Goat anti-mouse) (1:500)	Mesoderm
β-III tubulin	Mouse mAb	1:300	Alexa Fluor-488 (Goat anti-mouse) (1:500)	Ectoderm neuronal
FOXA2	Rabbit pAb	1:1000	Cy3-Fluor (Donkey anti-rabbit) (1:1000)	Endoderm

2.2.4.3 Karyotyping of newly derived iPSCs

To determine if the derived iPSCs maintained normal chromosomal number and integrity post-reprogramming, the iPSCs were cultured using the feeder-free method until the third passage, where after they were sent to the National Health Laboratory Services (NHLS) lab for karyotyping. Karyotyping analysis was performed using the Giemsa staining (G-band) method. Briefly, the cells were arrested at the metaphase of the mitotic stage by treating with

colchicine or colcemid. The cells were thereafter fixed with Carnoy's fixation solution (3:1 methanol to glacial acetic acid), trypsinised and collected by centrifugation followed by staining with Giemsa staining solution (Bickmore; Francke & Oliver, 1978).

2.3 Results

2.3.1 Derivation, isolation and expansion of iPSC clones

Control and patient dermal fibroblasts were infected with the SeVdp vector that contains the pluripotency factors (*OCT4; SOX2; KLF4, C-MYC*). The infected fibroblasts were cultured on iMEF feeder layer in hESC medium as described in the methods. Eight to 10 clones per iPSC line were picked and expanded or frozen in liquid nitrogen for later use. Two patient fibroblasts (Patient A and Patients B) and familial Control fibroblast line were reprogrammed into iPSCs. Ten clones were picked for both the familial Control and Patient A were successfully expanded up to passage 3. Two clones from each line were characterised (Table 2.4). The selected clones for the familial Control and Patient A were successfully characterised (Fig. 2.2 A-D). Eight iPSC clones were picked for Patient B and two clones were initially selected for characterisation. The third clone was expanded for characterisation as the second clone indicated poor cell growth and lack of ESC-like morphology up to passage 6 (P6). Similarly, the third clone indicated partial reprogramming. Therefore, only one out of three clones for Patient B were successfully characterised (Fig. 2.2E). Partially reprogrammed clones showed a difference in their morphology compared to fully reprogrammed cells. They appeared slightly dome- or flat-shaped with no clear edge around each colony compared to the normal flat shape. The colonies were small and differentiated at faster rate than the fully reprogrammed cells on a MEF feeder layer (Fig. 2.3E). Although partially reprogrammed cells expressed stem cell markers such as OCT4 and TRA-1-60, they were difficult to maintain in culture and did not differentiate into the three germ layers as they tended to disintegrate at the EB stage, or they maintained their epithelial-like morphology after re-adherence of EBs during differentiation. Figure 2.3A-C indicates difference in morphology between iPSCs during day 11 and day 20 of reprogramming. The selected clones indicated ESC-like morphology at P2, a flat ESC-like morphology with an edge around the colony and a 2:1 nuclear to cytoplasm ratio as previously described by Takahashi et al. (2007). iPSCs cultured under feeder-free conditions (Fig. 2.3D) display a monolayer compared to the colonies observed on a feeder layer.

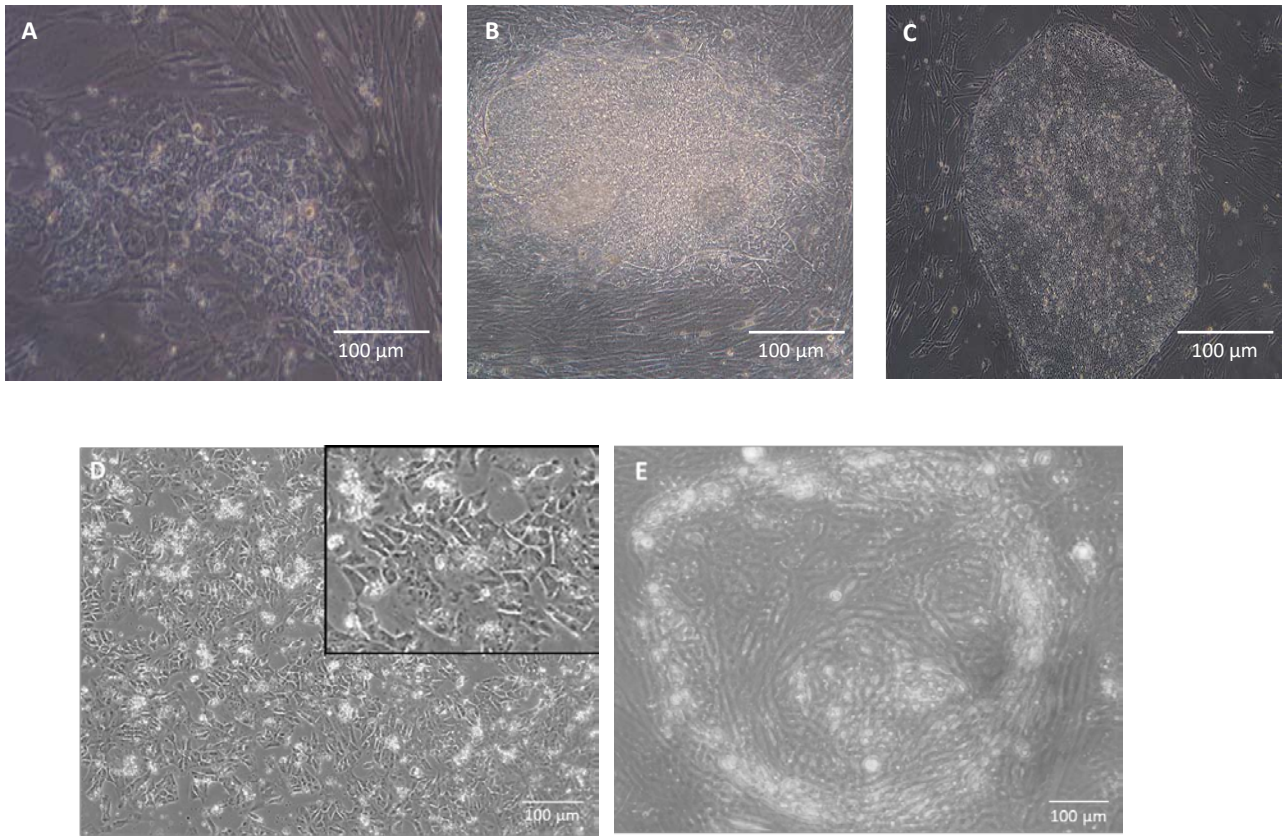

Figure 2.3 Morphology of reprogrammed iPSCs. (**A)** Cells undergoing reprogramming on day 11 post-infection showing a MET morphology. **(B)** Reprogrammed cells on day 20 showing formation of a colony with ESC-like defined border. (**C)** iPSC colony at passage 2 (P2) post-reprogramming. (**D)** iPSCs cultured under feeder-free conditions proliferate as a monolayer. **(E)** The flattened colony indicates a partially reprogrammed cell after six passages.

TABLE 2.4: Patient and control iPSC clones characterised in this study

Sample	iPSC clones (C)	Expression of stem cell genes (ICC & RT-PCR)	Karyotyping	*in vitro* differentiation to 3 germ layers
Familial Control	FAM_C1	✓	✓	✓
	FAM_C2	✓	✓	✓
Patient A	Pt A_C1	✓	✓	✓
	Pt A_C2	✓	✓	✓
Patient B	Pt B_C1	✓	✓	✓
	Pt B_C2	Characterisation was discontinued for C2 and C3 due to partial reprogramming observed at P6.		
	Pt B_C3			

Familial control (FAM); Patient A (Pt A); Patient B (Pt B); Clone (C)

2.3.2 Expression of stem cell genes in derived iPSCs

To determine whether the derived iPSCs express stem cell genes, feeder-free cell culture was performed (section 2.2.3.3) and mRNA expression was analysed by qPCR. Expression levels of the stem cell markers (*OCT4*, *NANOG* and *SOX2)* were higher in derived iPSC lines compared to control dermal fibroblasts (Fig. 2.4A). The expression levels of KLF-4were notably similar to the levels observed in control dermal fibroblasts (Fig. 2.4A). KLF-4 is reported to regulate NANOG expression (Zhang et al., 2010), and KLF-2 and KLF-5 can also regulate NANOG expression (Chan et al., 2009). Therefore, the low *KLF-4* levels in derived iPSCs may be due the redundancy with other KLF proteins which also bind to NANOG to maintain pluripotency and self-renewal. Immunocytochemistry (ICC) was also performed to determine protein expression of pluripotency markers in derived iPSCs. Figure 2.4B indicates that the iPSCs stained positive for OCT3/4 which localises in the nucleus, and TRA-1-60 which is a surface marker found in pluripotent stem cells. The results indicate that reprogramming of dermal fibroblasts with the SeVdp vector induced endogenous expression of stem cell genes. Analysis for clearance of SeVdp backbone was determined and indicated that SeVdp was silenced in the iPSC lines used in this study (data not shown).

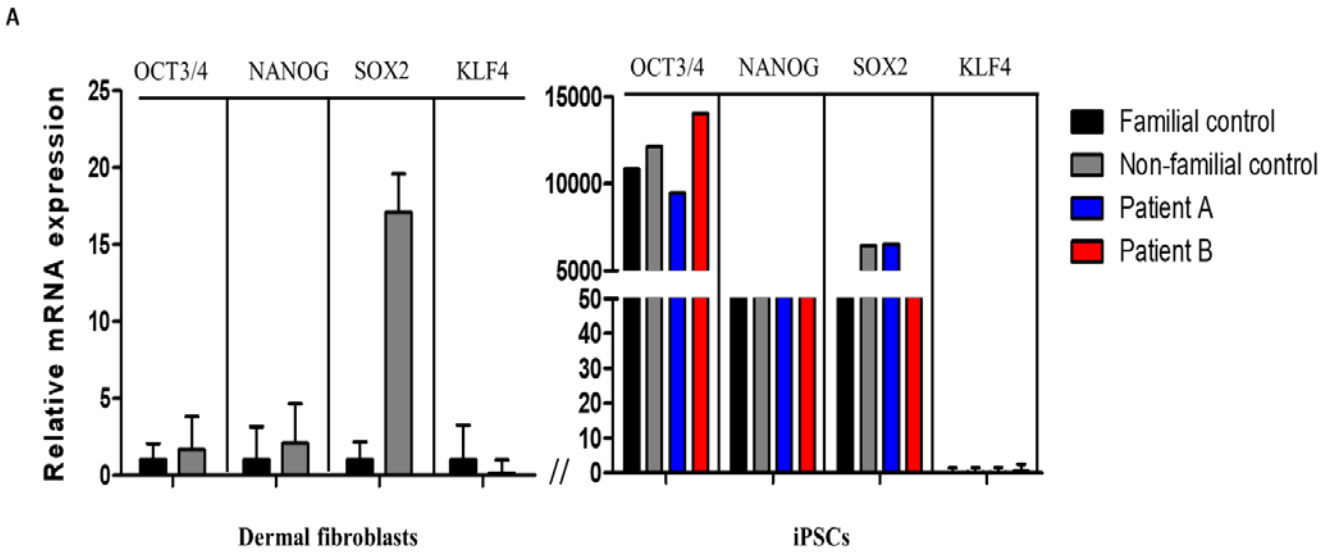

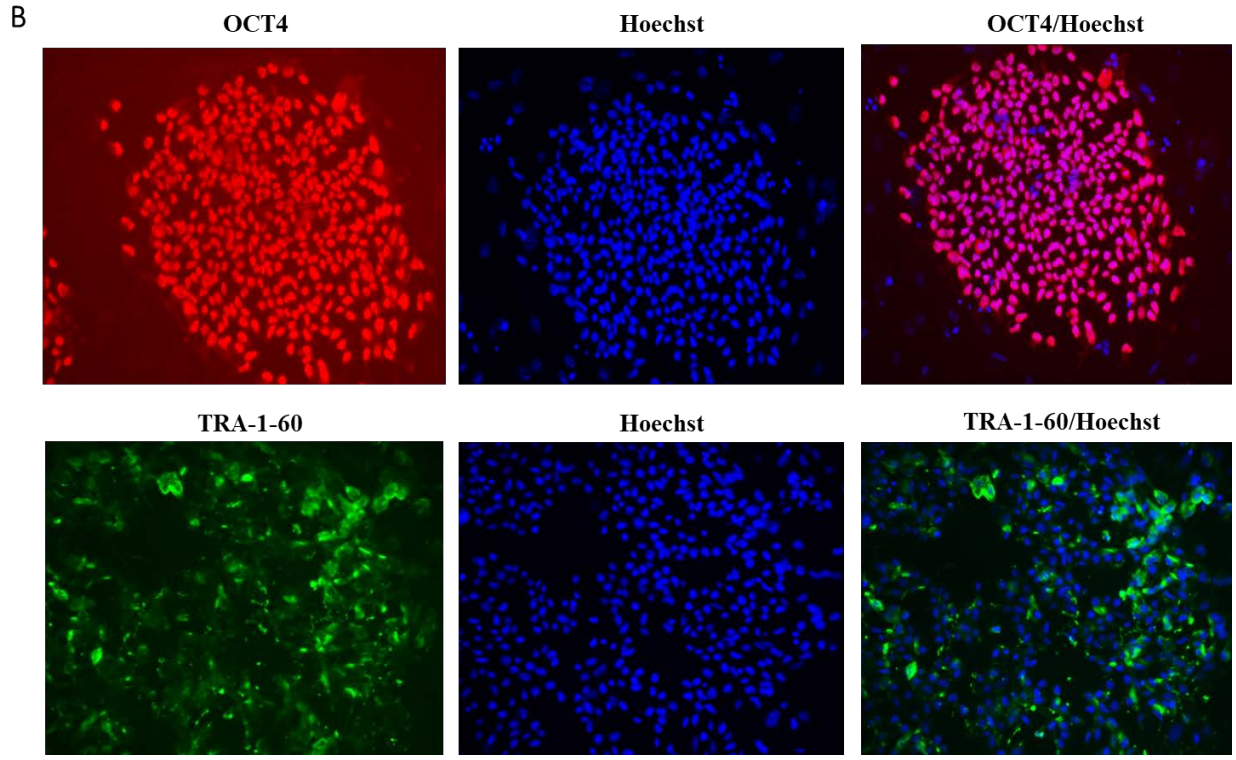

Figure 2.4 Expression of pluripotency markers. (A) qPCR analysis indicating high mRNA expression of stem cell genes (*OCT4*, *NANOG*, *SOX2* and *KLF-4*) in derived iPSCs compared to dermal fibroblasts of control samples. n=3 (SEM). **(B)** immunocytochemistry results show a representation of iPSCs that stain positive for OCT3/4 and TRA-1-60 pluripotency markers (scale bar = 100 µm).

2.3.3 *In vitro* differentiation of derived iPSCs

To determine the pluripotency of derived iPSCs, *in vitro* differentiation via EB formation was performed. Figure 2.5 shows images of well-formed EBs cultured in suspension (A) and EBs that have been cultured in adherent culture plate with outgrowths of differentiating cells (B). Figure 2.5C shows the presence of nuclear-localised FOXA2 protein expressed in the endoderm. Figure 2.5D shows positive staining of α-SMA which is a mesoderm marker that is prevalent in cells of mesenchymal origin. Figure 2.5E shows detection of β-III tubulin which is a neuronal marker demonstrating successful differentiation of iPSCs into the ectodermal lineage.

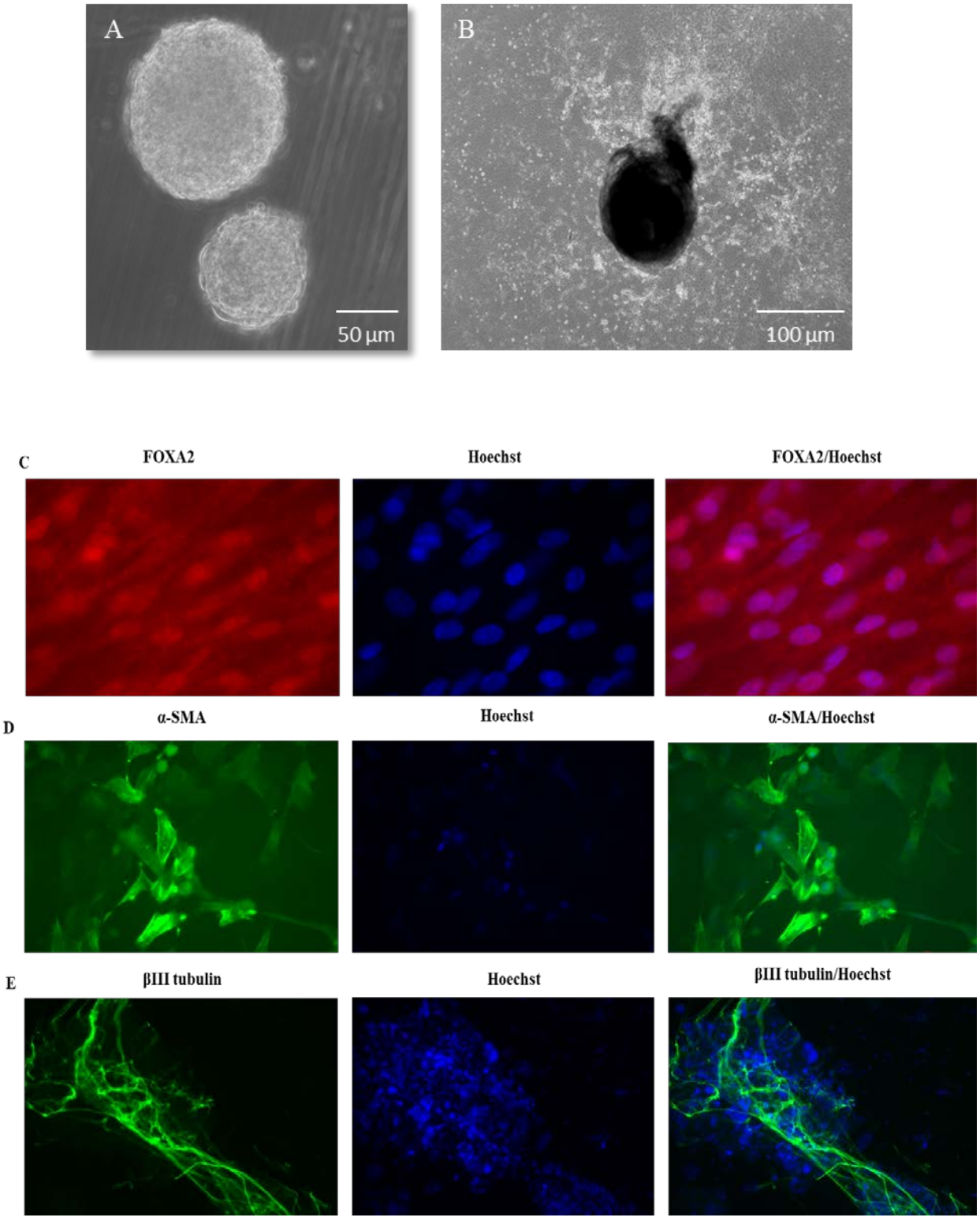

Figure 2.5 *in vitro* differentiation of derived iPSCs. (A) Embryoid bodies (EBs) in suspension culture. **(B)** Re-adhered EBs with cell outgrowths during in vitro differentiation. **(C)** Immunocytochemistry showing Positive staining of FOXA2 expressed in the endodermal germ layer (scale bar = 20 µm), **(D)** α-SMA expressed in the mesodermal germ layer (scale bar = 50 µm) and **(E)** β-III tubulin expressed in the ectodermal germ layer (scale bar = 100 µm).

2.3.4. Karyotyping of derived iPSCs

All the fully reprogrammed iPSC clones were further characterised by determining whether they maintained normal karyotype after reprogramming. The iPSC lines demonstrated normal karyotyping and no chromosomal aberrations (see appendix).

2.4 Discussion

Dermal fibroblasts from two affected siblings and familial control (i.e. genetically related) of the South African kindred, were successfully reprogrammed into iPSCs using the Sendai virus vector containing four of the pluripotency factors (*OCT4; SOX2; KLF-4; c-MYC*). Two clones per iPSC line were selected for characterisation. Both clones for Patient A and the familial control expressed ESC markers (*OCT4, NANOG, SOX2* and TRA-1-60) either by qPCR or ICC assay (Fig. 2.4A-B) and were further demonstrated pluripotency by successfully differentiating (*in vitro*) into the three germ layers (i.e. endoderm, mesoderm and ectoderm) (Fig. 2.5C-E). Moreover, karyotype analysis indicated that the selected iPSC clones indicated genome stability with no chromosomal aberrations (Appendix). Only one clone for Patient B was fully characterised as two out of three selected clones demonstrated partial reprogramming. The morphology of partially reprogrammed iPSCs did not fully resemble that of ESCs and were not further characterised, although they expressed all the ESC markers. The reprogramming efficiency in these cells was therefore low despite the use of the SeVdp vector. Some studies suggest that reprogramming efficiency can be improved by 80% if repeated cycles of SeVdp infection are performed (Nishimura et al., 2011). It should be noted that a single round of SeVdp infection was performed in this study. Interestingly, other studies contest the notion that partially reprogrammed iPSCs are not pluripotent (Tonge et al., 2014; Vidal et al., 2015). A study by Tonge et al. (2014) indicated that partially reprogrammed derived iPSCs from mouse fibroblasts, which they labelled “F-Class cells” are at an alternative pluripotent state as they expressed Oct4 and Nanog as well as other pluripotent genes such as *Sall4*. They also showed that the F-class cells had a different morphology as they did not express E-cadherin 1, which is highly expressed in ESCs. They further suggested that continuous infection cycles with exogenous OSKM factors can drive “F-Class cells” into complete reprogramming. Another study showed that partially reprogrammed mouse iPSCs that remained in the intermediate state for up to 20 passages could progress to a fully reprogrammed state by maintaining them in serum-free medium supplemented with bFGF compared to the serum containing medium supplemented with the Leukemia inhibitory factor (LIF) (Kim et al., 2014). This study further supports that partially reprogrammed cells can be induced to progress into a fully reprogrammed state under specific conditions. The use of enhancers such as valproic acid, ascorbic acid and butyrate

have been shown to improve reprogramming efficiency (Chen et al., 2016; Ebrahimi, 2015; Liang et al., 2010). These studies therefore indicate that partially reprogrammed clones can be converted to fully reprogrammed iPSCs by using enhancers and repeated treatment with the SeVdp vector containing the stem cell genes. Therefore, future work will include enhancing the reprogramming efficiency of partially reprogrammed in this study, especially for Patient B clones.

Although KLF-4 is used for iPSC reprogramming, its endogenous expression in fully reprogrammed iPSCs was shown to be similar to fibroblasts (Takahashi, 2007), a finding which was also observed in this study. The role of KLF-4 is reported to maintain pluripotency and self-renewal in pluripotent stem cells. A study by Zhang et al. (2010) demonstrated that KLF-4 expression in mouse ES cells prevents terminal differentiation. Most importantly, they indicated that KLF-4 binds to NANOG to maintain pluripotency in mouse ES cells via the LIF-STAT3 pathway. Other studies have also suggested that KLF-4 acts as an enhancer of pluripotency genes (e.g. OCT3/4 and SOX2) during reprogramming (Guo et al., 2010; Takahashi, 2007). Furthermore, KLF-4 is suggested to be involved in chromatin remodelling during reprogramming for activation of stem cell genes. There is also functional redundancy of the KLF family of proteins, where KLF-2 and KLF-5 also bind to the NANOG promoter region (Chan et al., 2009). It is therefore plausible that the low KLF-4 levels detected in derived iPSCs for this study may have been due to the redundancy with other KLF proteins.

The iPSC technology is a promising tool for patient-specific disease modelling, cell replacement therapy and regenerative medicine. However, there is also a need to overcome some of the challenges experienced during iPSC reprograming such as low reprogramming efficiency and partial reprogramming. Furthermore, genetic and clone variation are hurdles that still need to be addressed (Ohnuki & Takahashi, 2015; Rouhani et al., 2014). Recognising some of these challenges in this study, future work will require that more clones be further characterised, particularly for Patient B. Nevertheless, derivation of patient-specific iPSCs in this study has thus produced a platform to further derive tissue-specific cells types that are affected in POIKTMP, and to explore the mechanism(s) by which the *FAM111B* mutation induces POIKTMP, focusing on the fibrosis phenotype which is the primary cause of death in the South African family (Khumalo et al., 2006; Mercier et al., 2013).

Chapter 3

Using iPSC-derived mesenchymal stem/stromal cells (iPSC-MSCs) to explore the role of FAM111B in the expression of genes involved in fibrogenesis

3.1 Introduction

Wound healing is a tightly regulated process, its dysregulation causes extensive deposition of the ECM causing fibrosis which leads to impaired tissue remodelling and ultimately organ failure (Henderson & Iredale, 2007; Krenning et al., 2010; Wynn, 2008). In some disease conditions such as chronic kidney disease, cardiac fibrosis and liver cirrhosis, the onset of fibrosis can be traced to an acute injury, which progresses to become chronic thus leading to fibrosis. In hereditary fibrosing poikiloderma (POIKTMP) which is caused by mutations in the *FAM111B* gene, it has not been elucidated how these mutations result in the onset or progression of fibrosis. As a first approach to investigating this problem, this chapter explores the question of whether the *FAM111B* mutation activates the fibrotic process by altering the expression key pro-fibrotic molecules. As previously described (chapter 1), the primary effector cells in wound healing are fibroblasts, which break down the damaged extracellular matrix via matrix metalloproteinases and deposit newly synthesised type I and type III collagen required for wound healing and tissue repair (Fig. 1.6). There is also recruitment of pericytes, macrophages and mesenchymal cells/stromal which are activated to form myofibroblasts that produce new collagen and other ECM proteins. Epithelial cells which undergo EMT, are also activated and recruited for collagen deposition, and also contribute to fibrogenesis in impaired tissue repair (Rockey et al., 2015; Talele et al., 2015; Wynn, 2007, 2010).

It was observed that most of the affected tissues in POIKTMP are of mesenchymal lineage (e.g. tendons, skeletal muscle and connective tissue). Mesenchymal stem/stromal cells have notably been implicated in augmenting fibrosis as they are also recruited and activated by TGF-β and/or CTGF cytokine to differentiate into myofibroblasts during wound healing and fibrosis (LeBleu et al., 2013; Tan et al., 2011). Furthermore, MSCs have also been indicated to either attenuate fibrosis. For example, during tissue injury MSCs home to the site of injury and induce immunomodulation which results in the inhibition of T-cell and B-cell lymphocyte proliferation as well as stimulating an anti-inflammatory response

(Corcione et al., 2006; Di Nicola et al., 2002). Due to their role in immunomodulation and fibrosis, it is suggested that timing of MSC treatment for clinical application is critical for effective immunomodulation and anti-fibrotic response (Hayes et al., 2015). It has been suggested in some studies that for effective MSC treatment in lung injury, for example, treatment must be performed 48 hours post-injury to prevent fibrogenesis. Late MSC treatment is suggested to induce fibrosis as it overlaps with tissue remodelling which is associated with high levels of anti-inflammatory cytokines (e.g. TGF-β) which activate myofibroblasts. Treatment with MSCs during tissue remodelling therefore results in their differentiation into myofibroblast thereby contributing to an increased number of myofibroblasts and their activity leading to fibrosis (Popova et al., 2010).

In systemic sclerosis (SSc), MSCs have been shown to express high levels of α-SMA and type I collagen, suggesting that baseline expression of these pro-fibrotic markers is elevated in this condition. This is further suggested by the finding that they have low potential to differentiate into vascular smooth muscle cells (Hegner et al., 2016). Hegner et al. (2016) showed by RNA and protein expression assays that MSCs from SSc patients particularly do not express high levels of connective tissue growth factor (CTGF) and bFGF, which are required for vascular smooth muscle differentiation. Furthermore, it is proposed that in familial disorders such systemic sclerosis, precursor cells such as MSCs could be the source of the disease phenotype (Hegner et al., 2016; Larghero et al., 2008).

In this chapter, to test whether the *FAM111B* mutation results in increased levels of pro-fibrotic markers, mesenchymal stem/stromal cells were derived from patient and control iPSCs, and tested for changes in expression of pro-fibrotic markers α-SMA, type I and type III collagen

Different protocols have been used for derivation of MSCs from iPSCs (iPSC-MSCs), and though there is no standardised method of derivation, characterisation of derived MSCs has been done by comparing iPSC-MSC gene expression profile and multi-lineage differentiation to that of bone marrow-derived MSCs, which are used as bona fide MSCs (Bianco et al., 2008). Mesenchymal stem/stromal cells previously derived from human ESCs were shown to be derived by treating hESCs with small molecules such as Rho-associated kinase (ROCK) inhibitor for 10 days (Tan et al., 2011), or TGF-β/BMP inhibitor for 28 days (Sánchez et al., 2011). Derivation of iPSC-MSCs by other investigators has also been shown to further require a variation of small molecules such as TGF-β, activin-A, retinoic acid,

ascorbic acid, platelet-derived growth factor (PDGF) and MSC-specific medium (Diederichs & Tuan, 2014; Kang et al., 2015; Lian et al., 2010; Moslem et al., 2015; Zou et al., 2013). Moreover, other studies have demonstrated effective differentiation of iPSCs into MSCs via standard embryoid body (EB) formation, while others showed direct iPSC to MSCs differentiation to be effective (Diederichs & Tuan, 2014; Lian et al., 2010). Interestingly, derivation of fibroblast-like cells from iPSCs required similar differentiation molecules used to derive iPSC-MSCs. However, due to the heterogeneity of these cells (Itoh et al., 2013), it is difficult to fully distinguish whether iPSC-derived fibroblasts are true fibroblasts or MSCs as these cell lines both exhibit the same morphology and phenotypic profile. It is therefore reasonable to identify these cells as mesenchymal stem/stromal cells.

To investigate the role of the *FAM111B* mutation in the expression of pro-fibrotic markers in POIKTMP patients, the objectives in this chapter were to:

a) Differentiate iPSC into MSCs (iPSC-MSCs)

b) Determine whether iPSC-MSCs express typical MSC markers, and whether they possess the multi-lineage capacity to undergo osteogenic and adipogenic differentiation

c) Determine whether there are differences in the expression of pro-fibrotic and adipogenic markers between patient and control cells

3.2 Materials and methods

3.2.1 Deriving mesenchymal stem/stromal cells from iPSCs

The iPSC-MSCs in this study were derived using a modified protocol by Itoh et al. (2013), where TGF-β2 was omitted and ascorbic acid was the primary molecule used to drive iPSCs towards the mesodermal lineage via EB formation and finally into mesenchymal stem/stromal cells (Fig. 3.1). Transforming growth factor (TGF)-β2 was omitted in the differentiation of iPSC to obtain progenitor cells of mesenchymal lineage for further differentiation into the affected tissue such as skeletal muscle, and to determine whether patient cells exhibited a myofibroblast phenotype without TGF-β treatment.

Two patients and two control iPSC lines were manually passaged from the iMEF feeder layer as previously and transferred onto non-adherent 100 mm petri dishes for formation of EBs. The EBs were maintained in hESC medium (K/ODMEM; 20% KO-SR; 1% NEAA; 1% GlutaMax; 0.05 mM β-mercaptoethanol) without bFGF and supplemented with 0.3 mM ascorbic acid (AA), and insulin-transferrin-selenium (ITS-A) supplement (Thermo Fisher Scientific, Waltham, MA, USA). The EBs were maintained in hESC medium (w/o bFGF) for six days and medium was changed every two days. Six days after EB formation the well-formed EBs were collected into 15 ml conical tubes and centrifuged at 300 x g for two minutes. After centrifugation, the supernatant was removed and the EBs transferred onto gelatin-coated 6-well plates and maintained in high-glucose DMEM supplemented with 20% FBS, 1% Pen-strep and 0.3 mM ascorbic acid for 10 days, with medium change every 2-3 days. After 10 days, the cell outgrowths were passaged by first aspirating the differentiation medium and washing the cells twice with 1x PBS. The cells were passaged with 0.5 ml of 0.25% trypsin/EDTA per well and incubated at 37° C for five minutes. Thereafter 4.5 ml of growth medium was added to the cells for deactivation of trypsin/EDTA, collected and centrifuged at 2000 rpm for five minutes at room temperature (RT). Following centrifugation, the supernatant was removed, and the pellet was resuspended in one ml growth medium. The resuspended cells were thereafter added onto gelatin-coated culture dishes for expansion and formation of MSCs in DMEM supplemented with 10% FBS and 1% Pen-strep. The cells were maintained in culture and passaged every seven days up to passage six before characterisation for MSC markers.

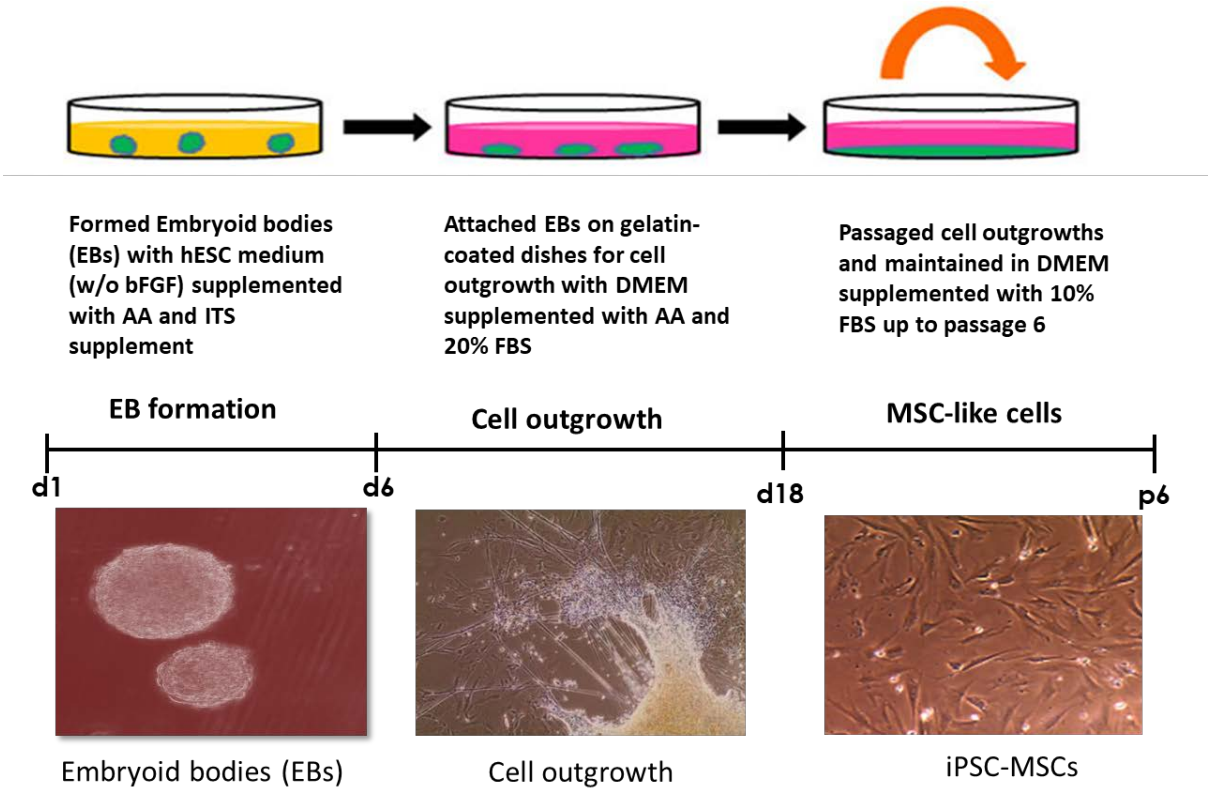

Figure 3.1 Derivation of iPSC-MSCs. The schematic diagram shows the step-wise approach used to derive MSCs from iPSCs. Adhered embryoid bodies (EBs) were maintained in basal medium supplemented with 20% FBS and ascorbic acid to induce mesenchymal differentiation. Fibroblast-like cells were maintained in culture for six passages prior to characterisation. The timeline shows the duration of each differentiation step for deriving iPSC-MSCs (protocol adapted from *Itoh et al. 2013*). (scale bar = 100 µm)

3.2.2 Characterisation of iPSC-derived mesenchymal stem/stromal cells (iPSC-MSCs)

3.2.2.1 Determining expression of MSC markers in iPSC-MSCs

At passage six (P6), the derived iPSC-MSCs were characterised by qPCR analysis for expression of MSC markers. RNA extraction and qPCR (section 2.2.4.1.1 and 2.2.4.1.2, page 45) were performed to detect the expression of CD73, CD90 and alpha-smooth muscle actin (α-SMA) markers which are commonly expressed by MSCs. Adipose-derived MSCs which were kindly donated by Professor Michael Pepper (University of Pretoria, Pretoria, South Africa), were used as a positive control for characterisation of iPSC-MSCs as they are known to also express these markers.

3.2.2.2 Osteogenic differentiation of iPSC-MSCs

To determine the multipotency of iPSC-derived MSCs, 1 x 10^5 cells/well were seeded onto gelatin-coated wells in a 6-well plate and were maintained in standard growth medium (DMEM; 10% FBS; 1% Pen-strep) until they reached confluence. The confluent iPSC-MSCs were maintained in standard growth medium supplemented with 50 µM ascorbate-2-phosphate, 10 mM β-glycerophosphate and 1 µM dexamethasone, which activate expression of osteogenic transcription factors such as RUNX2 and synthesis of collagen (Langenbach & Handschel, 2013). Osteogenic differentiation was induced for 21 days, with fresh medium added every three days. Figure 3.2 shows the osteogenic cocktail used for differentiation and the timeline of differentiation. At day 21, the cells were either harvested for qPCR analysis to determine the expression of osteogenic markers and/or stained with Alizarin Red S stain to detect calcium deposition (Jaiswal et al., 1997; Kang et al., 2014; Pittenger, 1999). For qPCR analysis, the osteogenic markers used to detect successful differentiation were alkaline phosphatase (AP), RUNX2 and osteocalcin.

Osteogenic cocktail

Reagent	Final Conc.
Ascorbate-2-phosphate	50 µM
Dexamethasone	1 µM
β-glycerophosphate	10 mM

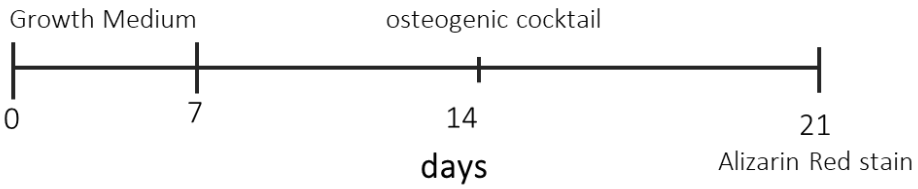

Figure 3.2 Osteogenic differentiation. iPSC-MSCs were maintained in growth medium for 7 days. From day 7 until day 21 the iPSC-MSCs were maintained in growth medium supplemented with the osteogenic cocktail indicated in the table. At day 21 the differentiated cells were stained with Alizarin red stain and compared with undifferentiated cells which were maintained in standard growth medium for 21 days.

Table 3.1: Primer sequences for osteogenic genes

Gene	Primer sequence	NM Sequence	Size (bp)
AP (F)	5'-ATC TGA CCC TCC CAG TCT C-3'	XM_006710546.3	165
AP (R)	5'-GAG TGA GTG AGT GAG CAA GG-3'		
hRUNX2 (F)	5'-CCACCTCTGACTTCTGCCTC-3'	NM_001024630.3	108
hRUNX2 (R)	5'-ATGAAATGCTTGGGAACTGC-3'		
hOC/BGLAP (F)	5'-GGCAGCGAGGTAGTGAAGAG-3'	NM_199173.5	158
hOC/BGLAP (R)	5'-CGATAGGCCTCCTGAAAGC-3'		

3.2.2.2.1 Alizarin Red S (ARS) staining

For detection of calcium deposition following 21-day of osteogenic differentiation, medium was aspirated, and the cells were washed twice with 1X PBS. After rinsing the cells with PBS, the cells were fixed with 10% formalin for 30 minutes at room temperature (RT). After fixing, the cells were washed twice with double-distilled water (ddH_2O). One ml of Alizarin red stain (0.14%; pH 4.13) was thereafter added to the cells and incubated in the dark at RT for 1 hour (h). Following ARS staining, the cells were rinsed five times and thereafter viewed under the Evos XL Core (Life technologies) light microscope with a 20x objective.

3.2.2.3 Adipogenic differentiation of iPSC-MSCs

The derived iPSC-MSCs were further differentiated into adipocytes to determine their multipotency as MSCs are known to have the capacity to undergo into osteogenic, adipogenic and chondrogenic differentiation. For adipogenic differentiation, the iPSC-MSCs were cultured onto gelatin-coated 6-well plates at 5000 cell/cm^2 for seven days and maintained in growth medium (DMEM; 10% FBS; 1% Pen-strep). On day seven growth medium was supplemented with the adipogenic cocktail containing 0.5 mM 3-Isobutyl-1-methylxanthine (IBMX) (Sigma-Aldrich, St Louis, MO), 10 µg/ml insulin (Thermo Fisher Scientific, Waltham, MA, USA), 1 µM Dexamethasone (activates expression of C/EBPα and PPARγ) (Sigma-Aldrich, St Louis, MO) and 100 µM indomethacin (Sigma-Aldrich, St Louis, MO). Adipogenic differentiation was induced from day seven until day 21, with medium change every 2-3 days (see Fig 3.3 for schematic presentation). The undifferentiated iPSCs-MSCs

were maintained in growth medium until day 21, with medium change every 2-3 days. Adipogenic differentiation was thereafter analysed by qPCR or Oil Red O staining. Adipose-derived MSCs (AD-MSCs) were used as a positive control for characterisation of iPSC-MSCs. Messenger RNA (mRNA) expression for early adipogenic markers peroxisome proliferator-activated receptor γ (PPARγ), CCAAT/enhancer binding protein α (C/EBPα), and late adipogenic markers fatty-acid binding protein-4 (FABP4) were analysed by qPCR in differentiated iPSC-MSCs.

Adipogenic cocktail

Reagent	Final Conc.
3-Isobutyl-1-methylxanthine	0.5 mM
Dexamethasone	1 µM
Insulin	10 µg/ml
Indomethacin (FW 357.8 g/mol)	100 µM

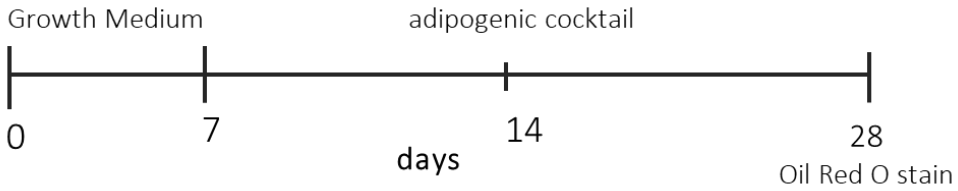

Figure 3.3 Adipogenic differentiation. iPSC-MSCs were maintained in growth medium until confluence on day 7. Growth medium was medium supplemented with the adipogenic cocktail (see table) for adipogenic induction. At day 21 the differentiated cells were stained with oil red O stain which stain lipid droplets red and compared with undifferentiated cells, which were maintained in standard growth medium for 21 days.

Table 3.2: Primer sequences for adipogenic genes

Gene	Primer sequence	NM Sequence	Size (bp)
PPARγ (F)	5'-ATTGACCCAGAAAGCGATTC-3'	NM_001354668.1	154
PPARγ (R)	5'-CAAAGGAGTGGGAGTGGTCT'		
hCAAT/EBPα (F)	5'-GCAAACTCACCGCTCCAATG-3'	NM_001287435.1	247
hCAAT/EBPα (R)	5'-TTAGGTTCCAAGCCCCAAGTC-3'		
hFABP4 (F)	5'-GGGACGTTGACCTGGACTGA-3'	NM_001442.2	113
hFABP4 (R)	5'-GGGAGAAAATTACTTGCTTGCTAAA-3'		

3.2.2.3.1 Oil Red O staining in adipocytes derived from iPSC-MSCs

Following adipogenic differentiation, the cells were washed twice with 1x PBS and fixed for 10 minutes with 10% formalin at room temperature (RT). After 10 minutes, fresh 10% formalin was added, and the cells were incubated for 1 hour (h) at RT. After 1 h, formalin was aspirated, and the cells were washed twice with distilled water and thereafter incubated with 60% isopropanol for five minutes. Thereafter, isopropanol was removed, and the cells were air-dried for five minutes followed by incubation with 60% Oil Red O (ORO) (Sigma-Aldrich, St Louis, MO) for 15 minutes. Following ORO staining, the cells were washed 4x with distilled water and air-dried prior to viewing at 200x magnification with the Evos XL Core Microscope (Thermo Fisher Scientific, Waltham, MA, USA).

3.2.3 Analysis of fibrotic markers in iPSC-MSCs

The iPSC-MSCs were cultured in growth medium (DMEM; 10% FBS; 1% Pen-strep) to determine if patients' cells express high levels of key fibrotic markers, which are collagen type 1A1 (COL1A1), 3A1 (COL3A1) and α-SMA. Once the iPSC-MSCs reached confluence they were harvested for RNA extraction as previously described (section 2.2.4.1.1) and analysed by qPCR (section 2.2.4.1.2). Extraction of RNA and qPCR were performed as previously described, and expression of COL1A1, COL3A1 and α-SMA mRNA levels were measured and compared between patients and controls.

3.2.3.1 Picrosirius Red (PSR) staining in iPSC-MSCs

Picrosirius red staining was performed to determine whether patient cells synthesised increased levels of type I and III collagen compared to controls. Briefly, patient and control iPSC-MSCs were seeded onto gelatin-coated 6-well culture plates at 0.1 x 10^6 cell/well. The cells were maintained in growth medium (DMEM; 10% FBS; 1% Pen-strep), with medium change every 2 days until the cells reached 80% confluence. At 80% confluence the cells were maintained in low serum (1% FBS) for 24 h. Following 24 h cell-culture in low serum, the cells were washed twice with 1x PBS and fixed with 1 ml Bouin's solution and incubated at room temperature (RT) for 2 h. After fixation, the cells were washed twice with 1x PBS, followed by incubation with shaking in 1 ml of 0.1% Picrosirius red (PSR) stain for 2 h at

RT. After 2 h incubation, the cells were washed 3x with 0.1% acetic acid and air-dried at RT for five minutes. Collagen staining imaging was captured at 200X magnification.

The PSR-collagen stain was eluted by incubating the cells with 0.1 N sodium hydroxide (NaOH) with shaking for 90 minutes at RT. The eluted stain was quantified using the spectrophotometer at the optical density of 540 nm. Rat tail collagen I was used as a standard.

3.2.4 Western blotting

3.2.4.1 Protein quantification

Patient and control iPSC-MSCs were cultured to 90% confluence. Three-hundred µl of radioimmunoprecipitation assay (RIPA) buffer containing protease inhibitors were added to each 10-cm culture plate for cell lysis and collection. The lysate was centrifuged at 12 000 rpm and 4 ºC for 20 minutes. The supernatant was collected into a fresh microfuge tube, and protein concentration was quantified using the Bicinchoninic acid assay (BCA) assay (Thermo Fisher Scientific, Waltham, MA, USA). Briefly, a 1:8 dilution was prepared for the BCA solution and bovine serum albumin (BSA), which was used as a standard. The samples were also prepared at 1:8 dilution in a 96-well plate. The 96-well plate was incubated at 37º C for 30 minutes and the absorbance was thereafter read at 562 nm using the RT-2100C microplate reader (Rayto Life & Analytical Sciences, Shenzhen, China). The standard curve and protein concentration were analysed on Microsoft Excel using the linear equation [(y = a*x + b) where: y = Protein concentration; x = Absorbance; a = Slope and b = Background Signal]. The protein samples were stored at -80º C for later use or long-term storage.

3.2.4.2 Sodium-dodecyl-sulphate polyacrylamide gel electrophoresis (SDS-PAGE)

The SDS-PAGE gels were prepared using the BioRad electrophoresis apparatus (Biorad Mini PROTEAN©). Ten-percent resolving gels were prepared on 1.5 mm (thick) plates and 5% stacking gels were prepared for loading the samples (see appendix). Laemali sample buffer (2X) was added to each sample and boiled at 95º C for five minutes. Thirty micrograms of protein for each sample were loaded onto the gels and electrophoresed at 110

volts (V) in 1X running buffer for 90-120 minutes at room temperature. The loading control used was rabbit polyclonal anti-p38 (Cell Signalling Technology, Danvers, MA, USA) which is a 40 kDa protein.

3.2.4.3 Nitrocellulose membrane electro-transfer

Following SDS-PAGE, the resolving gels and nitrocellulose transfer membrane (Amersham Biosciences, UK) were soaked in in 1X transfer buffer (see appendix) for 10 minutes. The resolving gels and the transfer membranes were "sandwiched" between cassettes and placed in a running tank. The electro-transfer was performed at 100V and 4º C for 1 h.

3.2.4.4 Chemiluminescence protein detection

Following electro-transfer, the nitrocellulose membrane was soaked in Ponceau stain for three minutes for detection of transfer efficiency. The membranes were thereafter washed 3 x 5 minutes with shaking in Tris-buffered saline-0.1% Tween-20 solution (0.1% TBS-T). The membranes were incubated in blocking buffer in containing TBS-T and 5% fat-free milk for 1 h at RT with shaking. The membranes were thereafter washed 3 x 5 minutes with shaking in 0.1% TBS-T. For detection of α-SMA protein (37 kDa) (Abcam, UK) one membrane was incubated in anti-α-SMA primary antibody (1:500) diluted in blocking buffer overnight at 4º C with shaking. The other membrane was incubated with anti-p38 primary antibody (1:5000) and used as a loading control.

Following overnight incubation, the membranes were washed 3 x 5 minutes with shaking in 0.1% TBS-T and thereafter incubated for 2 h (RT) in horseradish peroxidase-conjugated goat-anti rabbit secondary antibody (Biorad, Hercules, CA, USA) at 1:1000 for α-SMA and 1:5000 for p38. The membranes were thereafter washed 3 x 5 minutes with shaking in 0.1% TBS-T and incubated in chemiluminescence reagent for 3-5 minutes and developed the blots in the dark using X-ray film for signal detection. The blots were thereafter scanned for densitometric readings and further analysis.

3.2.5 Statistical analysis

Statistica Software version 13.2 (Dell Inc.) was used for statistical analysis of all data in this study. The qPCR results were analysed according to Schmittgen & Livak (Schmittgen & Livak, 2008) method, which was added to the Minimum Information for Publication of Quantitative Real-Time PCR Experiments (MIQE) guidelines (Bustin et al., 2009). The results are presented as mean ±SEM, and differences between two samples were analysed by Student's t-test, independent by group or variable. To determine significant differences in three or more groups, Breakdown & one-way analysis of variance (ANOVA) was used, with Tukey honest significant difference (HSD) as the post-hoc test. Data were considered statistically significant at $p < 0.05$. Graphs were plotted with GraphPad Prism version 5.0 (GraphPad, San Diego, CA).

3.3 Results

3.3.1. Characterisation of iPSC-derived MSCs (iPSC-MSCs)

3.3.1.1 iPSC-MSCs express MSC markers

The derived iPSC-MSCs were first characterised by their cellular morphology followed by the expression of typical MSC surface markers. The cell morphology of the newly derived iPSC-MSCs showed the typical fibroblast-like cell morphology as seen in adipose-derived MSCs (Fig 3.4A). Quantitative real-time PCR (qPCR) was performed to detect expression of typical MSC markers in iPSC-derived MSCs. As can be seen (Fig. 3.4B-D), the iPSC-MSCs expressed high levels of CD73 ($p < 0.001$), CD90 ($p < 0.05$) and α-SMA ($p < 0.05$) compared iPSCs. Interestingly, low levels of CD90 expression were detected in iPSCs, which is not typically expressed in pluripotent stem cells. These results indicate that the iPSC-MSC were successfully differentiated towards the mesenchymal lineage. Some variations were observed between the familial and non-familial controls with regards to CD90 expression (Fig. 3.4C) where the non-familial control showed higher expression of CD90 compared to the familial control as well as patient samples. This may have been due to differences in the genetic background of the non-familial control as genetic variation affects the expression of different genes in unrelated or non-isogenic samples.

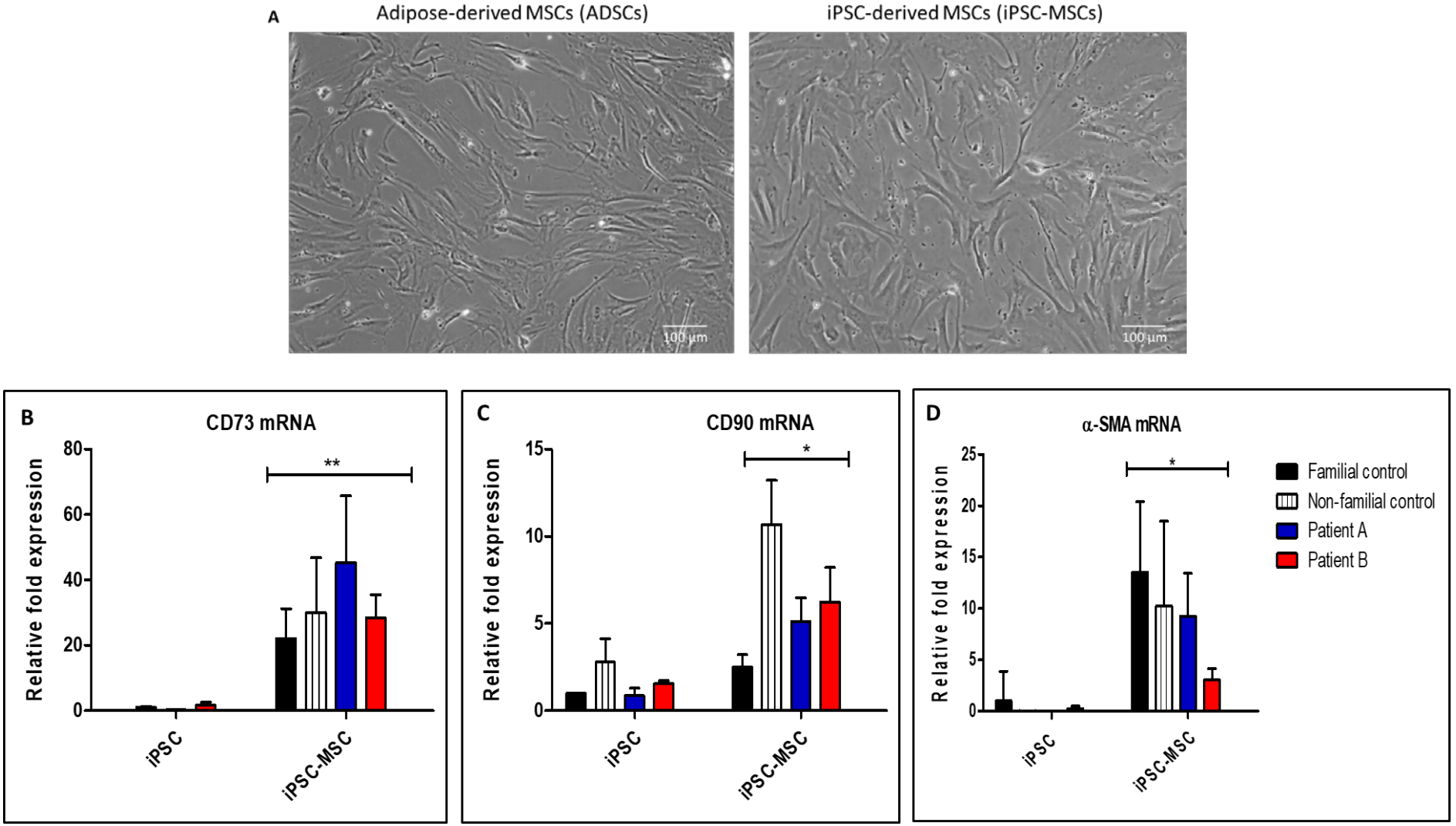

Figure 3.4 Expression of MSC markers in iPSC-derived MSCs (iPSC-MSCs). (A) The cell morphology of derived iPSC-MSCs was compared to *bona fide* adipose-derived MSCs (AD-MSCs) **(B-D)** The expression of MSC-specific gene markers (CD73; CD90; α-SMA) in iPSC-MSCs was compared with undifferentiated iPSCs. Data are presented as mean ± SEM (n = 4). * $p < 0.05$; ** $p < 0.001$.

3.3.1.2 iPSC-MSCs stain positive for Alizarin red stain and express osteogenic markers

One of the key characteristics of mesenchymal stem/stromal cells is their trilineage multipotency. To determine whether iPSC-derived MSCs are multipotent, they were induced towards osteogenic differentiation by maintaining the cells in growth medium supplemented with 50 µM ascorbate-2-phosphate, 10 mM β-glycerophosphate and 1 µM dexamethasone for 21 days, with medium change every 2-3 days. At day 21, the differentiated iPSC-MSCs were subjected to Alizarin Red S (ARS) stain for detection of mineralisation through calcium deposition. The successful differentiation of iPSC-MSC towards the osteogenic lineage was revealed by the orange-red ARS. The iPSC-MSCs that stained positive for ARS stain appeared orange-red and the undifferentiated iPSC-MSC showed a slightly reddish stain thus indicating non-mineralisation (Fig.3.5 A and B). Alizarin red staining in the familial control and Patient A was less extensive compared to the non-familial control and Patient B. Two biological repeats were performed for osteogenic differentiation and ARS stain and similar results were obtained. This was further confirmed by the expression of osteogenic markers, that the familial control and Patient A cells had low levels of *RUNX2* a master transcription factor for osteogenic differentiation, and alkaline phosphatase (AP) which is an early osteogenic marker which is sustained till day 21. The non-familial control and Patient B indicated high levels of *RUNX2* and AP (Fig 3.5Ci and Ciii), which is consistent with the high ARS staining compared to the familial control and Patient A. This variation in the familial control and Patient A may be due to clone variation. The expression of *osteocalcin* mRNA (Fig. 5Cii) was similar in both differentiated and undifferentiated cells. This finding is consistent with the finding by Jaiswal et al. (1997) who also showed that osteocalcin is expressed in similar levels in both differentiated and undifferentiated MSCs.

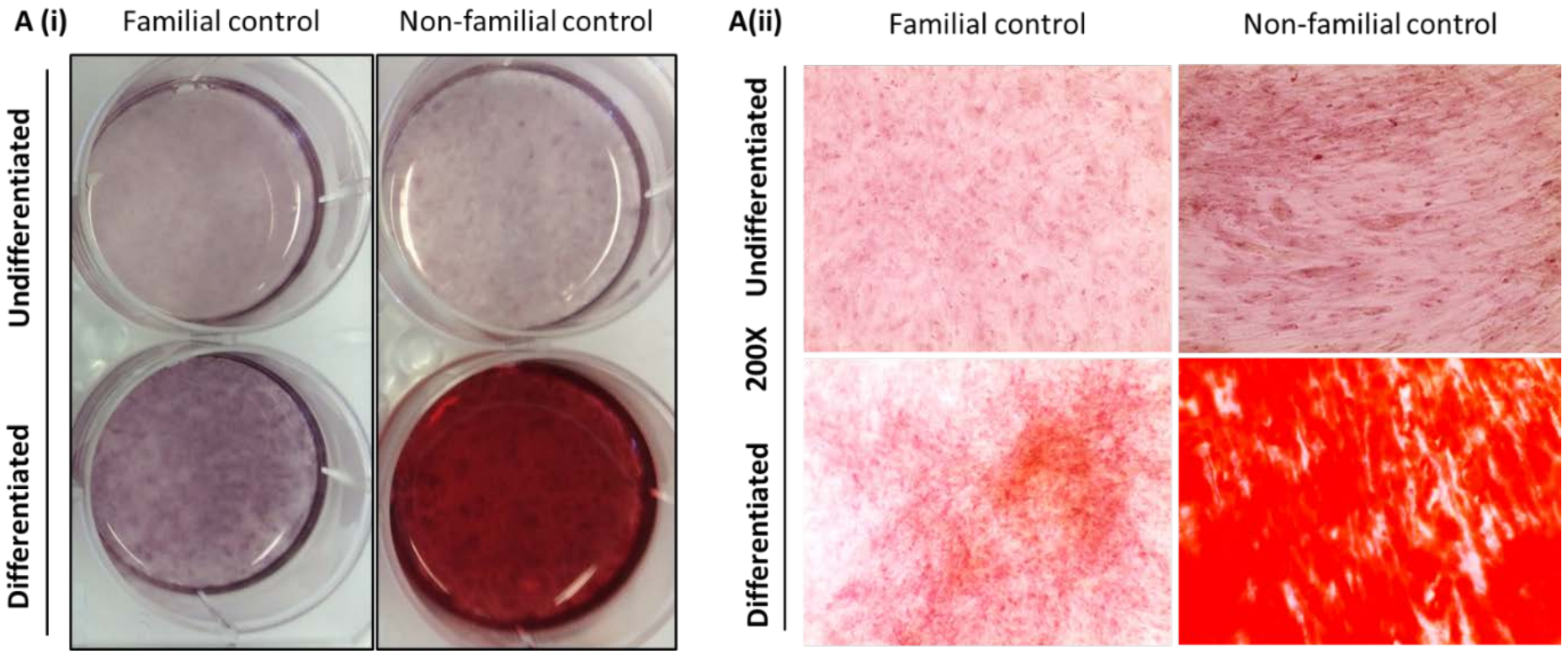
A (i)
Familial control
Non-familial control
Undifferentiated
Differentiated
A(ii)
Familial control
Non-familial control
Undifferentiated
200X
Differentiated

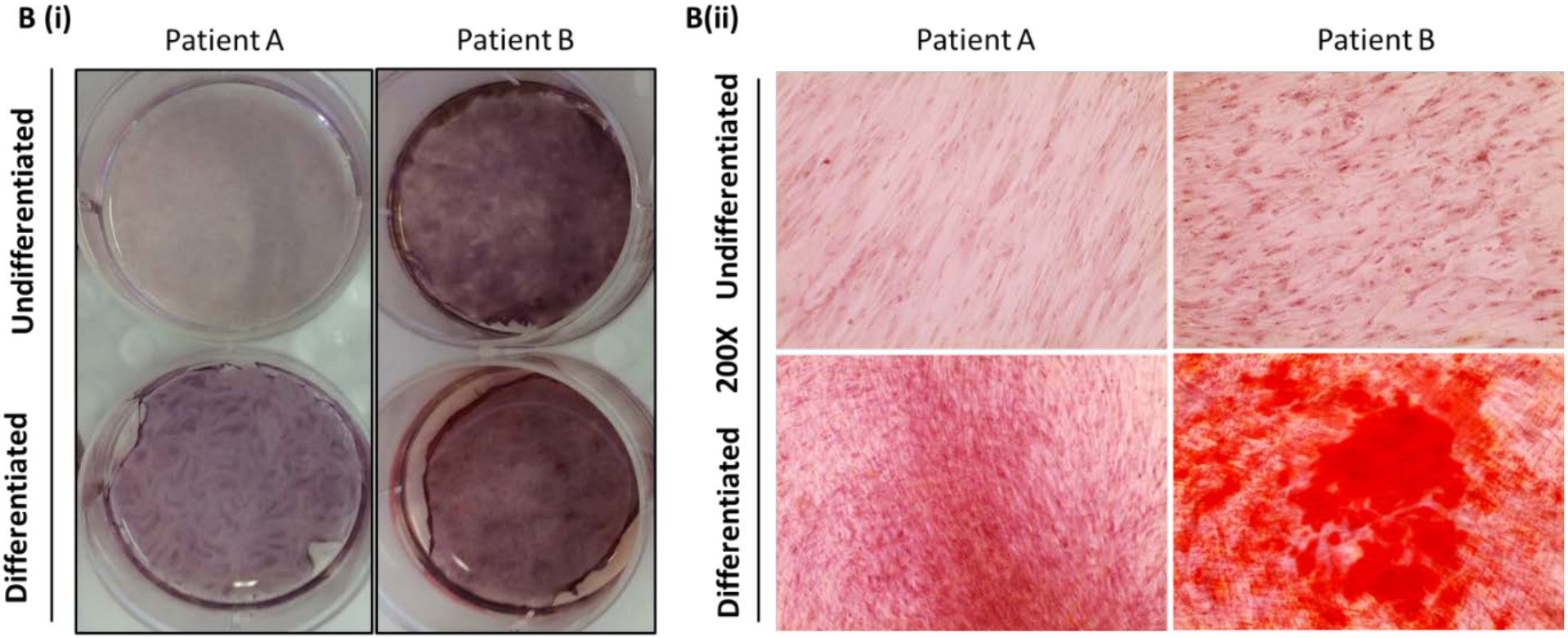
B (i)
Patient A
Patient B
Undifferentiated
Differentiated
B(ii)
Patient A
Patient B
Undifferentiated
Differentiated
200X

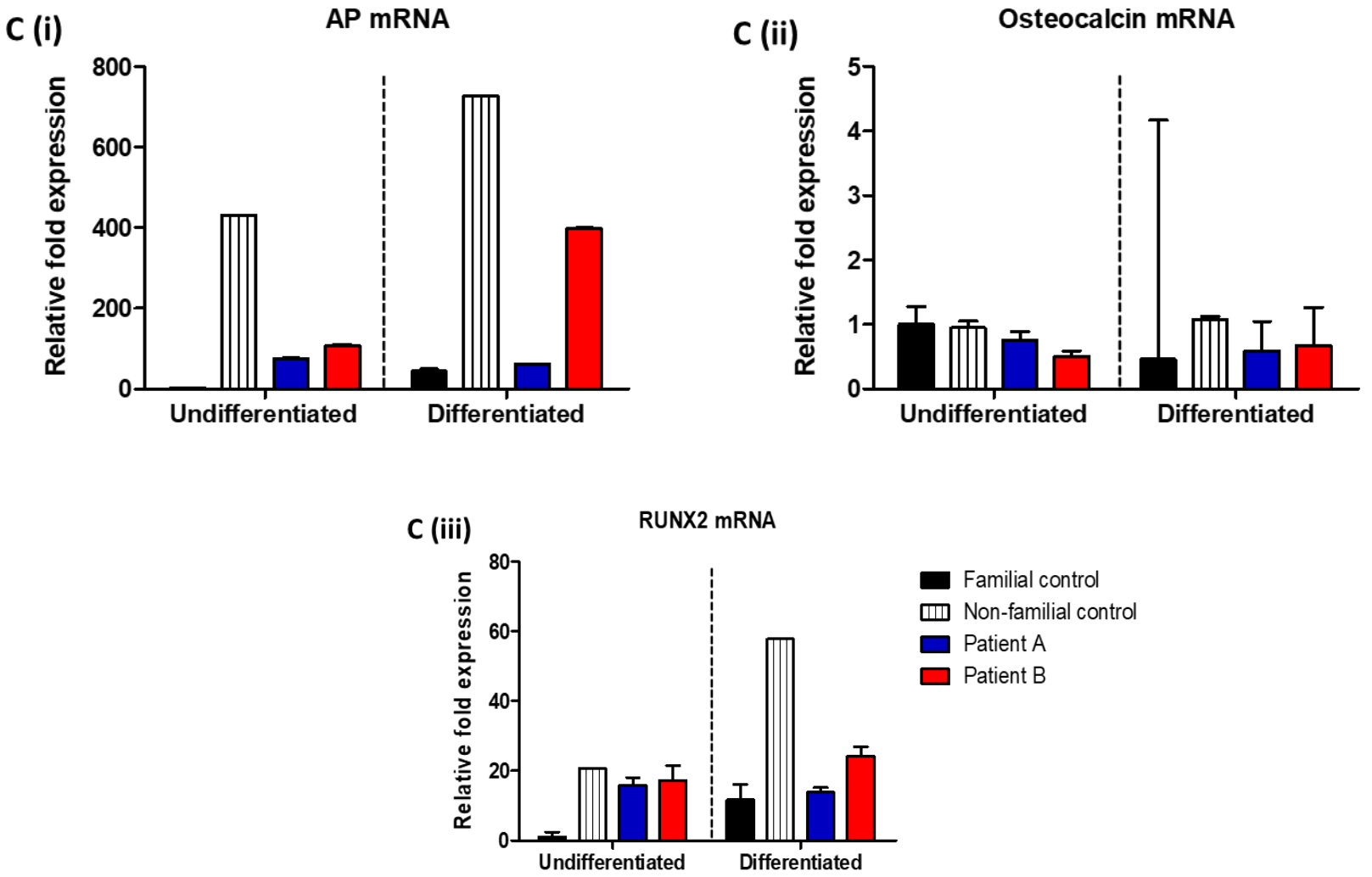

Figure 3.5: Alizarin red staining and expression of osteogenic markers. (Ai; ii) iPSC-derived MSCs were differentiated towards the osteogenic lineage and stained with alizarin red S (ARS) stain. **(Bi; ii)** Alizarin red staining and microscopic imaging of ARS in differentiated and undifferentiated control iPSC-MSC samples. Alizarin red staining and microscopic imaging of in differentiated and undifferentiated patient iPSC-MSC samples. **(Ci-iii)** mRNA expression of osteogenic markers (*AP*, *osteocalcin* and *RUNX2*) was analysed in differentiated iPSC-MSCs and compared to undifferentiated cells. Two biological repeats were performed for osteogenic differentiation and ARS stain. Data presented as mean ± SEM (n = 2).

3.3.1.3 iPSC-MSC show limited Oil red O staining and low levels of adipogenic markers

To determine the ability of iPSC-MSCs to differentiate towards the adipogenic lineage, they were maintained in growth medium supplemented with adipogenic cocktail (0.5 mM IBMX, 1 µM dexamethasone, 100 µM indomethacin, and 10 µg/ml insulin) for 21 days. After 21 days of adipogenic induction oil red O (ORO) staining was performed. Adipose-derived MSC (AD-MSCs) which were used as a positive control indicated positive staining of ORO and high expression of adipogenic markers (PPARγ; C/EBPα; FABP4) (Fig. 3.6A) compared to undifferentiated cells (Figure 3.6B). By day 21 of adipogenic differentiation, the iPSC-MSCs revealed smaller and fewer lipid droplets after ORO staining [Fig 3.6 C (i)]. Expression of *PPARγ* [Fig. 3.6C (ii)] and *C/EBPα* [Fig. 3.6C (iii)] mRNA, which are early adipogenic markers as well as *FABP4* [Fig 3.6C (iv)] a late marker, indicated low or similar expression levels as undifferentiated cells. The qPCR data thus confirmed the low ORO staining indicating that expression of the key adipogenic genes were induced at very low levels. Three biological repeats were performed for the 21-day differentiation with similar findings, and two biological repeats were performed for the 30-day adipogenic induction. Extension of adipogenic differentiation in iPSC-MSCs to 30 days indicated a slight increase in adipocytes indicated by ORO staining (Fig 3.6D), however, high variation in the expression of adipogenic genes 30 days post-induction. These results demonstrate that iPSC-derived MSCs have less adipogenicity compared to AD-MSCs

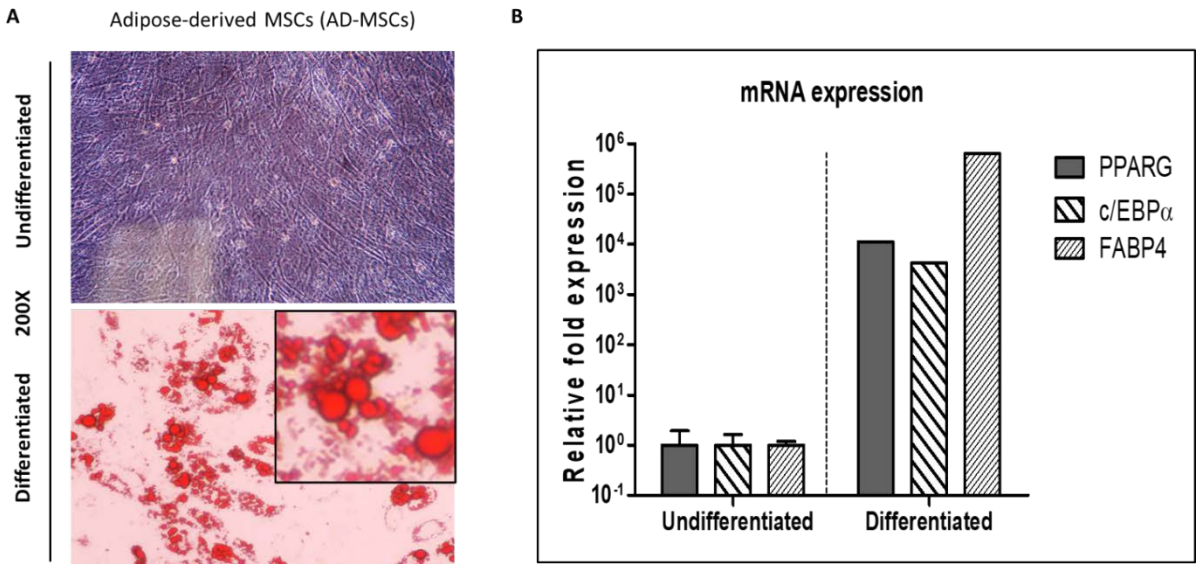

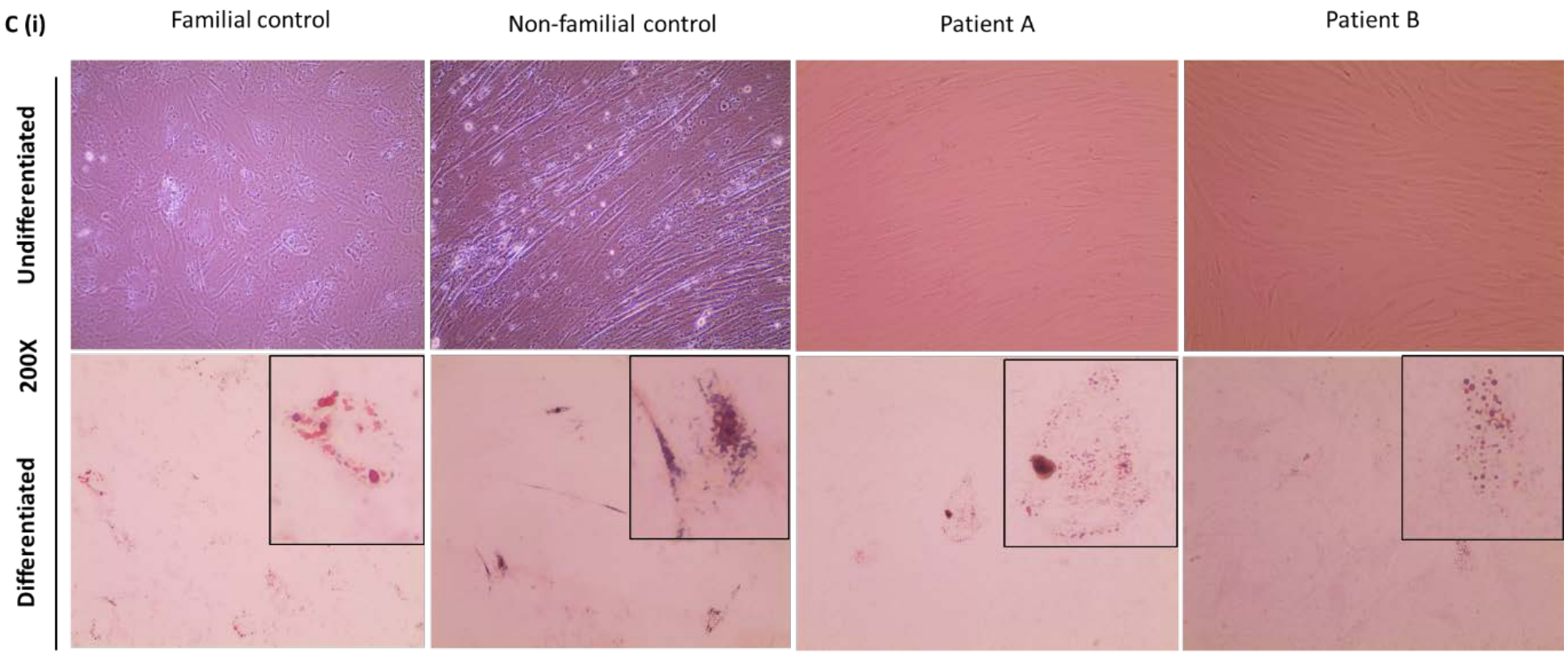
C (i)
Familial control
Non-familial control
Patient A
Patient B
Undifferentiated
200X
Differentiated

C (ii)

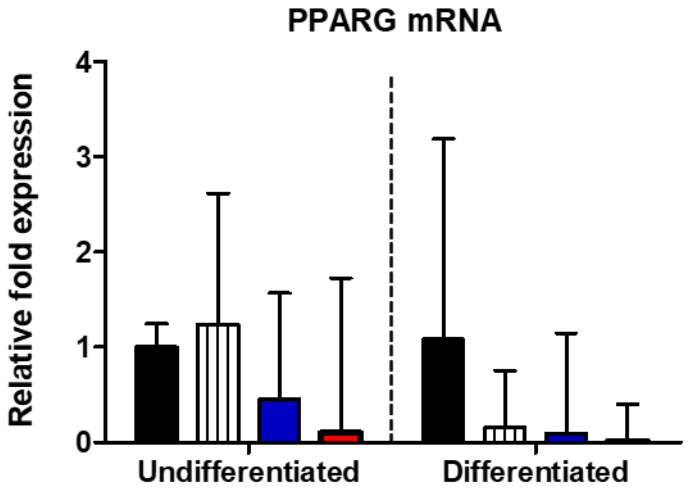
PPARG mRNA
Relative fold expression
4
3
2
1
0
Undifferentiated
Differentiated

C (iii)

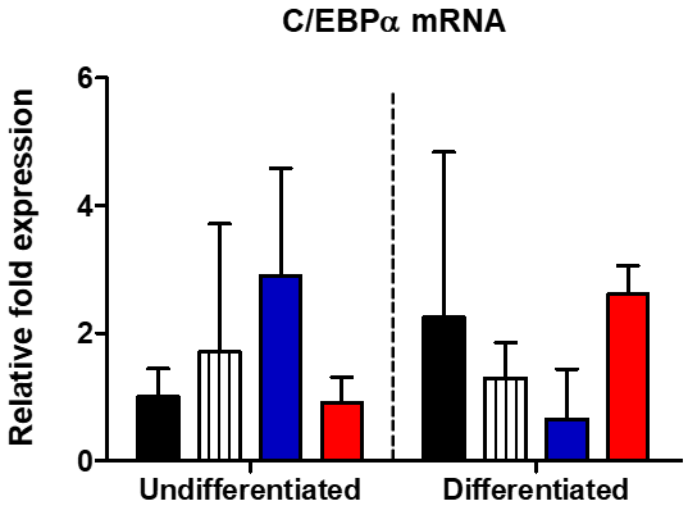
C/EBPα mRNA
Relative fold expression
6
4
2
0
Undifferentiated
Differentiated

C (iv)

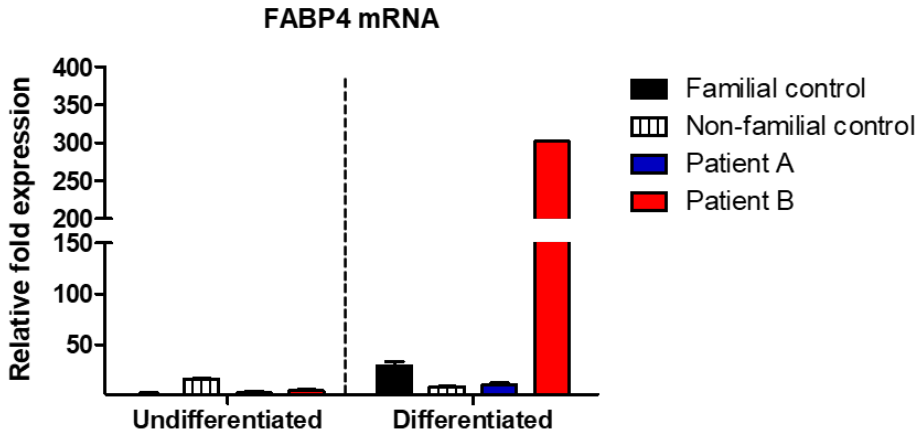
FABP4 mRNA
Relative fold expression
400
350
300
250
200
150
100
50
Undifferentiated
Differentiated
Familial control
Non-familial control
Patient A
Patient B

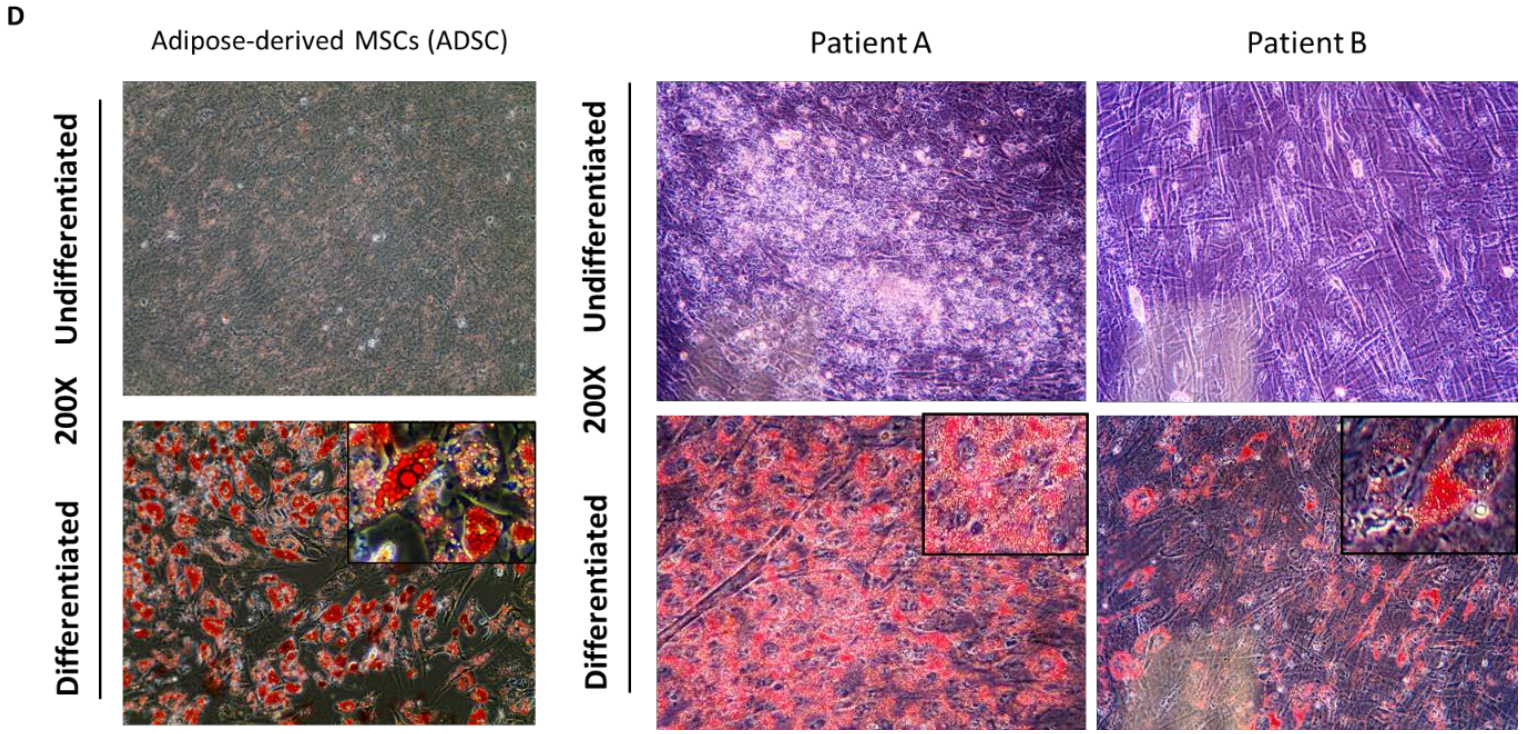

Figure 3.6 Analysis of adipogenic differentiation in iPSC-MSCs. Patient and control iPSC-MSCs were differentiated for 21 days and stained with Oil Red O (ORO). **(A)** Adipose-derived MSCs (AD-MSCs) show positive ORO staining of lipid droplets and **(B)** high expression of adipogenic genes (PPARγ, C/EBPα and FABP4) compared to undifferentiated cells. **(Ci)** Oil red staining and expression of adipogenic genes **(Cii)** PPARG; **(Ciii)** C/EBPα; **(Civ)** FABP4 in differentiated and undifferentiated patient and control cells at day-21 of differentiation. **(D)** iPSC-MSCs showed a slight increase in lipid droplets following ORO staining after 30 days of adipogenic differentiation. Data are presented as mean ± SEM (n = 3).

3.3.2 Expression of pro-fibrotic markers in patient-derived iPSC-MSCs

3.3.2.1 Patient-derived iPSC-MSCs do not express higher levels of pro-fibrotic markers than control cells

The hallmark of POIKTMP is multi-systemic fibrosis, specifically of the skin, skeletal muscle and tendons with lung fibrosis being the leading cause of death (Khumalo et al., 2006; Mercier et al., 2013). Since the mechanism by which the *FAM111B* mutation induces fibrosis in POIKTMP patients is currently unknown, we hypothesised that the mutation leads to the overexpression of pro-fibrotic markers and increases deposition of collagen type I and III. To test this hypothesis, endogenous expression of key pro-fibrotic makers (α-SMA; COL1A1, COL3A1) were analysed by qPCR in iPSC-MSCs. The aim was to determine if the patient iPSC-MSCs overexpress these pro-fibrotic markers similarly to systemic sclerosis (Gabrielli et al., 2009; LeRoy, 1974).

When the mRNA expressions of *COL1A1*, *COL3A1* and *α-SMA* were analysed in this study, there was no statistical difference between patients and controls (Fig. 3.7A). Protein analysis of α-SMA showed overall non-statistical significance between patients and controls (Fig. 3.7B). These results indicate that under the culture conditions of these experiments the patient iPSC-MSCs do not overexpress COL1A1, COL3A and α-SMA pro-fibrotic markers.

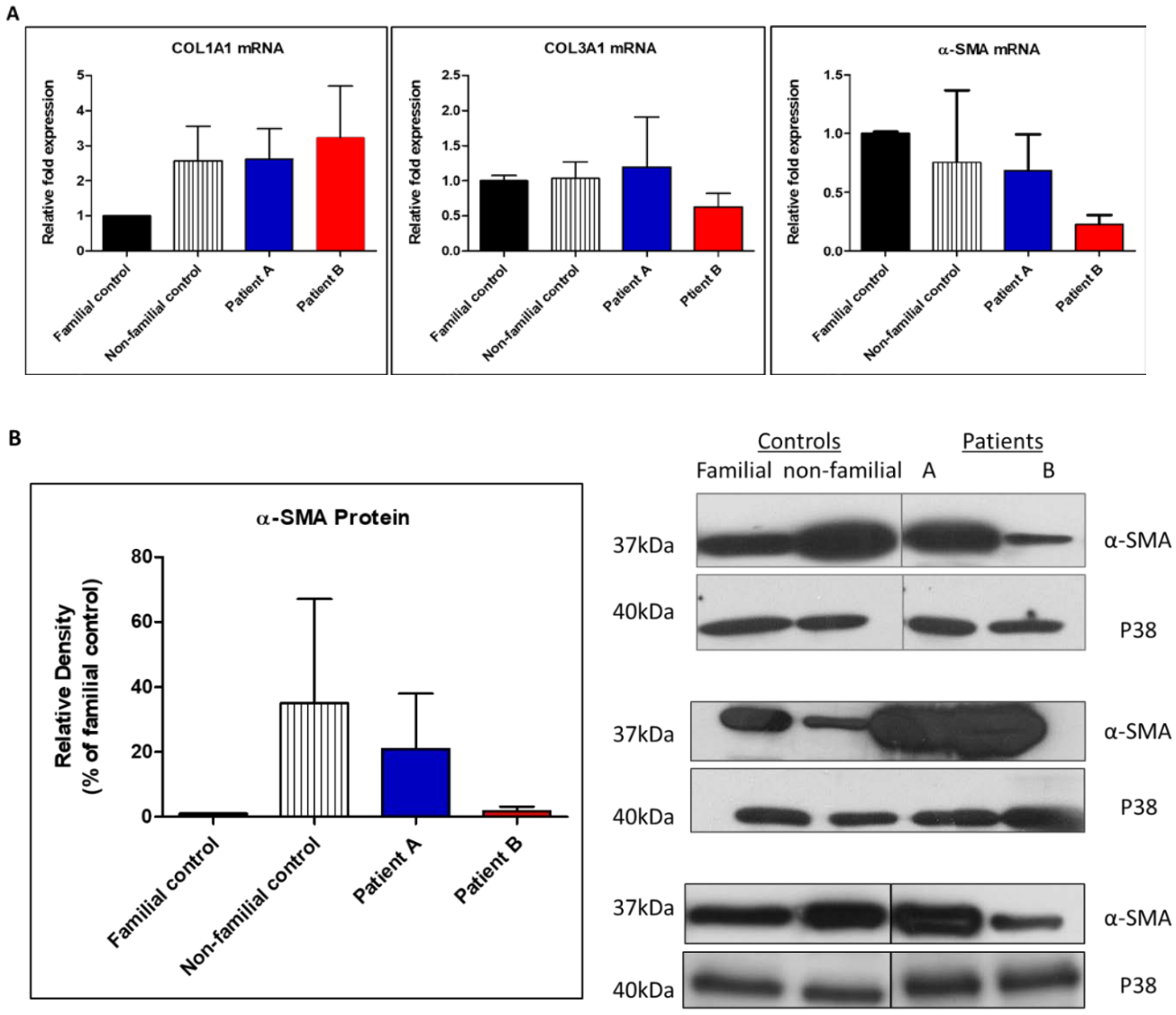

Figure 3.7 Expression of fibrosis markers in patient and control iPSC-MSCs. (A) Endogenous mRNA expression for COL1A1; COL3A1 and α-SMA was measured in patient and control iPSC-MSCs. **(B)**. Western blotting and densitometric analysis for α-SMA protein expression (shown in % relative to the familial control) was performed in patient and control iPSC-MSCs. Data are presented as mean ± SEM (n = 4). * $p < 0.05$; ** $p < 0.01$

3.3.2.2 Patient cells reveal normal collagen levels following picrosirius red staining and quantification

Since fibrosis is not only caused by high collagen expression but could have also been caused by a dysregulation in the breakdown of collagens and other ECM proteins. This would result in an accumulation of these proteins. Therefore, the next experiment was to determine if there are changes in total collagen content between POIKTMP patients and controls. Patient and control iPSC-MSCs were seeded onto gelatin-coated culture plates and

maintained in standard growth medium till the cells reached 80% confluence. When confluent, they were maintained in DMEM supplemented with 1% FBS for 24 h and thereafter stained with Picrosirius red. Two biological repeats were performed for PSR staining and quantification. Picrosirius red (PSR) staining, which stains collagen indicated similar amounts of collagen between patients and controls (Fig 3.8A). The quantified PSR stain also demonstrated that patients and control iPSC-MSCs contained similar amount of collagen (Fig. 3.8B). These results indicate that the patient cells contain normal levels of collagen proteins.

Overall, these results indicate that POIKTMP is distinct from other hereditary fibrotic disorders such as SSc, which show that patient fibroblasts and MSCs express high levels of these pro-fibrotic markers *in vitro* (LeRoy, 1974; Lu et al., 2017a; Vanneaux et al., 2013). It should be noted, in interpreting these experiments, that *in vitro* culture seems to upregulate the basal levels fibrotic proteins, such as collagens: this might mask any differences that might been seen between patient and control cells.

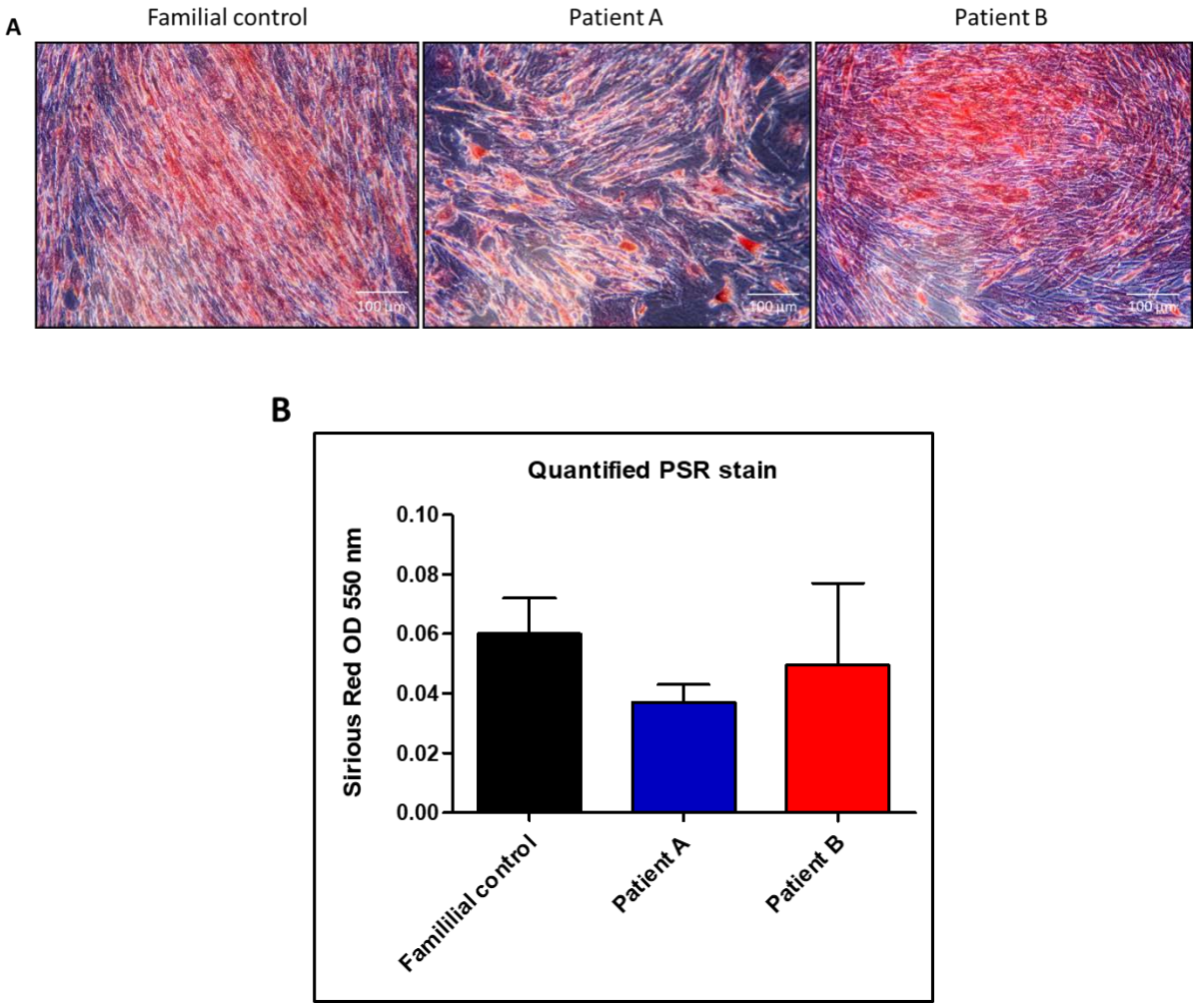

Figure 3.8 Staining and quantification of collagen in iPSC-MSCs. (A) Picrosirius red staining of collagen in Patient and control iPSC-MSCs. **(B)** Spectrophotometric quantification of eluted Picrosirius red stain as a measure of total collagen in patient and control iPSC-MSCs. Data are presented as mean ± SEM (n = 2) (scale bar = 100 µm).

3.4 Discussion

3.4.1. iPSC-derived mesenchymal stem/stromal cells demonstrate MSC characteristics with reduced adipogenicity

Multi-systemic fibrosis is the primary phenotype in POIKTMP, and pulmonary fibrosis is the cause of death in the South African kindred. It was therefore valuable to determine, in cell specific assays, whether the *FAM111B* mutation results in an increasing the expression or accumulation of key fibrotic markers including COL1A1, COL3A1 and α-SMA.

Most of the affected tissues in POIKTMP are of mesenchymal lineage, therefore, iPSCs were differentiated into mesenchymal stem/stromal cells (iPSC-MSCs) to determine expression of key pro-fibrotic markers in patient cells. Derivation of iPSC-MSCs was performed via embryoid body formation, with ascorbic acid and serum as the main molecules used to drive mesodermal/mesenchymal lineage differentiation. Characterisation of iPSC-MSCs revealed that these cells have the fibroblast-like morphology and express typical MSCs markers (CD73, CD90 and α-SMA). Osteogenic and adipogenic differentiation in iPSC-MSCs indicated that iPSC-MSCs possess adequate osteogenic differentiation and limited adipogenicity. Analysis of osteogenic differentiation also revealed some variation between samples. For example, the familial control and Patient A indicated moderate Alizarin red S (ARS) staining for detection of mineralisation in osteogenic cells, which was supported by the low expression of osteogenic markers (*AP* and *RUNX2*) in these samples. The non-familial control and Patient B on the other hand, showed extensive osteogenic induction (Fig. 3.5 B-C). These findings thus indicate that the variation between samples may be due to clone variation and not the POIKTMP condition as Patient A showed less osteogenic differentiation and Patient B showed high osteogenicity. Other clones for the familial control and Patient A need to be tested osteogenic differentiation.

Limited adipogenic induction was observed in all iPSC-MSC samples. Following a 21-day adipogenic induction, all iPSC-MSCs demonstrated less adipogenic differentiation with very small and few lipid droplets compared to adipose-derived MSCs (AD-MSCs) (Fig 3.6 A-C). Furthermore, qPCR analysis indicated low expression of adipogenic genes (PPARγ; C/EBPα and FABP4) in differentiated iPSC-MSCs. Though there was a slight increase in adipogenesis after a 30-day induction, the areas of differentiation in iPSC-MSCs remained sparse. Similar findings were reported by Kang et al. (2015), who demonstrated that

iPSC-derived MSCs retain adequate osteogenic and chondrogenic differentiation capacity but less adipogenicity. Though a different method was used to derive MSCs from iPSCs in this study compared to a study by Kang et al. (2015), the same results were obtained in both studies, thus indicating that limited adipogenicity is a feature of iPSC-MSCs. Chondrogenic differentiation though not performed in this study was conducted by Dr Robea Ballo, who reported that iPSC-MSCs derived in this study indicated adequate chondrogenic differentiation (data not shown). Overall, the iPSC-MSCs demonstrated sufficient MSC phenotype and characteristics.

3.4.2 Changes in the expression of key pro-fibrotic markers were not detected in patient cells carrying the *FAM111B* mutation

Endogenous expression of pro-fibrotic markers was analysed in iPSC-MSCs to determine whether the *FAM111B* mutation increases expression of these genes thereby leading to fibrosis. The data in this study indicated that patient cells express similar levels of *COL1A1*, *COL3A1* and *α-SMA* compared to controls. Protein expression of α-SMA also indicated similar levels between patients and controls, thus suggesting that patient iPSC-MSCs remained in a non-myofibroblast state. Picrosirius red staining and quantification also indicated similar levels of collagen deposition between patient and control cells, which confirmed qPCR and western blot data. These findings indicate that FAM111B mutation does not alter the expression of pro-fibrotic markers analysed in this study, thereby suggesting that fibrosis may be a secondary effect of the gene mutation. The data in this study further indicate that POIKTMP differs from conditions such as SSc, which have been shown to cause constitutive expression of pro-fibrotic markers in affected (LeRoy, 1974).

Hereditary fibrosing poikiloderma studies have revealed variation in the phenotype caused by FAM1111B mutations. It is suggested that mutations located on codons 625, 627 and 628 (see Table 1.2) have a severe phenotype and early onset of the disease (Takeichi et al., 2016). However, other cases with varying phenotype from the South African kindred have been reported by Seo et al. (2016) and Goussot et al. (2017). A study by Seo et al. (2016) showed that the *FAM111B* mutation (c.1261_1263delAAG, p.Lys421del) causes exocrine pancreatic dysfunction, and a study by Goussot et al. (2017) reported a case of pancreatic cancer associated with another *FAM111B* mutation (c.1884T>A, p.Ser628Arg).

The fibrosis phenotype has been shown to be extensive in the South African kindred (Khumalo et al., 2006) while other cases have primarily reported muscle degeneration and elastic sclerosis in the skin (Mercier et al., 2013). These studies further expand the possible role of FAM111B in cellular processes. This chapter has shown that FAM111B does not alter the expression and pro-fibrotic genes as postulated, however, since wound healing is a complex process, the role of FAM111B cannot be completely excluded from this process. Since FAM111B has also been indicated to play a role in cell proliferation, though the mechanism has not been described (Aviner et al., 2015), it is therefore, suggested that FAM111B modulates cell proliferation during wound healing. The next chapter of this study will thus explore this hypothesis.

Because no animal model exists for studying this condition due to lack of FAM111B homologues in *Mus musculus* species, the use of derived iPSCs for further differentiation into other affected cells types proves to be an advantage as derivation of other cell types may reveal new insights into the mechanism by which FAM111B induces fibrosis. For example, using iPSC-derived alveolar epithelial cells as another cellular model may indicate if derived alveolar cells from affected individuals continuously undergo epithelial-mesenchymal transition (EMT) that is known to occur during tissue repair and fibrosis (Coward et al., 2010; Li et al., 2016). Also, iPSCs can be used to derive organoids for skin and lung tissue, which could mimic the 3D structure and function of that specific cell type more effectively than 2D cultures (Dutta et al.). Studies have shown the successful derivation of 3D organoids for modelling of neurodegenerative diseases such as neural crest cell to model Alzheimer's Disease (Raja et al., 2016). Furthermore, the use of 3D matrices for creating an in vivo microenvironment could also improve the current models for studying fibrosis in vitro (Jeon et al., 2016; Xu et al., 2015). Application of these model systems would hopefully improve future work into understanding the mechanism by which the *FAM111B* mutation induces multi-systemic fibrosis in POIKTMP patients.

Chapter 4

FAM111B mutation affects cell proliferation in poikiloderma patient-derived iPSC-MSCs

4.1 Introduction

In normal tissue fibroblasts are in a quiescent state but during wound healing they are activated to proliferate and transdifferentiate into myofibroblasts resulting in collagen and ECM production (Wynn, 2008; Yeo et al., 2018). There is also recruitment of bone marrow-derived mesenchymal stem/stromal cells that convert into myofibroblasts that further contribute to the synthesis of collagen and other ECM proteins (Chakraborty et al., 2014; Wynn, 2008). Upon completion of tissue repair the myofibroblasts are removed by apoptosis and senescence. However, the signals that lead to apoptosis or senescence have not been clearly defined (Desmoulière et al., 1995; Krizhanovsky et al., 2008). It has also been shown that the myofibroblasts that escape apoptosis and/or senescence revert to their inactive fibroblast state. For instance, a study by Desai et al. (2014) showed in adipose-derived MSCs that their exposure to TGF-β leads to myofibroblast formation and treatment with growth factors such as bFGF reverses the myofibroblast phenotype. Another *in vitro* study by Garrison et al. (2013) demonstrated that foetal and adult lung fibroblasts treated with TGF-β transdifferentiate into myofibroblasts and revert to their fibroblast state when treated with prostaglandin E2 (PGE_2).

In contrast to normal wound healing, during fibrosis, myofibroblasts evade apoptosis and persist in their active state, which results in further proliferation and ongoing collagen and ECM production (Horowitz et al., 2016; Vancheri et al., 2010). A study by van Spreeuwel et al. (2017), for example, showed that in cardiac fibrosis there is an increased number of resident fibroblasts which cause excessive production and deposition of collagen and other ECM proteins. A study on experimental idiopathic pulmonary fibrosis (IPF) study showed that primary fibroblasts obtained from patients with IPF proliferated faster compared to lung fibroblasts obtained from healthy individuals (Raghu et al., 1988). Furthermore, lung fibrosis studies using the bleomycin mouse model for fibrosis also indicated that there is an increase in the number of lung fibroblasts which correlates to increased collagen and other ECM proteins (Blaauboer et al., 2013; Chen et al., 2008; Löfdahl et al., 2018).

There have been a number of studies that have revealed that the increase in cell proliferation during fibrosis is caused by the upregulation of proteins involved in the cell cycle such as cyclin D1, which activates cell cycle progression from the G1 to S-phase. For example, a study by Watts et al. (2006) showed that a population of fibroblasts derived from lung biopsies of patients with IPF expressed higher levels of cyclin D1 via activation of the Rho A kinase pathway. Another study also indicated that alveolar epithelial cells obtained from patients with IPF differentiate into myofibroblasts via EMT and express high levels of cyclin D1 (Akram et al., 2014). These studies thus indicate that increased cell proliferation observed in fibrosis is also caused by cell cycle changes.

As briefly discussed in the literature review (section 1.4), FAM111A and FAM111B have been shown to play a role in cell proliferation and cell cycle progression. Both proteins have been reported to be associated with the DREAM complex which regulates cell cycle repression and activation (Litovchick et al., 2007). The ChIP Enrichment Analysis (ChEA) data indicated that the FAM111B promoter specifically binds to E2F1 in breast cancer cells (MCF7) and to E2F4 in lymphoblastoid cells (http://amp.pharm.mssm.edu/lib/chea.jsp). E2F1 has been described to activate expression of target genes, while E2F4 has more recently been suggested to have dual ability to repress and activate expression of target genes (Lee et al., 2012). Since both transcription factors form part of the DREAM complex, they possibly activate FAM111B expression during cell cycle progression (Popov & Petrov, 2014; Sadasivam & DeCaprio, 2013).

In support of this hypothesis, a study by Aviner et al. (2015) was the first to show that FAM111B is expressed in a cell cycle-dependent manner. Using multi-omic analysis (transcriptomics and proteomics) they showed that in synchronised HeLa S3 cellsFAM111B expression increases at the G1→S transition, with an mRNA peak at G1 and a protein peak at the S-phase, and low at the G2/M phase. Furthermore, their data indicate that FAM111B expression correlates with PCNA expression in these cells. Because FAM111B peaks at S-phase, they propose that FAM111B may be involved in DNA replication or forms part of the S-phase machinery.

Interestingly, cancer-associated studies have also shown a link between FAM111B and cancer progression. A study by Peng et al. (2008) reported that FAM111B (also known as the cancer-associated nuclear protein (CANP) mRNA expression is higher in human foetal tissue and cancer cells, compared to differentiating cells and adult tissues. They further

reported that FAM111B mRNA levels are higher in hepatic carcinoma cells compared to HepG2 cells. A separate study using integrated bioinformatic analysis of public microarray data revealed that FAM111B is among the top genes that are upregulated in lung squamous cell carcinoma (Zhang et al., 2017). These results overall suggest that in various types of cancer, FAM111B is upregulated and overexpressed. A complementary approach was to ask whether FAM111B is reduced in cancer cells following treatment with anticancer agents. In the first of such studies using a transcriptomic approach, Yue et al. (2015) showed that FAM111B was downregulated over 20-fold in a pancreatic cancer cell line (PANC-1) following dual treatment with metformin and aspirin. Another study by Baselet et al. (2017) indicated that the expression levels of FAM111B together with *MKI67,* which encodes a cell proliferation marker, were decreased in endothelial cells that were subjected to a single x-ray dose of ionizing radiation, which inhibits cell proliferation. These studies indicate that FAM111B is among the genes, including cell cycle genes which are altered during cancer treatment. It should be noted when interpreting these experiments, that one cannot distinguish between two possible interpretations: i.e. whether a decrease in the proliferation of cancer cells is a downstream consequence to a decrease in FAM111B expression, or whether FAM111B expression is decreased due to the global effect of anti-cancer drugs.

Another important connector is that several studies have shown similarities in the pathogenesis of fibrosis and cancer (Kalluri, 2016; Schäfer & Werner, 2008; Vancheri et al., 2010). Though distinct in their onset and progression, there are clear parallels as well as common cellular and molecular mechanisms that are activated in fibrosis and cancer (Schäfer & Werner, 2008). For instance, studies have shown that tumour stroma resembles the granulation tissue of wound healing, which also comprises of inflammatory cells and myofibroblasts (Balkwill et al., 2005). Furthermore, cancer has also been hypothesised to be an “overhealing wound” as malignant tumours have often been found to occur at sites of chronic injury caused by chronic inflammation (Schäfer & Werner, 2008). Also, it was previously postulated that chronic irritation and previous injuries are preconditions for tumorigenesis (Dvorak, 1986). Moreover, long-term inflammatory cells in chronic inflammation act as tumour promoters thus creating what is known as a neoplastic tissue with a microenvironment that is favourable for tumour growth and progression (Balkwill et al., 2005). In neoplastic tissue there are also tumour-associated macrophages (TAMs) that acquire the type 2 (M2) macrophage phenotype which further induces secretion of anti-inflammatory cytokines (IL-10 and TGF-β) to promote tumour proliferation, progression and

ECM deposition (Balkwill et al., 2005; Obermueller et al., 2004; Pollard, 2004). Activation of the EMT pathways has also been shown to contribute to tumour stroma which increases susceptibility to tumour formation and metastasis in liver fibrosis (Sawada et al., 2001; Tse & Kalluri, 2007). Additionally, as in fibrosis, tumour-associated myofibroblasts have been indicated to exhibit high proliferation and migratory phenotype thus inducing tumour invasion and metastasis (Liu et al., 2011; Spector et al., 2012). Moreover, the presence of myofibroblasts in cancer stromal tissues, similar to those in fibrotic tissues produce higher levels of collagen I; this regulates the expression of genes involved cell signalling and metabolism for tumour progression, apoptosis and invasion (Spector et al., 2012). Increased collagen and ECM production has also been associated with downregulation of E-cadherin (cell-cell adhesion marker) in cancer epithelial cells. It was previously shown in an *in vitro* study that pancreatic cancer cells (PANC-1) cultured on type I and III collagen result in downregulation of E-cadherin expression compared to PANC-1 cells that were cultured on fibronectin or type IV collagen (Menke et al., 2001). This study further showed that the loss of E-cadherin results in epithelial-to-mesenchymal morphology.

Microarray studies have revealed further similarities in gene expression patterns between early wound healing and cancer. For example, Chang et al. (2004) indicated that the gene expression signature of serum-activated fibroblasts was similar to that of cancer cells as it included high expression of cell cycle genes (e.g. *E2F1*) and extracellular matrix remodelling genes (e.g. *LOXL2*) which are involved in cancer progression and metastasis. Importantly, in relation to the work in this thesis, there has also been an identification of mutations in genes associated with cell cycle progression in fibrosis and cancer. A study by Guyard et al. (2017), for example, identified by next-generation sequencing (NGS), mutations in *p53*, *β-catenin* (*CTNNB1*) and the *phosphatase and tensin homolog* (*PTEN*) genes from patients who presented with lung fibrosis-associated lung cancer. It is well established that mutations in the *p53* tumour suppressor gene lead to aberrant DNA repair and deregulated cell cycle arrest causing tumorigenesis (Rivlin et al., 2011; Vancheri et al., 2010). β-catenin, which activates the Wnt signalling pathway during development is also involved in cell proliferation by activating transcription of cycling D1 (Olmeda et al., 2003). Mutations in the *β-catenin* gene (exon 3) have been associated with colorectal cancer (Ilyas et al., 1997; Johnson et al., 2005). A study by Kaler et al. (2012) showed that co-culture of human colorectal carcinoma cells HCT116 (which harbour the wildtype and mutant *β-catenin* alleles) with THP1 macrophages induce enhanced Wnt-signalling in the tumour stroma, thus

changing the anti-tumour properties of macrophages into tumour-associated macrophages. In fibrosis, it seems most likely, that mutations in β-catenin induce increased proliferation of myofibroblasts and expression of ECM proteins by activation of M2 macrophages that secrete growth factors which further activate the TGF-β pathway, leading to expression of collagen I and other ECM proteins (Enzo et al., 2015; Zhou et al., 2012). Mutation on the *PTEN* gene which encodes a tumour suppressor lead to cancer caused by increased cell proliferation and downregulation of cyclin kinase inhibitor p21 (Sun et al., 1999). Furthermore, knockout of *PTEN (PTEN* $^{-/-}$*)* in fibroblasts derived from IPF lung biopsies caused formation of myofibroblasts (White et al., 2006).

Overall, these studies indicate that mutations in genes that are associated with cell proliferation and cell cycle progression potentially cause fibrosis and/or cancer. This link is important as mutations in the *FAM111B* gene are associated with fibrosis and cancer (Goussot et al., 2017; Mercier et al., 2013). It is, therefore, plausible that FAM111B is also the link between fibrosis and cancer. This notion is supported by a case report by Goussot et al. (2017) which indicated that a *FAM111B* mutation causes pancreatic cancer instead of the fibrotic phenotype commonly observed in POIKTMP cases. These results suggest that description of the POIKTMP phenotype should be expanded to include cancer predisposition.

In summary, the studies above have revealed tantalising evidence that FAM111B plays a role in cell proliferation and that increased cell proliferation during wound healing and tissue repair is also a key factor in chronic wound repair and fibrosis. To date there have been no studies to determine whether cells carrying a FAM111B mutation have an altered proliferation potential as compared with normal cells. The derivation of patient and control cells derived from iPSCs has enabled this question to be explored. The approach taken to address this hypothesis was therefore:

a) To determine if there are differences in cell proliferation rates between patient and control iPSC-MSCs.
b) To determine whether there is increased expression of FAM111B in rapidly dividing cells (iPSCs) compared to adult cells (dermal fibroblasts) and multipotent stem cells (iPSC-MSCs).
c) To determine whether FAM111B expression is differentially expressed during cell cycle progression as indicated by Aviner et al. (2015), and if so, whether its expression is altered in patients compared to controls.

4.2 Materials & methods

4.2.1 Growth rate of patient and control iPSC-MSCs

To investigate the involvement of FAM111B in cell cycle regulation, a 6-day growth curve for patients and control iPSC-MSCs was performed. The iPSC-MSCs were seeded onto gelatin-coated 6-well plates at 3 x 10^4 cells per well to prevent myofibroblast morphology which MSCs exhibit when cultured on uncoated plastic dishes (Kanta, 2015). Each sample was seeded in duplicates for each day count and maintained in standard growth medium (DMEM; 10% FBS; 1% P/S). The cell counts were performed every 2 days for 6 days. Briefly, growth medium was aspirated, and cells were washed twice with 1X PBS, followed by a five minutes incubation with trypsin/EDTA at 37° C to dislodge the cells. Trypsin/EDTA was deactivated with two ml growth medium and 12 µl of medium containing cells was mounted onto a haemocytometer (Marienfeld Superior, Germany) for cell count. Cells were counted at their log-phase on days 0, 2, 4 and 6. Cell doubling time was calculated at the log phase using the following equation: $DT = T\ ln2/ln\ (Xe/Xb)$ in which T is the incubation time in hours, Xb is the cell number at the beginning of the incubation time and Xe is the cell number at the end of incubation time (Aliborzi et al., 2016).

4.2.2 Synchronisation of patient and control iPSC-MSCs

For analysis of FAM111B expression in synchronised cells, iPSC-MSCs were synchronised using double thymidine block (Banfalvi, 2011). Because different cells have different properties, it is not a simple matter to decide how to the blocking should be conducted, it was thus necessary to optimise the blocking time and the concentration of thymidine. This was done using the control iPSC-MSCs. Briefly, 2x10^5 iPSC-MSCs were seeded onto gelatin-coated 100 mm culture plates using standard growth medium (DMEM; 10% FBS; 1% P/S). When the cells reached 40-45% confluence, they were arrested at the G1/S phase by blocking with 4 mM thymidine (Sigma Aldrich, St Louis, MO) prepared in basal DMEM for 24 hours (h). After the first 24 h thymidine block, the cells were released from the G1/S arrest by removing growth medium and rinsing the cells twice with 1X PBS. Fresh growth medium was added for 12 h before the second thymidine block. Following the second 24 h block, the cells were washed twice with PBS and fresh growth medium for harvesting. For mRNA analysis, the cells were harvested at 0, 2, 6, 12 and 15 h timepoints, which coincide with the

G1/S, early S, late S and G2/M cell cycle phases. For mRNA analysis qPCR was performed as described below. The proliferating nuclear antigen (PCNA) which is known as a sliding clamp at the DNA replication fork (Dieckman et al., 2012; Moldovan et al., 2007) was used as a G1 and S-phase marker for qPCR analysis. Aurora kinase A (AURKA) which is involved in the regulation of centrosome maturation and spindle formation during mitosis (Marumoto et al., 2005; Nikonova et al., 2013) was used as a marker for cells analysed at the G2/M phase. Therefore, it is suggested that the pancreatic cancer phenotype in the POIKTMP case report by Goussot et al. (2017) is due to the FAM111B mutation in the affected person.

For FAM111B protein determination in synchronised iPSC-MSCs, 4 mM double thymidine block (24 h thymidine, 12 h release, 24 h thymidine) was performed to obtain a cell population arrested at the G1/S and S-phase. To obtain a cell population arrested at the G2/M phase, a single 24 h thymidine (4 mM) block was performed, followed by an 18 h nocodazole (150 ng/ml) block. Cells arrested at the M-phase were collected by shaking off the rounded cells and collecting them into a 15 ml tube and centrifuged at 1500 RPM for 5min at RT. The supernatant was removed, and the cells were rinsed with 1X PBS, centrifuged and pooled with the adhered cells which were arrested at the G2-phase for analysis.

4.2.3 Flow cytometry

For validation of cell synchronisation, the familial control was prepared for flow cytometry post-thymidine and nocodazole block. For analysis of DNA content at the G1 and S-phase, the iPSC-MSCs were rinsed with twice 1X PBS and trypsinised using trypsin/EDTA for five minutes and thereafter collected and centrifuged at 1500 RPM for five minutes at RT. The cell pellet was resuspended in 2 ml 1X PBS for cell counting. Cells were fixed by adding eight ml of ice-cold 70% ethanol to the cell suspension and stored at -20° C for 1 h. After 1 h, the cells were centrifuged at 1500 RPM for five min at RT followed by removal of the supernatant and rinsing the cells with 1X PBS to remove excess ethanol. The cells were rinsed twice 1 ml PBS and after removal of the supernatant were incubated with 0.5 ml of FxCycle™ PI/RNase Staining Solution (Life Technologies) at RT for 30 minutes in the dark. The stained cell pellets were thereafter for distribution of DNA content by flow cytometry.

4.2.4 RNA isolation and analysis

4.2.4.1 RNA extraction

For analysis of mRNA extraction, total RNA isolation from cells using the High Pure RNA Isolation Kit (Roche) per the manufacturer's instructions. Briefly, 0.2 ml of 100% chloroform was added to every 1 ml of the cell lysates, vigorously mixed by inverting for 15 seconds (s) and incubated at room temperature for 15 minutes. The lysates were thereafter centrifuged at 4 °C and 12 000 x *g* for 15 min. After centrifugation, the aqueous phase which contained RNA was transferred into new microfuge tube and equal volume of 70% ethanol was added to aqueous phase and mixed 10 times by pipetting up and down. The aqueous mixture was then transferred into a High Pure filter tube and 2 ml collection tube and thereafter centrifuged at 10 000 rpm for one minute. The flow-through was discarded and each sample was treated with 100 µl of DNase I for removal of genomic DNA contamination, and incubated at room temperature for 15 min. Following DNase I treatment, the samples were washed by adding 500 µl of Wash Buffer I and centrifuged at 10 000 rpm for one minute. The flow-through was discarded and the samples were washed again with 200 µl of Wash Buffer I and centrifuged as before. Following washes with Buffer I the samples were washed by adding 500 µl of Wash Buffer II and centrifuged at 10 000 rpm for one minute The flow-through was discarded and washed again with 200 µl of Wash Buffer II and thereafter centrifuged at 13 000 rpm for two minutes The flow-through was discarded and the samples were opened and incubated at room temperature for five minutes to allow evaporation of ethanol from the wash buffers. After five minutes, 30 µl of the Elution buffer were added to each sample and total RNA was measured using a nanodrop spectrophotometer (ND-1000, Thermo Fisher). RNA purity was measured at A260/A280 ratio. To determine RNA integrity one µg RNA was run on a non-denaturing 1% agarose gel containing ethidium bromide and electrophoresed at 100 volts (V) for 45 minutes The gel was viewed under UV light for detection of 28S and 18S ribosomal RNA bands.

4.2.4.2 cDNA synthesis

For cDNA synthesis, 0.5-1 µg RNA from each sample was reverse transcribed by addition of Oligo (dT) primers and running the reaction in the PCR machine at 42° C for five minutes, followed by adding the cDNA mastermix (1 mM dNTPs; 2.5 mM $MgCl_2$; 1x RT Buffer; 1 U/µl RNase inhibitor; 20 U M-MLV Reverse Transcriptase) [all reagents purchased from Promega except for dNTPs (Bioline)].

4.2.4.3 Quantitative real-time PCR (qPCR)

The quantitative real-time PCR (qPCR) Mastermix constituted of 200 ng of cDNA, 0.2 µM of forward and reverse primers, 1X (5 µl) SYBR Green I Mastermix (Life Technologies) and water to the final volume of 10 µl per sample. The qPCR reaction was performed using the StepOne Plus machine (Applied Biosystems, Life Technologies) at 95 °C denaturation for 15 s and 60° C annealing for one minute for 40 cycles. The results were analysed by relative quantitation using the delta delta (ΔΔ) Ct method, where samples were first normalised to β-glucuronidase (GUSβ) and/or β-actin housekeeping genes. Fold change ($2^{-\Delta\Delta Ct}$) was analysed by determining differences between the normalised target sample and normalised calibrator (control sample). Human dermal fibroblasts (HDFs) were used as negative controls for the expression of pluripotency markers.

Table 4.1: Primer sequences for FAM111B, PCNA and AURKA genes

Gene	Primer sequence	NM Sequence	Size (bp)	Reference
PCNA (F)	5’-AGGACCTGTTAAGGCTACA–3’	NM_182649	91	Aviner et al. 2015
PCNA (R)	5’-CCAAGGTATCCGCGTTATC–3’			
FAM111B (F)	5'-GACCGTAGTGTGTTTACAGCA-3'	NM_001142704.1	171	https://pga.mgh.harvard.edu/
FAM111B (R)	5'-GCACTTGAGAGGCATTCCTAAAT-3'			
AURKA (F)	5’-AGGACCTGTTAAGGCTACA–3’	NM_003600.3	104	Aviner et al. 2015
AURKA (R)	5’-GAGCCTGGCCACTATTTAC–3			

4.2.5 Western blotting

4.2.5.1 Cell harvesting & protein quantification

Patient and control iPSC-MSCs were culture to 90% confluence. Three-hundred µl of radioimmunoprecipitation assay (RIPA) buffer containing protease inhibitors were added to each 10-cm culture plate for cell lysis and collection. The lysate was centrifuged at 12 000 rpm and 4º C for 20 minutes. The supernatant was collected into a fresh microfuge tube, and protein concentration was quantified using the Bicinchoninic acid assay (BCA) assay (Thermo Fisher Scientific, Waltham, MA, USA). Briefly, a 1:8 dilution was prepared for the BCA solution and bovine serum albumin (BSA), which was used as a standard. The samples were also prepared at 1:8 dilution in a 96-well plate. The 96-well plate was incubated at 37º C for 30 minutes and the absorbance was thereafter read at 562 nm using the RT-2100C microplate reader (Rayto Life & Analytical Sciences, Shenzhen, China). The standard curve and protein concentration were analysed on Microsoft Excel using the linear equation [(y = a*x + b) where: y = Protein concentration; x = Absorbance; a = Slope and b = Background Signal]. The protein samples were stored at -80º C for later use or long-term storage.

4.2.5.2 Sodium-dodecyl-sulphate polyacrylamide gel electrophoresis (SDS-PAGE)

The SDS-PAGE gels were prepared using the BioRad electrophoresis apparatus (Biorad Mini PROTEAN©). Ten-percent resolving gels were prepared on 1.5 mm (thick) plates and 5% stacking gels were prepared for loading the samples (see appendix). Laemali sample buffer (2X) was added to each sample and boiled at 95º C for five minutes. Thirty micrograms of protein for each sample were loaded onto the gels and electrophoresed at 110 volts (V) in 1X running buffer for 90-120 minutes at room temperature. The loading control used was rabbit polyclonal anti-p38 (Cell Signalling Technology, Danvers, MA, USA) which is a 40 kDa protein.

4.2.5.3 Nitrocellulose membrane electro-transfer

Following SDS-PAGE, the resolving gels and nitrocellulose transfer membrane (Amersham Biosciences, UK) were soaked in in 1X transfer buffer (see appendix) for 10 minutes. The resolving gels and the transfer membranes were "sandwiched" between cassettes and placed in a running tank. The electro-transfer was performed at 100V and 4º C for 1 h.

4.2.5.4 Chemiluminescence protein detection

Following electro-transfer, the nitrocellulose membrane was soaked in Ponceau stain (see appendix) for three min for detection of transfer efficiency. The membranes were thereafter washed 3 x 5 minutes with shaking in 0.1% TBS-T (see appendix). The membranes were incubated in blocking buffer in containing TBS-T and 5% fat-free milk for 1 h at RT with shaking. The membranes were thereafter washed 3 x 5 minutes with shaking in 0.1% TBS-T. For detection cyclin B1 (55 kDa) (Cell Signalling Technology, Danvers, MA, USA) and FAM111B (55kDa) (Santa Cruz) proteins, the membranes were incubated in anti-cyclin B1 primary antibody (1:1000) and anti-FAM111B antibody (1:100) diluted in blocking buffer overnight at 4º C with shaking. The other membrane was incubated with anti-p38 primary antibody (1:5000) and used as a loading control.

Following overnight incubation, the membranes were washed 3 x 5 min with shaking in 0.1% TBS-T and thereafter incubated for 2 h (RT) in horseradish peroxidase-conjugated goat-anti mouse secondary antibody (Biorad, Hercules, CA, USA) at 1:2000 for cyclin B1, donkey-anti-goat (1:2000) and goat-anti rabbit (1:5000) for p38. The membranes were thereafter washed 3 x 5 minutes with shaking in 0.1% TBS-T and incubated in chemiluminescence reagent for 3-5 minutes and developed the blots in the dark using X-ray film for signal detection. The blots were thereafter scanned for densitometric readings and further analysis.

4.2.6 Statistical analysis

Statistica Software version 13.3 (Dell Inc.) was used for statistical analysis of all data in this study. The qPCR results were analysed according to Schmittgen & Livak (Schmittgen & Livak, 2008) method, which was added to the Minimum Information for Publication of Quantitative Real-Time PCR Experiments (MIQE) guidelines (Bustin et al., 2009). The results are presented as mean ±SEM, and differences between two samples were analysed by Student's t-test, independent by group or variable. To determine significant differences in three or more groups, Breakdown & one-way analysis of variance (ANOVA) was used, with Tukey honest significant difference (HSD) as the post-hoc test. Data were considered statistically significant at $p < 0.05$. Graphs were plotted with GraphPad Prism version 5.0 (GraphPad, San Diego, CA).

4.3 Results

One of the key characteristics of fibrosis is that in response to wounding, cells are stimulated to undergo proliferation by the growth factors that are released from the wounded tissue by invading inflammatory cells (Diegelmann & Evans, 2004). It was therefore hypothesised that the iPSC-derived mesenchymal stem/stromal cells from poikiloderma patients might proliferate at a more rapid rate than the equivalent control cells, contributing towards the increase in fibrotic tissues.

4.3.1 Patient-specific iPSC-MSCs show a higher cell proliferation rate compared to control cells

To test this hypothesis, the first aim was to determine whether iPSC-MSCs from patients proliferated faster than those of controls. Briefly, the iPSC-MSCs were seeded at a density of 3 x 10^4 per well in gelatin-coated six-well plates and each sample was cultured in duplicates. The cells were manually counted every 2 days for 8 days. The experiments were carried out three times in duplicate and the combined results are presented in Figure 4.1. As can be seen, after 6 days there were approximately 2.5 times more patient cells (6 x 10^5) than controls (1.6 x 10^5). Doubling time calculations revealed that control cells had an average doubling time of 55 hours compared to patient cells, which had a doubling time of 33 hours. These results provide solid evidence that FAM111B protein does indeed play a role in regulating cell proliferation.

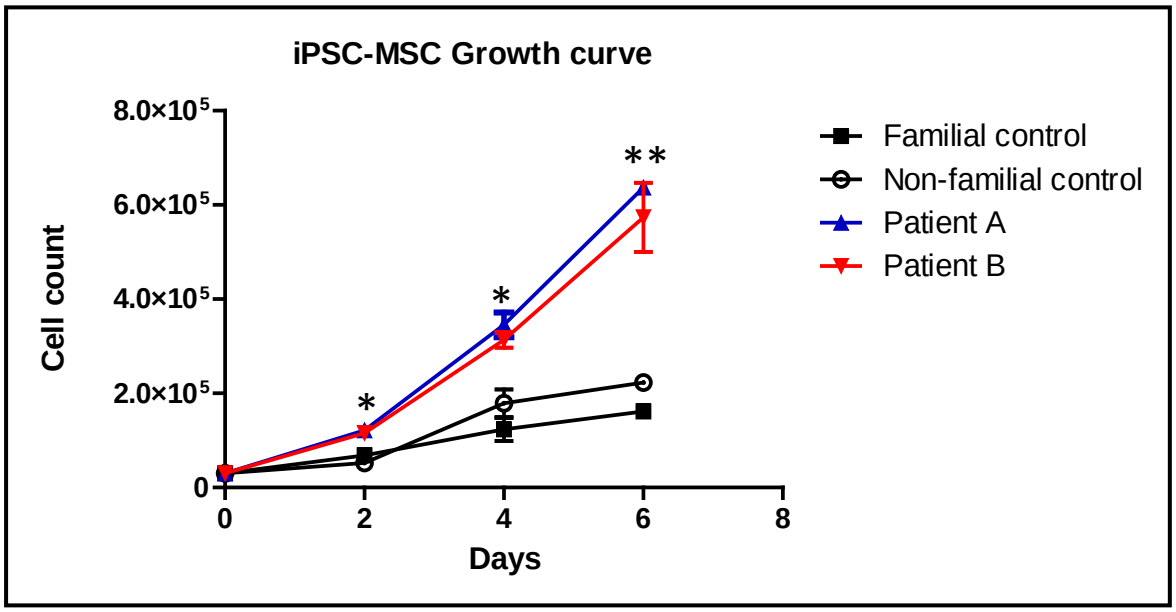

Fig. 4.1 Growth curve of patient and control iPSC-MSCs. Patients and controls iPSC-MSCs were cultured for 8-days and counted every two days to determine the growth rate Data presented as mean ± SEM. (n = 3). * $p < 0.05$; ** $p < 0.01$; *** $p < 0.001$

4.3.2 FAM111B expression in dermal fibroblasts, iPSCs and iPSC-derived MSCs

The next aim was to determine a) whether the level of FAM111B expression is different between patient and controls cells and b) whether different cell types express different levels of FAM111B (Fig. 4.2). If so, this might give a clue as to what role or how FAM111B might be influencing cell proliferation. In the first set of experiments, FAM111B mRNA levels were determined in three cell lines, dermal fibroblasts, iPSCs and iPSC-MSCs, as follows: Dermal fibroblasts and iPSC-MSCs were cultured on gelatin-coated culture plates and maintained in standard growth medium till they reached 90% confluence. The iPSCs were cultured under feeder-free conditions and analysed when they reached 90% confluence. Cells were then harvested and analysed for mRNA expression as previously described in the chapter 2 (sections 2.2.4.1). Of importance, it should be noted that all experiments were done at the same time or in the same run in order to minimize technical variations. Three biological repeats were performed with each biological repeat conducted as described. The results in Fig. 4.2 show that the iPSCs, somewhat surprisingly, showed higher FAM111B mRNA expression ($p \leq 0.001$) compared to fibroblasts and iPSC-MSCs, with Patient A iPSCs showing the highest expression levels (Fig. 4.2A). The results further show that dermal fibroblasts have a lower expression of FAM111B mRNA compared iPSCs but slightly higher

levels when compared to iPSC-MSCs (Fig. 4.2A). The iPSC-MSCs showed lower FAM111B mRNA expression when compared to fibroblasts and iPSCs. The high levels of FAM111B in iPSCs is interesting because it is known that these cells have a faster cell cycle than cells of later lineages, including differentiated cells (Coronado et al., 2013; Kapinas et al., 2013).

Next, FAM111B mRNA expression was compared between patients and controls (Fig. 4.2B). Patient primary skin fibroblasts showed slightly higher FAM111B expression compared to the familial and non-familial controls. The non-familial control showed significantly lower mRNA levels ($p \leq 0.001$) compared to patients and the familial control (see discussion) For iPSCs, FAM111B mRNA levels were similar between patients and controls with no statistical difference (n.s). When comparing FAM111B expression between patients and controls in iPSC-MSCs, there was no statistical difference between patients and controls though the non-familial control showed comparably low FAM111B levels. Furthermore, patient iPSC-MSCs had similar FAM111B levels as the familial control. Overall, the results suggest that a) iPSCs have a significantly higher FAM111B expression compared to dermal fibroblasts and iPSC-MSCs, and b) in these analyses of non-synchronised cell cultures, there is no statistical difference in FAM111B expression detectable between patients and controls.

From these results one can conclude that a) differences in cell proliferation between patient and control cells are not due to the overall level of FAM111B mRNA which implies b) that the FAM111B mutation does not result in higher levels of gene expression or steady state levels of the protein. However, it is possible that FAM111B expression is cell-cycle regulated, and if so, the study of asynchronous population of cells would not reveal any differences.

A

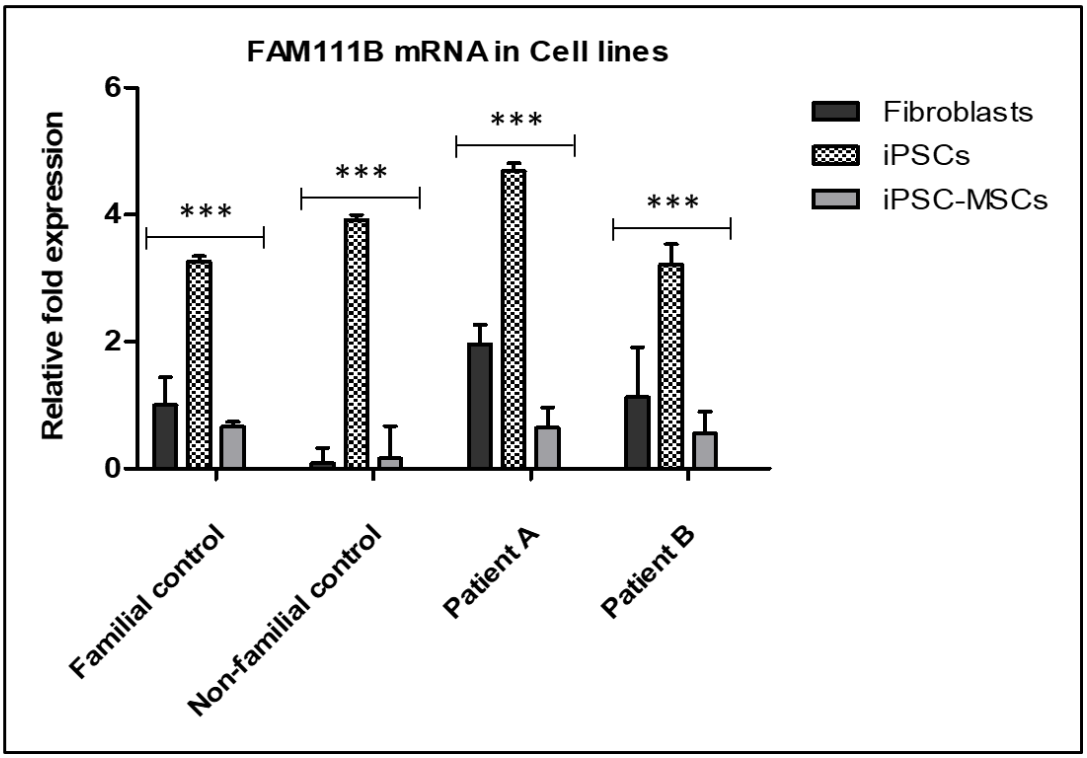

B

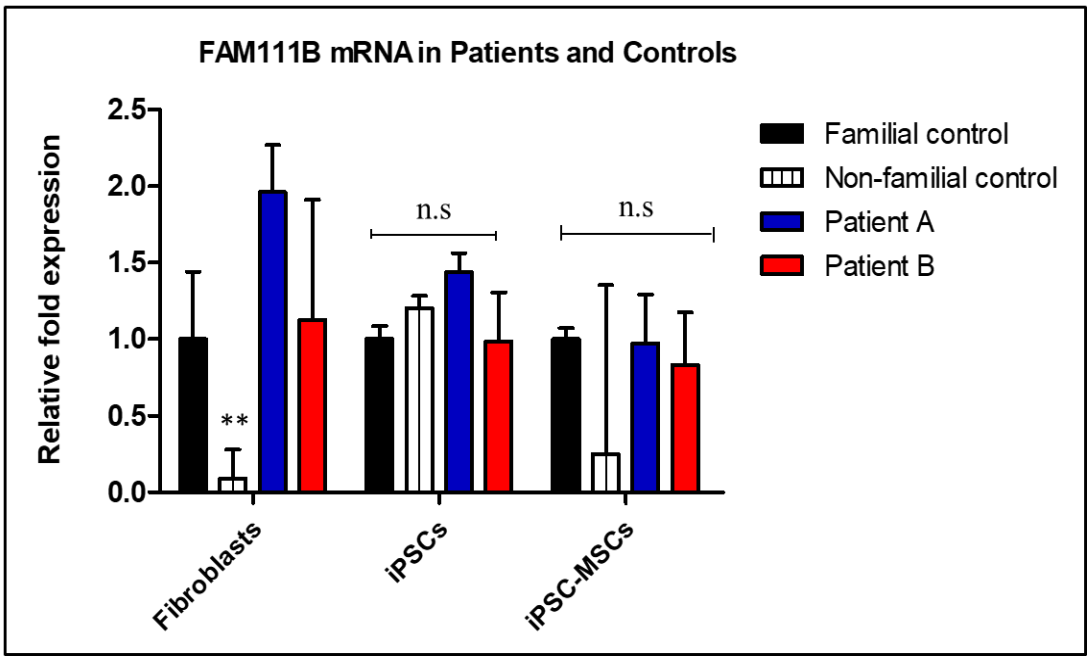

Fig. 4.2 Analysis of FAM111B mRNA expression in different cells lines and between patients and controls. (A) FAM111B mRNA expression was analysed in fibroblasts, iPSC and iPSC-MSCs. **(B)** FAM111B expression was compared between patient and control iPSC-MSCs. Data presented as mean ± SEM (n = 4). * $p \leq 0.05$; ** $p \leq 0.01$; *** $p \leq 0.001$. Non-significant data shown by n.s.

4.3.3 Optimising cell synchronisation in patient and control iPSC-MSCs using double-thymidine block

Because there were no statistical differences in FAM111B RNA expression in non-synchronised cells, it was recognised that a more targeted or fine-tuned approach would be necessary to analyse possible differences at different stages of the cell cycle, especially as Aviner et al. (2015) had recently shown that in HeLa cells that FAM111B was cell cycle regulated. In order to conduct analyses of synchronised cells it was first necessary to establish the conditions (doses of drugs, timing), to effectively synchronise the iPSC-MSCs. Firstly, I tested the reproducibility of the data obtained by Aviner et al. (2015) in synchronised HeLa cells. The HeLa cells were synchronised by double-thymidine block for 19 hours (h), with release for nine hours in between blocks. Cells were harvested at 2-h intervals for 14 h post the second thymidine block (Fig. S1). The data in the present study correlated with the findings of Aviner et al. (2015) that FAM111B mRNA expression in HeLa cells peaks at 14-hours post-thymidine release, which is indicated to be the G1-phase. Similarly, PCNA and AURKA expression patterns were comparable to the those shown by Aviner et al. (2015) that PCNA (Fig. S1A) and FAM111B (Fig. S1C) peak at 14 h and AURKA peaks between 6- and 8-h post-thymidine release (Fig. S1B). Thus, the synchronisation data of HeLa cells in this study showed reproducibility with this method and was therefore adopted for this current study.

Synchronisation of iPSC-MSCs was initially performed using the parameters similar to those of Aviner et al. (2015). However, there were no clear peaks in PCNA and AUKRA mRNA expression when using this protocol. It was therefore deduced that this may have been due to a longer doubling time in iPSC-MSCs compared to HeLa cells which have a doubling time of 16 hours. To correct for this problem, optimisation experiments were first performed on one cell line (Familial control) to establish the best synchronization protocol and to determine synchronisation efficiency. A 30-h thymidine block (2 mM) was performed followed by a 15-h release and a final 30-h thymidine block for synchronisation of iPSC-MSCs. The cells were thereafter harvested at 5-h intervals for 30 h. Careful analysis of the 30-h timepoint showed two cell cycle rounds as PCNA (Fig. S2A) and FAM111B (Fig. S2C) expression peaked at 15- and 30- h, while AURKA peaked at 25-hours (Fig. S2B) post-double thymidine block. The iPSC-MSCs were thereafter synchronised by double thymidine block for 24 h and harvested at 3-h intervals up to 24 h after the second thymidine block to analyse a single cycle round. In this experiment, the results showed that the cell cycle marker

PCNA peaked at 3-,15- and 24-hours post-thymidine release (Fig. S3A). Aurora kinase A mRNA expression indicated a gradual increase, peaking at 6 h (Fig. S3B) and FAM111B mRNA peaked at 15- and 18 h post-double thymidine release (Fig. S3C). The results from these experiments indicated poor synchronisation as indicated by PCNA which peaked at different timepoints. It was therefore postulated that the 2 mM thymidine concentration was too low for synchronisation of iPSC-MSCs. The concentration was thereafter doubled to 4 mM which improved synchronisation as indicated by flow cytometry data which measures DNA content (ploidy) during cycle progression, where diploid (2N) cells are detected at G0/G1 and tetraploid (4N) cells are detected at S- and G2/M phase (Fig. S4A-D). Cells were harvested at 0 h (G1/S), 2 h (S-phase), 6 h (G2/M) and 15 h (early G1-phase) post-double thymidine release. The 12 h timepoint was omitted in the optimised synchronisation protocol as it either showed a similar pattern of synchronisation with the 15-h timepoint as indicated by flow cytometry (Fig. S5) or it demonstrated large variations (high SEM), especially in AURKA mRNA expression between experiments (Fig. S6A). This pattern was observed in the three biological repeats performed.

Using the optimised double thymidine (4 mM) blocking method, the iPSC-MSCs were arrested at the G1/S phase for 24 h, followed by a 12 h release and a second thymidine block (4 mM) for 23 hours was carried out (Whitfield et al., 2002). Following cell cycle arrest, the cells were released from the block and harvested at 0 h, 2 h, 6 h and 15 post-thymidine treatment. Flow cytometric analysis (Fig. 4.3A) showed that in the untreated asynchronous control cells, 80% of the asynchronous cell population remained at the G0/G1 phase. Typically, one would expect MORE cells to be in G0/G1 at time zero (straight after arrest) and drop thereafter, as cells move out of G1 into S/G2 and then rise again as cells go through mitosis and re-enter G1. However, in these experiments at zero hour, the number of cells in G1 DROPPED to 58%. Thereafter, the number of cells in G1 stayed at the level of about 55-58% and rose again to 66% in 15 h. The time zero result thus indicates that thymidine arrests the cells at G1/S and not G0/G1 (Bjursell & Reichard, 1973), and that the cells in G0/G1 follow the predicted pattern. The analysis of cells in S and /G2 are more informative in cell cycle progression. In asynchronous cells, there are 13% of cells in G2 and 6% in M. At 2 h, there was 17% of cells in G2 and 26% of cells in S-phase. At 6 h, there was an increase in the population of cells at the G2/M phase, followed by a decrease at 15 h. While these results are encouraging and suggest at least some of the cells have been effectively synchronised by the double-thymidine treatment, the results for time zero which

show a high population of cells arrested at G1 and S, and the very high levels of cells in G1 throughout cell cycle progression make it difficult to provide firm conclusions.

In the final set of experiments, cell synchronisation efficiency was therefore determined by analysis of cell cycle genes- PCNA and AURKA at timepoints 0, 2, 6 and 15 h. PCNA is involved in DNA replication and its expression is typically increased at G1, peaking at S-phase and lowest at G2/M (Morris & Mathews, 1989). In Figure 4.3B, PCNA expression in the familial control indicates unchanged expression levels in all the timepoints. The non-familial control also shows similar expression for PCNA between 0 and 2 h timepoints, with a slight decrease at 6 h and returning to similar levels at 15 h. Patient cells had a high expression of PCNA at 0 h, with Patient A showing a 1.7-fold increase compared to the controls, and Patient B showing a two-fold increase compared to controls. Patient A showed a 2.5-fold increase and Patient B a 3.8-fold increase in PCNA mRNA expression at 2 h. At 6 h PCNA levels in Patient A and Patient B cells decreased by 50% with a further decrease at 15 h. The PCNA data thus indicates that at least some of the cells were successfully synchronised as it peaked at the G1/S and S phase where it is known to be high as it is involved in DNA replication. Furthermore, PCNA levels were relatively higher in the patient cells compared to controls (although no statistical differences were observed).

Aurora kinase A (AURKA), which is involved in spindle formation during the mitotic phase was also analysed in synchronised iPSC-MSCs. In control cells, AURKA mRNA showed a gradual increase between 0 and 6 h, peaking at 6 h. At 15 h, there was a decrease in AURKA in the familial control and non-familial control (Fig. 4.3C). (It was observed that the non-familial control expressed slightly high AURKA levels compared to the familial control). Patient cells, similarly, showed a gradual increase of AURKA mRNA expression between time 0 and 6 h, peaking at 6 h. At 15 h both Patient A and Patient B showed a slight increase in AURKA levels (Fig. 4.3C). The AURKA expression further indicated measurable synchronisation as it peaked at 6 h which correlates with the G2/M phase.

Although the flow cytometric data (Fig. 4.3A) showed that a high population of synchronised cells remained at the G1 phase, changes in the expression of PCNA and AURKA (Fig. 4.3 B-C) in patient and control cells at each timepoint indicated changes as the cell cycle progressed. These results provide slightly more convincing evidence that at least a subpopulation of cells was synchronised by double thymidine block. The qPCR data show that expression of PCNA mRNA levels (Fig. 4.3B) coincides with the S-phase, which occurs

2 h post-thymidine block for a 4-6 h duration. As PCNA expression decreased at 6 h, it was also observed that AURKA mRNA levels peaked at 6 h (Fig. 4.3C), suggesting entry into the G2/M phase in both patients and controls. The data at 15 h indicate completion of the G2/M phase and entry into early G1 phase.

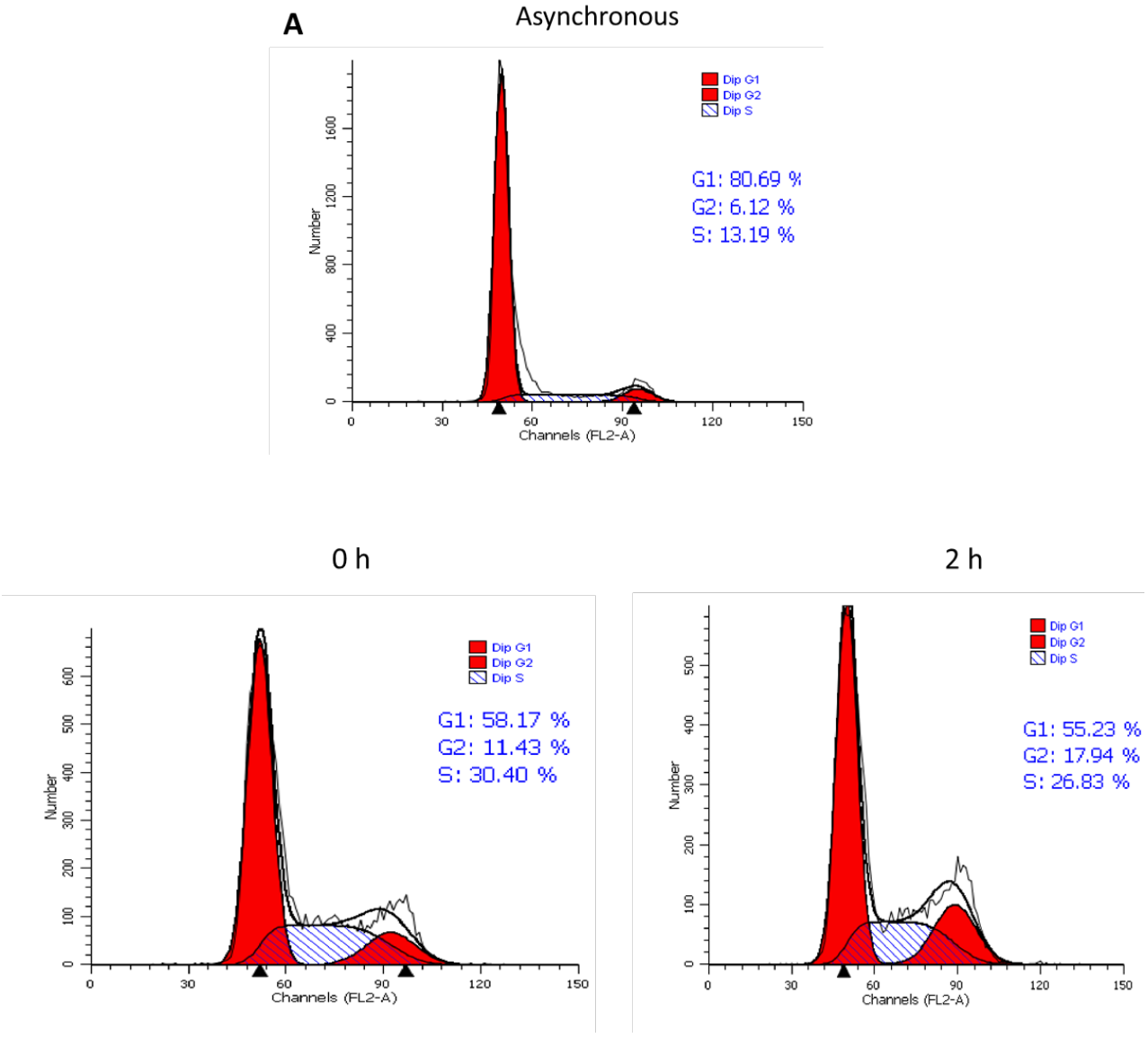

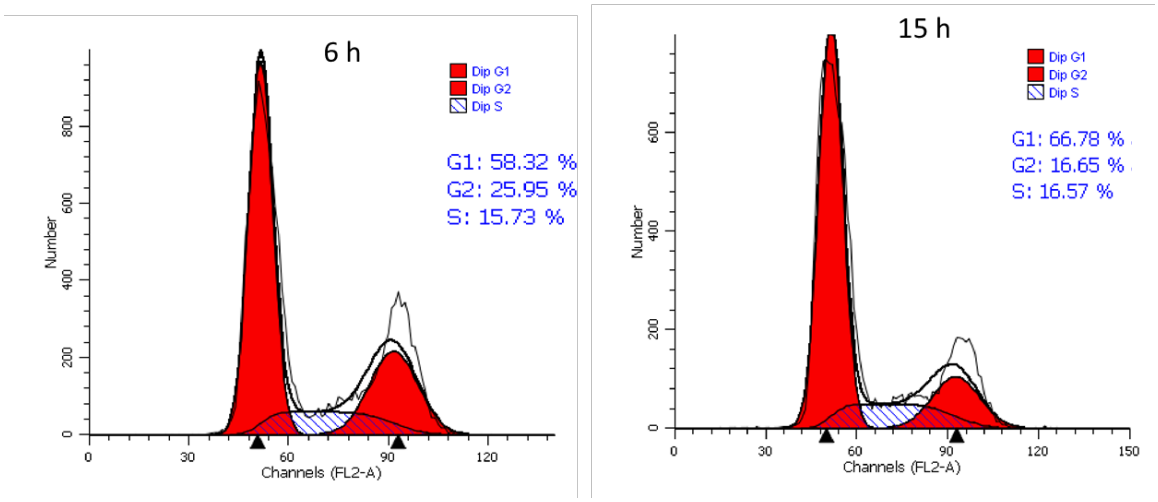

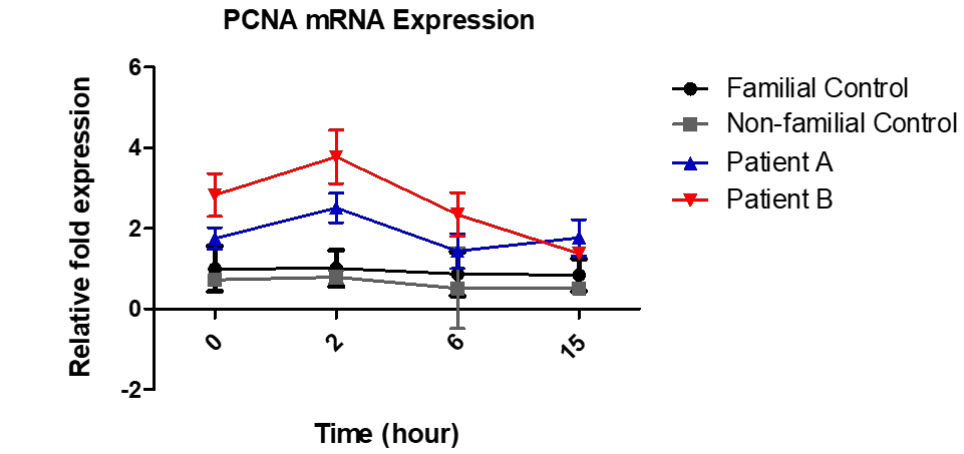

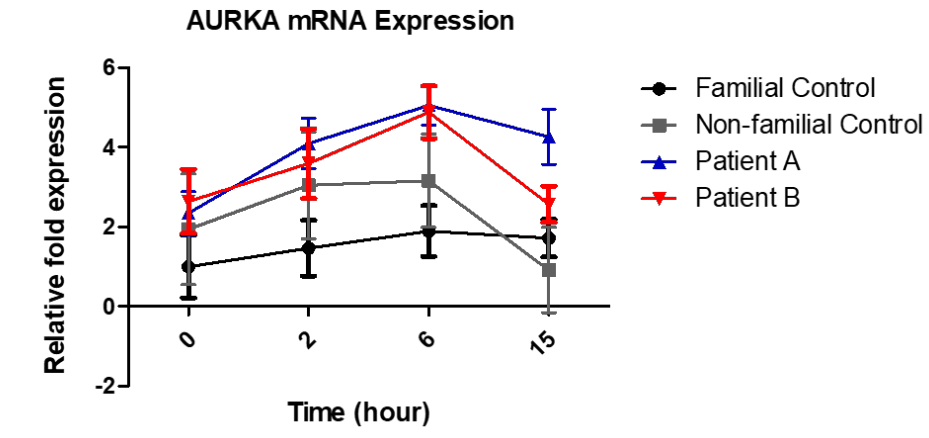

Fig. 4.3 Representative histograms of DNA content in synchronised cells by flow cytometry and mRNA expression of cell cycle genes. Patient and control iPSC-MSCs were synchronised by a 24 h double-thymidine block (4 mM), followed by release and harvesting of the cells at 0 h, 2 h, 6 h and 15 h post-thymidine block. **(A)** Flow cytometry shows cell population of the familial control at each cycle phase at the optimised timepoints. The different timepoints represent the G1/S phase (0 h), S-phase (2 h) G2/M phase (6 h) and early G1-phase (15 h). **(B)** PCNA mRNA and **(C)** AURKA mRNA expression were analysed at 0, 2, 6 and 15 h. Data presented as mean ± SEM (n = 3).

4.3.4 FAM111B mRNA expression is higher in synchronised patient cells compared to control cells

To determine whether FAM111B levels of expression are altered in patient cells during cell cycle progression (as compared to control cells), the iPSC-MSCs were synchronised by double-thymidine block as previously described and were harvested at 0 h, 2 h, 6 h, and 15 h timepoints after release from thymidine block. Real-time qPCR was thereafter performed to determine FAM111B mRNA expression in these synchronised cells. The results reveal that FAM111B mRNA expression peaked at 2 h (Fig. 4.4) and at 6 h there was a decrease in FAM111B expression followed by a slight increase at 15 h.

Patient cells showed significantly higher FAM111B mRNA levels than controls, with Patient A indicating a six-fold ($p \leq 0.01$) higher level and Patient B showing a five-fold ($p \leq 0.01$) increase in mRNA levels compared to control cells at 0 h (Fig. 4.4). At 2 h, FAM111B expression peaked to 7-fold ($p < 0.05$) in the patient cells compared to controls. At 6 h FAM111B mRNA levels decreased but remained significantly high ($p < 0.05$) in patient cells compared to controls. At 15 h, mRNA levels were similar between patient cells and the familial control. The non-familial control on the other hand, showed significantly low FAM111B mRNA levels at 15 h ($p < 0.05$) (Fig. 4.4), possibly due to variations in genetic background. The 12 h timepoint was omitted in this experiment as it demonstrated large variations (high SEM) in FAM111B mRNA expression in the patient cells and the non-familial control after three biological repeats (Fig. S6B). This suggests a technical error which masked whether there is statistical difference between patient and control cells at this timepoint.The overall data showed that a) FAM111B mRNA is temporally expressed in synchronized cells, peaking at the S-phase which is represented by the 2 h timepoint in this study; and b) FAM111B mRNA expression is very much higher in patients cells compared to controls between 0 h and 6 h timepoints. Interestingly, FAM111B expression pattern appears to be similar to the PCNA expression pattern, where both genes were increased at 2 h (S-phase) and decreased at 6 h (G2/M) (Fig 4.3 B) particularly in the patient cells, which suggests that FAM111B is involved in DNA replication.

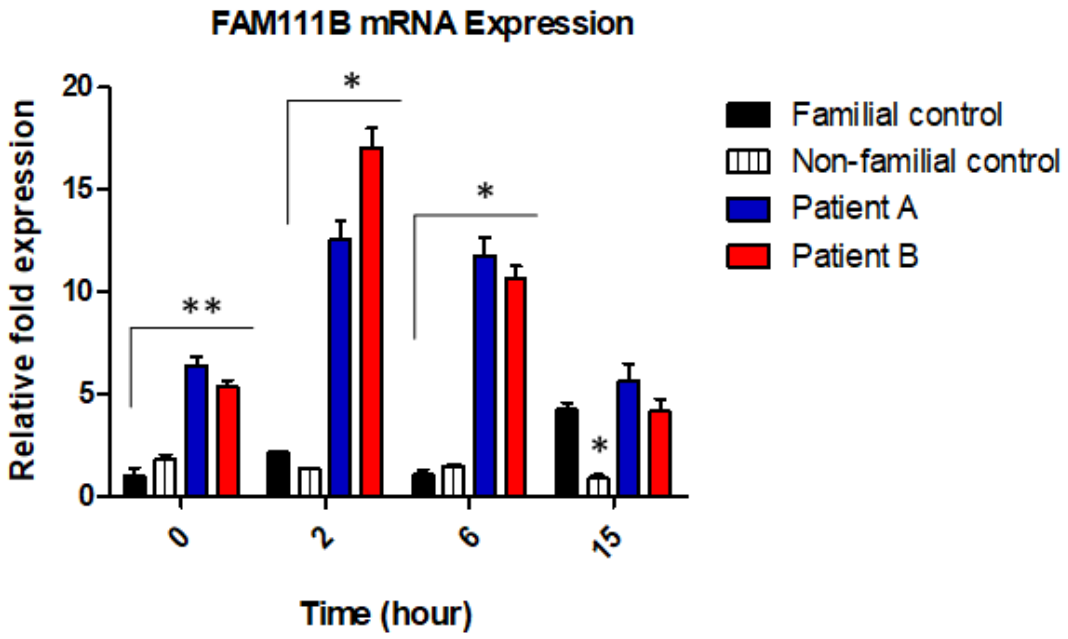

Fig. 4.4 FAM111B mRNA expression in patient and control iPSC-MSCs. Synchronised cells were analysed for FAM111B mRNA expression at time 0 h, 2 h, 6 h and 15 h, which represent the G1/S, S and G2/M phases of the cell cycle. Data presented as mean ± SEM (n = 3) * $p < 0.05$; ** $p < 0.01$; *** $p < 0.001$

4.3.5 Detection of FAM111B protein in patient and control cells

The next step was to determine if FAM111B protein expression correlated with mRNA expression. To analyse FAM111B protein expression at the different phases of the cell cycle the thymidine-nocodazole method was used. Briefly, to obtain cells arrested at the G1/S and S-phase double-thymidine (4 mM) block was performed as described in section 4.2.2. To obtain cells arrested at the G2/M phase, the iPSC-MSCs were treated for 18 h with nocodazole (150 ng/ml) after a single 24 h thymidine block. Nocodazole, which arrest cells at G2/M phase by inhibiting formation of mitotic spindle (Banfalvi, 2011) was added to obtain a higher cell population at the G2/M for protein quantification. Flow cytometric data of the familial control was used to confirm efficient synchronisation in iPSC-MSCs following cell synchronisation by thymidine-nocodazole block (Fig. 4.5A). As with the flow cytometry data in Figure 4.3A, a high percentage of cells (55-58%) remained at the G1-phase as shown in Figure 4.5A. The percentage of cells at early (2 h) and late (4 h) S-phase were at 25% and 15%, respectively. Flow cytometry data further showed that 31.69% of the cell population was arrested at the G2/M phase following nocodazole block (Fig. 4.5).

Western blot analysis of cyclin B1 (CCNB1), which increases during the G2/M phase was further performed to confirm synchronisation of both patient and control cells by indicating a high expression at the G2/M-phase compared to the early S- and late S-phase. The densitometric graph indicates that cyclin B1 protein levels were slightly higher in the patient cells at early S-phase, decreased at late S-phase and increased at G2/M as expected (Fig. 4.5 B). Three biological repeats were performed in this experiment. Though cyclin B1 protein levels in the synchronised iPSC-MSCs were slightly increased at G2/M, with Patient B indicating higher expression compared to controls and Patient A (though not statistically significant), the data indicates that a population of cells were synchronised, and also that some cells may have escaped cell cycle arrest even after nocodazole block which arrests cells at G2/M phase.

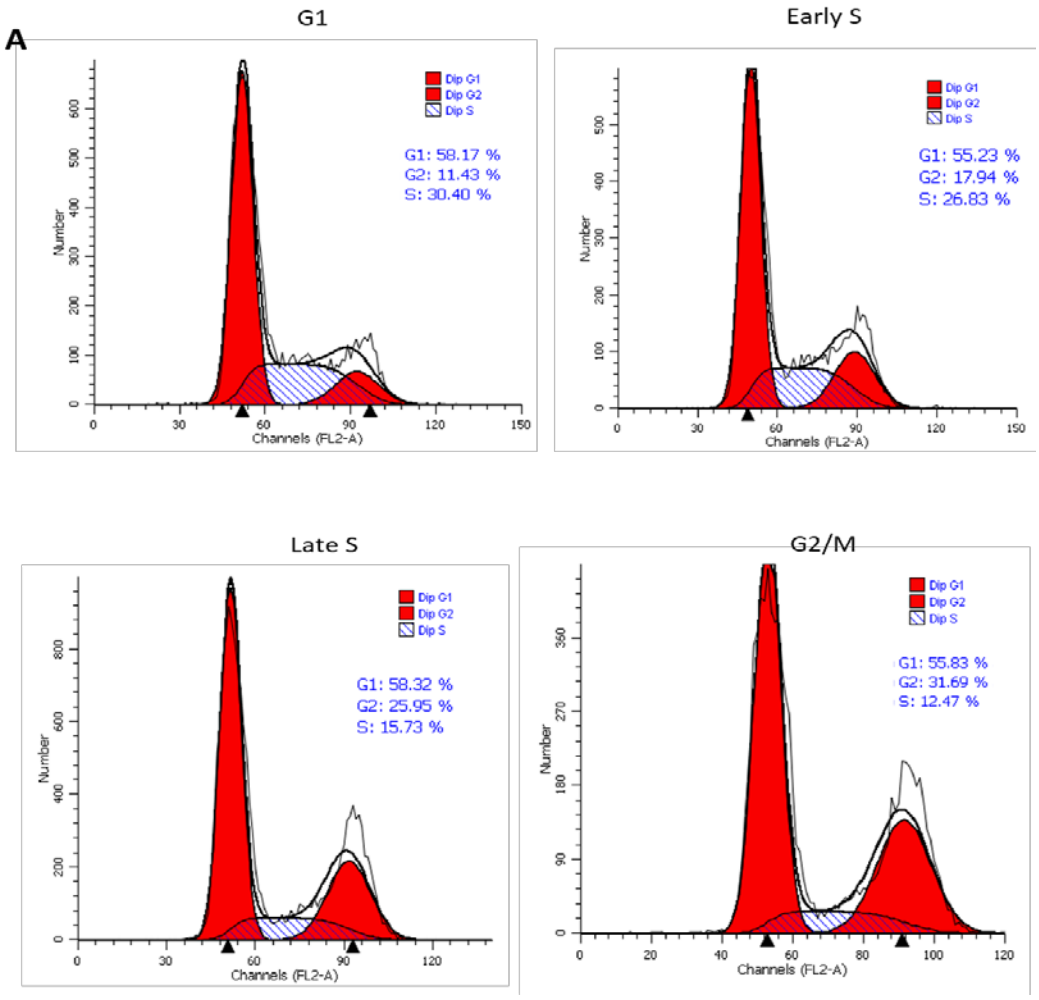

B

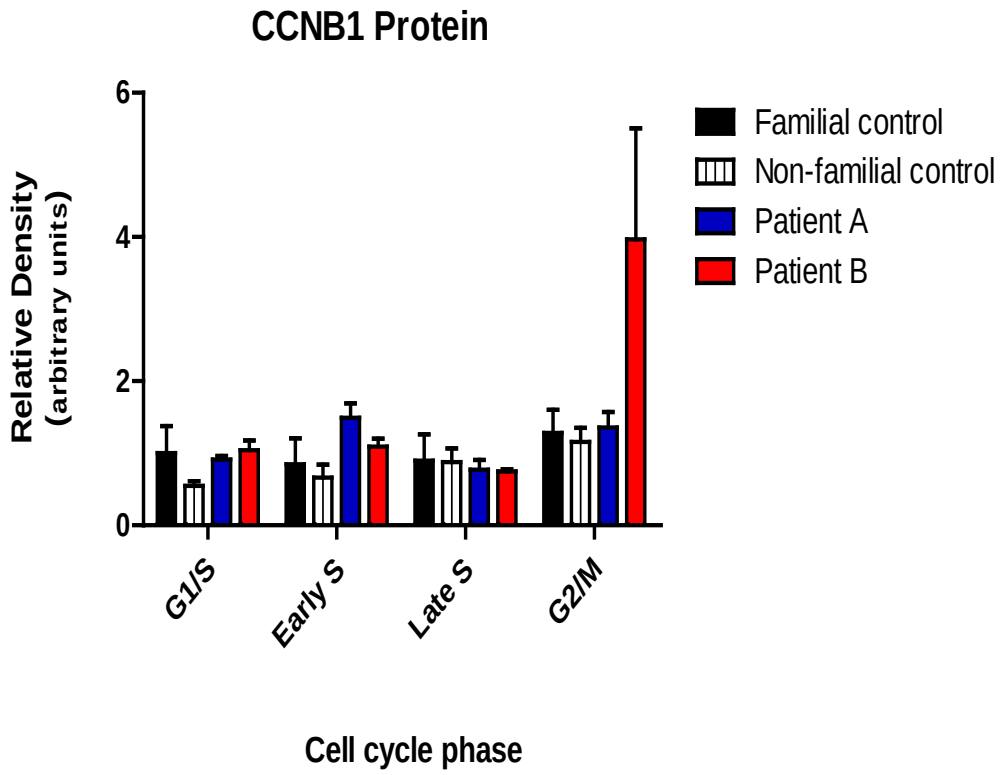
CCNB1 Protein
Relative Density
(arbitrary units)
6
4
2
0
G1/S
Early S
Late S
G2/M
Cell cycle phase
Familial control
Non-familial control
Patient A
Patient B

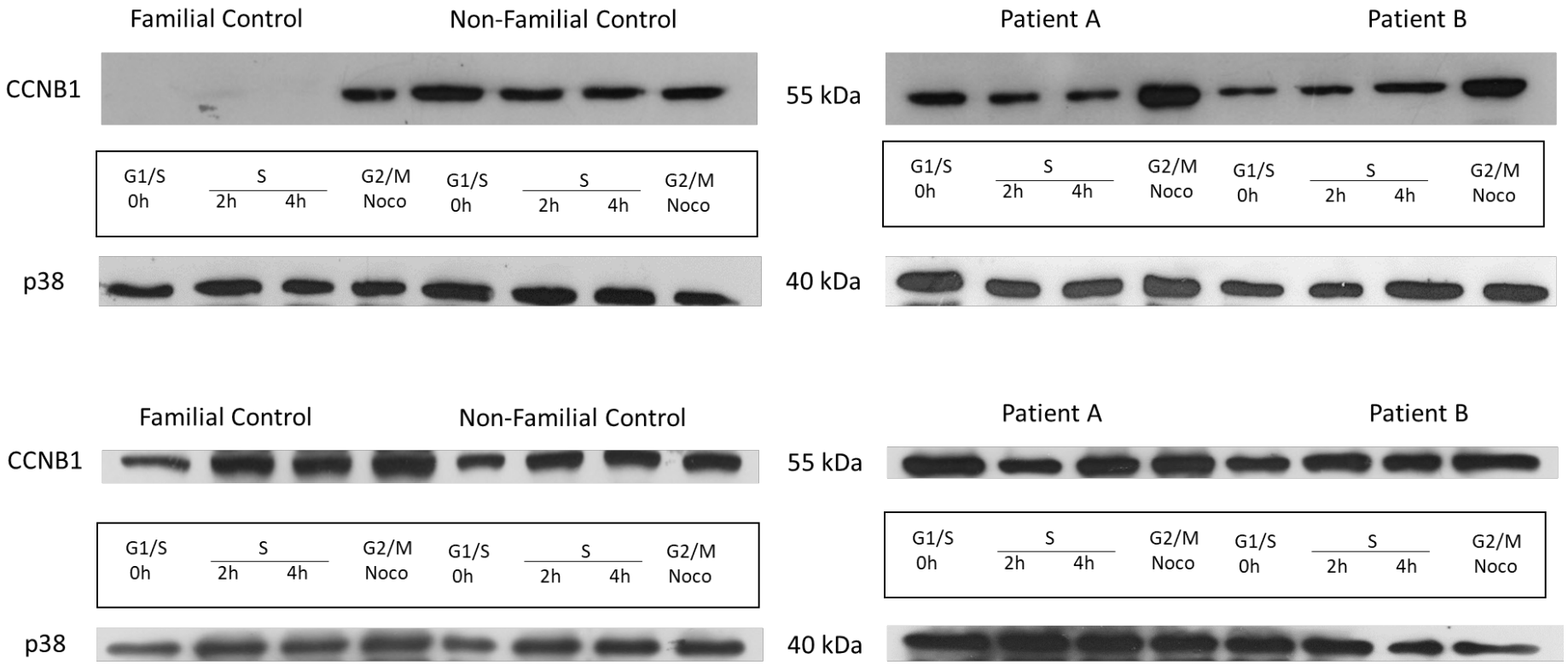

Fig. 4.5 Flow cytometric analysis of DNA content and protein expression of cyclin B1 in iPSCs-MSCs synchronised by thymidine-nocodazole block (A) Familial control iPSC-MSCs were used optimise and determine synchronisation efficiency by flow cytometry at G1/S, early S-phase, late S-phase and G2/M-phase (n = 2). **(B)** Cyclin B1 (CCNB1) protein expression was analysed by western blotting (blots and graph) in synchronised patient and control cells Anti-p38 antibody was used a loading control. Data presented as ± SEM (n = 3).

Next, FAM111B was analysed by western blotting in synchronised cells to determine whether the mRNA levels (Fig. 4.4) correlate with protein levels. In particular the aim was to 1) determine whether there are higher levels of FAM111B protein in patient versus control cells, and 2) whether there is any detectable difference in pattern of FAM111B expression compared to controls. The currently available anti-FAM111B antibodies do not detect the predicted molecular size of 72 kDa for FAM111B, including the antibody used in this study, possibly due to posttranslational modifications that occur during protein synthesis (Umar et al., 1996). The available antibodies commonly show clear detection of FAM111 B protein with the molecular weight of 55 kDa, which is size that was detected by the antibody used in this study (sc-246547). Densitometric analysis was used to measure the ratio of protein levels expressed in patient cells relative to the familial control for quantification of FAM111B protein levels detected by western blotting. The densitometric data indicate that FAM111B protein levels are similar at the G1/S and S-phase (2 h and 4 h) (Fig 4.6A). FAM111B protein levels are slightly higher in the early S-phase (2 h) and lower in the G2/M phase, however, no statistical differences were observed. Slight differences were also observed between patients and controls where patient cells expressed high levels of FAM111B protein in the early S-phase (2 h) compared to controls. Interestingly, FAM111B levels were reduced in patient cells compared to controls at the G2/M phase though no statistical difference was observed. Overall, these western blot results thus do not reveal a correlation in FAM111B mRNA (Fig. 4.4) and protein expression (Fig. 4.6A). It should be noted however, that there were variations in FAM111B protein levels between the experimental runs as indicated by the western blots in Figure 4.6B (i-iii). The variations observed in the western blots may be due to a lag in protein synthesis; but they may also be attributed to some of the challenges experienced with western blotting where the housekeeping protein levels are elevated in some experimental runs as observed in this study where p38 levels varied as shown in Figure 4.6 B (i) and (ii).

The overall FAM111B results reveal temporal expression patterns and statistical differences in mRNA expression between patient and control cells (Fig. 4.4). Though changes in FAM111B protein expression pattern were subtle, they appeared to be similar to the mRNA expression pattern (Fig 4.6A), particularly in the early S-phase represented by the 2 h timepoint. However, other synchronisation methods such as serum starvation (Achille et al., 2011; Davis et al., 2001) should be applied to confirm the findings in this study. Also, the

application of proteomics should be used to overcome some of the limitation and challenges experienced with western blotting

A

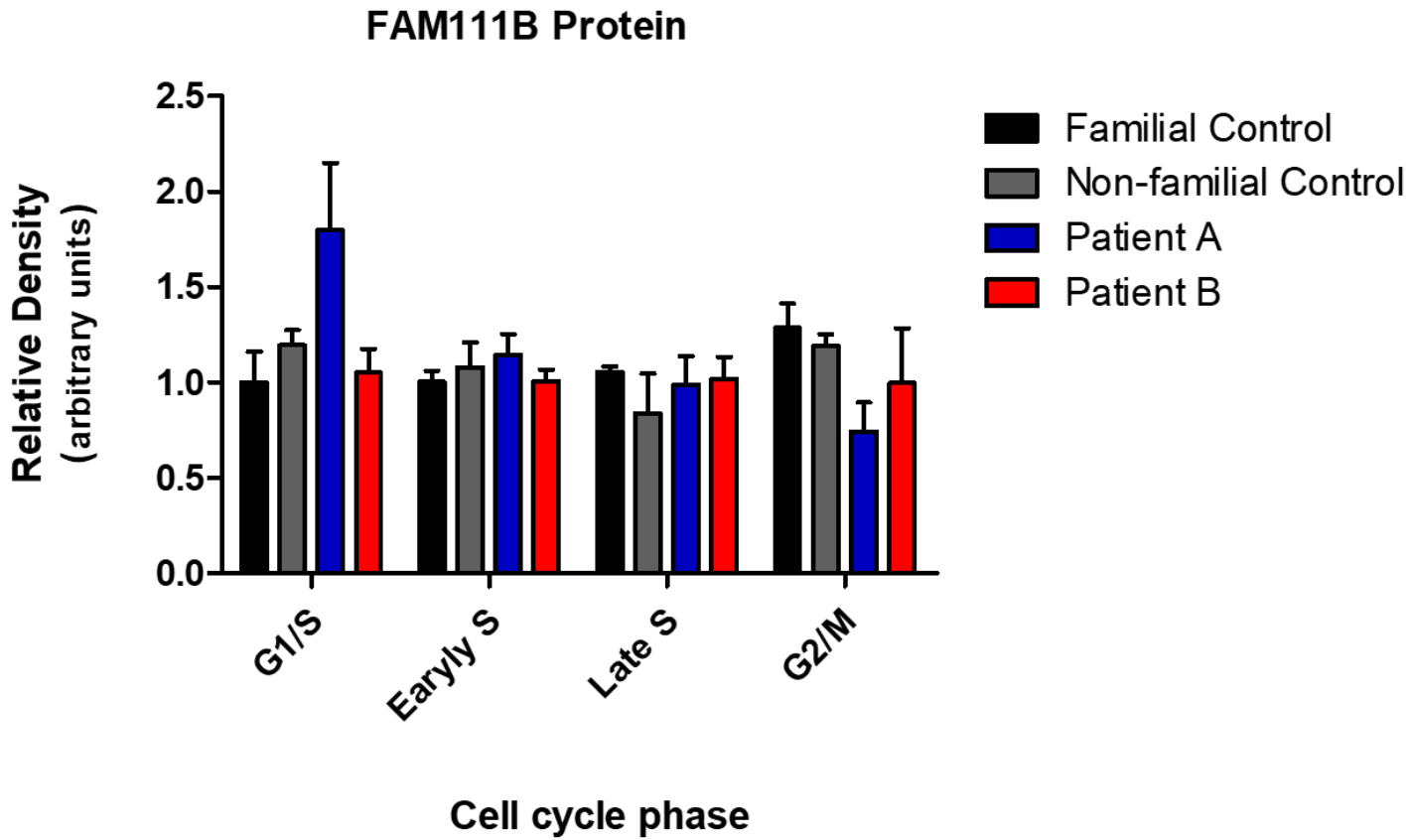
FAM111B Protein
Relative Density
(arbitrary units)
2.5
2.0
1.5
1.0
0.5
0.0
G1/S
Earyly S
Late S
G2/M
Cell cycle phase
Familial Control
Non-familial Control
Patient A
Patient B

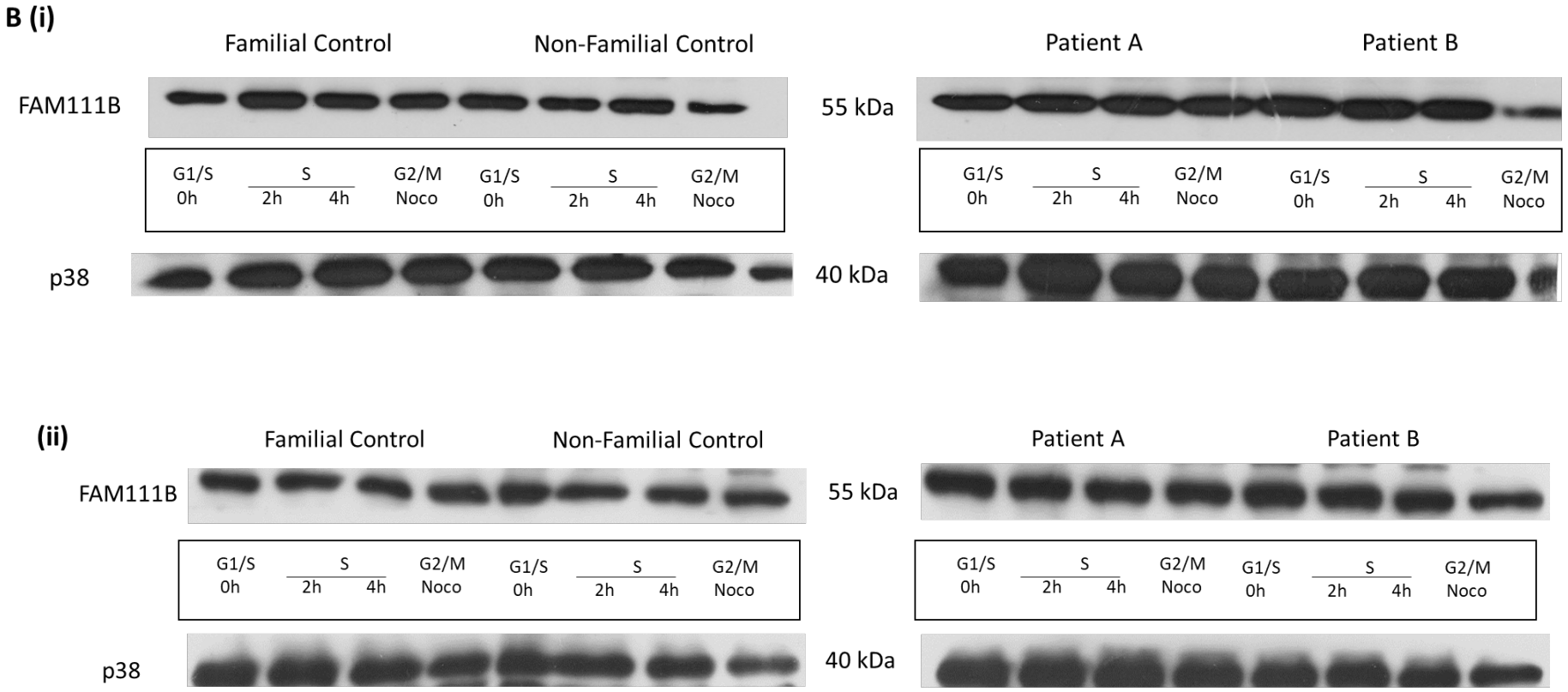
B (i)
Familial Control
Non-Familial Control
Patient A
Patient B
FAM111B
55 kDa
G1/S 0h
S 2h 4h
G2/M Noco
G1/S 0h
S 2h 4h
G2/M Noco
G1/S 0h
S 2h 4h
G2/M Noco
G1/S 0h
S 2h 4h
G2/M Noco
p38
40 kDa
(ii)
Familial Control
Non-Familial Control
Patient A
Patient B
FAM111B
55 kDa
G1/S 0h
S 2h 4h
G2/M Noco
G1/S 0h
S 2h 4h
G2/M Noco
G1/S 0h
S 2h 4h
G2/M Noco
G1/S 0h
S 2h 4h
G2/M Noco
p38
40 kDa

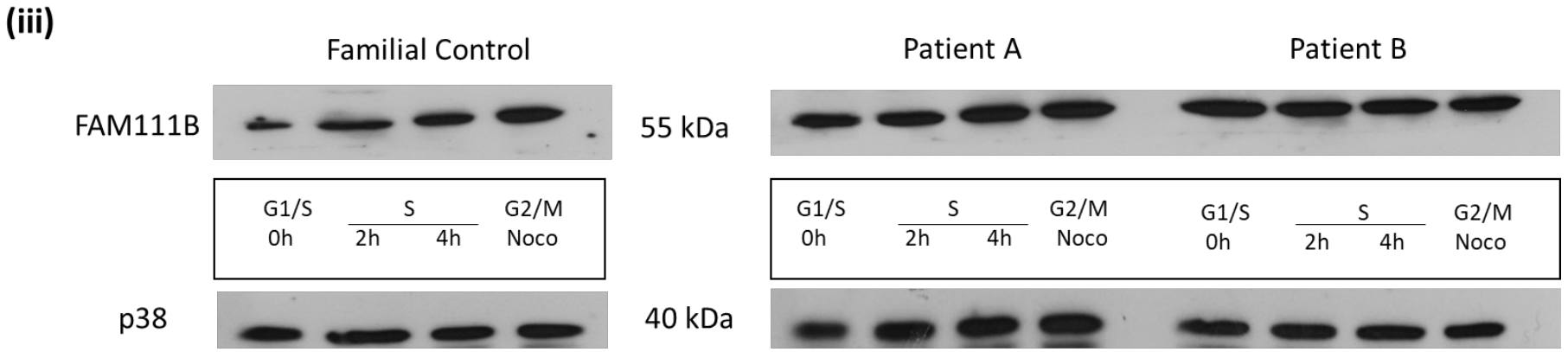

Figure 4.6 FAM111B protein expression in synchronised iPSC-MSCs. Patient and control iPSC-MSCs were synchronised by thymidine-nocodazole block. Double thymidine (4 mM) block was performed for isolation of cells arrested at the G1 and S phase. Cells at the early S-phase were harvest 2 h post-thymidine release and cells at the late S-phase were harvested 4 h post-thymidine release. Cells arrested at the G2/M were collected after 18 h of nocodazole (150 ng/ml) treatment. Anti-FAM111B antibody was used to detect FAM111B protein expression between patients and controls. **(A)** Graphical representation of relative FAM111B expression following normalisation with anti-p38 antibody which was used a loading control. Graph presented as ± SEM (n =3). **(B i-iii)** Western blots indicating FAM111B protein expression between patients and controls.

4.4 Discussion

During the course of this study, reports were published on the involvement of FAM111B in cell proliferation and cell cycle progression (Aviner et al., 2015). These reports led to the hypothesis that the FAM111B mutation may promote fibrosis by modulating the cell proliferation. The aim in this chapter was therefore, to determine whether patient cells proliferated at a different rate compared to control cells, and whether the mutation in the *FAM111B* gene alters its level of expression in the patient cells.

A standard growth curve was performed to determine the proliferation rate of patient and control cells, and notably, patient cells showed higher cell proliferation rate compared to control cells, with the average doubling time of 33 hours in patient cells versus 55 hours in control cells. Studies have indicated varying doubling times for mesenchymal stem/stromal cells derived from bone marrow, adipose and/or umbilical cord tissue ranging from 40 to 50 hours (Heo et al., 2016; Mennan et al., 2016). The control iPSC-MSCs in this study indicate similar doubling times as the primary mesenchymal stem/stromal cells as well as iPSC-MSCs reported by other investigators (Diederichs & Tuan, 2014). The differences in the growth rate of patient cells thus suggests that the FAM111B mutation is associated with the modulation of cell proliferation in this condition. It would have been of interest to determine if dermal fibroblasts showed similar trends between patients and controls, however, this was not possible because of the limited supply of patient dermal fibroblasts. Skin biopsies will need to be obtained to address this gap.

The thymidine block protocol used to synchronise cells in culture works by increasing the intracellular pool of deoxy-thymidine triphosphate (dTTP) which results in the inhibition of deoxy-cytidine diphosphate (dCDP) thereby inhibiting DNA replication (Bjursell & Reichard, 1973; Uzbekov, 2004). Double thymidine block is used as the first thymidine block arrests cells which are at the G1/S boundary and the second thymidine block arrests cells which have escaped the first block (Tobey et al., 1966; Uzbekov, 2004). It has also been shown that thymidine blocks nucleolar RNA which prevents ribosomal RNA synthesis. The advantage of thymidine is that it is a reversible inhibitor, therefore, upon release the synchronised cells progress into the S-phase to complete at least one full cell cycle (Banfalvi, 2011; Chen & Deng, 2018). Expression of cell cycle-regulated genes is analysed in synchronised cells at specific timepoints which represent a duration of each phase for one cell

cycle upon thymidine release (Banfalvi, 2011). However, since double-thymidine block arrests DNA and ribosomal RNA synthesis it is therefore recommended that it not be used to synchronise cells with cell cycle duration longer than 16-18 hours (Uzbekov, 2004).

After carrying out a double thymidine block of iPSC-MSCs in this study, flow cytometry data showed that a low percentage of cells progressed through the cell cycle and at least 60% of the cell population remained at G1. These results, therefore, demonstrate that this method was inefficient to synchronise iPSC-MSCs. There are a number of possible explanations for this: 1) it may have been due to an inappropriately low thymidine concentration of 4 mM which was used in this study. Investigators commonly use thymidine concentrations of 2 mM to 5 mM, particularly in HeLa cells and other cancer cells (Aviner et al., 2015; Banfalvi, 2011; Whitfield et al., 2002). Higher thymidine concentrations of 10 mM have been previously used to synchronise other cells such as CHO cells (Tobey et al., 1967). Therefore, higher thymidine concentrations may be needed to synchronise iPSC-MSCs for future work. 2) Studies have also reported that some synchronised cells lose their synchrony post-thymidine release, which reduces the number of synchronous cells that complete the cell cycle. This may have also contributed to the low synchronisation of iPSC-MSCs in the current study (Darzynkiewicz et al., 2011; Pederson & Robbins, 1971). 3) Synchronisation methods such as serum starvation and other chemical inhibitors such as nocodazole (arrest the cells at the G2/M-phase) and aphidicolin (arrests cells at G1) have also been used in other studies (Uzbekov, 2004). Synchronisation of MSCs has been previously performed in other studies, for example, Achille et al. (2011) synchronised bone marrow-derived MSCs (BM-MSCs) by serum starvation for 20 hours and harvested the cells between 10 and 32 hours after serum addition. Their study indicated that these cells have an extended cell cycle of over 24 hours as the G1-phase lasted 14-15 hours, the S-phase lasting 8-9 hours and G2/M phase lasting 3-4 hours. Furthermore, they showed that BM-MSCs enter the G1-phase 15 hours post-serum addition and enter the S- and G2/M phases 24- and 27 hours post-serum addition respectively. Another study using serum starvation showed that human dermal fibroblasts and adipose-derived MSCs enter the S-phase 20 hours- and the G2/M phase 24 hours post-serum addition (Chen et al., 2012). These studies, therefore, suggest that serum starvation may be a more suitable method for synchronising cells with a longer doubling time and/or longer cell cycle duration.

The double-thymidine block has also been reported to synchronise a low percentage of cells compared to serum starvation as the cells are captured at fixed timepoints by this method thus leading to a loss of subtle shifts in gene expression during cell cycle progression (Bjursell & Reichard, 1973). Furthermore, there have been debates that whole-culture synchronisation cannot be performed as synchronisation only aligns a small population of cells (Cooper et al., 2008). Another study by Cooper et al. (2006) also argues that chemical synchronisation by nocodazole only arrests cells at G2 prior to mitosis and therefore produce a mixed population of cells that have G2-DNA content and G1-DNA due to some cells escaping synchronisation, further masking the expression of cell cycle genes. These studies therefore indicate that there are limitations to the respective synchronisation methods, hence specific methods need to be applied for specific cell types that have a lengthy cell cycle duration.

Although the above studies suggest that serum starvation is the preferable method to synchronise even whole-cell culture, especially mesenchymal cells, there are currently no studies that have investigated the cell cycle duration of iPSC-derived MSCs. Furthermore, there is no current data which compares cell cycle duration between primary MSCs and iPSC-MSCs. Future work will, therefore, address this gap in order to optimise synchronisation of iPSC-MSCs and as to verify whether there is actual correlation between FAM111B mRNA and protein expression.

Despite the evident problems with synchronization of the iPSC-MSCs, there was useful information that could be gleaned from the cell cycle experiments. Analysis of FAM111B expression in synchronised patient and control iPSC-MSCs showed that FAM111B mRNA expression is temporally expressed, peaking at 2-hours (S-phase) as well as at 15-hour (G1 phase) timepoints. Though there was slight variation in the peak of FAM111B mRNA expression between this study and the findings by Aviner et al. (2015), who showed that FAM111B mRNA peaks at the G1-phase. This variation may have been due to the different cell types and analytical methods used for both these studies. Aviner et al. (2015) measured FAM111B mRNA expression by RNA-seq in HeLa cells, while the current study measured relative FAM111B mRNA expression in synchronised iPSC-MSCs using by quantitative real-time PCR. Furthermore, the inconclusive protein data in this study limited further analysis of FAM111B between the current study and the findings by Aviner et al. (2015). However, the findings in this study are in line with the findings by Aviner et al.

(2015) that FAM111B mRNA expression is associated with the G1→S cell cycle progression, peaking the at S-phase and that FAM111B is co-expressed with PCNA expression which also peaked at 2 hours (S-phase). The elevated levels of expression of FAM111B at S phase are in line with ChEA data (http://amp.pharm.mssm.edu/lib/chea.jsp), which shows that the FAM111B promoter region contains a binding site for the E2F-1 transcriptional activator known to be involved in the regulation of cell cycle transition into the S-phase. A recent study by Melling (2018) showed that the FAM111B promoter activity is increased in synchronised human lung carcinoma cell line (H1299) that were transfected with plasmids expressing E2F1 and E4orf6/7 which is a viral (adenovirus) analogue to human p107. Protein interaction assays such the chromatin immunoprecipitation (ChIP) assay could be performed to determine whether there is FAM111B-E2F1 interaction at the G1 and S-phase to confirm the abundance of FAM111B protein in patient cells compared to controls. Furthermore, a report by Peng et al. (2008), stated that FAM111B/CANP levels are higher in foetal tissue and cancer cells compared to differentiating and adult cells. Foetal and cancer cells are known to exhibit higher cell proliferation rates compared to normal adult cells. Though different cell lines were used in this study, the data corroborates the report by Peng et al. (2008) as the results in this study showed that iPSCs, which have high proliferation rate express significantly higher levels FAM111B mRNA compared to dermal fibroblasts and iPSC-MSCs. These results further support the findings that FAM111B mRNA in synchronised iPSC-MSCs is temporally expressed and that patient cells express significantly higher levels than normal.

Protein quantification was also performed to determine whether there is a correlation between FAM111B mRNA and protein expression. However, there was no correlation between mRNA and protein expression nor were there any statistical differences in protein expression between patient and control iPSC-MSCs. Given that it was clear that not all cells were adequately synchronised, one cannot draw any conclusions from these results. These experiments will be repeated once the cell cycle duration and the effective synchronisation method for iPSC-MSCs are established.

While inefficient cell synchronisation may be the main conceivable reason for the differences in FAM111B mRNA and protein expression, other factors which may affect protein expression should also be considered, such mRNA-protein ratio as well as the specificity and/or effectiveness of the antibody used in this study. Studies have shown that

there are variations in transcription and translation rates which affect protein abundance (Lin & Amir, 2018; Liu et al., 2016). It has also been indicated that the mRNA-protein relationship is influenced by modulation of mRNA translation by the binding of non-coding RNAs (e.g. miRNA) on the regulatory elements of the transcript (Ebert & Sharp, 2012; Liu et al., 2016). The ubiquitin-proteasome pathway (UPP) has also been shown to influence protein levels and half-life independent of the mRNA levels. Furthermore, the delay in protein synthesis also contributes to the non-correlation with mRNA. For instance, a study by (Jovanovic et al., 2015) showed that mRNA levels of immune genes in mouse dendritic cells are elevated 3 hours after stimulation with lipopolysaccharide (LPS) while protein levels were elevated only 12 hours post-LPS stimulation. Another factor that could be considered to cause the differences in FAM111B mRNA and protein expression relates to the antibody used in this study. The Human Protein Atlas (www.proteinatlas.org) reported in their detection of FAM111B that the antibody staining of FAM111B in human tonsil tissue was inconsistent with RNA expression. Though the present study used a different antibody (sc-246547) compared to the Human Protein Atlas (HPA038637) similar findings were observed. Lastly, it is also important to note that though data by Aviner et al. (2015) showed similar pattern of FAM111B mRNA and protein expression in HeLa cells, their study also indicates that certain cell cycle genes with high mRNA and translation do not show similar protein data, and further state that protein expression of these cell cycle genes is not reflected by steady-state protein accumulation. Clearly, future work will include optimising antibody detection and specificity.

As mentioned above, the FAM111B protein levels may be due to posttranslational modifications such as ubiquitination which is known to modulate protein expression during cellular processes such as cell cycle progression (Liu et al., 2016). Interestingly, ubiquitin binding sites have been identified on FAM111B and are reported to be localised on lysine (K) 382, K429 and K62 (www.genecards.org). Functional studies, however, are needed to confirm activity on these ubiquitin sites. It should also be noted that gene mutations in some hereditary disorders may also show equivalent mRNA and/or protein expression as the wildtype. For example, a study by Devine et al. (2011) indicated that the protein levels of the mutant LRRK2 protein which causes autosomal dominant Parkinson's disease, were similar between patient and control fibroblasts. Another study indicated that protein expression of the mutant Four and a half LIM domain protein 1 (FHL1), which causes Reducing Body Myopathy (RBM) due to poor myotube differentiation, was similar to the wildtype in induced

C2C12 mouse myoblast cells. In this condition, the mutant gene causes protein aggregates that inhibit normal myotube differentiation (Wilding et al., 2014). These studies thus indicate that though comparable protein levels can be observed between affected and unaffected cells, the pathogenesis of these conditions may be caused by protein modifications which are not detected by protein quantification.

The data in this chapter demonstrates that patient cells exhibit a higher proliferation rate than control cells, and that elevated FAM111B mRNA levels may be associated with increased cell proliferation as recent studies have indicated that FAM111B is be involved in cell proliferation, though the mechanism of action is undefined. Future work will include investigating FAM111B protein expression in synchronised cells using the serum starvation method which may yield better results compared to the thymidine method used in this current study. Posttranslational modification (e.g. ubiquitination) assays and immuno-detection assays will also be performed to determine FAM111B localisation during cell cycle progression, and whether there is modulation of the ubiquitin proteasome system in FAM111B degradation. Future work will, furthermore, focus on FAM111B protein expression, activity and regulation as it will reveal the mechanism by which the mutation causes POIKTMP for clinical application in the affected persons.

Chapter 5

General discussion and conclusion

5.1 Summary of key findings

Mutations in the *FAM111B* gene are associated with hereditary fibrosing poikiloderma with tendon contractures, myopathy and pulmonary fibrosis (POIKTMP). Since the putative function of FAM111B has not been described, this study aimed to investigate its involvement in fibrogenesis in a South African family carrying an autosomal dominant FAM111B mutation (c. 1861 T>G p. Tyr621Asp.). While it was hypothesised that FAM111B influences expression of pro-fibrotic genes, the findings in this study revealed that patient cells carrying the FAM111B mutation express normal levels of pro-fibrotic markers (COL1A1, COL3A1 and α-SMA). Collagen content also indicated to be unaffected in the patient cells, thereby confirming the expression data. These results, therefore, indicate that FAM111B does not directly induce fibrosis via the dysregulation of pro-fibrotic markers.

Recent studies have indicated that FAM111B is among the uncharacterised proteins involved in cell proliferation and cell cycle progression (Aviner et al., 2015; Baselet et al., 2017). To determine the basis of cell cycle modulation in this condition, a growth curve was performed to determine the proliferation rate between patient and control cells. The results showed that patient cells have over 2-fold cell proliferation compared to the control cells. Cell cycle experiments were therefore, performed to determine whether there is an association between FAM111B expression and cell cycle progression. The results revealed that FAM111B mRNA expression is cell cycle-regulated, peaking at the S-phase. Most importantly, they showed that patient cells express significantly high FAM111B mRNA levels compared to control cells in a cell cycle-dependent manner. Protein data were, however, inconclusive as the iPSC-MSCs indicated poor synchronisation for protein analysis. This may have been caused by the synchronisation method and/or the cell type used in this study. Taken together, this study has firstly, revealed that the cells derived from the South African patients carrying a *FAM111B* mutation have higher proliferation rate than the unaffected control cells. Secondly, though further experimentation is required in synchronised cells for protein analysis, mRNA data in this study indicate strong evidence that FAM111B is cell cycle-regulated and that it is highly expressed in the patient cells compared to controls. In summary, the data in this study suggest that the FAM111B mutation modulates

cell proliferation in persons with POIKTMP, which plausibly contributes to the phenotype in this condition.

5.2 Creating *in vitro* cell models to elucidate FAM111B function

Hereditary fibrosing poikiloderma (POIKTMP) in the South African family presents primarily with fibrosis in skeletal muscle, skin and lungs (Khumalo et al., 2006; Mercier et al., 2013). Based on the findings in this study the FAM111B mutation alters cell proliferation in the patient cells, but it is unclear how the mutation causes myopathy or tendon contractures. Fibrosis in skeletal muscle has been indicated to be caused by the continuous cycle of myofiber degeneration and regeneration, followed by excessive proliferation of fibroblasts as well as increased production of ECM proteins (Serrano & Munoz-Canoves, 2010). In the patients with POIKTMP there is also muscle fragmentation that is replaced by fatty infiltration. Fatty infiltration is suggested to be caused by differentiation of fibro/adipogenic progenitor cells that are found in the interstitial space of skeletal muscle (Uezumi et al., 2011). It is probable that the FAM111B mutation contributes to the continuous cycle of muscle degeneration and fibrosis via fibro/adipogenic progenitors as they are able differentiate into fibroblasts and/or adipocytes during muscle repair, however, further studies need to be performed. Tendon contractures which are described as thickening of the tendons due to increased collagen deposition (Nolan, 1992) may be a secondary effect of this condition as their aetiology is unclear in literature.

The current *in vitro* study used the iPSC-derived mesenchymal stem/stromal cells to investigate their proliferation and expression of pro-fibrotic factors as they have the potential to differentiate into myocytes as well as myofibroblasts under specific conditions (Desai et al., 2014; Xu et al., 2017). The limitation of this cellular model is that it could not recapitulate some of the fibrotic features observed in POIKTMP due to time constraints and the complexity of fibrosis (Mercier et al., 2013). Also, a 2D monolayer culture system was used in this study which has its limitation in mimicking the 3D *in vivo* microenvironment or complete disease modelling (Antoni et al., 2015; Duval et al., 2017). Furthermore, no chemical or mechanical insults were applied to iPSC-MSCs such as treatment with TGF-β or scratch assays to induce *in vitro* “wounding healing” or “fibrosis” to determine cell proliferation and fibrogenesis in these experimental conditions. Improving this *in vitro*

model will provide greater insights into understanding the role of FAM111B during wound healing and fibrosis.

The patient-derived iPSCs provide an infinite source for creation of *in vitro* tissue-specific models for studying POIKTMP. The unknown function of FAM111B thus requires that iPSCs be further differentiated into other cell types that are affected in this condition to gain more insight into the onset of this fibroproliferative condition. Firstly, it is crucial that a 3D culture system be used to mimic the *in vivo* milieu. Studies have shown that culturing human MSCs in hydrogel scaffolds stimulated with CTGF or TGF-β leads to their differentiation into myofibroblasts and increase production of ECM proteins (Xu et al., 2017). Furthermore, differentiation of iPSC-MSCs into skeletal myocytes to investigate the onset of myopathy in this condition may also reveal the role of FAM111B in myocyte degeneration and fatty infiltration observed in POIKTMP. In addition, the Protein Atlas database (www.proteinatlas.org) has indicated that FAM111B expression is high in tissues of the endodermal lineage such as the pancreas, lung and prostate; these are some of the tissues that are affected in POIKMTP cases or prostate cancer linked to FAM111B (Akamatsu et al., 2012; Goussot et al., 2017; Mercier et al., 2013; Takeichi et al., 2016); therefore, cellular modelling must also be directed towards these cell types to gain more understanding into the function of FAM111B. The derived patient-specific iPSCs could also be differentiated into 3D skin and/or lung organoids under the 3D culture system (Ho et al., 2018; Miller et al., 2019; Zuppinger, 2016). Recent studies have shown that 3D cell culture models develop tissue stroma and the heterogenous cell type found in the specific tissue (Dutta et al.). For instance, a study by (Hohwieler et al., 2016) showed that iPSC-derived pancreatic organoids formed mature acinar/ductal structures which also produced enzymes such as carbonic anhydrase. Another study by Dye et al. (2015) demonstrated that iPSC-derived lung organoids presented with epithelial structures that resembled the proximal airway and were also associated with mesenchymal cells which expressed α-SMA.

There are still challenges in the creation of iPSC-derived *in vitro* models that mimic molecular changes at different stages of disease progression (Miller et al., 2013). Creation of these *in vitro* models is not only expensive, but it is also laborious and requires further troubleshooting to obtain a culture model that best mimics the structure and function of the specific tissue (Dye et al., 2015; Miller et al., 2019). Furthermore, there is also a challenge of self-organisation of organoid cell cultures as they do not always undergo uniform self-organization (Ho et al., 2018). Moreover, it is also important to determine the lifespan of the

derived cell types and to match it to the primary cells as it is known that cellular reprogramming also alters the epigenetic signature of the reprogrammed cells. For example, iPSC-MSCs have been shown to exhibit similar characteristics as primary MSCs (Diederichs & Tuan, 2014; Frobel et al., 2014; Kang et al., 2015). They have also been shown to maintain a distinct epigenetic signature and acquire rejuvenation-associated gene signature compared to primary MSCs (Frobel et al., 2014; Spitzhorn et al., 2019). A study by Frobel et al. (2014) showed that redifferentiation of iPSCs that were derived BM- MSCs into iPSC-MSCs acquire moderate age-related DNA methylation compared to BM-MSCs and were estimated to be younger than the donor MSCs. In contrast, a recent study by Fernandez-Rebollo et al. (2019) indicated that iPSC-MSCs acquire similar changes in morphology as primary MSCs and display similar senescence-associated metabolomic phenotype. Furthermore, they reach growth arrest at cumulative population doubling (CPD) of 17 compared to primary MSCs that reached growth arrest at CPD of 21. Therefore, it is important to determine the aging of the cell type used for disease modelling. Another challenge is aging the iPSC-derived disease models as they "age" at a different pace as primary cells.

Creation of an isogenic lines in this study is required for future work to eliminate the genetic background of non-isogenic cell lines which contributes to the variation of the results observed in this study. The clustered regularly interspaced short palindromic repeat-Cas9 (CRISPR-Cas9) system is a gene editing tool which can be used to create isogenic cell lines by performing a homolog-directed repair (HDR) where the Cas9 endonuclease is directed to the target DNA locus by guide RNAs to repair the target mutation (Ran et al., 2013). Gene editing of patient-derived cells by the CRISPR-Cas9 system will therefore, allow for comparison of the wildtype and mutant cells from the same donor and further reveal some of the subtle phenotypic differences that may have been masked by the genetic background of non-isogenic donor cells (Bassett, 2017; Grobarczyk et al., 2015). The generation of FAM111B isogenic cell lines will further yield conclusive findings such as whether the *FAM111B* mutation alters expression of pro-fibrotic markers since no differences were observed when compared with the non-isogenic control cells. Furthermore, the creation of patient-derived isogenic iPSCs will contribute to understanding the fibrotic phenotype affecting the different cell types as well as its mechanism in different disease models that will be derived for this condition.

5.3 Functional characterisation of FAM111B

Further characterisation of the FAM111B protein is also required as gene mutations may cause molecular modifications during protein expression and folding. Bioinformatic data have, for instance, indicated that there are ubiquitination sites on the FAM111B protein and are localised on lysine (K) 382, K429 and K62 (www.genecards.org). It has also been indicated that FAM111B forms part of the ubiquitin-mediated proteolysis pathway (UMPP) (Guo et al., 2011) and that FAM111B is frequently mutated in renal cell carcinoma (Rydzanicz et al., 2013). The FAM111B mutation in this study is located at the loop region (p. Tyr621Asp.) of the catalytic domain (Mercier et al., 2013), therefore it is likely that it affects the catalytic activity of this protein. Based on the current findings that the mutation induces increased cell proliferation in patient cells, this suggests a gain-of-function mutation as hypothesised by Mercier et al. (2013). A gain-of-function mutations exert effects which the wild-type gene does not (van Oijen & Slootweg, 2000). It is, therefore, possible that the FAM111B mutation in the South African family acquires new function in proliferating cells. Further experiments such as *in vitro* wounding or stress assays need to be performed as the gain-of-function phenotype in patient cells may lead to increased cell proliferation. Furthermore, since FAM111B is described as a serine/cysteine protease it is also likely that the mutation may lead to autoactivation or inhibit inactivation of the catalytic site leading to POIKTMP, as observed in gain-of-function mutations on the cationic trypsinogen enzyme which causes hereditary pancreatitis (Sahin-Tóth & Tóth, 2000). Moreover, the FAM111B-fibrosis and FAM111B-cancer link should be further explored as it may also reveal the role of FAM111B in fibrosis and cancer. For, instance, a study by Fernandez-Retana et al. (2017) showed that FAM111A and FAM111B form part of the degradome-related genes which are upregulated in cervical cancer as they are also involved in the breakdown of the extracellular matrix for cancer metastasis.

5.4 Potential treatment for POIKTMP

The standard treatment for fibrotic diseases such as systemic sclerosis, hepatic fibrosis, idiopathic pulmonary fibrosis (IPF) and nephrogenic systemic fibrosis is targeted downstream kinases in the TGF-β and PDGF receptor signalling pathway (Daniels et al., 2004; Kay & High, 2008). For example, Imatinib mesylate inhibits tyrosine kinase activation to prevent binding of TGF-β to SMAD-independent receptors (e.g. PI3K/Akt/ c-Abl) as well as PDGF

signalling. Imatinib has been shown to particularly target the non-receptor tyrosine kinase-cellular Abelson (c-Abl) as well as the non-canonical TGF-β pathway (Kay & High, 2008).

Most of these therapeutic drugs such as Pirfenidone aim to target TGF-β and its pathway. Although some improvement has been observed, it should be noted that TGF-β plays an essential role in cellular processes such as proliferation, cell migration and differentiation; therefore, its inhibition may have long-term negative consequences. Some studies have therefore reported that the timing of treating fibrosis using TGF-β inhibitors is crucial as treating early may worsen the condition while treating later may greatly improve the condition (Edgley et al., 2012). Some promising studies have demonstrated that targeting the EMT process during fibrosis may be effective in treating fibrosis. For example, a study by Kim et al. (2017) demonstrated that the use of chromones which are present in plant flavones can downregulate EMT-associated genes. This study demonstrated that Eupatilin, a chromone derivative successfully downregulated lymphocyte infiltration, collagen I, periostin and α-SMA expression as well as overall ECM deposition in IPF lung fibroblasts and hepatic stellate cells *in vitro* (Kim et al., 2017). Corticosteroids which function as anti-inflammatory agents to prevent the activation of pro-inflammatory factors have also been used to treat idiopathic pulmonary fibrosis (Walter et al., 2006). These therapeutic agents, however, have proven to be ineffective for long-term treatment of fibrosis.

Since FAM111B is associated with fibrosis and cancer (Fernandez-Retana et al., 2017; Mercier et al., 2013; Yue et al., 2015), it is of interest, based on the findings in this study, if the repurposing of cancer-drugs can be used to treat POIKTMP as it induces increased cell proliferation in the affected persons. Recent studies have indicated that co-treatment of cancer-associated fibroblasts with cisplatin and pirfinedone leads to increased apoptosis and reduced cancer progression in non-small cell lung cancer (NSCLC) cell lines and prostate (Mediavilla-Varela et al., 2016). Furthermore, treatment of pulmonary fibrosis with histone deacetylase (HDAC) inhibitors such as Suberanilohydroxamic acid (SAHA) which is used to treat T-cell lymphoma was shown to reduce inflammation in IPF lung cells by inhibiting biosynthesis of Leukotriene B4 (LTB4) enzyme required for chemotactic activity of leukocytes in mouse acute lung infection model (Lu et al., 2017b). Another study indicated that treatment of IPF lung cells with UCN-01, (7-hydroxystaurosporinean), an anti-cancer drug that is currently tested in phase II clinical trial (http://clinicaltrials.gov) increases expression of the Forkhead box O3 (FoxO3) transcription factor. This transcription factor was found to be downregulated in fibroblasts obtained from human IPF lung and those from a

mouse bleomycin model. Treatment of the cells with UNC-01 leads to increased FoxO3 protein levels which indicated to reduce cell proliferation and expression of pro-fibrotic markers such as COL1A1, COL3A1 and α-SMA (Al-Tamari et al., 2017). These studies, though in early stages thus indicate that anti-cancer drugs can be repurposed for treatment of fibrosis by also targeting cell proliferation which is also observed in the POIKTMP condition.

5.5 Conclusion and Future work

This study revealed that FAM111B mutation increases proliferation of patient cells. It further showed that FAM111B mRNA is increased in the patient cells. However, protein data for FAM111B expression during cell cycle progression was inconclusive. Therefore, determination of the cell cycle duration in the derived iPSC-MSCs is important for determining whether there are differences in the expression of FAM111B protein in patient cells.

Future work will also focus on developing the 3D disease model(s) to elucidate the function of FAM111B. Together with the UCT FAM111B group, future work will also focus on protein characterisation and enzymatic activity, particularly during cell cycle progression as the current data indicate its involvement in DNA synthesis. Furthermore, FAM111B expression and its role in cancer cells will be explored as it may perform similar function in POIKTMP.

Reference List

Achille, V., Mantelli, M., Arrigo, G., Novara, F., Avanzini, M. A., Bernardo, M. E., et al. (2011). Cell-cycle phases and genetic profile of bone marrow-derived mesenchymal stromal cells expanded in vitro from healthy donors. *J Cell Biochem, 112*(7), 1817-1821.

Akamatsu, S., Takata, R., Haiman, C. A., Takahashi, A., Inoue, T., Kubo, M., et al. (2012). Common variants at 11q12, 10q26 and 3p11.2 are associated with prostate cancer susceptibility in Japanese. [10.1038/ng.1104]. *Nat Genet, 44*(4), 426-429.

Akhmetshina, A., Palumbo, K., Dees, C., Bergmann, C., Venalis, P., Zerr, P., et al. (2012). Activation of canonical Wnt signalling is required for TGF-β-mediated fibrosis. [Article]. *Nature Communications, 3*, 735.

Akram, K. M., Lomas, N. J., Forsyth, N. R., & Spiteri, M. A. (2014). Alveolar epithelial cells in idiopathic pulmonary fibrosis display upregulation of TRAIL, DR4 and DR5 expression with simultaneous preferential over-expression of pro-apoptotic marker p53. *Int J Clin Exp Pathol, 7*(2), 552-564.

Al-Tamari, H. M., Dabral, S., Schmall, A., Sarvari, P., Ruppert, C., Paik, J., et al. (2017). FoxO3 an important player in fibrogenesis and therapeutic target for idiopathic pulmonary fibrosis. *EMBO Molecular Medicine*, e201606261.

Alabert, C., Bukowski-Wills, J. C., Lee, S. B., Kustatscher, G., Nakamura, K., de Lima Alves, F., et al. (2014). Nascent chromatin capture proteomics determines chromatin dynamics during DNA replication and identifies unknown fork components. *Nat Cell Biol, 16*(3), 281-293.

Aliborzi, G., Vahdati, A., Mehrabani, D., Hosseini, S. E., & Tamadon, A. (2016). Isolation, Characterization and Growth Kinetic Comparison of Bone Marrow and Adipose Tissue Mesenchymal Stem Cells of Guinea Pig. *International journal of stem cells, 9*(1), 115-123.

Ansorge, M., Sapudom, J., Chkolnikov, M., Wilde, M., Anderegg, U., Möller, S., et al. (2017). Mimicking Paracrine TGFβ1 Signals during Myofibroblast Differentiation in 3D Collagen Networks. *Scientific Reports, 7*(1), 5664.

Antoni, D., Burckel, H., Josset, E., & Noel, G. (2015). Three-dimensional cell culture: a breakthrough in vivo. *Int J Mol Sci, 16*(3), 5517-5527.

Arber, C., Precious, S. V., Cambray, S., Risner-Janiczek, J. R., Kelly, C., Noakes, Z., et al. (2015). Activin A directs striatal projection neuron differentiation of human pluripotent stem cells. *Development, 142*(7), 1375-1386.

Arpino, V., Brock, M., & Gill, S. E. (2015). The role of TIMPs in regulation of extracellular matrix proteolysis. *Matrix Biology, 44–46*, 247-254.

Aso, M., Kondo, M., Suemune, H., & Hecht, S. M. (1999). Chemistry of the Bleomycin-Induced Alkali-Labile DNA Lesion. *Journal of the American Chemical Society, 121*(39), 9023-9033.

Aso, Y., Yoneda, K., & Kikkawa, Y. (1976). Morphologic and biochemical study of pulmonary changes induced by bleomycin in mice. *Lab Invest, 35*(6), 558-568.

Aviner, R., Shenoy, A., Elroy-Stein, O., & Geiger, T. (2015). Uncovering Hidden Layers of Cell Cycle Regulation through Integrative Multi-omic Analysis. *PLoS Genetics, 11*(10), e1005554.

Avior, Y., Sagi, I., & Benvenisty, N. (2016). Pluripotent stem cells in disease modelling and drug discovery. [Review]. *Nat Rev Mol Cell Biol, 17*(3), 170-182.

Ayaub, E. A., Dubey, A., Imani, J., Botelho, F., Kolb, M. R. J., Richards, C. D., et al. (2017). Overexpression of OSM and IL-6 impacts the polarization of pro-fibrotic macrophages and the development of bleomycin-induced lung fibrosis. *Scientific Reports, 7*(1), 13281.

B. Moore, B., Lawson, W. E., Oury, T. D., Sisson, T. H., Raghavendran, K., & Hogaboam, C. M. (2013). Animal Models of Fibrotic Lung Disease. *American Journal of Respiratory Cell and Molecular Biology, 49*(2), 167-179.

Baghbaderani, Behnam A., Tian, X., Neo, Boon H., Burkall, A., Dimezzo, T., Sierra, G., et al. (2015). cGMP-Manufactured Human Induced Pluripotent Stem Cells Are Available for Pre-clinical and Clinical Applications. *Stem Cell Reports, 5*(4), 647-659.

Bahr, A., De Graeve, F., Kedinger, C., & Chatton, B. (1998). Point mutations causing Bloom's syndrome abolish ATPase and DNA helicase activities of the BLM protein. [Original Paper]. *Oncogene, 17*, 2565.

Baker, A. H., Edwards, D. R., & Murphy, G. (2002). Metalloproteinase inhibitors: biological actions and therapeutic opportunities. [10.1242/jcs.00063]. *Journal of Cell Science, 115*(19), 3719.

Balkwill, F., Charles, K. A., & Mantovani, A. (2005). Smoldering and polarized inflammation in the initiation and promotion of malignant disease. *Cancer Cell, 7*(3), 211-217.

Banfalvi, G. (2011). Overview of cell synchronization. *Methods Mol Biol, 761*, 1-23.

Barakat, T. S., Ghazvini, M., de Hoon, B., Li, T., Eussen, B., Douben, H., et al. (2015). Stable X chromosome reactivation in female human induced pluripotent stem cells. *Stem cell reports, 4*(2), 199-208.

Barnes, J., & Mayes, M. D. (2012). Epidemiology of systemic sclerosis: incidence, prevalence, survival, risk factors, malignancy, and environmental triggers. *Curr Opin Rheumatol, 24*(2), 165-170.

Barnum, K. J., & O'Connell, M. J. (2014). Cell Cycle Regulation by Checkpoints. *Methods in molecular biology (Clifton, N.J.), 1170*, 29-40.

Barrientos, S., Stojadinovic, O., Golinko, M. S., Brem, H., & Tomic-Canic, M. (2008). Growth factors and cytokines in wound healing. [WRR410 pii ;10.1111/j.1524-475X.2008.00410.x doi]. *Wound.Repair Regen., 16*(5), 585-601.

Baselet, B., Belmans, N., Coninx, E., Lowe, D., Janssen, A., Michaux, A., et al. (2017). Functional Gene Analysis Reveals Cell Cycle Changes and Inflammation in Endothelial Cells Irradiated with a Single X-ray Dose. *Frontiers in Pharmacology, 8*, 213.

Bassett, A. R. (2017). Editing the genome of hiPSC with CRISPR/Cas9: disease models. *Mammalian genome : official journal of the International Mammalian Genome Society, 28*(7-8), 348-364.

Baxter, R. M., Crowell, T. P., McCrann, M. E., Frew, E. M., & Gardner, H. (2005). Analysis of the tight skin (Tsk1//+) mouse as a model for testing antifibrotic agents. *Lab Invest, 85*(10), 1199-1209.

Beers, J., Linask, K. L., Chen, J. A., Siniscalchi, L. I., Lin, Y., Zheng, W., et al. (2015). A cost-effective and efficient reprogramming platform for large-scale production of integration-free human induced pluripotent stem cells in chemically defined culture. [Article]. *Scientific Reports, 5*, 11319.

Berardis, S., Dwisthi Sattwika, P., Najimi, M., & Sokal, E. M. (2015). Use of mesenchymal stem cells to treat liver fibrosis: Current situation and future prospects. *World Journal of Gastroenterology : WJG, 21*(3), 742-758.

Bertoli, C., Skotheim, J. M., & de Bruin, R. A. (2013). Control of cell cycle transcription during G1 and S phases. *Nat Rev Mol Cell Biol, 14*(8), 518-528.

Beyer, C., Schett, G., Distler, O., & Distler, J. H. W. (2010). Animal models of systemic sclerosis: Prospects and limitations. *Arthritis & Rheumatism, 62*(10), 2831-2844.

Bianco, P., Robey, P. G., & Simmons, P. J. (2008). Mesenchymal Stem Cells: Revisiting History, Concepts, and Assays. *Cell stem cell, 2*(4), 313-319.

Bickmore, W. A.

Biernacka, A., Dobaczewski, M., & Frangogiannis, N. G. (2011). TGF-beta signaling in fibrosis. *Growth Factors, 29*.

Bjursell, G., & Reichard, P. (1973). Effects of thymidine on deoxyribonucleoside triphosphate pools and deoxyribonucleic acid synthesis in Chinese hamster ovary cells. *J Biol Chem, 248*(11), 3904-3909.

Blaauboer, M. E., Emson, C. L., Verschuren, L., van Erk, M., Turner, S. M., Everts, V., et al. (2013). Novel combination of collagen dynamics analysis and transcriptional profiling reveals fibrosis-relevant genes and pathways. *Matrix Biology, 32*(7), 424-431.

Blanpain, C., Lowry, W. E., Geoghegan, A., Polak, L., & Fuchs, E. (2004). Self-renewal, multipotency, and the existence of two cell populations within an epithelial stem cell niche. *Cell, 118*(5), 635-648.

Boisset, J.-C., & Robin, C. (2012). On the origin of hematopoietic stem cells: Progress and controversy. *Stem Cell Research, 8*(1), 1-13.

Bonella, F., Stowasser, S., & Wollin, L. (2015). Idiopathic pulmonary fibrosis: current treatment options and critical appraisal of nintedanib. *Drug Design, Development and Therapy, 9*, 6407-6419.

Borthwick, L. A., Wynn, T. A., & Fisher, A. J. (2013). Cytokine mediated tissue fibrosis(). *Biochimica et biophysica acta, 1832*(7), 1049-1060.

Buganim, Y., Faddah, D. A., Cheng, A. W., Itskovich, E., Markoulaki, S., Ganz, K., et al. (2012). Single-cell gene expression analyses of cellular reprogramming reveal a stochastic early and hierarchic late phase. *Cell, 150*(6), 1209-1222.

Buganim, Y., Faddah, D. A., & Jaenisch, R. (2013). Mechanisms and models of somatic cell reprogramming. *Nature reviews. Genetics, 14*(6), 427-439.

Bustin, S. A., Benes, V., Garson, J. A., Hellemans, J., Huggett, J., Kubista, M., et al. (2009). The MIQE Guidelines: Minimum Information for Publication of Quantitative Real-Time PCR Experiments. [10.1373/clinchem.2008.112797]. *Clinical Chemistry, 55*(4), 611.

Caminati, A., Madotto, F., Cesana, G., Conti, S., & Harari, S. (2015). Epidemiological studies in idiopathic pulmonary fibrosis: pitfalls in methodologies and data interpretation. [10.1183/16000617.0040-2015]. *European Respiratory Review, 24*(137), 436.

Cantone, I., Bagci, H., Dormann, D., Dharmalingam, G., Nesterova, T., Brockdorff, N., et al. (2016). Ordered chromatin changes and human X chromosome reactivation by cell fusion-mediated pluripotent reprogramming. [Article]. *Nature Communications, 7*, 12354.

Carthy, J. M., Garmaroudi, F. S., Luo, Z., & McManus, B. M. (2011). Wnt3a induces myofibroblast differentiation by upregulating TGF-beta signaling through SMAD2 in a beta-catenin-dependent manner. *PLoS One, 6*(5), e19809.

Cerdan, C., & Bhatia, M. (2010). Novel roles for Notch, Wnt and Hedgehog in hematopoesis derived from human pluripotent stem cells. *Int J Dev Biol, 54*(6-7), 955-963.

Chakraborty, S., Chopra, P., Ambi, S. V., Dastidar, S. G., & Ray, A. (2014). Emerging therapeutic interventions for idiopathic pulmonary fibrosis. *Expert Opinion on Investigational Drugs, 23*(7), 893-910.

Chan, K. K.-K., Zhang, J., Chia, N.-Y., Chan, Y.-S., Sim, H. S., Tan, K. S., et al. (2009). KLF4 and PBX1 Directly Regulate NANOG Expression in Human Embryonic Stem Cells. *STEM CELLS, 27*(9), 2114-2125.

Chang, H. Y., Sneddon, J. B., Alizadeh, A. A., Sood, R., West, R. B., Montgomery, K., et al. (2004). Gene expression signature of fibroblast serum response predicts human cancer progression: similarities between tumors and wounds. *PLoS Biol, 2*(2), E7.

Chasseuil, E., McGrath, J. A., Seo, A., Balguerie, X., Bodak, N., Chasseuil, H., et al. (2019). Dermatological manifestations of hereditary fibrosing poikiloderma with tendon contractures, myopathy and pulmonary fibrosis (poiktmp): a case series of 28 patients. *British Journal of Dermatology, 0*(ja).

Cheifetz, S., Hernandez, H., Laiho, M., ten, D. P., Iwata, K. K., & Massague, J. (1990). Distinct transforming growth factor-beta (TGF-beta) receptor subsets as determinants of cellular responsiveness to three TGF-beta isoforms. *J.Biol.Chem., 265*(33), 20533-20538.

Chen, G., & Deng, X. (2018). Cell Synchronization by Double Thymidine Block. *Bio-protocol, 8*(17), e2994.

Chen, M., Huang, J., Yang, X., Liu, B., Zhang, W., Huang, L., et al. (2012). Serum Starvation Induced Cell Cycle Synchronization Facilitates Human Somatic Cells Reprogramming. *PLOS ONE, 7*(4), e28203.

Chen, X., Sun, R., Hu, J., Mo, Z., Yang, Z., Liao, D., et al. (2008). Attenuation of Bleomycin-Induced Lung Fibrosis by Oxymatrine Is Associated with Regulation of Fibroblast Proliferation and Collagen Production in Primary Culture. *Basic & Clinical Pharmacology & Toxicology, 103*(3), 278-286.

Chen, X., Zhai, Y., Yu, D., Cui, J., Hu, J. F., & Li, W. (2016). Valproic Acid Enhances iPSC Induction From Human Bone Marrow-Derived Cells Through the Suppression of Reprogramming-Induced Senescence. *J Cell Physiol, 231*(8), 1719-1727.

Chilosi, M., Poletti, V., Zamo, A., Lestani, M., Montagna, L., Piccoli, P., et al. (2003). Aberrant Wnt/beta-catenin pathway activation in idiopathic pulmonary fibrosis. *Am J Pathol, 162*(5), 1495-1502.

Choe, K. N., & Moldovan, G. L. (2017). Forging Ahead through Darkness: PCNA, Still the Principal Conductor at the Replication Fork. *Mol Cell, 65*(3), 380-392.

Chou, B. K., Mali, P., Huang, X., Ye, Z., Dowey, S. N., Resar, L. M., et al. (2011). Efficient human iPS cell derivation by a non-integrating plasmid from blood cells with unique epigenetic and gene expression signatures. *Cell Res, 21*(3), 518-529.

Christner, P. J., Peters, J., Hawkins, D., Siracusa, L. D., & Jiménez, S. A. (1995). The tight skin 2 mouse. *Arthritis & Rheumatism, 38*(12), 1791-1798.

Chung, E., & Son, Y. (2014). Crosstalk between mesenchymal stem cells and macrophages in tissue repair. [journal article]. *Tissue Engineering and Regenerative Medicine, 11*(6), 431-438.

Clevers, H., & Nusse, R. (2012). Wnt/beta-catenin signaling and disease. *Cell, 149*(6), 1192-1205.

Cooper, S., Chen, K. Z., & Ravi, S. (2008). Thymidine block does not synchronize L1210 mouse leukaemic cells: implications for cell cycle control, cell cycle analysis and whole-culture synchronization. *Cell Proliferation, 41*(1), 156-167.

Cooper, S., Iyer, G., Tarquini, M., & Bissett, P. (2006). Nocodazole does not synchronize cells: implications for cell-cycle control and whole-culture synchronization. *Cell Tissue Res, 324*(2), 237-242.

Corcione, A., Benvenuto, F., Ferretti, E., Giunti, D., Cappiello, V., Cazzanti, F., et al. (2006). Human mesenchymal stem cells modulate B-cell functions. *Blood, 107*(1), 367-372.

Coronado, D., Godet, M., Bourillot, P.-Y., Tapponnier, Y., Bernat, A., Petit, M., et al. (2013). A short G1 phase is an intrinsic determinant of naïve embryonic stem cell pluripotency. *Stem Cell Research, 10*(1), 118-131.

Coward, W. R., Saini, G., & Jenkins, G. (2010). The pathogenesis of idiopathic pulmonary fibrosis. *Ther Adv Respir Dis, 4*(6), 367-388.

Daniels, C. E., Wilkes, M. C., Edens, M., Kottom, T. J., Murphy, S. J., Limper, A. H., et al. (2004). Imatinib mesylate inhibits the profibrogenic activity of TGF-beta and prevents bleomycin-mediated lung fibrosis. *J Clin Invest, 114*(9), 1308-1316.

Darby, I., Skalli, O., & Gabbiani, G. (1990). Alpha-smooth muscle actin is transiently expressed by myofibroblasts during experimental wound healing. *Lab Invest, 63*(1), 21-29.

Darzynkiewicz, Z., Halicka, H. D., Zhao, H., & Podhorecka, M. (2011). Cell synchronization by inhibitors of DNA replication induces replication stress and DNA damage response: analysis by flow cytometry. *Methods in molecular biology (Clifton, N.J.), 761*, 85-96.

Davis, P. K., Ho, A., & Dowdy, S. F. (2001). Biological methods for cell-cycle synchronization of mammalian cells. *Biotechniques, 30*(6), 1322-1326, 1328, 1330-1321.

de Wert, G., & Mummery, C. (2003). Human embryonic stem cells: research, ethics and policy. *Hum Reprod, 18*(4), 672-682.

Denham, J. W., & Hauer-Jensen, M. (2002). The radiotherapeutic injury – a complex 'wound'. *Radiotherapy and Oncology, 63*(2), 129-145.

Denton, C. P., Merkel, P. A., Furst, D. E., Khanna, D., Emery, P., Hsu, V. M., et al. (2007). Recombinant human anti-transforming growth factor beta1 antibody therapy in systemic sclerosis: a multicenter, randomized, placebo-controlled phase I/II trial of CAT-192. *Arthritis Rheum, 56*(1), 323-333.

Desai, V. D., Hsia, H. C., & Schwarzbauer, J. E. (2014). Reversible Modulation of Myofibroblast Differentiation in Adipose-Derived Mesenchymal Stem Cells. *PLOS ONE, 9*(1), e86865.

Desmouliere, A., Geinoz, A., Gabbiani, F., & Gabbiani, G. (1993). Transforming growth factor-beta 1 induces alpha-smooth muscle actin expression in granulation tissue

myofibroblasts and in quiescent and growing cultured fibroblasts. *J Cell Biol, 122*(1), 103-111.

Desmoulière, A., Redard, M., Darby, I., & Gabbiani, G. (1995). Apoptosis mediates the decrease in cellularity during the transition between granulation tissue and scar. *The American Journal of Pathology, 146*(1), 56-66.

Devine, M. J., Kaganovich, A., Ryten, M., Mamais, A., Trabzuni, D., Manzoni, C., et al. (2011). Pathogenic LRRK2 Mutations Do Not Alter Gene Expression in Cell Model Systems or Human Brain Tissue. *PLOS ONE, 6*(7), e22489.

Di Nicola, M., Carlo-Stella, C., Magni, M., Milanesi, M., Longoni, P. D., Matteucci, P., et al. (2002). Human bone marrow stromal cells suppress T-lymphocyte proliferation induced by cellular or nonspecific mitogenic stimuli. *Blood, 99*(10), 3838-3843.

Dieckman, L. M., Freudenthal, B. D., & Washington, M. T. (2012). PCNA structure and function: insights from structures of PCNA complexes and post-translationally modified PCNA. *Sub-cellular biochemistry, 62*, 281-299.

Diederichs, S., & Tuan, R. S. (2014). Functional comparison of human-induced pluripotent stem cell-derived mesenchymal cells and bone marrow-derived mesenchymal stromal cells from the same donor. *Stem Cells Dev, 23*(14), 1594-1610.

Diegelmann, R. F., & Evans, M. C. (2004). Wound healing: an overview of acute, fibrotic and delayed healing. *Front Biosci., 9*, 283-289.

Ding, H., Zhou, D., Hao, S., Zhou, L., He, W., Nie, J., et al. (2012). Sonic Hedgehog Signaling Mediates Epithelial–Mesenchymal Communication and Promotes Renal Fibrosis. *Journal of the American Society of Nephrology, 23*(5), 801-813.

Do, N. N., & Eming, S. A. (2016). Skin fibrosis: Models and mechanisms. *Current Research in Translational Medicine, 64*(4), 185-193.

Donohoe, M. E., Silva, S. S., Pinter, S. F., Xu, N., & Lee, J. T. (2009). The pluripotency factor Oct4 interacts with Ctcf and also controls X-chromosome pairing and counting. [10.1038/nature08098]. *Nature, 460*(7251), 128-132.

Dutta, D., Heo, I., & Clevers, H. Disease Modeling in Stem Cell-Derived 3D Organoid Systems. *Trends in Molecular Medicine, 23*(5), 393-410.

Duval, K., Grover, H., Han, L. H., Mou, Y., Pegoraro, A. F., Fredberg, J., et al. (2017). Modeling Physiological Events in 2D vs. 3D Cell Culture. *Physiology (Bethesda), 32*(4), 266-277.

Dvorak, H. F. (1986). Tumors: wounds that do not heal. Similarities between tumor stroma generation and wound healing. *N Engl J Med, 315*.

Dye, B. R., Hill, D. R., Ferguson, M. A. H., Tsai, Y.-H., Nagy, M. S., Dyal, R., et al. (2015). In vitro generation of human pluripotent stem cell derived lung organoids. *eLife, 4*, e05098.

Ebert, Margaret S., & Sharp, Phillip A. (2012). Roles for MicroRNAs in Conferring Robustness to Biological Processes. *Cell, 149*(3), 515-524.

Ebrahimi, B. (2015). Reprogramming barriers and enhancers: strategies to enhance the efficiency and kinetics of induced pluripotency. *Cell Regeneration, 4*(1), 10.

Edgley, A. J., Krum, H., & Kelly, D. J. (2012). Targeting Fibrosis for the Treatment of Heart Failure: A Role for Transforming Growth Factor-β. *Cardiovascular Therapeutics, 30*(1), e30-e40.

Ellis, N. A., Groden, J., Ye, T.-Z., Straughen, J., Lennon, D. J., Ciocci, S., et al. (1995). The Bloom's syndrome gene product is homologous to RecQ helicases. *Cell, 83*(4), 655-666.

Enzo, M. V., Rastrelli, M., Rossi, C. R., Hladnik, U., & Segat, D. (2015). The Wnt/β-catenin pathway in human fibrotic-like diseases and its eligibility as a therapeutic target. *Molecular and cellular therapies, 3*, 1-1.

Ercan, S. (2015). Mechanisms of x chromosome dosage compensation. *Journal of genomics, 3*, 1-19.

Evans, P. M., Zhang, W., Chen, X., Yang, J., Bhakat, K. K., & Liu, C. (2007). Kruppel-like factor 4 is acetylated by p300 and regulates gene transcription via modulation of histone acetylation. *J Biol Chem, 282*(47), 33994-34002.

Fan, Z., Beresford, P. J., Zhang, D., & Lieberman, J. (2002). HMG2 interacts with the nucleosome assembly protein SET and is a target of the cytotoxic T-lymphocyte protease granzyme A. *Mol Cell Biol, 22*(8), 2810-2820.

Feng, B., Jiang, J., Kraus, P., Ng, J. H., Heng, J. C. D., Chan, Y. S., et al. (2009). Reprogramming of fibroblasts into induced pluripotent stem cells with orphan nuclear receptor Esrrb. *Nat Cell Biol, 11*.

Fernandez-Rebollo, E., Franzen, J., Hollmann, J., Ostrowska, A., Oliverio, M., Sieben, T., et al. (2019). Senescence-associated metabolomic phenotype in primary and iPSC-derived mesenchymal stromal cells. *bioRxiv*, 542357.

Fernandez-Retana, J., Zamudio-Meza, H., Rodriguez-Morales, M., Pedroza-Torres, A., Isla-Ortiz, D., Herrera, L., et al. (2017). Gene signature based on degradome-related genes can predict distal metastasis in cervical cancer patients. *Tumor Biology, 39*(6), 1010428317711895.

Fine, D. A., Rozenblatt-Rosen, O., Padi, M., Korkhin, A., James, R. L., Adelmant, G., et al. (2012). Identification of FAM111A as an SV40 host range restriction and adenovirus helper factor. *PLoS Pathog, 8*(10), e1002949.

Fischer, I. A., Kazandjieva, J., Vassileva, S., & Dourmishev, A. (2005). Kindler syndrome: a case report and proposal for clinical diagnostic criteria. *Acta Dermatovenerol Alp Pannonica Adriat, 14*(2), 61-67.

Fischer, M., & Müller, G. A. (2017). Cell cycle transcription control: DREAM/MuvB and RB-E2F complexes. *Critical Reviews in Biochemistry and Molecular Biology, 52*(6), 638-662.

Forbes, S. J., Russo, F. P., Rey, V., Burra, P., Rugge, M., Wright, N. A., et al. (2004). A significant proportion of myofibroblasts are of bone marrow origin in human liver fibrosis. *Gastroenterology, 126*(4), 955-963.

Foster, D. A., Yellen, P., Xu, L., & Saqcena, M. (2010). Regulation of G1 Cell Cycle Progression: Distinguishing the Restriction Point from a Nutrient-Sensing Cell Growth Checkpoint(s). *Genes & Cancer, 1*(11), 1124-1131.

Francke, U., & Oliver, N. (1978). Quantitative analysis of high-resolution trypsin-Giemsa bands on human prometaphase chromosomes. *Human Genetics, 45*(2), 137-165.

Frobel, J., Hemeda, H., Lenz, M., Abagnale, G., Joussen, S., Denecke, B., et al. (2014). Epigenetic Rejuvenation of Mesenchymal Stromal Cells Derived from Induced Pluripotent Stem Cells. *Stem Cell Reports, 3*(3), 414-422.

Fusaki, N., Ban, H., Nishiyama, A., Saeki, K., & Hasegawa, M. (2009a). Efficient induction of transgene-free human pluripotent stem cells using a vector based on Sendai virus, an RNA virus that does not integrate into the host genome. *Proc Jpn Acad Ser B Phys Biol Sci, 85*.

Fusaki, N., Ban, H., Nishiyama, A., Saeki, K., & Hasegawa, M. (2009b). Efficient induction of transgene-free human pluripotent stem cells using a vector based on Sendai virus, an RNA virus that does not integrate into the host genome. [JST.JSTAGE/pjab/85.348 pii]. *Proc.Jpn.Acad.Ser.B Phys.Biol.Sci., 85*(8), 348-362.

Gabbiani, G. (2003). The myofibroblast in wound healing and fibrocontractive diseases. *J Pathol, 200*.

Gabbiani, G., Hirschel, B. J., Ryan, G. B., Statkov, P. R., & Majno, G. (1972). Granulation tissue as a contractile organ. A study of structure and function. *J Exp Med, 135*(4), 719-734.

Gabrielli , A., Avvedimento , E. V., & Krieg , T. (2009). Scleroderma. *New England Journal of Medicine, 360*(19), 1989-2003.

Garg, K., Corona, B. T., & Walters, T. J. (2015). Therapeutic strategies for preventing skeletal muscle fibrosis after injury. *Frontiers in Pharmacology, 6*, 87.

Garrison, G., Huang, S. K., Okunishi, K., Scott, J. P., Kumar Penke, L. R., Scruggs, A. M., et al. (2013). Reversal of myofibroblast differentiation by prostaglandin E(2). *Am J Respir Cell Mol Biol, 48*(5), 550-558.

Gelse, K., Poschl, E., & Aigner, T. (2003). Collagens--structure, function, and biosynthesis. *Adv. Drug Deliv. Rev, 55*(12), 1531-1546.

Ghaedi, M., Calle, E. A., Mendez, J. J., Gard, A. L., Balestrini, J., Booth, A., et al. (2013). Human iPS cell-derived alveolar epithelium repopulates lung extracellular matrix. [68793 pii ;10.1172/JCI68793 doi]. *J.Clin.Invest, 123*(11), 4950-4962.

Gładych, M., Andrzejewska, A., Oleksiewicz, U., & Estécio, M. R. H. (2015). Epigenetic mechanisms of induced pluripotency. *Contemporary Oncology, 19*(1A), A30-A38.

Gonzalez, D. M., & Medici, D. (2014). Signaling mechanisms of the epithelial-mesenchymal transition. *Science signaling, 7*(344), re8-re8.

Goussot, R., Prasad, M., Stoetzel, C., Lenormand, C., Dollfus, H., & Lipsker, D. (2017). Expanding phenotype of hereditary fibrosing poikiloderma with tendon contractures, myopathy, and pulmonary fibrosis caused by FAM111B mutations: Report of an additional family raising the question of cancer predisposition and a short review of early-onset poikiloderma. *JAAD Case Reports, 3*(2), 143-150.

Green, M. C., Sweet, H. O., & Bunker, L. E. (1976). Tight skin, a new mutation of the mouse causing excessive growth of connective tissue and skeleton. [Article]. *American Journal of Pathology, 82*(3), 493-512.

Grobarczyk, B., Franco, B., Hanon, K., & Malgrange, B. (2015). Generation of Isogenic Human iPS Cell Line Precisely Corrected by Genome Editing Using the CRISPR/Cas9 System. *Stem Cell Rev, 11*(5), 774-787.

Grskovic, M., Javaherian, A., Strulovici, B., & Daley, G. Q. (2011). Induced pluripotent stem cells - opportunities for disease modelling and drug discovery. *Nat Rev Drug Discov, 10*.

Guarino, M., Tosoni, A., & Nebuloni, M. (2009). Direct contribution of epithelium to organ fibrosis: epithelial-mesenchymal transition. *Hum Pathol, 40*.

Guo, G., Gui, Y., Gao, S., Tang, A., Hu, X., Huang, Y., et al. (2011). Frequent mutations of genes encoding ubiquitin-mediated proteolysis pathway components in clear cell renal cell carcinoma. *Nat Genet, 44*(1), 17-19.

Guo, Y. L., Chakraborty, S., Rajan, S. S., Wang, R., & Huang, F. (2010). Effects of oxidative stress on mouse embryonic stem cell proliferation, apoptosis, senescence, and self-renewal. *Stem Cells Dev, 19*.

Guo, Z., Higgins, C. A., Gillette, B. M., Itoh, M., Umegaki, N., Gledhill, K., et al. (2013). Building a microphysiological skin model from induced pluripotent stem cells. *Stem Cell Research & Therapy, 4*(Suppl 1), S2-S2.

Gurdon, J. B. (1962). The transplantation of nuclei between two species of Xenopus. *Developmental Biology, 5*(1), 68-83.

Guyard, A., Danel, C., Théou-Anton, N., Debray, M.-P., Gibault, L., Mordant, P., et al. (2017). Morphologic and molecular study of lung cancers associated with idiopathic pulmonary fibrosis and other pulmonary fibroses. [journal article]. *Respiratory Research, 18*(1), 120.

Hall, M. C., Young, D. A., Waters, J. G., Rowan, A. D., Chantry, A., Edwards, D. R., et al. (2003). The comparative role of activator protein 1 and Smad factors in the regulation of Timp-1 and MMP-1 gene expression by transforming growth factor-beta 1. [10.1074/jbc.M212334200 doi ;M212334200 pii]. *J.Biol.Chem., 278*(12), 10304-10313.

Han, J. W., & Yoon, Y.-s. (2011). Induced Pluripotent Stem Cells: Emerging Techniques for Nuclear Reprogramming. *Antioxidants & Redox Signaling, 15*(7), 1799-1820.

Handy, D. E., Castro, R., & Loscalzo, J. (2011). Epigenetic Modifications: Basic Mechanisms and Role in Cardiovascular Disease. *Circulation, 123*(19), 2145-2156.

Hanna, J., Markoulaki, S., Schorderet, P., Carey, B. W., Beard, C., Wernig, M., et al. (2008). Direct reprogramming of terminally differentiated mature B lymphocytes to pluripotency. *Cell, 133*.

Harrison, J. H., Jr., & Lazo, J. S. (1988). Plasma and pulmonary pharmacokinetics of bleomycin in murine strains that are sensitive and resistant to bleomycin-induced pulmonary fibrosis. *J Pharmacol Exp Ther, 247*(3), 1052-1058.

Hayes, M., Curley, G. F., Masterson, C., Devaney, J., O'Toole, D., & Laffey, J. G. (2015). Mesenchymal stromal cells are more effective than the MSC secretome in diminishing injury and enhancing recovery following ventilator-induced lung injury. *Intensive Care Med Exp, 3*(1), 29.

Hegner, B., Schaub, T., Catar, R., Kusch, A., Wagner, P., Essin, K., et al. (2016). Intrinsic Deregulation of Vascular Smooth Muscle and Myofibroblast Differentiation in Mesenchymal Stromal Cells from Patients with Systemic Sclerosis. *PLoS ONE, 11*(4), e0153101.

Henderson, N. C., & Iredale, J. P. (2007). Liver fibrosis: cellular mechanisms of progression and resolution. *Clin Sci (Lond), 112*(5), 265-280.

Heo, J. S., Choi, Y., Kim, H.-S., & Kim, H. O. (2016). Comparison of molecular profiles of human mesenchymal stem cells derived from bone marrow, umbilical cord blood, placenta and adipose tissue. *International journal of molecular medicine, 37*(1), 115-125.

Hezroni, H., Sailaja, B. S., & Meshorer, E. (2011). Pluripotency-related, valproic acid (VPA)-induced genome-wide histone H3 lysine 9 (H3K9) acetylation patterns in embryonic stem cells. *J Biol Chem, 286*(41), 35977-35988.

Higuchi, A., Ling, Q.-D., Kumar, S. S., Munusamy, M. A., Alarfaj, A. A., Chang, Y., et al. (2014). Generation of pluripotent stem cells without the use of genetic material. [Mini Review]. *Laboratory Investigation, 95*, 26.

Hinz, B. (2007). Formation and function of the myofibroblast during tissue repair. *J Invest Dermatol, 127*(3), 526-537.

Ho, B. X., Pek, N. M. Q., & Soh, B.-S. (2018). Disease Modeling Using 3D Organoids Derived from Human Induced Pluripotent Stem Cells. *International Journal of Molecular Sciences, 19*(4), 936.

Hohwieler, M., Illing, A., Hermann, P. C., Mayer, T., Stockmann, M., Perkhofer, L., et al. (2016). Human pluripotent stem cell-derived acinar/ductal organoids generate human pancreas upon orthotopic transplantation and allow disease modelling. [10.1136/gutjnl-2016-312423]. *Gut*.

Holt, D. J., Chamberlain, L. M., & Grainger, D. W. (2010). Cell-cell signaling in co-cultures of macrophages and fibroblasts. *Biomaterials, 31*(36), 9382-9394.

Horowitz, J. C., Osterholzer, J. J., Marazioti, A., & Stathopoulos, G. T. (2016). "Scar-cinoma": viewing the fibrotic lung mesenchymal cell in the context of cancer biology. *The European respiratory journal, 47*(6), 1842-1854.

Hossini, A. M., Megges, M., Prigione, A., Lichtner, B., Toliat, M. R., Wruck, W., et al. (2015). Induced pluripotent stem cell-derived neuronal cells from a sporadic Alzheimer's disease donor as a model for investigating AD-associated gene regulatory networks. [journal article]. *BMC Genomics, 16*(1), 84.

Hu, S., Wilson, K. D., Ghosh, Z., Han, L., Wang, Y., Lan, F., et al. (2013). MicroRNA-302 Increases Reprogramming Efficiency via Repression of NR2F2. *Stem cells (Dayton, Ohio), 31*(2), 259-268.

Huangfu, D., Maehr, R., Guo, W., Eijkelenboom, A., Snitow, M., & Chen, A. E. (2008). Induction of pluripotent stem cells by defined factors is greatly improved by small-molecule compounds. *Nat Biotech., 26*.

Hulmes, D. J. (2002). Building collagen molecules, fibrils, and suprafibrillar structures. [10.1006/jsbi.2002.4450 doi ;S1047847702944503 pii]. *J.Struct.Biol., 137*(1-2), 2-10.

Ilyas, M., Tomlinson, I. P., Rowan, A., Pignatelli, M., & Bodmer, W. F. (1997). Beta-catenin mutations in cell lines established from human colorectal cancers. *Proc Natl Acad Sci U S A, 94*(19), 10330-10334.

Itoh, M., Umegaki-Arao, N., Guo, Z., Liu, L., Higgins, C. A., & Christiano, A. M. (2013). Generation of 3D skin equivalents fully reconstituted from human induced pluripotent stem cells (iPSCs). [10.1371/journal.pone.0077673 doi ;PONE-D-13-17268 pii]. *PLoS.One., 8*(10), e77673.

Iwano, M., Plieth, D., Danoff, T. M., Xue, C., Okada, H., & Neilson, E. G. (2002). Evidence that fibroblasts derive from epithelium during tissue fibrosis. *The Journal of Clinical Investigation, 110*(3), 341-350.

Jaiswal, N., Haynesworth, S. E., Caplan, A. I., & Bruder, S. P. (1997). Osteogenic differentiation of purified, culture-expanded human mesenchymal stem cells in vitro. *Journal of Cellular Biochemistry, 64*(2), 295-312.

Jeon, O. H., Panicker, L. M., Lu, Q., Chae, J. J., Feldman, R. A., & Elisseeff, J. H. (2016). Human iPSC-derived osteoblasts and osteoclasts together promote bone regeneration in 3D biomaterials. [Article]. *Scientific Reports, 6*, 26761.

Jia, G., Chandriani, S., Abbas, A. R., DePianto, D. J., N'Diaye, E. N., Yaylaoglu, M. B., et al. (2017). CXCL14 is a candidate biomarker for Hedgehog signalling in idiopathic pulmonary fibrosis. *Thorax*.

Jinnin, M. (2010). Mechanisms of skin fibrosis in systemic sclerosis. *J Dermatol, 37*(1), 11-25.

Jobard, F., Bouadjar, B., Caux, F., Hadj-Rabia, S., Has, C., Matsuda, F., et al. (2003). Identification of mutations in a new gene encoding a FERM family protein with a pleckstrin homology domain in Kindler syndrome. *Hum Mol Genet, 12*(8), 925-935.

Johnson, V., Volikos, E., Halford, S. E., Eftekhar Sadat, E. T., Popat, S., Talbot, I., et al. (2005). Exon 3 beta-catenin mutations are specifically associated with colorectal carcinomas in hereditary non-polyposis colorectal cancer syndrome. *Gut, 54*(2), 264-267.

Jovanovic, M., Rooney, M. S., Mertins, P., Przybylski, D., Chevrier, N., Satija, R., et al. (2015). Dynamic profiling of the protein life cycle in response to pathogens. *Science, 347*(6226), 1259038.

Kagawa, S., Matsuo, A., Yagi, Y., Ikematsu, K., Tsuda, R., & Nakasono, I. (2009). The time-course analysis of gene expression during wound healing in mouse skin. *Legal Medicine, 11*(2), 70-75.

Kaler, P., Augenlicht, L., & Klampfer, L. (2012). Activating Mutations in β-Catenin in Colon Cancer Cells Alter Their Interaction with Macrophages; the Role of Snail. *PLOS ONE, 7*(9), e45462.

Kalluri, R. (2016). The biology and function of fibroblasts in cancer. *Nat Rev Cancer, 16*.

Kalluri, R., & Neilson, E. G. (2003). Epithelial-mesenchymal transition and its implications for fibrosis. *J Clin Invest, 112*(12), 1776-1784.

Kang, R., Luo, Y., Zou, L., Xie, L., Lysdahl, H., & Jiang, X. (2014). Osteogenesis of human induced pluripotent stem cells derived mesenchymal stem cells on hydroxyapatite contained nanofibers. *RSC Adv, 4*.

Kang, R., Zhou, Y., Tan, S., Zhou, G., Aagaard, L., Xie, L., et al. (2015). Mesenchymal stem cells derived from human induced pluripotent stem cells retain adequate osteogenicity and chondrogenicity but less adipogenicity. [journal article]. *Stem Cell Research & Therapy, 6*(1), 144.

Kanta, J. (2015). Collagen matrix as a tool in studying fibroblastic cell behavior. *Cell adhesion & migration, 9*(4), 308-316.

Kapinas, K., Grandy, R., Ghule, P., Medina, R., Becker, K., Pardee, A., et al. (2013). The Abbreviated Pluripotent Cell Cycle. *Journal of cellular physiology, 228*(1), 9-20.

Kastan, M. B., & Bartek, J. (2004). Cell-cycle checkpoints and cancer. [10.1038/nature03097]. *Nature, 432*(7015), 316-323.

Kawamura, T., Suzuki, J., Wang, Y. V., Menendez, S., Morera, L. B., & Raya, A. (2009). Linking the p53 tumour suppressor pathway to somatic cell reprogramming. *Nature., 460*.

Kay, J., & High, W. A. (2008). Imatinib mesylate treatment of nephrogenic systemic fibrosis. *Arthritis & Rheumatism, 58*(8), 2543-2548.

Kazlouskaya, V., Feldman, E. J., Jakus, J., Heilman, E., & Glick, S. (2018). A Case of Hereditary Fibrosing Poikiloderma with Tendon Contractures, Myopathy, and Pulmonary Fibrosis (POIKTMP) with the Emphasis on Cutaneous Histopathological Findings. *J Eur Acad Dermatol Venereol*.

Khumalo, N. P., Pillay, K., Beighton, P., Wainwright, H., Walker, B., Saxe, N., et al. (2006). Poikiloderma, tendon contracture and pulmonary fibrosis: a new autosomal dominant syndrome? [BJD7473 pii ;10.1111/j.1365-2133.2006.07473.x doi]. *Br.J.Dermatol., 155*(5), 1057-1061.

Kim, C., Wong, J., Wen, J., Wang, S., Wang, C., Spiering, S., et al. (2013). Studying arrhythmogenic right ventricular dysplasia with patient-specific iPSCs. *Nature, 494*(7435), 105-110.

Kim, H.-S., Kim, J.-H., Lee, J. Y., Yoon, Y.-M., Kim, I.-H., Yoon, H.-S., et al. (2017). Small molecule-mediated reprogramming of epithelial-mesenchymal transition thereby blocking fibrosis. [10.1101/106591]. *bioRxiv*.

Kim, J. S., Choi, H. W., Araúzo-Bravo, M. J., Schöler, H. R., & Do, J. T. (2015). Reactivation of the inactive X chromosome and post-transcriptional reprogramming of Xist in iPSCs. [10.1242/jcs.154294]. *Journal of Cell Science, 128*(1), 81.

Kim, J. S., Choi, H. W., Choi, S., Seo, H. G., Moon, S.-H., Chung, H.-M., et al. (2014). Conversion of Partially Reprogrammed Cells to Fully Pluripotent Stem Cells Is Associated with Further Activation of Stem Cell Maintenance- and Gamete Generation-Related Genes. *Stem Cells and Development, 23*(21), 2637-2648.

Kitano, K., Kim, S.-Y., & Hakoshima, T. (2010). Structural Basis for DNA Strand Separation by the Unconventional Winged-Helix Domain of RecQ Helicase WRN. *Structure, 18*(2), 177-187.

Krenning, G., Zeisberg, E. M., & Kalluri, R. (2010). The origin of fibroblasts and mechanism of cardiac fibrosis. *J Cell Physiol, 225*.

Krieg, T., Abraham, D., & Lafyatis, R. (2007). Fibrosis in connective tissue disease: the role of the myofibroblast and fibroblast-epithelial cell interactions. *Arthritis Res Ther, 9 Suppl 2*, S4.

Krizhanovsky, V., Yon, M., Dickins, R. A., Hearn, S., Simon, J., Miething, C., et al. (2008). Senescence of activated stellate cells limits liver fibrosis. *Cell, 134*(4), 657-667.

Kunisada, Y., Tsubooka-Yamazoe, N., Shoji, M., & Hosoya, M. (2012). Small molecules induce efficient differentiation into insulin-producing cells from human induced pluripotent stem cells. *Stem Cell Res, 8*(2), 274-284.

Lam, A. P., & Gottardi, C. J. (2011a). beta-catenin signaling: a novel mediator of fibrosis and potential therapeutic target. *Curr Opin Rheumatol, 23*(6), 562-567.

Lam, A. P., & Gottardi, C. J. (2011b). β-catenin signaling: a novel mediator of fibrosis and potential therapeutic target. *Current Opinion in Rheumatology, 23*(6), 562-567.

Langenbach, F., & Handschel, J. (2013). Effects of dexamethasone, ascorbic acid and β-glycerophosphate on the osteogenic differentiation of stem cells in vitro. *Stem Cell Research & Therapy, 4*(5), 117.

Larghero, J., Farge, D., Braccini, A., Lecourt, S., Scherberich, A., Foïs, E., et al. (2008). Phenotypical and functional characteristics of in vitro expanded bone marrow mesenchymal stem cells from patients with systemic sclerosis. [10.1136/ard.2007.071233]. *Annals of the Rheumatic Diseases, 67*(4), 443.

Larizza, L., Roversi, G., & Volpi, L. (2010). Rothmund-Thomson syndrome. [1750-1172-5-2 pii ;10.1186/1750-1172-5-2 doi]. *Orphanet.J.Rare.Dis., 5*, 2.

Laskin, D. L., Sunil, V. R., Gardner, C. R., & Laskin, J. D. (2011). Macrophages and Tissue Injury: Agents of Defense or Destruction? *Annual review of pharmacology and toxicology, 51*, 267-288.

Lauer-Fields, J. L., Chalmers, M. J., Busby, S. A., Minond, D., Griffin, P. R., & Fields, G. B. (2009). Identification of specific hemopexin-like domain residues that facilitate

matrix metalloproteinase collagenolytic activity. [M109.016873 pii ;10.1074/jbc.M109.016873 doi]. *J.Biol.Chem., 284*(36), 24017-24024.

Laurent, G. J. (1987). Dynamic state of collagen: pathways of collagen degradation in vivo and their possible role in regulation of collagen mass. *Am.J.Physiol, 252*(1 Pt 1), C1-C9.

Leask, A., & Abraham, D. J. (2004). TGF-beta signaling and the fibrotic response. [10.1096/fj.03-1273rev doi ;18/7/816 pii]. *FASEB J., 18*(7), 816-827.

LeBleu, V. S., Taduri, G., O'Connell, J., Teng, Y., Cooke, V. G., Woda, C., et al. (2013). Origin and Function of Myofibroblasts in Kidney Fibrosis. *Nature medicine, 19*(8), 1047-1053.

Lee, H., Ragusano, L., Martinez, A., Gill, J., & Dimova, D. K. (2012). A dual role for the dREAM/MMB complex in the regulation of differentiation-specific E2F/RB target genes. *Mol Cell Biol, 32*(11), 2110-2120.

LeRoy, E. C. (1974). Increased collagen synthesis by scleroderma skin fibroblasts in vitro: a possible defect in the regulation or activation of the scleroderma fibroblast. *J Clin Invest, 54*(4), 880-889.

Lewandowski, J., Kolanowski, T. J., & Kurpisz, M. (2017). Techniques for the induction of human pluripotent stem cell differentiation towards cardiomyocytes. *Journal of Tissue Engineering and Regenerative Medicine, 11*(5), 1658-1674.

Ley, B., & Collard, H. R. (2013). Epidemiology of idiopathic pulmonary fibrosis. *Clinical epidemiology, 5*, 483-492.

Li, H. O., Zhu, Y. F., Asakawa, M., Kuma, H., Hirata, T., Ueda, Y., et al. (2000). A cytoplasmic RNA vector derived from nontransmissible Sendai virus with efficient gene transfer and expression. *J Virol, 74*(14), 6564-6569.

Li, M., Luan, F., Zhao, Y., Hao, H., Zhou, Y., Han, W., et al. (2016). Epithelial-mesenchymal transition: An emerging target in tissue fibrosis. *Experimental Biology and Medicine, 241*(1), 1-13.

Li, Y., Feng, H., Gu, H., Lewis, D. W., Yuan, Y., Zhang, L., et al. (2013). The p53–PUMA axis suppresses iPSC generation. [Article]. *Nature Communications, 4*, 2174.

Li, Y., Foster, W., Deasy, B. M., Chan, Y., Prisk, V., Tang, Y., et al. (2004). Transforming growth factor-beta1 induces the differentiation of myogenic cells into fibrotic cells in injured skeletal muscle: a key event in muscle fibrogenesis. *Am J Pathol, 164*.

Lian, Q., Zhang, Y., Zhang, J., Zhang, H. K., Wu, X., & Lam, F. F. (2010). Functional mesenchymal stem cells derived from human induced pluripotent stem cells attenuate limb ischemia in mice. *Circulation, 121*.

Liang, G., Taranova, O., Xia, K., & Zhang, Y. (2010). Butyrate promotes induced pluripotent stem cell generation. *J Biol Chem., 285*.

Lin, J., & Amir, A. (2018). Homeostasis of protein and mRNA concentrations in growing cells. [10.1101/255950]. *bioRxiv*.

Lindor, N. M., Furuichi, Y., Kitao, S., Shimamoto, A., Arndt, C., & Jalal, S. (2000). Rothmund-Thomson syndrome due to RECQ4 helicase mutations: report and clinical and molecular comparisons with Bloom syndrome and Werner syndrome. [10.1002/(SICI)1096-8628(20000131)90:3<223::AID-AJMG7>3.0.CO;2-Z pii]. *Am.J.Med.Genet., 90*(3), 223-228.

Litovchick, L., Sadasivam, S., Florens, L., Zhu, X., Swanson, S. K., Velmurugan, S., et al. (2007). Evolutionarily Conserved Multisubunit RBL2/p130 and E2F4 Protein Complex Represses Human Cell Cycle-Dependent Genes in Quiescence. *Molecular Cell, 26*(4), 539-551.

Liu, M., Xu, J., & Deng, H. (2011). Tangled fibroblasts in tumor-stroma interactions. *Int J Cancer, 129*(8), 1795-1805.

Liu, Y., Beyer, A., & Aebersold, R. (2016). On the Dependency of Cellular Protein Levels on mRNA Abundance. *Cell, 165*(3), 535-550.

Liu, Y., & West, S. C. (2008). More complexity to the Bloom's syndrome complex. *Genes Dev, 22*(20), 2737-2742.

Löfdahl, A., Rydell-Törmänen, K., Larsson-Callerfelt, A.-K., Wenglén, C., & Westergren-Thorsson, G. (2018). Pulmonary fibrosis in vivo displays increased p21 expression reduced by 5-HT2B receptor antagonists in vitro – a potential pathway affecting proliferation. *Scientific Reports, 8*(1), 1927.

Loh, Y.-H., Wu, Q., Chew, J.-L., Vega, V. B., Zhang, W., Chen, X., et al. (2006). The Oct4 and Nanog transcription network regulates pluripotency in mouse embryonic stem cells. [Article]. *Nature Genetics, 38*, 431.

Lu, J., Liu, Q., Wang, L., Tu, W., Chu, H., Ding, W., et al. (2017a). Increased expression of latent TGF-β-binding protein 4 affects the fibrotic process in scleroderma by TGF-β/SMAD signaling. [Research Article]. *Laboratory Investigation, 97*, 591.

Lu, W., Yao, X., Ouyang, P., Dong, N., Wu, D., Jiang, X., et al. (2017b). Drug Repurposing of Histone Deacetylase Inhibitors That Alleviate Neutrophilic Inflammation in Acute Lung Injury and Idiopathic Pulmonary Fibrosis via Inhibiting Leukotriene A4 Hydrolase and Blocking LTB4 Biosynthesis. *Journal of Medicinal Chemistry, 60*(5), 1817-1828.

Lunyak, V. V., & Rosenfeld, M. G. (2008). Epigenetic regulation of stem cell fate. *Human Molecular Genetics, 17*(R1), R28-R36.

Ma, D., Wei, H., Lu, J., Ho, S., Zhang, G., Sun, X., et al. (2013). Generation of patient-specific induced pluripotent stem cell-derived cardiomyocytes as a cellular model of arrhythmogenic right ventricular cardiomyopathy. [ehs226 pii ;10.1093/eurheartj/ehs226 doi]. *Eur.Heart J., 34*(15), 1122-1133.

MacArthur, B. D., Sevilla, A., Lenz, M., Müller, F.-J., Schuldt, B. M., & Schuppert, A. A. (2012). Nanog-dependent feedback loops regulate murine embryonic stem cell heterogeneity. *Nat Cell Biol, 14*.

Macris, M. A., Krejci, L., Bussen, W., Shimamoto, A., & Sung, P. (2006). Biochemical characterization of the RECQ4 protein, mutated in Rothmund-Thomson syndrome. *DNA Repair (Amst), 5*(2), 172-180.

Maherali, N., Sridharan, R., Xie, W., Utika, J., Eminli, S., Arnold, K., et al. (2007). Directly reprogrammed fibroblasts show global epigenetic remodeling and widespread tissue contribution. *Cell Stem Cell, 1*.

Malik, N., & Rao, M. S. (2013). A review of the methods for human iPSC derivation. *Methods Mol Biol, 997*, 23-33.

Mann, C. J., Perdiguero, E., Kharraz, Y., Aguilar, S., Pessina, P., Serrano, A. L., et al. (2011). Aberrant repair and fibrosis development in skeletal muscle. *Skelet Muscle, 1*.

Marion, N. W., & Mao, J. J. (2006). Mesenchymal stem cells and tissue engineering. [S0076-6879(06)20016-8 pii ;10.1016/S0076-6879(06)20016-8 doi]. *Methods Enzymol., 420*, 339-361.

Marumoto, T., Zhang, D., & Saya, H. (2005). Aurora-A — A guardian of poles. [Review Article]. *Nature Reviews Cancer, 5*, 42.

Massague, J. (2004). G1 cell-cycle control and cancer. [10.1038/nature03094]. *Nature, 432*(7015), 298-306.

Masur, S. K., Dewal, H. S., Dinh, T. T., Erenburg, I., & Petridou, S. (1996). Myofibroblasts differentiate from fibroblasts when plated at low density. *Proc Natl Acad Sci U S A, 93*(9), 4219-4223.

Maurer, B., & Distler, O. (2011). Emerging targeted therapies in scleroderma lung and skin fibrosis. *Best Practice & Research Clinical Rheumatology, 25*(6), 843-858.

McKleroy, W., Lee, T. H., & Atabai, K. (2013). Always cleave up your mess: targeting collagen degradation to treat tissue fibrosis. *Am J Physiol Lung Cell Mol Physiol, 304*(11), L709-721.

Mediavilla-Varela, M., Boateng, K., Noyes, D., & Antonia, S. J. (2016). The anti-fibrotic agent pirfenidone synergizes with cisplatin in killing tumor cells and cancer-associated fibroblasts. *BMC Cancer, 16*(1), 176.

Menendez, S., Camus, S., & Izpisua Belmonte, J. C. (2010). p53: guardian of reprogramming. *Cell Cycle, 9*.

Menke, A., Philippi, C., Vogelmann, R., Seidel, B., Lutz, M. P., Adler, G., et al. (2001). Down-Regulation of E-Cadherin Gene Expression by Collagen Type I and Type III in Pancreatic Cancer Cell Lines. *Cancer Research, 61*(8), 3508.

Mennan, C., Brown, S., McCarthy, H., Mavrogonatou, E., Kletsas, D., Garcia, J., et al. (2016). Mesenchymal stromal cells derived from whole human umbilical cord exhibit similar properties to those derived from Wharton's jelly and bone marrow. *FEBS Open Bio, 6*(11), 1054-1066.

Mercier, S., Kury, S., Salort-Campana, E., Magot, A., Agbim, U., Besnard, T., et al. (2015). Expanding the clinical spectrum of hereditary fibrosing poikiloderma with tendon contractures, myopathy and pulmonary fibrosis due to FAM111B mutations. *Orphanet J Rare Dis, 10*, 135.

Mercier, S., Küry, S., Shaboodien, G., Houniet, Darren T., Khumalo, Nonhlanhla P., Bou-Hanna, C., et al. (2013). Mutations in FAM111B Cause Hereditary Fibrosing Poikiloderma with Tendon Contracture, Myopathy, and Pulmonary Fibrosis. *American Journal of Human Genetics, 93*(6), 1100-1107.

Merkle, Florian T., & Eggan, K. (2013). Modeling Human Disease with Pluripotent Stem Cells: from Genome Association to Function. *Cell Stem Cell, 12*(6), 656-668.

Miller, A. J., Dye, B. R., Ferrer-Torres, D., Hill, D. R., Overeem, A. W., Shea, L. D., et al. (2019). Generation of lung organoids from human pluripotent stem cells in vitro. *Nature Protocols, 14*(2), 518-540.

Miller, J. D., Ganat, Y. M., Kishinevsky, S., Bowman, R. L., Liu, B., Tu, E. Y., et al. (2013). Human iPSC-based Modeling of Late-Onset Disease via Progerin-induced Aging. *Cell stem cell, 13*(6), 691-705.

Minor, R. R. (1980). Collagen metabolism: a comparison of diseases of collagen and diseases affecting collagen. *Am.J.Pathol., 98*(1), 225-280.

Mitsui, K., Tokuzawa, Y., Itoh, H., Segawa, K., Murakami, M., Takahashi, K., et al. (2003). The homeoprotein Nanog is required for maintenance of pluripotency in mouse epiblast and ES cells. *Cell, 113*.

Moldovan, G.-L., Pfander, B., & Jentsch, S. (2007). PCNA, the Maestro of the Replication Fork. *Cell, 129*(4), 665-679.

Moreno-Layseca, P., & Streuli, C. H. (2014). Signalling pathways linking integrins with cell cycle progression. *Matrix Biology, 34*, 144-153.

Moretti, A., Laugwitz, K. L., Dorn, T., Sinnecker, D., & Mummery, C. (2013). Pluripotent stem cell models of human heart disease. *Cold Spring Harb Perspect Med, 3*(11).

Morris, G. F., & Mathews, M. B. (1989). Regulation of proliferating cell nuclear antigen during the cell cycle. *J Biol Chem, 264*(23), 13856-13864.

Moslem, M., Eberle, I., Weber, I., Henschler, R., & Cantz, T. (2015). Mesenchymal Stem/Stromal Cells Derived from Induced Pluripotent Stem Cells Support CD34pos Hematopoietic Stem Cell Propagation and Suppress Inflammatory Reaction. *Stem Cells International, 2015*, 14.

Nagase, H., & Woessner, J. F., Jr. (1999). Matrix metalloproteinases. *J.Biol.Chem., 274*(31), 21491-21494.

Nakagawa, M., Koyanagi, M., Tanabe, K., Takahashi, K., Ichisaka, T., Aoi, T., et al. (2008). Generation of induced pluripotent stem cells without Myc from mouse and human fibroblasts. [nbt1374 pii ;10.1038/nbt1374 doi]. *Nat.Biotechnol., 26*(1), 101-106.

Nakanishi, M., & Otsu, M. (2012). Development of Sendai virus vectors and their potential applications in gene therapy and regenerative medicine. *Curr Gene Ther, 12*(5), 410-416.

Narayanan, A. S., Page, R. C., & Swanson, J. (1989). Collagen synthesis by human fibroblasts. Regulation by transforming growth factor-beta in the presence of other inflammatory mediators. *Biochem.J., 260*(2), 463-469.

Nguyen, H. N., Byers, B., Cord, B., Shcheglovitov, A., Byrne, J., Gujar, P., et al. (2011). LRRK2 mutant iPSC-derived DA neurons demonstrate increased susceptibility to oxidative stress. *Cell Stem Cell, 8*(3), 267-280.

Nie, Z., Hu, G., Wei, G., Cui, K., Yamane, A., Resch, W., et al. (2012). c-Myc is a universal amplifier of expressed genes in lymphocytes and embryonic stem cells. *Cell, 151*(1), 68-79.

Nikonova, A. S., Astsaturov, I., Serebriiskii, I. G., Dunbrack, R. L., & Golemis, E. A. (2013). Aurora-A kinase (AURKA) in normal and pathological cell growth. *Cellular and molecular life sciences : CMLS, 70*(4), 661-687.

Nishimura, K., Ohtaka, M., Takada, H., Kurisaki, A., Tran, N. V. K., Tran, Y. T. H., et al. (2017). Simple and effective generation of transgene-free induced pluripotent stem cells using an auto-erasable Sendai virus vector responding to microRNA-302. *Stem Cell Research, 23*, 13-19.

Nishimura, K., Sano, M., Ohtaka, M., Furuta, B., Umemura, Y., Nakajima, Y., et al. (2011). Development of defective and persistent Sendai virus vector: a unique gene delivery/expression system ideal for cell reprogramming. [M110.183780 pii ;10.1074/jbc.M110.183780 doi]. *J.Biol.Chem., 286*(6), 4760-4771.

Nofal, A., & Salah, E. (2013). Acquired poikiloderma: proposed classification and diagnostic approach. [S0190-9622(12)00679-2 pii ;10.1016/j.jaad.2012.06.015 doi]. *J.Am.Acad.Dermatol., 69*(3), e129-e140.

Nolan, J. F. (1992). Tendon contractures in hypercholesterolaemia. *J R Soc Med, 85*(8), 496-497.

Normand, J., & Karasek, M. A. (1995). A method for the isolation and serial propagation of keratinocytes, endothelial cells, and fibroblasts from a single punch biopsy of human skin. *In Vitro Cellular & Developmental Biology - Animal, 31*(6), 447-455.

Novak, M. L., & Koh, T. J. (2013). Macrophage phenotypes during tissue repair. *J Leukoc Biol, 93*(6), 875-881.

Nusse, R. (2005). Wnt signaling in disease and in development. *Cell Res, 15*(1), 28-32.

Obermueller, E., Vosseler, S., Fusenig, N. E., & Mueller, M. M. (2004). Cooperative autocrine and paracrine functions of granulocyte colony-stimulating factor and granulocyte-macrophage colony-stimulating factor in the progression of skin carcinoma cells. *Cancer Res, 64*(21), 7801-7812.

Oh, Y., Wei, H., Ma, D., Sun, X., & Liew, R. (2012). Clinical applications of patient-specific induced pluripotent stem cells in cardiovascular medicine. [heartjnl-2011-301317 pii ;10.1136/heartjnl-2011-301317 doi]. *Heart, 98*(6), 443-449.

Ohnuki, M., & Takahashi, K. (2015). Present and future challenges of induced pluripotent stem cells. *Philosophical Transactions of the Royal Society B: Biological Sciences, 370*(1680), 20140367.

Okumura-Nakanishi, S., Saito, M., Niwa, H., & Ishikawa, F. (2005). Oct-3/4 and Sox2 regulate Oct-3/4 gene in embryonic stem cells. *J Biol Chem, 280*(7), 5307-5317.

Olmeda, D., Castel, S., Vilaró, S., & Cano, A. (2003). Beta-catenin regulation during the cell cycle: implications in G2/M and apoptosis. *Molecular biology of the cell, 14*(7), 2844-2860.

Panning, B., Dausman, J., & Jaenisch, R. (1997). X Chromosome Inactivation Is Mediated by Xist RNA Stabilization. *Cell, 90*(5), 907-916.

Parker, M. W., Rossi, D., Peterson, M., Smith, K., Sikstrom, K., White, E. S., et al. (2014). Fibrotic extracellular matrix activates a profibrotic positive feedback loop. *J Clin Invest, 124*(4), 1622-1635.

Pasque, V., Tchieu, J., Karnik, R., Uyeda, M., Dimashkie, A. S., Case, D., et al. (2014). X Chromosome Reactivation Dynamics Reveal Stages of Reprogramming to Pluripotency. *Cell, 159*(7), 1681-1697.

Pederson, T., & Robbins, E. (1971). A method for improving synchrony in the G2 phase of the cell cycle. *J Cell Biol, 49*(3), 942-945.

Pekkanen-Mattila, M., Ojala, M., Kerkelä, E., Rajala, K., Skottman, H., & Aalto-Setälä, K. (2012). The Effect of Human and Mouse Fibroblast Feeder Cells on Cardiac Differentiation of Human Pluripotent Stem Cells. *Stem Cells International, 2012*, 10.

Peng, S. Y., Yip, H. S., Pan, H. W., & Hsu, H. C. (2008). 437 CANP, A NOVEL CANCER ASSOCIATED NUCLEOPROTEIN, IS FREQUENTLY OVEREXPRESSED IN HEPATOCELLULAR CARCINOMA AND ITS DOWNREGULATION ASSOCIATED WITH REDUCED INVASION CAPABILITY. *Journal of Hepatology, 48*, S167.

Pittenger, M. F. (1999). Multilineage potential of adult human mesenchymal stem cells. *Science, 284*.

Pohlers, D., Brenmoehl, J., Loffler, I., Muller, C. K., Leipner, C., Schultze-Mosgau, S., et al. (2009). TGF-beta and fibrosis in different organs - molecular pathway imprints. [S0925-4439(09)00135-5 pii ;10.1016/j.bbadis.2009.06.004 doi]. *Biochim.Biophys.Acta, 1792*(8), 746-756.

Pollard, J. W. (2004). Tumour-educated macrophages promote tumour progression and metastasis. *Nat Rev Cancer, 4*.

Polo, Jose M., Anderssen, E., Walsh, Ryan M., Schwarz, Benjamin A., Nefzger, Christian M., Lim, Sue M., et al. (2012). A Molecular Roadmap of Reprogramming Somatic Cells into iPS Cells. *Cell, 151*(7), 1617-1632.

Polonchuk, L., Chabria, M., Badi, L., Hoflack, J.-C., Figtree, G., Davies, M. J., et al. (2017). Cardiac spheroids as promising in vitro models to study the human heart microenvironment. *Scientific Reports, 7*(1), 7005.

Popov, B., & Petrov, N. (2014). pRb-E2F signaling in life of mesenchymal stem cells: Cell cycle, cell fate, and cell differentiation. *Genes & Diseases, 1*(2), 174-187.

Popova, A. P., Bozyk, P. D., Goldsmith, A. M., Linn, M. J., Lei, J., Bentley, J. K., et al. (2010). Autocrine production of TGF-β1 promotes myofibroblastic differentiation of neonatal lung mesenchymal stem cells. *American Journal of Physiology - Lung Cellular and Molecular Physiology, 298*(6), L735-L743.

Potten, C. S., & Loeffler, M. (1990). Stem cells: attributes, cycles, spirals, pitfalls and uncertainties. Lessons for and from the crypt. *Development, 110*(4), 1001-1020.

Przepiorski, A., Sander, V., Tran, T., Hollywood, J. A., Sorrenson, B., Shih, J.-H., et al. (2018). A Simple Bioreactor-Based Method to Generate Kidney Organoids from Pluripotent Stem Cells. *Stem Cell Reports, 11*(2), 470-484.

Raghu, G., Chen, Y. Y., Rusch, V., & Rabinovitch, P. S. (1988). Differential proliferation of fibroblasts cultured from normal and fibrotic human lungs. *Am Rev Respir Dis, 138*(3), 703-708.

Rahl, P. B., Lin, C. Y., Seila, A. C., Flynn, R. A., Mccuine, S., Burge, C. B., et al. (2010). c-Myc regulates transcriptional pause release. *Cell, 141*.

Raja, W. K., Mungenast, A. E., Lin, Y.-T., Ko, T., Abdurrob, F., Seo, J., et al. (2016). Self-Organizing 3D Human Neural Tissue Derived from Induced Pluripotent Stem Cells Recapitulate Alzheimer's Disease Phenotypes. *PLOS ONE, 11*(9), e0161969.

Ramonet, D., Podhajska, A., Stafa, K., Sonnay, S., Trancikova, A., Tsika, E., et al. (2012). PARK9-associated ATP13A2 localizes to intracellular acidic vesicles and regulates cation homeostasis and neuronal integrity. *Human Molecular Genetics, 21*(8), 1725-1743.

Ran, F. A., Hsu, P. D., Wright, J., Agarwala, V., Scott, D. A., & Zhang, F. (2013). Genome engineering using the CRISPR-Cas9 system. *Nat Protoc, 8*(11), 2281-2308.

Ribes, V., & Briscoe, J. (2009). Establishing and interpreting graded Sonic Hedgehog signaling during vertebrate neural tube patterning: the role of negative feedback. *Cold Spring Harb Perspect Biol, 1*(2), a002014.

Richards, C. D., Kerr, C., Tong, L., & Langdon, C. (2002). Modulation of extracellular matrix using adenovirus vectors. *Biochem Soc Trans, 30*.

Rivlin, N., Brosh, R., Oren, M., & Rotter, V. (2011). Mutations in the p53 Tumor Suppressor Gene: Important Milestones at the Various Steps of Tumorigenesis. *Genes & cancer, 2*(4), 466-474.

Rockey, D. C., Bell, P. D., & Hill, J. A. (2015). Fibrosis--a common pathway to organ injury and failure. *N Engl J Med, 372*(12), 1138-1149.

Rosenbloom, J., Mendoza, F. A., & Jimenez, S. A. (2013). Strategies for anti-fibrotic therapies. *Biochimica et Biophysica Acta (BBA) - Molecular Basis of Disease, 1832*(7), 1088-1103.

Rouhani, F., Kumasaka, N., de Brito, M. C., Bradley, A., Vallier, L., & Gaffney, D. (2014). Genetic Background Drives Transcriptional Variation in Human Induced Pluripotent Stem Cells. *PLOS Genetics, 10*(6), e1004432.

Ruzek, M. C., Jha, S., Ledbetter, S., Richards, S. M., & Garman, R. D. (2004). A modified model of graft-versus-host–induced systemic sclerosis (scleroderma) exhibits all major aspects of the human disease. *Arthritis & Rheumatism, 50*(4), 1319-1331.

Ryan, S. D., Dolatabadi, N., Chan, S. F., Zhang, X., Akhtar, M. W., Parker, J., et al. (2013). Isogenic human iPSC Parkinson's model shows nitrosative stress-induced dysfunction in MEF2-PGC1alpha transcription. [S0092-8674(13)01422-0 pii ;10.1016/j.cell.2013.11.009 doi]. *Cell, 155*(6), 1351-1364.

Rydzanicz, M., Wrzesiński, T., Bluyssen, H. A. R., & Wesoły, J. (2013). Genomics and epigenomics of clear cell renal cell carcinoma: Recent developments and potential applications. *Cancer Letters, 341*(2), 111-126.

Sadasivam, S., & DeCaprio, J. A. (2013). The DREAM complex: Master coordinator of cell cycle dependent gene expression. *Nature reviews. Cancer, 13*(8), 585-595.

Sahin-Tóth, M., & Tóth, M. (2000). Gain-of-Function Mutations Associated with Hereditary Pancreatitis Enhance Autoactivation of Human Cationic Trypsinogen. *Biochemical and Biophysical Research Communications, 278*(2), 286-289.

Sánchez, L., Gutierrez-Aranda, I., Ligero, G., Rubio, R., Muñoz-López, M., García-Pérez, J. L., et al. (2011). Enrichment of Human ESC-Derived Multipotent Mesenchymal Stem Cells with Immunosuppressive and Anti-Inflammatory Properties Capable to Protect Against Experimental Inflammatory Bowel Disease. *STEM CELLS, 29*(2), 251-262.

Sawada, S., Murakami, K., Murata, J., Tsukada, K., & Saiki, I. (2001). Accumulation of extracellular matrix in the liver induces high metastatic potential of hepatocellular carcinoma to the lung. *Int J Oncol, 19*(1), 65-70.

Saxe, J. P., Tomilin, A., Schöler, H. R., Plath, K., & Huang, J. (2009). Post-translational regulation of Oct4 transcriptional activity. *PLoS ONE, 4*.

Schäfer, M., & Werner, S. (2008). Cancer as an overhealing wound: an old hypothesis revisited. [Review Article]. *Nature Reviews Molecular Cell Biology, 9*, 628.

Schmidt, R., & Plath, K. (2012). The roles of the reprogramming factors Oct4, Sox2 and Klf4 in resetting the somatic cell epigenome during induced pluripotent stem cell generation. *Genome Biology, 13*(10), 251.

Schmittgen, T. D., & Livak, K. J. (2008). Analyzing real-time PCR data by the comparative CT method. [10.1038/nprot.2008.73]. *Nat. Protocols, 3*(6), 1101-1108.

Schrier, D. J., & Phan, S. H. (1984). Modulation of bleomycin-induced pulmonary fibrosis in the BALB/c mouse by cyclophosphamide-sensitive T cells. *The American Journal of Pathology, 116*(2), 270-278.

Seaberg, R. M., & van der Kooy, D. (2003). Stem and progenitor cells: the premature desertion of rigorous definitions. *Trends Neurosci, 26*(3), 125-131.

Seki, T., & Fukuda, K. (2015). Methods of induced pluripotent stem cells for clinical application. *World journal of stem cells, 7*(1), 116-125.

Seo, A., Walsh, T., Lee, M. K., Ho, P. A., Hsu, E. K., Sidbury, R., et al. (2016). FAM111B Mutation Is Associated With Inherited Exocrine Pancreatic Dysfunction. *Pancreas, 45*(6), 858-862.

Serrano, A. L., & Munoz-Canoves, P. (2010). Regulation and dysregulation of fibrosis in skeletal muscle. *Exp Cell Res, 316*(18), 3050-3058.

Sert, M., Fakioglu, K., & Tetiker, T. (2009). Review of Two Siblings with Werner's Syndrome: A Case Report. *Case Reports in Medicine, 2009*.

Shi-Wen, X., Denton, C. P., McWhirter, A., Bou-Gharios, G., Abraham, D. J., du Bois, R. M., et al. (1997). Scleroderma lung fibroblasts exhibit elevated and dysregulated type I collagen biosynthesis. *Arthritis & Rheumatism, 40*(7), 1237-1244.

Sluijter, J. P., Smeets, M. B., Velema, E., Pasterkamp, G., & de Kleijn, D. P. (2004). Increase in collagen turnover but not in collagen fiber content is associated with flow-induced arterial remodeling. *J. Vasc. Res, 41*(6), 546-555.

Smith, G. P., & Chan, E. S. L. (2010). Molecular Pathogenesis of Skin Fibrosis: Insight from Animal Models. *Current rheumatology reports, 12*(1), 26-33.

Smith, Z. D., Sindhu, C., & Meissner, A. (2016). Molecular features of cellular reprogramming and development. [Review]. *Nat Rev Mol Cell Biol, 17*(3), 139-154.

Smithmyer, M. E., Sawicki, L. A., & Kloxin, A. M. (2014). Hydrogel scaffolds as in vitro models to study fibroblast activation in wound healing and disease. [10.1039/C3BM60319A]. *Biomaterials Science, 2*(5), 634-650.

Snoeck, H.-W. (2015). Modeling human lung development and disease using pluripotent stem cells. [10.1242/dev.115469]. *Development, 142*(1), 13.

Spector, I., Zilberstein, Y., Lavy, A., Nagler, A., Genin, O., & Pines, M. (2012). Involvement of Host Stroma Cells and Tissue Fibrosis in Pancreatic Tumor Development in Transgenic Mice. *PLOS ONE, 7*(7), e41833.

Spitzhorn, L.-S., Megges, M., Wruck, W., Rahman, M. S., Otte, J., Degistirici, Ö., et al. (2019). Human iPSC-derived MSCs (iMSCs) from aged individuals acquire a rejuvenation signature. *Stem Cell Research & Therapy, 10*(1), 100.

Srinageshwar, B., Maiti, P., Dunbar, G. L., & Rossignol, J. (2016). Role of Epigenetics in Stem Cell Proliferation and Differentiation: Implications for Treating Neurodegenerative Diseases. *International Journal of Molecular Sciences, 17*(2), 199.

Stadtfeld, M., Brennand, K., & Hochedlinger, K. (2008). Reprogramming of pancreatic beta cells into induced pluripotent stem cells. *Curr Biol, 18*.

Stadtfeld, M., & Hochedlinger, K. (2010). Induced pluripotency: history, mechanisms, and applications. *Genes Dev, 24*(20), 2239-2263.

Stewart, G. A., Hoyne, G. F., Ahmad, S. A., Jarman, E., Wallace, W. A., Harrison, D. J., et al. (2003). Expression of the developmental Sonic hedgehog (Shh) signalling pathway is up-regulated in chronic lung fibrosis and the Shh receptor patched 1 is present in circulating T lymphocytes. *J Pathol, 199*(4), 488-495.

Strutz, F., & Zeisberg, M. (2006). Renal Fibroblasts and Myofibroblasts in Chronic Kidney Disease. *Journal of the American Society of Nephrology, 17*(11), 2992-2998.

Sun, H., Lesche, R., Li, D. M., Liliental, J., Zhang, H., Gao, J., et al. (1999). PTEN modulates cell cycle progression and cell survival by regulating phosphatidylinositol 3,4,5,-trisphosphate and Akt/protein kinase B signaling pathway. *Proc Natl Acad Sci U S A, 96*(11), 6199-6204.

Tachibana, M., Amato, P., Sparman, M., Gutierrez, N. M., Tippner-Hedges, R., Ma, H., et al. (2013). Human embryonic stem cells derived by somatic cell nuclear transfer. *Cell, 153*(6), 1228-1238.

Takahashi, K. (2007). Induction of pluripotent stem cells from adult human fibroblasts by defined factors. *Cell, 131*.

Takahashi, K., & Yamanaka, S. (2006). Induction of pluripotent stem cells from mouse embryonic and adult fibroblast cultures by defined factors. [S0092-8674(06)00976-7 pii ;10.1016/j.cell.2006.07.024 doi]. *Cell, 126*(4), 663-676.

Takahashi, K., & Yamanaka, S. (2016). A decade of transcription factor-mediated reprogramming to pluripotency. [Perspectives]. *Nat Rev Mol Cell Biol, 17*(3), 183-193.

Takeichi, T., Nanda, A., Yang, H. S., Hsu, C. K., Lee, J. Y. Y., Al-Ajmi, H., et al. (2016). Syndromic inherited poikiloderma due to a de novo mutation in FAM111B. *British Journal of Dermatology*, n/a-n/a.

Talele, N. P., Fradette, J., Davies, J. E., Kapus, A., & Hinz, B. (2015). Expression of alpha-Smooth Muscle Actin Determines the Fate of Mesenchymal Stromal Cells. *Stem Cell Reports, 4*(6), 1016-1030.

Tan, Z., Su, Z.-y., Wu, R.-r., Gu, B., Liu, Y.-k., Zhao, X.-l., et al. (2011). Immunomodulative effects of mesenchymal stem cells derived from human embryonic stem cells in vivo and in vitro. *Journal of Zhejiang University. Science. B, 12*(1), 18-27.

Thomson, J. A., Eldor, J. I., Shapiro, S. S., & Waknitz, M. A. (1998). Embryonic Stem Cell Lines Derived from Human Blastocysts. *Science, 282*.

Tobey, R. A., Anderson, E. C., & Petersen, D. F. (1967). The effect of thymidine on the duration of G1 in Chinese hamster cells. *J Cell Biol, 35*(1), 53-59.

Tobey, R. A., Petersen, D. F., Anderson, E. C., & Puck, T. T. (1966). Life cycle analysis of mammalian cells. 3. The inhibition of division in Chinese hamster cells by puromycin and actinomycin. *Biophysical journal, 6*(5), 567-581.

Tonge, P. D., Corso, A. J., Monetti, C., Hussein, S. M. I., Puri, M. C., Michael, I. P., et al. (2014). Divergent reprogramming routes lead to alternative stem-cell states. [Article]. *Nature, 516*(7530), 192-197.

Trackman, P. C. (2005). Diverse biological functions of extracellular collagen processing enzymes. [10.1002/jcb.20605 doi]. *J.Cell Biochem., 96*(5), 927-937.

Trounson, A., & DeWitt, N. D. (2016). Pluripotent stem cells progressing to the clinic. [Perspectives]. *Nat Rev Mol Cell Biol, 17*(3), 194-200.

Tse, J. C., & Kalluri, R. (2007). Mechanisms of metastasis: Epithelial-to-mesenchymal transition and contribution of tumor microenvironment. *Journal of Cellular Biochemistry, 101*(4), 816-829.

Uezumi, A., Ikemoto-Uezumi, M., & Tsuchida, K. (2014). Roles of nonmyogenic mesenchymal progenitors in pathogenesis and regeneration of skeletal muscle. [Review]. *Frontiers in Physiology, 5*(68).

Uezumi, A., Ito, T., Morikawa, D., Shimizu, N., Yoneda, T., Segawa, M., et al. (2011). Fibrosis and adipogenesis originate from a common mesenchymal progenitor in skeletal muscle. *J Cell Sci, 124*(Pt 21), 3654-3664.

Umar, S., Malavasi, F., & Mehta, K. (1996). Post-translational modification of CD38 protein into a high molecular weight form alters its catalytic properties. *J Biol Chem, 271*(27), 15922-15927.

Ussar, S., Moser, M., Widmaier, M., Rognoni, E., Harrer, C., Genzel-Boroviczeny, O., et al. (2008). Loss of Kindlin-1 Causes Skin Atrophy and Lethal Neonatal Intestinal Epithelial Dysfunction. *PLOS Genetics, 4*(12), e1000289.

Usunier, B., #xEE, Benderitter, M., Tamarat, R., & Chapel, A. (2014). Management of Fibrosis: The Mesenchymal Stromal Cells Breakthrough. *Stem Cells International, 2014*, 26.

Uzbekov, R. E. (2004). Analysis of the cell cycle and a method employing synchronized cells for study of protein expression at various stages of the cell cycle. *Biochemistry (Mosc), 69*(5), 485-496.

van Amerongen, R., & Nusse, R. (2009). Towards an integrated view of Wnt signaling in development. *Development, 136*(19), 3205-3214.

van Oijen, M. G., & Slootweg, P. J. (2000). Gain-of-function mutations in the tumor suppressor gene p53. *Clin Cancer Res, 6*(6), 2138-2145.

van Spreeuwel, A. C. C., Bax, N. A. M., van Nierop, B. J., Aartsma-Rus, A., Goumans, M.-J. T. H., & Bouten, C. V. C. (2017). Mimicking Cardiac Fibrosis in a Dish: Fibroblast Density Rather than Collagen Density Weakens Cardiomyocyte Function. *Journal of Cardiovascular Translational Research*, 1-12.

Vancheri, C., Failla, M., Crimi, N., & Raghu, G. (2010). Idiopathic pulmonary fibrosis: a disease with similarities and links to cancer biology. [10.1183/09031936.00077309]. *European Respiratory Journal, 35*(3), 496.

Vanneaux, V., Farge-Bancel, D., Lecourt, S., Baraut, J., Cras, A., Jean-Louis, F., et al. (2013). Expression of transforming growth factor beta receptor II in mesenchymal stem cells from systemic sclerosis patients. *BMJ Open, 3*(1).

Vidal, Simon E., Stadtfeld, M., & Apostolou, E. (2015). F-Class Cells: New Routes and Destinations for Induced Pluripotency. *Cell Stem Cell, 16*(1), 9-10.

Viguet-Carrin, S., Garnero, P., & Delmas, P. D. (2006). The role of collagen in bone strength. *Osteoporosis International, 17*(3), 319-336.

Wakayama, T., & Yanagimachi, R. (1999). Cloning the laboratory mouse. *Seminars in Cell & Developmental Biology, 10*(3), 253-258.

Walter, N., Collard, H. R., & King, T. E., Jr. (2006). Current perspectives on the treatment of idiopathic pulmonary fibrosis. *Proc. Am. Thorac. Soc, 3*(4), 330-338.

Wang, J., Hao, J., Bai, D., Gu, Q., Han, W., Wang, L., et al. (2015). Generation of clinical-grade human induced pluripotent stem cells in Xeno-free conditions. *Stem Cell Research & Therapy, 6*, 223.

Warren, L., Ni, Y., Wang, J., & Guo, X. (2012). Feeder-Free Derivation of Human Induced Pluripotent Stem Cells with Messenger RNA. *Scientific Reports, 2*, 657.

Watanabe, K., Ueno, M., Kamiya, D., Nishiyama, A., Matsumura, M., Wataya, T., et al. (2007). A ROCK inhibitor permits survival of dissociated human embryonic stem cells. *Nature Biotechnology, 25*, 681.

Watts, K. L., Cottrell, E., Hoban, P. R., & Spiteri, M. A. (2006). RhoA signaling modulates cyclin D1 expression in human lung fibroblasts; implications for idiopathic pulmonary fibrosis. *Respiratory Research, 7*(1), 88.

Wernig, M., Meissner, A., Cassady, J. P., & Jaenisch, R. (2008). c-Myc is dispensable for direct reprogramming of mouse fibroblasts. *Cell Stem Cell, 2*.

White, E. S., Atrasz, R. G., Hu, B., Phan, S. H., Stambolic, V., Mak, T. W., et al. (2006). Negative regulation of myofibroblast differentiation by PTEN (Phosphatase and Tensin Homolog Deleted on chromosome 10). *American journal of respiratory and critical care medicine, 173*(1), 112-121.

Whitfield, M. L., Sherlock, G., Saldanha, A. J., Murray, J. I., Ball, C. A., Alexander, K. E., et al. (2002). Identification of genes periodically expressed in the human cell cycle and their expression in tumors. *Mol Biol Cell, 13*(6), 1977-2000.

Wilding, B. R., McGrath, M. J., Bonne, G., & Mitchell, C. A. (2014). FHL1 mutations that cause clinically distinct human myopathies form protein aggregates and impair myoblast differentiation. *Journal of Cell Science*, jcs.140905.

Willis, A. E., & Lindahl, T. (1987). DNA ligase I deficiency in Bloom's syndrome. [10.1038/325355a0]. *Nature, 325*(6102), 355-357.

Willis, B. C., duBois, R. M., & Borok, Z. (2006). Epithelial origin of myofibroblasts during fibrosis in the lung. *Proc Am Thorac Soc, 3*(4), 377-382.

Wilmut, I., Schnieke, A. E., McWhir, J., Kind, A. J., & Campbell, K. H. (1997). Viable offspring derived from fetal and adult mammalian cells. *Nature, 385*(6619), 810-813.

Wu, X., Li, Y., Crise, B., & Burgess, S. M. (2003). Transcription Start Regions in the Human Genome Are Favored Targets for MLV Integration. [10.1126/science.1083413]. *Science, 300*(5626), 1749.

Wynn, T. A. (2004). FIBROTIC DISEASE AND THE T(H)1/T(H)2 PARADIGM. *Nature reviews. Immunology, 4*(8), 583-594.

Wynn, T. A. (2007). Common and unique mechanisms regulate fibrosis in various fibroproliferative diseases. *J Clin Invest, 117*(3), 524-529.

Wynn, T. A. (2008). Cellular and molecular mechanisms of fibrosis. [10.1002/path.2277 doi]. *J.Pathol., 214*(2), 199-210.

Wynn, T. A. (2010). Fibrosis under arrest. *Nat Med, 16*.

Wynn, T. A. (2011). Integrating mechanisms of pulmonary fibrosis. *The Journal of Experimental Medicine, 208*(7), 1339-1350.

Wynn, T. A., & Ramalingam, T. R. (2012). Mechanisms of fibrosis: therapeutic translation for fibrotic disease. *Nat Med, 18*(7), 1028-1040.

Xia, H., Diebold, D., Nho, R., Perlman, D., Kleidon, J., Kahm, J., et al. (2008). Pathological integrin signaling enhances proliferation of primary lung fibroblasts from patients with idiopathic pulmonary fibrosis. *J Exp Med, 205*.

Xu, R., Besenbacher, F., & Chen, M. (2017). The 3D mechanical environment and chemical milieu influence the hMSC fibrogenesis and fibroblast-to-myofibroblast transition. [10.1039/C6RA25422E]. *RSC Advances, 7*(1), 20-25.

Xu, R., Taskin, M. B., Rubert, M., Seliktar, D., Besenbacher, F., & Chen, M. (2015). hiPS-MSCs differentiation towards fibroblasts on a 3D ECM mimicking scaffold. [Article]. *5*, 8480.

Yamamoto, T., Takagawa, S., Katayama, I., Yamazaki, K., Hamazaki, Y., Shinkai, H., et al. (1999). Animal Model of Sclerotic Skin. I: Local Injections of Bleomycin Induce Sclerotic Skin Mimicking Scleroderma. *Journal of Investigative Dermatology, 112*(4), 456-462.

Yamanaka, S. (2009). Elite and stochastic models for induced pluripotent stem cell generation. [10.1038/nature08180]. *Nature, 460*(7251), 49-52.

Yamasaki, S., Taguchi, Y., Shimamoto, A., Mukasa, H., Tahara, H., & Okamoto, T. (2014). Generation of Human Induced Pluripotent Stem (iPS) Cells in Serum- and Feeder-Free Defined Culture and TGF-β1 Regulation of Pluripotency. *PLOS ONE, 9*(1), e87151.

Yang, J., Li, S., He, X.-B., Cheng, C., & Le, W. (2016). Induced pluripotent stem cells in Alzheimer's disease: applications for disease modeling and cell-replacement therapy. *Molecular Neurodegeneration, 11*(1), 39.

Yang, Z., Sun, Z., Liu, H., Ren, Y. I., Shao, D., Zhang, W. E. I., et al. (2015). Connective tissue growth factor stimulates the proliferation, migration and differentiation of lung fibroblasts during paraquat-induced pulmonary fibrosis. *Molecular Medicine Reports, 12*(1), 1091-1097.

Yeo, S.-Y., Lee, K.-W., Shin, D., An, S., Cho, K.-H., & Kim, S.-H. (2018). A positive feedback loop bi-stably activates fibroblasts. *Nature Communications, 9*(1), 3016.

Yu, J. (2007). Induced pluripotent stem cell lines derived from human somatic cells. *Science, 318*.

Yu, J., Chau, K. F., Vodyanik, M. A., Jiang, J., & Jiang, Y. (2011). Efficient Feeder-Free Episomal Reprogramming with Small Molecules. *PLOS ONE, 6*(3), e17557.

Yue, W., Wang, T., Zachariah, E., Lin, Y., Yang, C. S., Xu, Q., et al. (2015). Transcriptomic analysis of pancreatic cancer cells in response to metformin and aspirin: an implication of synergy. [Article]. *Scientific Reports, 5*, 13390.

Zeisberg, E. M., Tarnavski, O., Zeisberg, M., Dorfman, A. L., McMullen, J. R., Gustafsson, E., et al. (2007). Endothelial-to-mesenchymal transition contributes to cardiac fibrosis. *Nat Med, 13*.

Zhang, F., Chen, X., Wei, K., Liu, D., Xu, X., Zhang, X., et al. (2017). Identification of Key Transcription Factors Associated with Lung Squamous Cell Carcinoma. *Medical Science Monitor : International Medical Journal of Experimental and Clinical Research, 23*, 172-206.

Zhang, J., Nuebel, E., Daley, G. Q., Koehler, C. M., & Teitell, M. A. (2012). Metabolic Regulation in Pluripotent Stem Cells during Reprogramming and Self-Renewal. *Cell stem cell, 11*(5), 589-595.

Zhang, N., Bailus, B. J., Ring, K. L., & Ellerby, L. M. (2016). iPSC-based drug screening for Huntington's disease. *Brain Res, 1638*(Pt A), 42-56.

Zhang, P., Andrianakos, R., Yang, Y., Liu, C., & Lu, W. (2010). Kruppel-like factor 4 (Klf4) prevents embryonic stem (ES) cell differentiation by regulating Nanog gene expression. *J Biol Chem, 285*(12), 9180-9189.

Zhang, Z., Zhang, J., Chen, F., Zheng, L., Li, H., Liu, M., et al. (2019). Family of hereditary fibrosing poikiloderma with tendon contractures, myopathy and pulmonary fibrosis caused by a novel FAM111B mutation. *J Dermatol*.

Zhao, H., Li, X., Zhao, S., Zeng, Y., Zhao, L., Ding, H., et al. (2014). Microengineered in vitro model of cardiac fibrosis through modulating myofibroblast mechanotransduction. *Biofabrication, 6*(4), 045009.

Zhou, B., Buckley, S. T., Patel, V., Liu, Y., Luo, J., Krishnaveni, M. S., et al. (2012). Troglitazone Attenuates TGF-β1-Induced EMT in Alveolar Epithelial Cells via a PPARγ-Independent Mechanism. *PLOS ONE, 7*(6), e38827.

Zou, L., Luo, Y., Chen, M., Wang, G., Ding, M., & Petersen, C. C. (2013). A simple method for deriving functional MSCs and applied for osteogenesis in 3D scaffolds. *Sci Rep, 3*.

Zunder, E. R., Lujan, E., Goltsev, Y., Wernig, M., & Nolan, G. P. (2015). A Continuous Molecular Roadmap to iPSC Reprogramming through Progression Analysis of Single-Cell Mass Cytometry. *Cell stem cell, 16*(3), 323-337.

Zuppinger, C. (2016). 3D culture for cardiac cells. *Biochimica et Biophysica Acta (BBA) - Molecular Cell Research, 1863*(7, Part B), 1873-1881.

Cell cycle supplemental Data

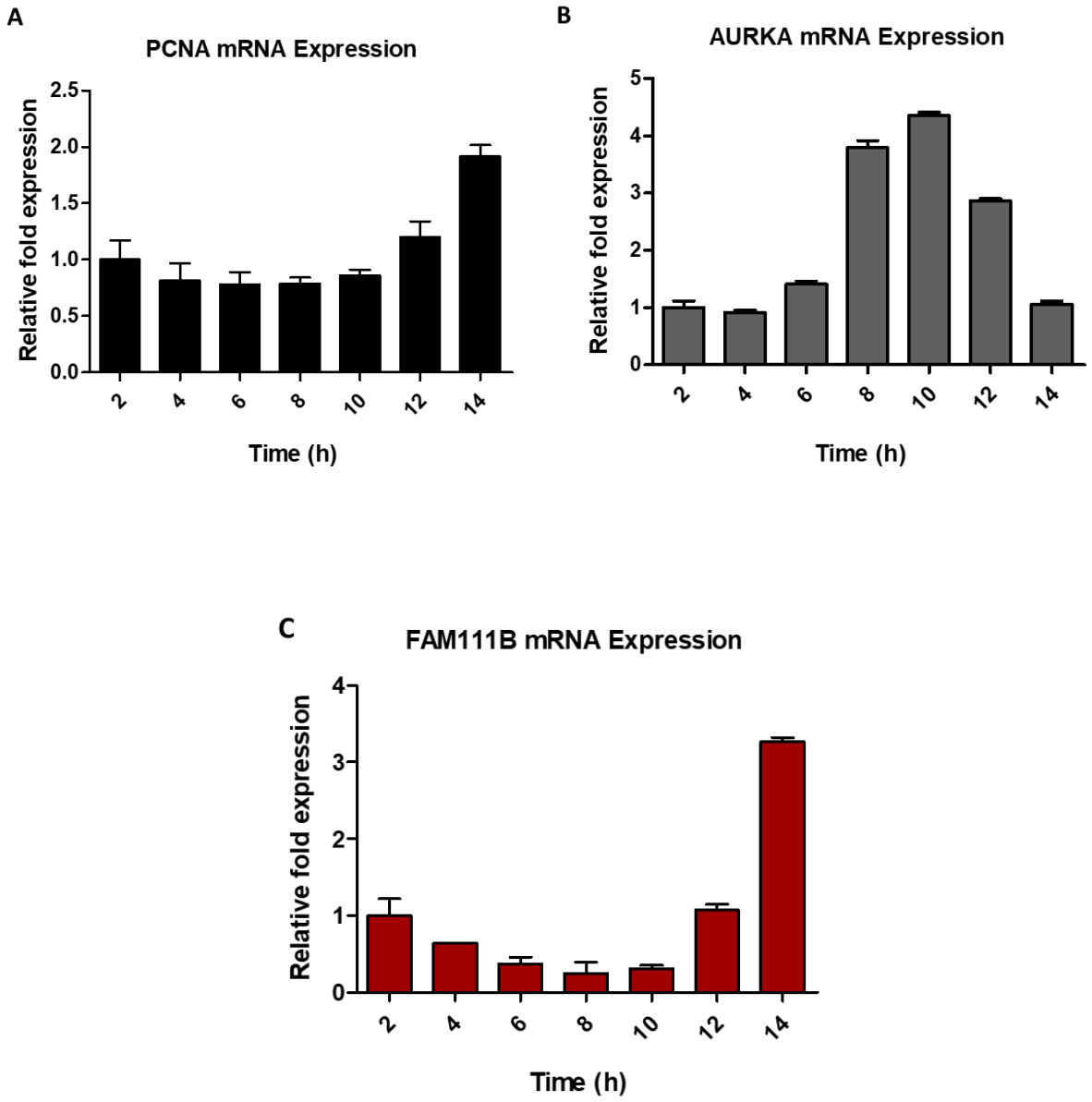

Figure S1: Synchronisation of HeLa cells with double-thymidine (2 mM) block. HeLa cells were arrested at G1/S using by double-thymidine (2 mM) block for 19 h with a 9-h release. (A) PCNA, (B) AURKA and (C) FAM111B mRNA expression levels were measured at 2, 4, 6, 8, 10, 12 and 14 h post-thymidine release. Data presented as mean ± SD (n =2).

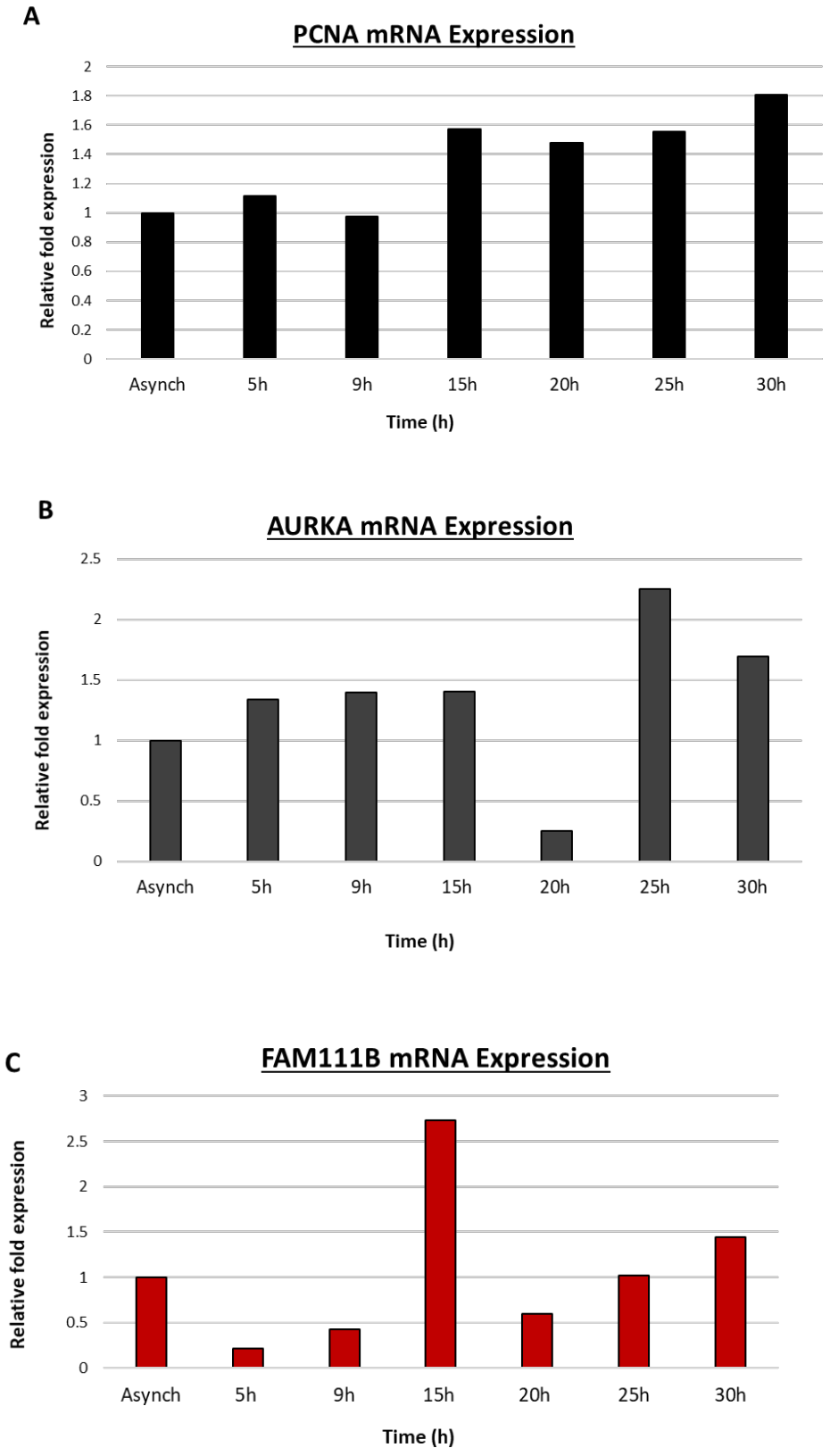

Figure S2: 30-hour synchronisation of control (familial) iPSC-MSCs with double-thymidine block (2 mM). Control iPSC-MSCs were arrested by double-thymidine (2 mM) block for 30 h with a 15-h release. mRNA expression of **(A)** PCNA, **(B)** AURKA and **(C)** FAM111B were analysed relative to asynchronous cells (G0) phase at 4-5 h intervals for 30 h post-thymidine block. (n =1).

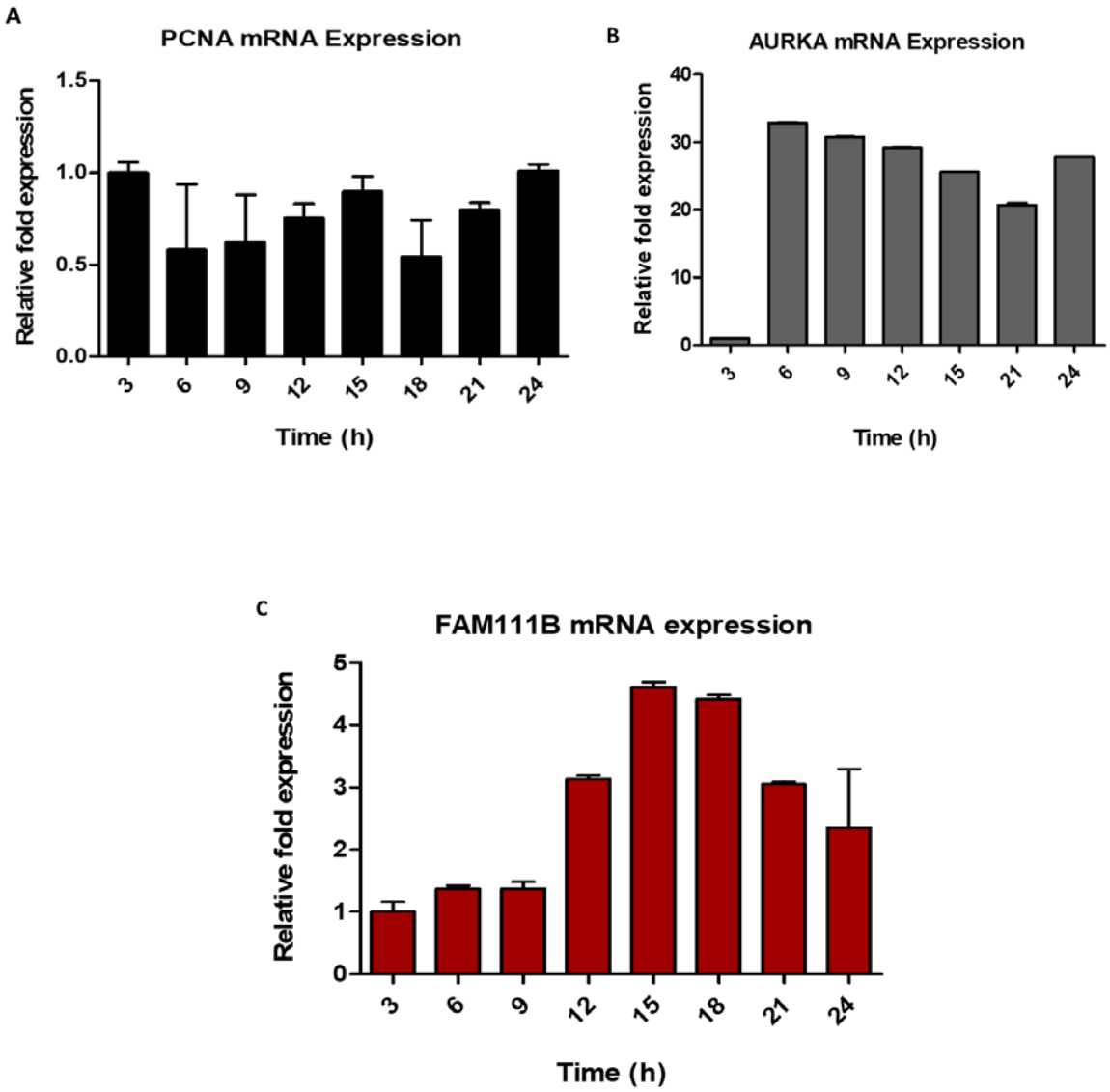

Figure S3: 24-hour synchronisation of control (familial) iPSC-MSCs with double-thymidine block (2 mM). Control iPSC-MSCs were arrested by double-thymidine (2 mM) block for 24 h with a 12-h release before the second thymidine block. mRNA expression of **(A)** PCNA, **(B)** AURKA and **(C)** FAM111B were analysed at 3-h intervals for 24 h post-thymidine block. Data presented as mean ± SD (n =2).

A

0 h (2 mM)

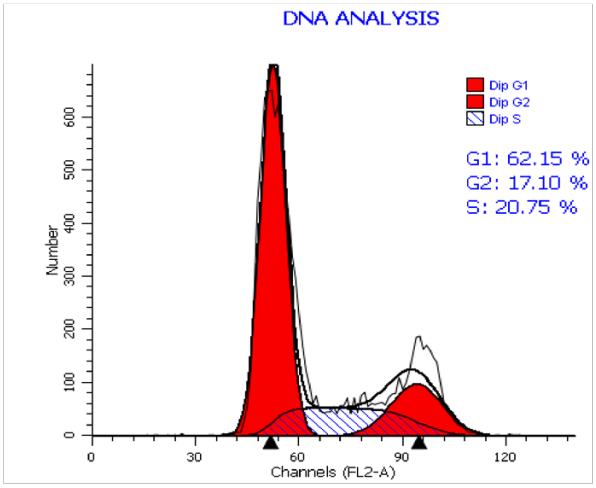

0 h (4 mM)

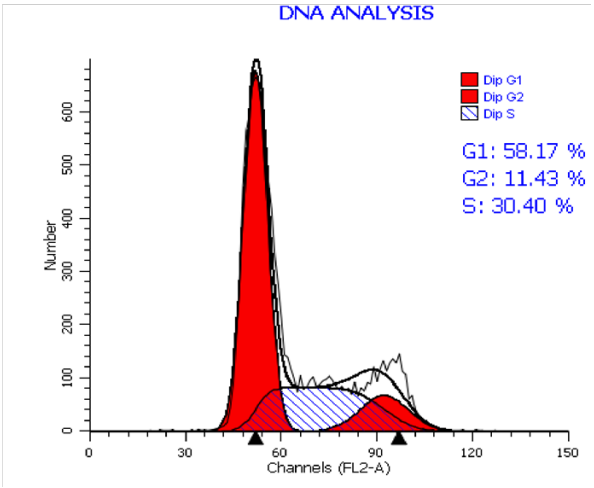

B

2 h (2 mM)

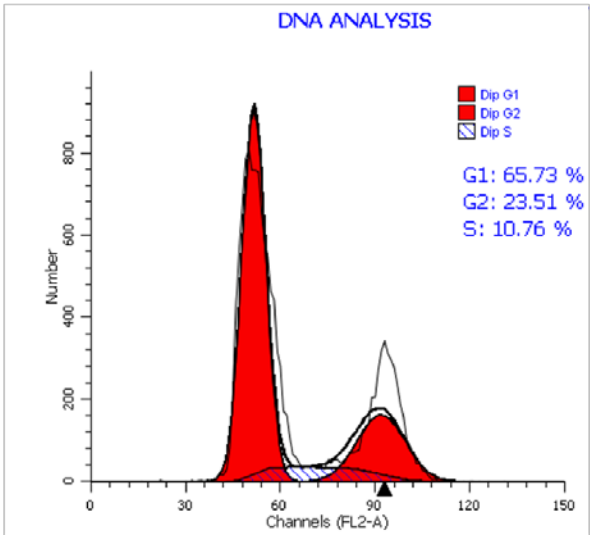

2 h (4 mM)

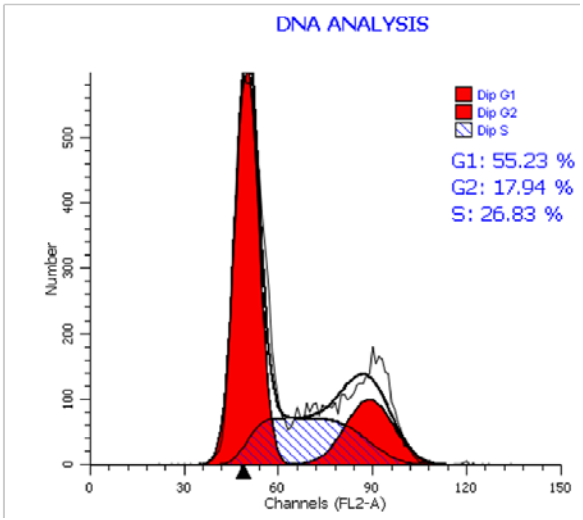

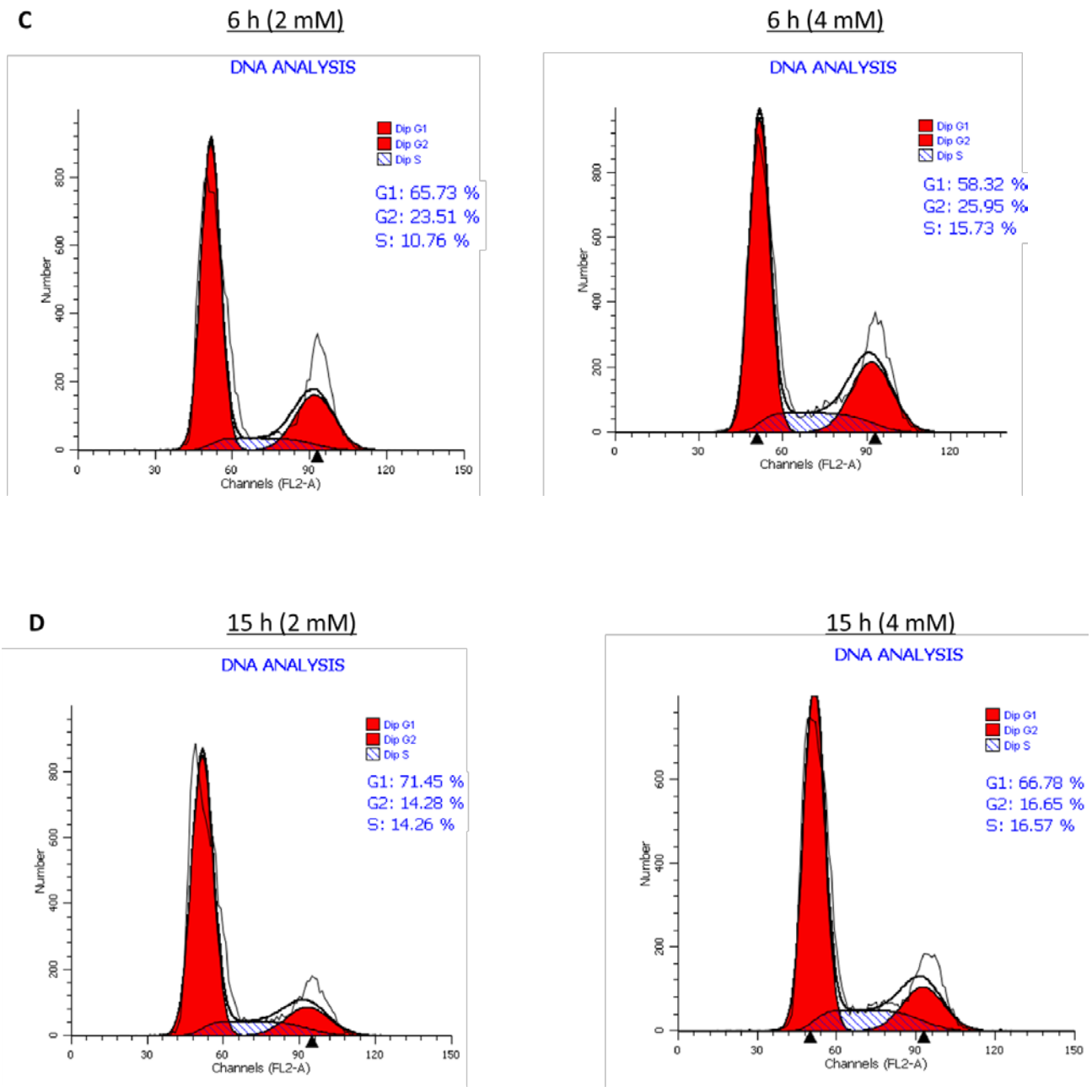

Figure S4: Flow cytometry of synchronised control (familial) iPSC-MSCs with 2 mM or 4 mM double-thymidine block. Control iPSC-MSCs were treated with 2 mM or 4 mM of thymidine for 24 h with a 12-h release before the second thymidine block. DNA content of synchronised cells was measured at **(A)** 0 h, **(B)** 2 h, **(C)** 6 h and **(D)** 15 h for the respective thymidine concentrations (2 mM and 4 mM) used. Data presented as mean ± SD (n =2).

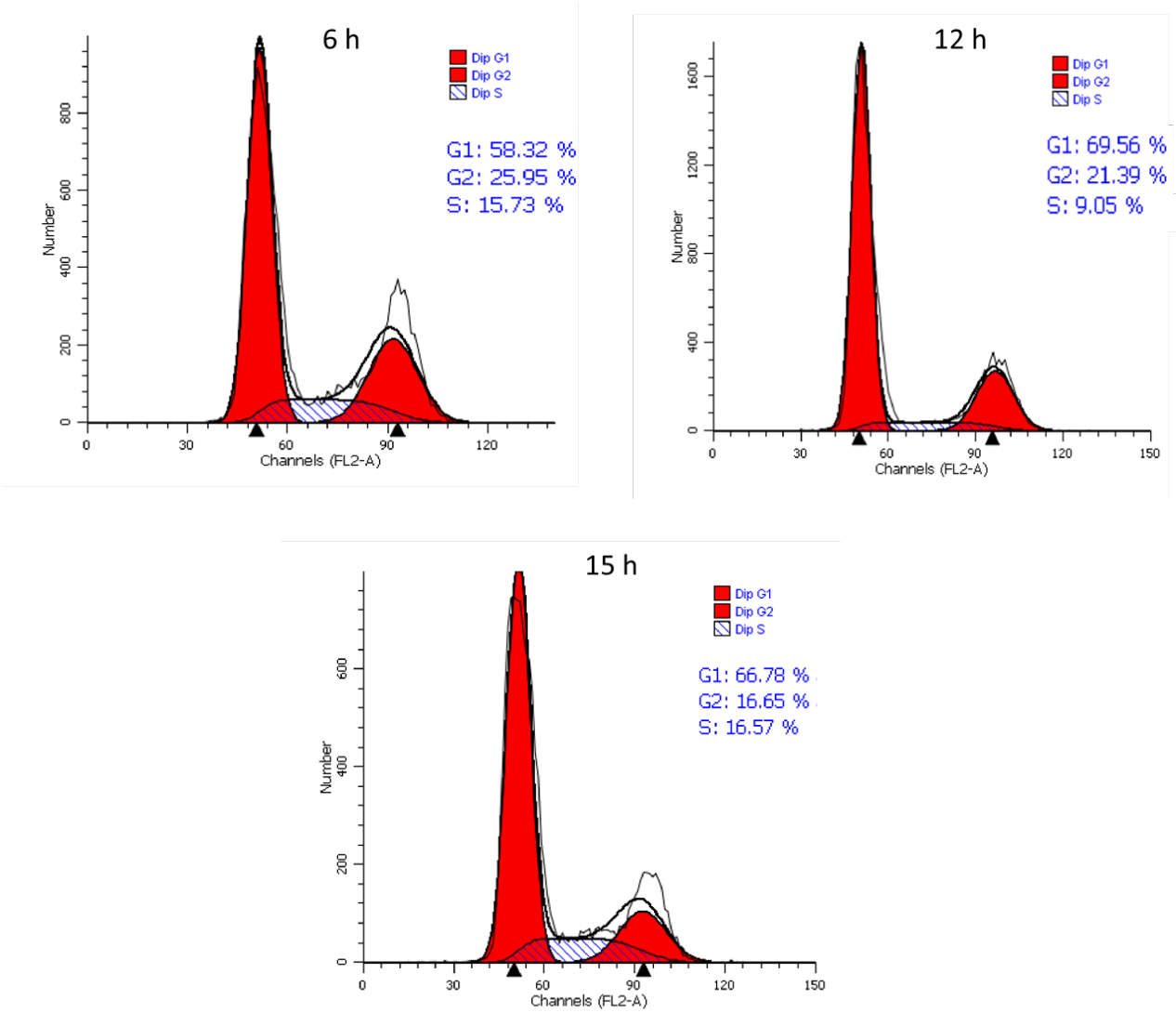

Figure S5: Flow cytometry analysis of synchronised control (familial) iPSC-MSCs at 6 h, 12 h and 15 h. Control iPSC-MSCs were treated with 4 mM of thymidine for 24 h with a 12-h release before the second thymidine block. DNA content in synchronised cells was compared at 6 h, 12 h and 15 h post-double-thymidine release. Data presented as mean ± SD (n =2).

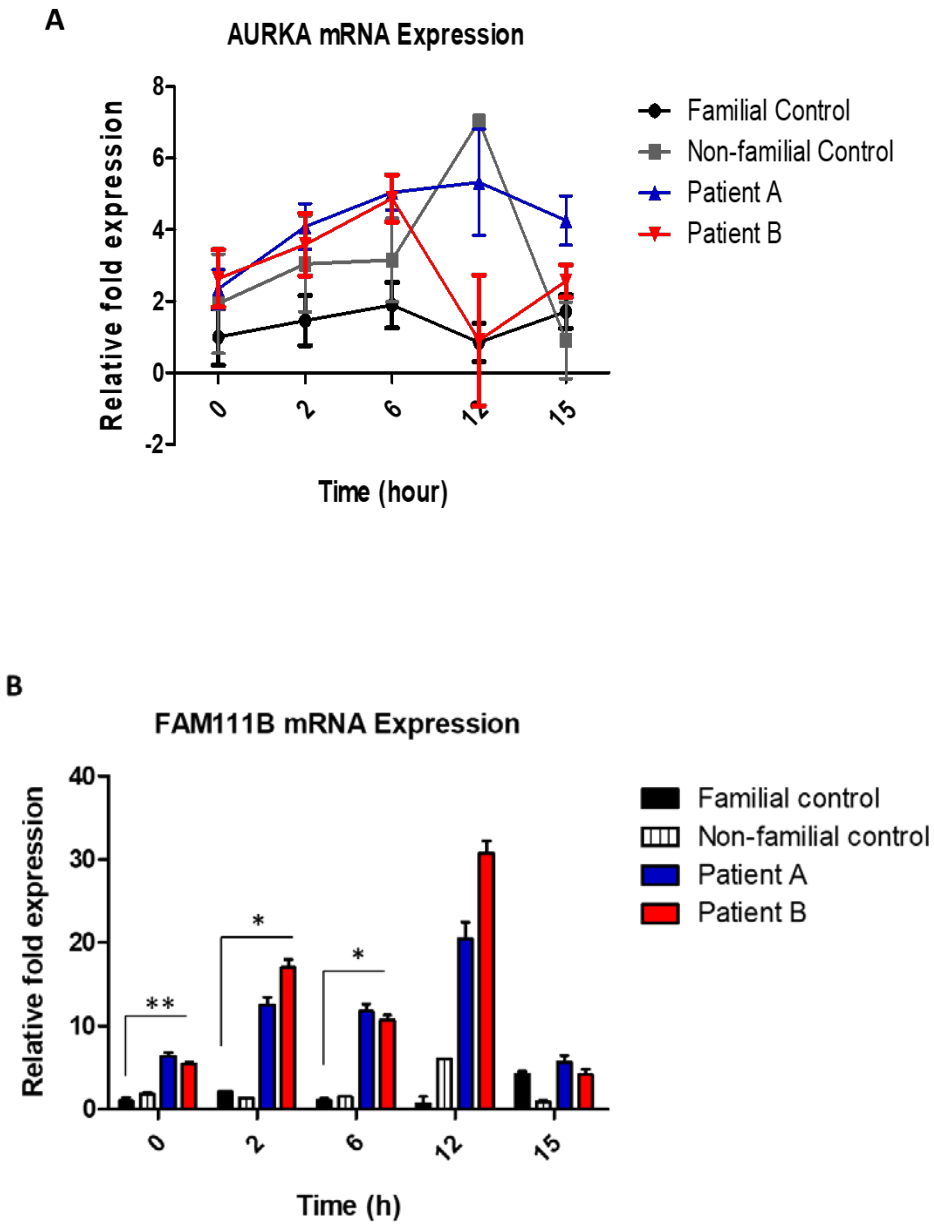

Figure S6: Expression of AURKA and FAM111B mRNA in synchronised patient and control iPSC-MSCs. The iPSC-MSCs were arrested by double-thymidine block for 24 h with a 12-h release before the second thymidine block. DNA content in synchronised cells was compared at 6 h, 12 h and 15 h post-double-thymidine release. **(A)** AURKA and **(B)** FAM111B mRNA expression were analysed at 0, 2, 6, 12 and 15 h. Data presented as mean ± SEM (n = 3). * $p < 0.05$; ** $p < 0.01$; *** $p < 0.001$

NATIONAL HEALTH LABORATORY SERVICE

Human Genetics - Groote Schuur

Tel No: 021 4044509 (Cyto) 021 4044449 (Molecular)
Fax No: 021 4044530 021 4044472
Practice No: 5200296
www.m:ulhtb.11cL1c.za

PO Box 3.J55S
Groote Schuur
7935

Labno **SCG0022205 (05/03/2014)**
Ref R-17

Age(Sex) DoB Not stated

DR BALLO
RM 6.01, LEVEL 6
ANATOMY BUILDING
UCT, MEDICAL SCHOOL
OBSERVATORY
7925

Ref Dr DR BALLO
Organisation Karyotyping **Ballo**
Hosp No **HFPI.2/Familial control**
Taken No Date Rcv'd 27/02/14 14:50
Report 17/03/14 13:41

LABORATORY REPORT

Specimen Stem Cell Collection
Tests ordered Bld Chr

BLOOD CHROMOSOME ANALYSIS

Chromosome analysis of 10 metaphase cells revealed the karyotype: 46,XX consistent with a normal female pattern.

No gross structural abnormality was detected on Giemsa banded metaphases. Chromosomal changes which may be clinically significant such as subtle rearrangements or micro-deletions may not be detected in some metaphase spreads.

The chromosome band resolution is approximately 400 g-bands.

This test was performed at NHLS Cytogenetics, C21, New GSH
Tel: 021 404 4509

Information regarding Genetic Services is available at
Tel: 021 406 6304 / 021 404 6235

Authorised by : T Ruppelt Medical Technologist Test(s): Bld Chr

--- End of Laboratory Report ---

NATIONAL HEALTH LABORATORY SERVICE

Human Genetics - Groote Schuur

Tel No: 021 4044509 (Cyto) 021 4044449 (Molecular)
Fax No: 021 4044530 021 4044472
Practice No: 5200296
www.madlab.uct.ac.za

PO Box 34555
Groote Schuur
7935

Labno **SCG0023263 (30/06/2014)** Patient **CTI.5/Non-familial control**
Ref R-18 Age(Sex) DoB Not stated

DR R BALLO
RM 6.01, LEVEL 6
ANATOMY BUILDING
UCT, MEDICAL SCHOOL
OBSERVATORY
7925

Ref Dr DR R BALLO
Organisation **Karyotyping Ballo**
Hosp No **CTI.5/Non-familial control**
Taken No Date Rcv'd26/06/14 00:00
Report 04/07/14 13:54

LABORATORY REPORT

Specimen Stem Cell Collection
Tests ordered Bld Chr

BLOOD CHROMOSOME ANALYSIS

Chromosome analysis of 10 metaphase cells revealed the karyotype: 46,XY, consistent with a normal male pattern.

No gross structural abnormality was detected on Giemsa banded metaphases. Chromosomal changes which may be clinically significant such as subtle rearrangements or micro-deletions may not be detected in some metaphase spreads.

The chromosome band resolution is approximately 400 g-bands.

This test was performed at NHLS Cytogenetics, C21, New GSH
Tel: 021 404 4509

Information regarding Genetic Services is available at
Tel: 021 406 6304 / 021 404 6235

Authorised by : N Jano Medical Technologist Test(s): Bld Chr

--- End of Laboratory Report ---

NATIONAL HEALTH LABORATORY SERVICE

Human Genetics - Groote Schuur

Tel No: 021 4044509 (Cyto) 021 4044449 (Molecular)
Fax No: 021 4044530 021 4044472
Pactice No: 5200296
wwi,i,·.tn.1<11:?b. 11Ct..1c.z.1

PO Box 3.J555
Groote Schuur
7935

Labno **SCG0023775 (15/08/2014)** Patient **HFP2.5/PatientA**
Ref R-20 Age(Sex) DoB Not stated

DR R BALLO
RM 6.01, LEVEL 6
ANATOMY BUILDING
UCT, MEDICAL SCHOOL
OBSERVATORY
7925

Ref Dr DR R BALLO
Organisation Karyotyping Ballo
Hosp No **HFP2.5/PatientA**
Taken No Date Rcv'dl2/08/14 15:45
Report 26/08/14 10:16

LABORATORY REPORT

Tests ordered Bld Chr

BLOOD CHROMOSOME ANALYSIS

Chromosome analysis of 10 metaphase cells revealed the karyotype: 46,XY, consistent with a normal male pattern.

No gross structural abnormality was detected on Giemsa banded metaphases. Chromosomal changes which may be clinically significant such as subtle rearrangements or micro-deletions may not be detected in some metaphase spreads.

The chromosome band resolution is approximately 500 g-bands.

This test was performed at NHLS Cytogenetics, C21, New GSH
Tel: 021 404 4509

Information regarding Genetic Services is available at
Tel: 021 406 6304 / 021 404 6235

Authorised by : N Jano Medical Technologist Test(s): Bld Chr

--- End of Laboratory Report ---

NATIONAL HEALTH LABORATORY SERVICE

Human Genetics - Groote Schuur

Tel No: 021404450 9 (Cyt o) 02140 44449 (Molecular)
Fax No: 0214044530 0214044472
Practice No: 5200296 *wi,i,·w.ma<lJ,lb.11ct.ac.z..1*

POBox34555
Groote Schuur
7935

Labno **SCG0024875 (20/11/2014)** Patient **HFP3.4/Patient B**
Ref R-22 Age(Sex) DoB Not stated

DR R BALLO
RM 6.01, LEVEL 6
ANATOMY BUILDING
UCT, MEDICAL SCHOOL
OBSERVATORY
7925

Ref Dr DR R BALLO
Organisation Karyotyping **Ballo**
Hosp No **HFP3.4/Patient B**
Taken No Date Rcv'dl7/ll/14 15:30
Report 12/12/14 13:59

LABORATORY REPORT

Specimen Stern Cell Collection
Tests ordered Bld Chr

BLOOD CHROMOSOME ANALYSIS

Chromosome analysis of 10 rnetaphase cells revealed the karyotype: 46,XX consistent with a normal female pattern.

No gross structural abnormality was detected on Giernsa banded metaphases. Chromosomal changes which may be clinically significant such as subtle rearrangements or micro-deletions may not be detected in some melaphase spreads.

The chromosome band resolution is approximately 400g-bands.

This test was performed at NHLS Cytogenetics, C21, New GSH
Tel: 021 404 4509

Information regarding Genetic Services is available at
Tel: 021 406 6304 / 021 404 6235

Authorised by : N Jano Medical Technologist Test(s): Bld Chr

--- End of Laboratory Report ---